Institute for Energy

Development of a European Procedure for Assessment of High Cycle Thermal Fatigue in Light Water Reactors: Final Report of the NESC-Thermal Fatigue Project

M. Dahlberg, K.-F. Nilsson, N. Taylor, C. Faidy, U. Wilke, S. Chapuliot, D. Kalkhof, I. Bretherton, M. Church, J. Solin, J. Catalano

2007

NESC

Network for Evaluating Structural Components

EUROPEAN COMMISSION
DIRECTORATE-GENERAL
Joint Research Centre
EUR 22763 EN

Mission of the Institute for Energy
The Institute for Energy provides scientific and technical support for the conception, development, implementation and monitoring of community policies related to energy. Special emphasis is given to the security of energy supply and to sustainable and safe energy production.

European Commission
Directorate-General Joint Research Centre (DG JRC)
http://www.jrc.ec.europa.eu/

Institute for Energy, Petten (the Netherlands)
http://ie.jrc.ec.europa.eu/

Contact details:
Nigel Taylor
Tel. + 31 (0) 224565202
E-mail: Nigel.Taylor@ec.europa.eu

Legal Notice

EUR 22763 EN
ISSN 1018-5593
Luxembourg: Office for Official Publications of the European Communities

NESC
Network for Evaluating Structural Components

DEVELOPMENT OF A EUROPEAN PROCEDURE FOR ASSESSMENT OF HIGH CYCLE THERMAL FATIGUE IN LIGHT WATER REACTORS

FINAL REPORT OF THE NESC-THERMAL FATIGUE PROJECT

EUR 22763 EN


NESC
Network for Evaluating Structural Components

NESC
Network for Evaluating Structural Components

Development of a European Procedure for Assessment of High Cycle Thermal Fatigue in Light Water Reactors: Final Report of the NESC-Thermal Fatigue Project

April 2007

EUR 22763 EN

Authors

M. Dahlberg, Inspecta
K.F. Nilsson, EC DG JRC
N. Taylor, EC DG JRC
C. Faidy, EDF
U. Wilke, EON
S. Chapuliot, CEA
D. Kalkhof, PSI (now HSK)
I. Bretherton, Serco (now HSE)
M. Church, NRG
J. Solin, VTT
J. Catalano Tractebel

Published by the

EUROPEAN COMMISSION

Directorate-General Joint Research Centre
Institute for Energy
1755 ZG Petten, The Netherlands


NESC
Network for Evaluating Structural Components

NESC
Network for Evaluating Structural Components

EXECUTIVE SUMMARY

In nuclear plant piping systems thermal fatigue damage can arise at locations where there is turbulent mixing of different temperature flows. The severity of this phenomenon can be difficult to assess via plant instrumentation due to the high frequencies involved. In Europe the existing approaches to high cycle thermal fatigue have been successful in providing margins against pipe ruptures. Nonetheless there have been instances of thermal fatigue damage and over the last 10 years several recent R&D programmes have been devoted to developing better understanding of the induced thermal loads and associated damage mechanisms. To exploit this work, in 2003 the Network for Evaluation of Structural Components (NESC) set up a project involving both utilities and R&D organizations. Its aim was to produce a consensus methodology for assessing high cycle thermal fatigue in piping components, with special attention to turbulent mixing phenomena at mixing tees in light water reactor systems. It has involved the collaboration of over 10 organisations from 5 European countries. All have participated on an 100% in-kind basis. Wherever possible, advantage has been taken of recent R&D work at national, European and international levels. The work programme focused on two main aspects:

a) creating a database of service and mock-up data for better understanding thermal fatigue damage mechanisms and for validating the procedure.

b) developing a European multi-level thermal fatigue damage procedure, which should reflect the multi-disciplinarity of the phenomenon (thermo hydraulic, material, strain evaluation through FEA, damage analysis, fracture mechanic, ISI performance).

The main findings and conclusions for each of these aspects are summarized in the following.

Data base thermal fatigue damage cases

- The project created a database of thermal fatigue damage cases, 45 of which relate to operational components and 5 to laboratory simulation tests. From the analysis of the operation data the following points emerge:
  - The cases examined confirm that the thermal loads are the main unknown factor for detailed assessment of thermal fatigue damage.
  - In several instances thermal fatigue damage has developed within short times, even less than a year. Hence the common classification of thermal fatigue as an ageing process (implying that its probability increases progressively with time) is potentially misleading.
  - A small number of damage cases with low nominal ΔT values (60 to 80^{o}C), were identified, but most of these apparently experienced periods of operation at higher ΔT values.
  - Cracks can appear both on un-flushed welds (not used in class 1 piping) and in the base material and can be oriented axially or circumferentially.

Cracks in welds tend to be deeper than those in base material (although it is noted that some deep cracks initiated in the weld counter bore radius).

- None of the through-wall cracks have lead to a pipe rupture during normal operation (although in some cases the dimensions would be assessed as critical for accident loads). All the cracks were detected by leakage in the system.
- Turbulent mixing alone rarely causes through-wall cracking of pipes, but leads to the development of local surface crazing. Crack depths depend on the mean stress values that are connected to the steady state stresses. Additional system or thermal loads can provide a level of stress sufficient to create through wall cracking.
- Stratification may occur in conjunction with turbulent mixing in dead legs. It is worth mentioning that stratification loads are easier to handle than turbulence and can frequently be controlled by temperature monitoring and application of suitable transfer functions (an exception is for steep gradients through the height of a pipe, for instance due to low velocity cold water flows in feedwater systems).
- A main risk factor for stratification is valve leakage. Thus valve leakage control is an effective measure against thermal fatigue in dead legs.

- Examination of the 5 laboratory simulations confirmed that these can successfully re-produce thermal fatigue damage. It is noted, however, that to achieve this under controlled test conditions these experiments used relatively high ΔT and low frequency values, so that the cycles to crack initiation ranging from several hundred up to several hundreds of thousands of cycles.

European Procedure for Assessment of Fatigue Damage under Turbulent Mixing

- A multi-level approach is proposed, which follows the French model and recognizes that despite recent R&D work on measurement and simulation of mixing conditions at Tee junctions, the description and quantification of the associated thermal loads remains a difficult task. The 4 levels are:
  - Level 1 uses a simple screening criteria expressed in terms of the (nominal) ΔT between the two mixing fluids
  - Level 2: the fatigue usage factor is determined by the so-called sinusoidal method, whereby the thermal loading is treated as an idealised sinusoidal wave
  - Level 3: the fatigue usage factor is determined by analysis of the complete local load spectra
  - Level 4 deals with the calculation of the growth of a detected or postulated crack-like flaw and is based on fracture mechanics principles.

  The first two levels have been considered in detail in this study.

- In Level 1 a screening criterion of $\Delta T = 80^{o}\mathrm{C}$ is proposed for turbulent mixing in Tees of austenitic materials. This can also be extended to other types of thermal loadings i.e. stratification and transients, for all types of components fabricated in austenitic materials. For Tees in carbon steel, a lower value of 50°C is set, reflecting the lower endurance limit of such steels and the greater uncertainty concerning the environment effect on fatigue strength. The project database of component damage cases broadly supports the validity of the screening criterion approach. Of the relatively small number of damage cases with slightly lower nominal ΔT values, several apparently experienced periods of operation at higher Δ*T* values. Rather than invalidating the proposed screening level, this highlights the need to verify that the "nominal" ΔT value used for the screening properly reflects the full range of past (or planned) operating conditions.

- Level 2 provides for the calculation of a fatigue usage factor based on the assumption of a sinusoidal thermal loading at the most damaging frequency for a given ΔT. Advice is given on selection of heat transfer coefficient, fatigue curves, fatigue strength reduction factors and plasticity correction factors. The inherent conservatism of the method has been demonstrated with the database of operational failure cases.
- In applying the above methods, sources of thermal loading other than turbulent mixing and/or system loads should be taken into consideration.
- Fatigue environmental effects have not to be taken in high cycle fatigue, but should be considered on a case-by-case basis for lower frequency stratification loads.

Further Work

- Level 3 and 4 of damage assessment methodology (detailed consideration of the thermal loading spectra and fatigue crack growth of detected or postulated crack-like flaws) should be detailed and validated.
- The database of thermal fatigue damage cases should be maintained and, where possible, further extended. Analysis of the data in relation to positive operating experience should be considered i.e. to account for cases where no damage has occurred (notwithstanding ΔT levels above the screening criterion level) in the assessment. For instance, the most recent EDF INTHERPOL test confirmed that class 1 piping weld with good surface finish can resist more than 500 000 cycles with ΔT = 120°C at low frequency without any damage.
- The procedure should be expanded to provide a more comprehensive basis for assessing the different aspects of thermal fatigue damage assessment and mitigation measures, for instance:
  - temperature monitoring for low frequency phenomena, stratification to support better understanding of these phenomena.
  - load sequence effects, in particular the effect of intermittent occurrence of large ΔT values on fatigue behaviour.
  - effective in-service inspection technology and procedures.

ACKNOWLEDGEMENTS

The support of SKI (Swedish Regulator), Ringhals AB and the European Commission is gratefully acknowledged. The authors would also like to thank other colleagues who have contributed to the work in the NESC-TF project, including Sander de Groot (NRG), Hans Leber (PSI) and John Taggart (Serco). For the proof reading and comments to this report, we are indebted to V. Radu (INR) and H. Finney (Inspecta).

TABLE OF CONTENTS

NESC
Network for Evaluating Structural Components

1 OBJECTIVE AND SCOPE

1.1 Background

Thermal fatigue is widely recognised as an important potential damage mechanism in cooling piping systems of light water reactors /1.1, 1.2/. While most common thermal fatigue issues are well understood and can be monitored by plant instrumentation systems, mixing tees present several distinct challenges for structural integrity assessment: the inherent difficult in determining the local thermal loads since these cannot be adequately monitored by common thermocouple instrumentation, the availability of appropriate high cycle fatigue data and the fatigue damage assessment process for variable loading histories. The components potentially affected by turbulent mixing include the surge and spray lines and several branch lines and nozzles (charging line, safety injection lines etc.).

A number of recent R&D programmes have considered thermal fatigue /turbulent mixing phenomenon. In Japan, extensive work has been performed both regarding the assessment process /1.3/ and environmental effect on the fatigue curves /1.4/ (although this aspect is less relevant in the high cycle regime for $N > 10^6$ cycles. The JSME has issued a code in 2003 on dealing with high-cycle thermal fatigue /1.5/. In the US thermal fatigue has been addressed as part of EPRI's Materials Reliability Project /1.6, 1.7/ with the aim to provide guidelines for evaluation, mitigation, monitoring and non-destructive examination. In parallel work is also underway concerning proposals to revise the ASME fatigue curves /1.8/, which would have consequences for thermal fatigue evaluation procedures. In Europe several national programmes are under way or have been completed in this area, notably the French studies /1.9/ which followed the leak at the Civaux plant in 1998.

The European Commission has promoted collaborative work in this area. The THERFAT project /1.10/ ran from December 2001 to November 2004. Its objectives were to advance the accuracy and reliability of thermal fatigue load determination in both engineering tools and research oriented approaches and to outline a science-based practical methodology for managing safety risks due to thermal fatigue. THERFAT has also produced a road-map for development of a European fatigue evaluation methodology and this challenge has been taken up in the NESC Thermal Fatigue project, which is the subject of this report.

1.2 Goal and Work Plan

The objective of the NESC Thermal Fatigue project was as initially stated follows:

> *"The development of a European methodology for assessing thermal fatigue in LWR components. The procedure should reflect the multi-disciplinarity of the thermal fatigue problem. It should be verified or validated by a database of suitable experimental and service data."*

It was subsequently agreed that the scope should be restricted to high cycle thermal fatigue in piping components, with special attention to turbulent mixing phenomena at mixing tees. To realise the above objective a three-phase work plan /1.11/ was agreed at the start of the project:

Phase 1: This consisted of three work packages i) WP Procedures, on the development of the multi-level framework proposed by EDF /1.12/ (Figure 1.1); ii) WP Database, involving compilation, classification and analysis of data from service data on components, from features tests and for materials properties testing and iii) WP Case Selection, to identify a sub-set of specific cases for the procedure verification; these should illustrate different typical in-service or design thermal fatigue problems and should be as complete as possible in terms of data.

Phase 2 In this Verification Phase, the selected cases from Phase 1 are analysed according to the draft procedure

Phase 3 Consensus and Recommended Procedure; this phase consisted of the integration of the Phase 1 and 2 results.

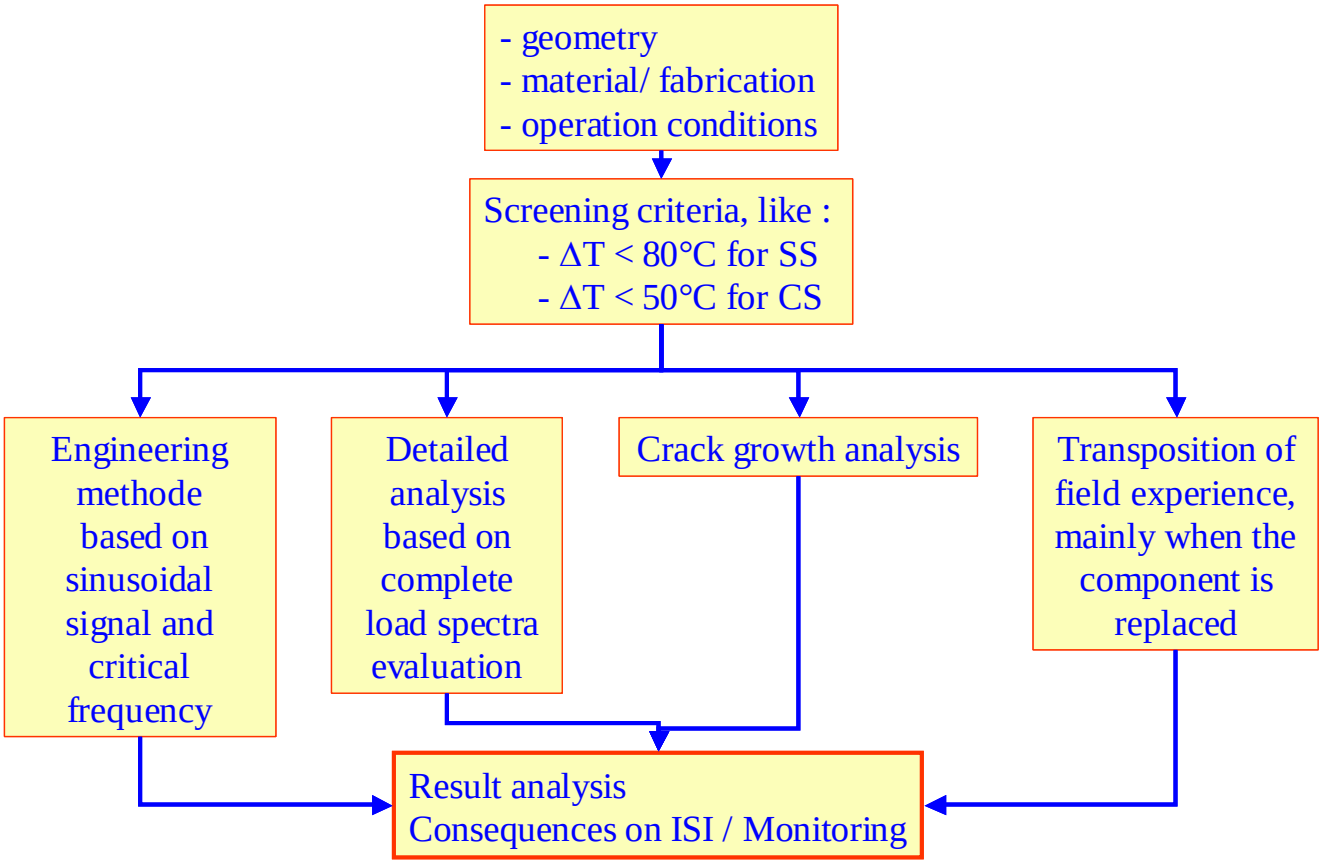

Figure 1.1: Schematic of the proposed thermal fatigue evaluation procedure /1.12/.

The present report summarises the results of the project. Chapter 2 identifies the fatigue issues addressed in the project. Chapter 3 considers the different forms of thermal fatigue relevant to LWR plant. Chapter 4 provides an overview of existing procedures, R&D work and laboratory simulations of relevant thermal fatigue phenomena. Chapter 5 deals with the database of operation instances of thermal fatigue and the analysis of the data collected. Chapter 6 discusses the critical issue of load determination. Chapter 7 deals with the fatigue damage assessment via fatigue curves. Chapter 8 presents the proposed procedure. Chapter 9 describes the verification calculations performed in the project. Finally Chapter 10 outlines areas for further R&D on this topic.

The main body of the report is complemented by 5 appendices, which provide more detailed information on the following aspects: Appendix A presents the failure case summary form used to compile the database of operation thermal fatigue cases; Appendix B considers the properties of the so-called sin-method, by which the temperature fluctuations are represented as a sine wave; Appendix C considers the code basis for thermal fatigue; Appendix D provides the background to the plasticity correction factors and Appendix E considers the fracture mechanic methods to be used for crack propagation analyses.

1.3 Project Organisation

NESC-TF is the fifth project of the Network for Evaluating Structural Components (NESC). NESC was set up over 10 years ago to address the verification of advanced structural integrity assessment techniques for safety-critical reactor components /1.13/. Through its self-funded activities and associated projects, partly funded by the European Commission's DG-RTD, it has developed a significant body of benchmark R&D data, in particular for large-scale tests performed under closely monitored conditions. The added value of combining the efforts of utilities, manufacturers and R&D organisations is stressed.

In the NESC-TF participation is subject to a commitment to contribute to the work of the project i.e in-kind contribution, whereby its funding is up to the participant. To promote exchange of data and open discussions between the participants, it was decided that the project group should be autonomous within NESC, although there was an obligation to report progress to the NESC Steering Committee. However the group's working documents are reserved to the participants of the project itself. NESC-TF has run from 2003 to 2006 and has involved the following 10 organisations (in alphabetical order)

- CEA, France
- Inspecta, Sweden (for Swedish utilities and the Swedish Nuclear Inspectorate)
- EDF, France
- EON Kernkraft, Germany
- Fortum, Finland
- JRC, European Commission
- NRG, The Netherlands
- Paul Scherrer Institute, Switzerland

- Serco, UK
- Tractebel, Belgium
- VTT, Finland

1.4 References

1.1 IAEA, “Assessment and management of ageing of major nuclear power plant components important to safety. Primary piping in PWRs”, TECDOC-1361, July 2003

1.2 C. Faidy et al, Thermal Fatigue of Reactor Components in OECD-NEA countries: a Three-fold Program to Enhance cooperation, Proc. SMiRT-18, Beijing, China, August 2005

1.3 N. Kasahara et al, Thermal Fatigue Evaluation Method based on power spectrum density functions against fluid temperature fluctuation, Proc. ASME PVP2005, Denver, Colorado, USA, July 2005.

1.4 M. Higuchi at al, “Development and Evaluation Method of Fatigue Damage on Operating Plant Components Considering Environmental Effects”, NEA/CSNI/R(2004)21 , Proc. 3rd Int. Conf. on Fatigue of Reactor Components, Seville, Spain, October 2004

1.5 JSME, Guideline for Evaluation of High-cycle Thermal Fatigue of a Pipe, S017-2003, 2003

1.6 J.D. Keller et al, “Thermal Cycling Screening Criteria and Evaluation Methodology and Application to Pressurized Water Reactor Branch Line Piping”, NEA/CSNI/R(2004)21, Proc. 3rd Int. Conf. on Fatigue of Reactor Components, Seville, Spain, October 2004

1.7 J.D. Keller et al, “Thermal Fatigue Management Guideline for Normally Stagnant Non-Isolable RCS Branch Lines”, NEA/CSNI/R(2004)21, Proc. 3rd Int. Conf. on Fatigue of Reactor Components, Seville, Spain, October 2004

1.8 W. J. O’Donnell et al, Proposed new fatigue design curves for carbon and low alloy steels in high temperature water, Proc. ASME PVP2005, July 2005, Denver, Colorado, USA

1.9 S. Chapuliot et al, Hydro-thermal-mechanical analysis of thermal fatigue in a mixing tee, Nuclear Engineering & Design, 235 (2005) 575-596

1.10 K.-J. Metzner & U. Wilke, European THERFAT project—thermal fatigue evaluation of piping system “Tee”-connections, Nuclear Engineering & Design, Vol.. 235, Issues 2-4 , 2005, 473-484

1.11 K.-F. Nilsson, N. Taylor, M. Dahlberg, C. Faidy, NESC Thermal Fatigue Project Proposed Work Programme, NESCDOC MAN (03) 05, December 2003

1.12 C. Faidy, ‘Thermal Fatigue in Mixing Areas: Status and Justification of French Assessment Method’, Proc. 3rd Int. Conf. on Fatigue of Reactor Components, EPRI 1011958, 2005.

1.13 N. Taylor & D.P.G. Lidbury, “Improving Structural Integrity Assessment Techniques”, 1st Symposium - Nuclear Pressure Equipment Expertise and Regulation, International Conference, Dijon, June 2005

2 BASIC FATIGUE ISSUES

Thermal fatigue is a potentially significant degradation mechanism in nuclear power plants which can also manifest itself as short-term process linked to specific operational conditions. In general, the common thermal fatigue issues ("plug type" transients and steady state stratification effects) are understood and can be controlled by plant instrumentation systems. However, incidents in some plants indicate that turbulent temperature mixing effects may occur, for instance in certain piping systems Tees, that cannot be adequately monitored by external surface thermocouples. Such high cyclic thermal loads can act in combination with the other thermal and system loads, leading to new complex load spectra.

Component design is typically carried out with conservatively specified lump design loads and various simplifying assumptions concerning thermal loads which are not adapted to quantify the existing safety margins for the complex thermal load spectra arsing from turbulent mixing phenomena. Usually more sophisticated fatigue analysis methods have to be applied to achieve reliable fatigue damage predictions e.g. 3-D finite element analyses or modifications of the K_e-factor considering the plastic material behaviour at local geometric discontinuities. The load input is of particular importance. Specified loads or measurement results can be used. For fatigue analyses only service level A and B (operational and upset condition loads) are relevant. Loads taken from the design specification include all potential system load cases - enveloping stipulated – up to "End of Life (EOL)". Sometimes level C loads (emergency condition), which are unlikely to occur, are classified as operational loads for certain systems. Therefore, they are included in the EOL fatigue analysis, although they may never appear. Load monitoring systems (bookkeeping of operational transients and load cycle numbers) are helpful to avoid conservative load assumptions because they register the operational loads which have really occurred during the plant operation period so far.

In a piping system different types of temperature loads may occur. High flow rates can cause "plug-type" transients; the associated temperature drop/rise produces a thermal shock type-load with high local stresses on the inner pipe surface. Under low flow rate conditions thermal stratification can occur in horizontal portions of a piping system, giving rise to a global "banana" type deflection and local "pear" type deformation of the pipe cross-section. Turbulent temperature mixing effects, which are the main focus of this report, may occur by mixing of different mass flows at Tee connections.

A consistent overall concept or guiding framework is required to help manage these fatigue related questions and to ensure appropriate co-operation between the different technical disciplines involved.

3 THERMAL LOADINGS

3.1 Thermal Transients

Major nuclear components are designed to resist low cycle thermal fatigue. Operating experience shows that only a limited number of cases involving cracks and leaks have been due to cyclic thermal shocks. Nevertheless, in some cases, for example for long term life cycle management, more realistic methods, potentially less conservative than the code-based design methods, can be proposed on a case by case basis.

Significant thermal transients can occur in the following way. Injection of hot or cold water with a high flow rate leads to a plug-type block of coolant, which produces a uniform change of temperature over the entire pipe cross section as it passes (Figure 3.1). Very "fast" transients with significant temperature differences may cause "thermal shocks". These plug-type transients may occur in horizontal and vertical piping systems. At cross-sections where such phenomena are expected, two measuring points are installed at the 12 and 6 o'clock positions for temperature monitoring.

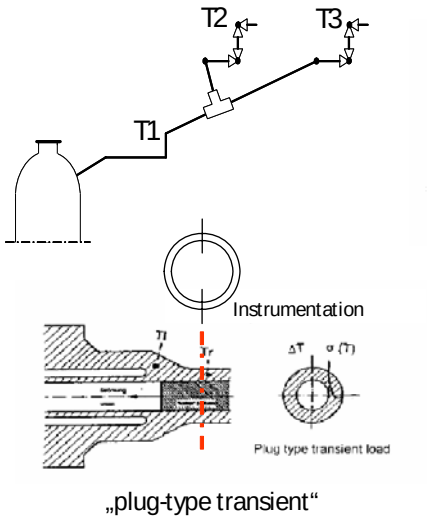

Figure 3.1: Schematic of plug-type transients.

3.2 Thermal Stratification

A thermally stratified fluid is when the fluid is layered with different temperatures. A change in temperature leads to a change in the water density. The warm water strives to rise and the cold water strives to settle at the bottom of the pipe. If the water is not sufficiently mixed, the cold and hot portions will separate over the cross-section of the pipe. Thus stratification is promoted by high temperature differences that increase the difference in density. The typical condition for occurrence of thermal stratification is when the flow

velocities are low and the thermal gradient through the height of the piping system is high. Increasing the flow velocity will enable mixing and remove the stratified state.

Stratification, like other thermal loads can occur in combination with turbulent mixing. Thermal stratification can occur in horizontal or vertical sections of the pipe, but also close to an elbow. The following sub-categorization is customary:

Global thermal stratification
When flow conditions change from stratification to no stratification, Figure 3.2, and back to stratification over a long horizontal section of a line. This is called *global thermal stratification.* The stratified state will cause the pipe to bend, resulting in loads on the pipe supports along the horizontal runs, on the elbows and on the nozzles at its ends. This stratification is more significant for long flexible horizontal pipe, with a very deep gradient (far away of a linear gradient through the height of the horizontal pipe). A large linear ΔT has no mechanical consequences on a flexible pipe.

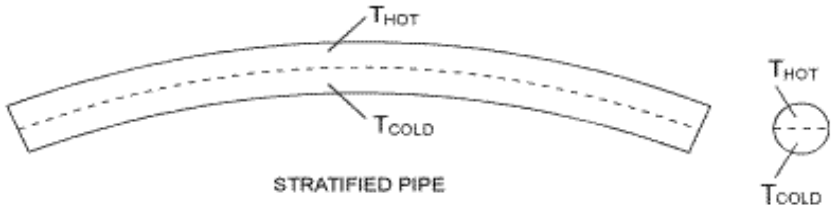

Figure 3.2: Schematic of a pipe with stratification.

Cyclic thermal stratification
If stratification can be present in a horizontal section of a pipe, the damage can be connected to changes in the elevation of the interface between the hot and cold portions, with deep gradient around the interface. This type of stratification is called *cyclic thermal stratification.* Stresses will arise with and without pipe restraints, with the case of no restraint shown in Figure 3.3. If the pipe is restrained net bending moments will arise. The stresses in the circumferential direction of the pipe are normally negligible.

Thermal cycling
Change in length of the stratified portion of a pipe is referred to as *thermal cycling.* This can be seen as axial motion of the interface between stratified and non-stratified water. A typical example is when turbulence in a main pipe penetrates into a connecting line of nominally stagnant water. The turbulent penetration fluctuates and produces cyclic axial movement of the stratification interface. This type of stratification is often associated with a leaking valve. Thermal cycling can also develop in a vertical section of the branch line and the interface may move cyclically over an elbow. See for example Figure 3.4. Thermal cycling is associated with stresses in both the axial and circumferential direction, depending on the interface height and inclination. See Figure 3.5.

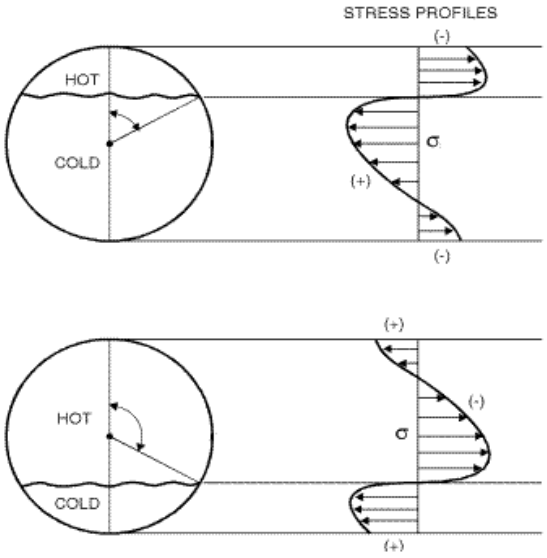

Figure 3.3: Cross section of an un-restrained pipe with stratification and the resulting axial stress profile; the circumferential stresses are small in comparison.

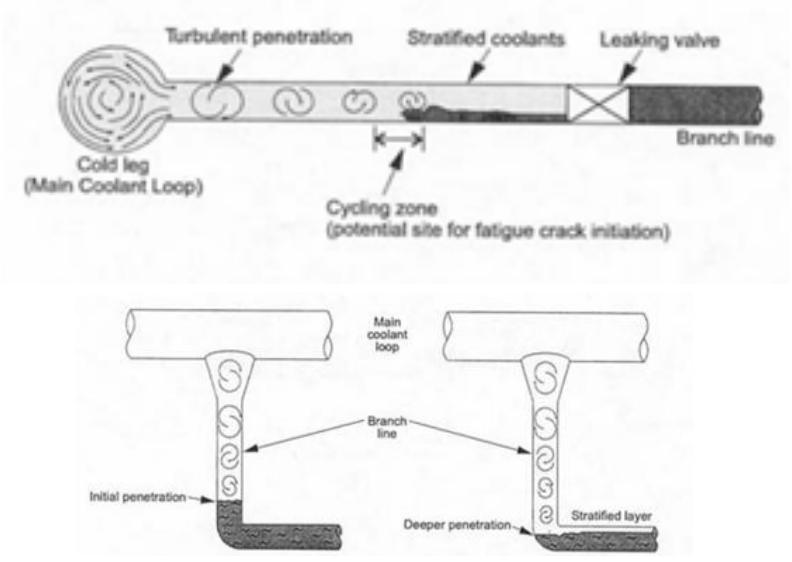

Figure 3.4: Thermal cycling in a straight pipe and an elbow

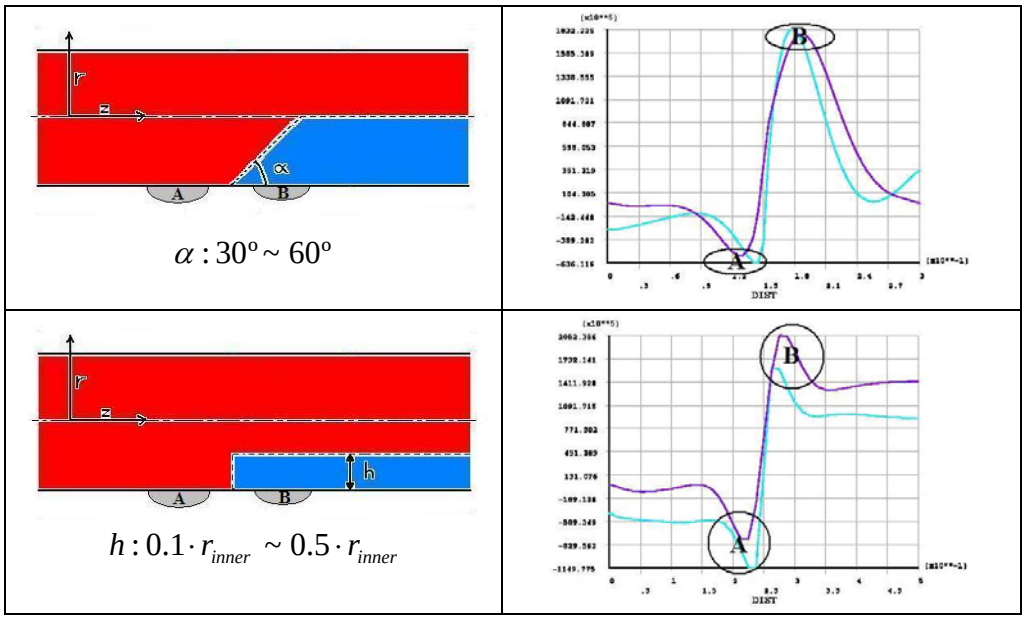

Figure 3.5: Axial and circumferential stress behaviour when varying the angle and the height of the stratification interface.

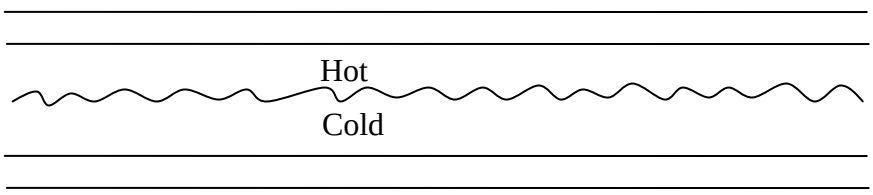

Figure 3.6: Thermal striping due to fluctuation of the interface in a stratified flow.

Striping (combined with stratification)
Stratification can also be associated with a higher frequency temperature variation, so called striping. Striping (in this context) can be seen as a rapid variation of the interface region between the hot and cold fluids. The damage rate, in this case, is directly connected to the thermal gradient in the interface area. This is illustrated in Figure 3.6. This case of loading is similar to the turbulent mixing case.

3.3 Turbulent High- Cyclic Thermal Loads

Turbulent mixing of hot and cold water is characterised by rapid and highly irregular fluid motions. These fluctuations will increase the transfer of energy and momentum as well as the heat convection transfer rate. Turbulence is associated with random fluctuations and the fluid motion occurs on several length scales. Generally, this makes the fluid motion extremely difficult to describe in detail. In the context of turbulent or mixing the

description of eddies are used. Eddies are small portions of fluid in irregular motion that exists for a short time before losing its identity. The temperature fluctuations near the pipe wall can be of the order of up to several Hz.

In turbulence the inertia forces are high in comparison to the viscous forces in the fluid. A common measure for this relation is the dimensionless Reynolds number. High Reynolds numbers will indicate higher levels of turbulence in comparison to organized laminar flow. In a tube Reynolds number is defined as $\mathrm{Re} = \frac{\rho u_m D}{\mu}$. Here, D is the pipe inner diameter, ρ is the fluid density, u_m is the mean velocity and μ is the viscosity. Reynolds number can be seen as a measure of the ratio between inertial forces and viscous forces. As a rule of thumb, $\mathrm{Re} \geq 2000$ can be used as a criterion for the onset of turbulent flow in a pipe.

A schematic of turbulent mixing is given in Figure 3.7. The random motion and temperature fluctuation near the wall will cause stresses in the wall section. The spatial distribution of the stresses implies a length correlation parameter. Quantification of the length correlation is not simple unless rather detailed information of the temperature fluctuations is available. In simplified models the temperature fluctuation is applied to a one dimensional model thus neglecting the spatial length scale dependence. (However, reportedly different EDF studies confirm that assumption is reasonable by comparing 1D model and 3D LES model.)

It should be noted that in some literature turbulent mixing is referred to as striping.

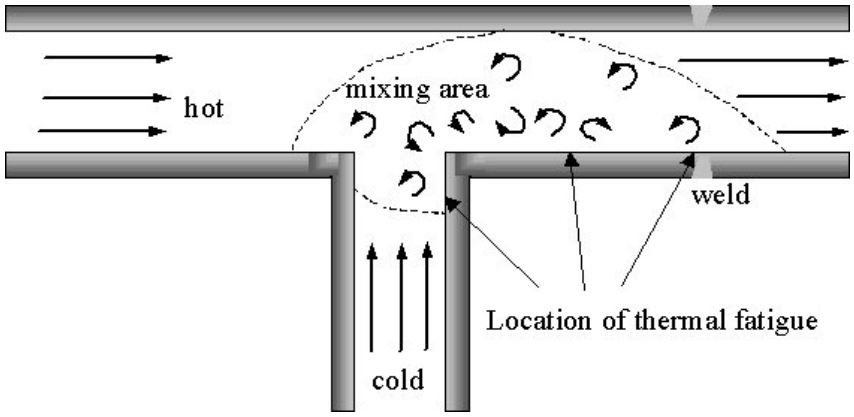

Figure 3.7: Turbulent mixing at a Tee.

4 EXISTING PROCEDURES AND EXPERTISE

4.1 European and International Procedures

4.1.1 German Approach (KTA 3201.4)

In German NPPs an integrity concept is applied according to the KTA rules for Class 1 components (see /4.1/ to /4.10/). In this temperature monitoring (stratification, plug-type transients, etc.) is a key issue. These rules can be compared with ASME Section III for Design and Section XI for Operation. KTA-rule 3201.4 contains an overall conceptual framework for the safeguarding of components integrity during plant operation, which has been used as basis for an overall integrity concept (Figure 4.1). A detailed description of an overall integrity evaluation of safety relevant systems regarding temperature loadings is documented in the THERFAT Project report /4.1/. The basic approach is:

- to demonstrate the current system/component integrity status and
- to safeguard the required component quality during the future plant operation correlated to the relevant potential degradation mechanisms and related to the safety significance of the system/component under consideration.

This can be applied for:

- Periodic safety reviews,
- Leak-before-break assessment,
- Optimisation of NDT-measures (extending intervals, optimisation of inspection extent etc.)
- Ageing management,
- System/component integrity evaluations for specific purposes e. g. to quantify the existing safety margins concerning fatigue (see section 4.2.2).

4.1.1.1 Determination of safety margins concerning thermal fatigue

In order to determine the safety margins the load/stress/fatigue determination route in combination with the load bearing capability has to be assessed. Technical codes and standards as the ASME-Code Section III for design and XI for operation, the French RCC-M Code, the British Standard BS 5500 or the German Safety Standard KTA are amongst others the basis for the fatigue analysis procedures.

As load input for the fatigue analysis either specified loads or temperature measurement results may be used (see section 6). Usually, for fatigue analyses only service level A and B are relevant. Loads taken from the design specification include all potential system load cases - enveloping stipulated - till “End of Life (EOL)”. Sometimes even plant level C loads (emergency condition) which are not likely to occur, are sometimes classified as operational load cases on the system level. Therefore, they are included in the EOL-fatigue evaluation with specified loads, although they may never appear. Trying to specify additional complex temperature phenomena may result in too conservative simplification or is done in such a detailed manner which is not suitable as data input for the common piping

system fatigue analysis. For fatigue relevant temperature transients and stratifications thermo couple measurements provide suitable data input concerning the cross section temperature distribution at important locations and the temperature variation along the length of piping system segments (Figure 4.2). Heat transfer coefficients derived from measurements are more realistic than nominal values given in codes or procedures. Mostly, operational load cycle numbers are smaller than the design specification data. The "bookkeeping" of load cycles provides the advantage that realistic values of the current fatigue usage factor can be determined and prediction for future time periods is available.

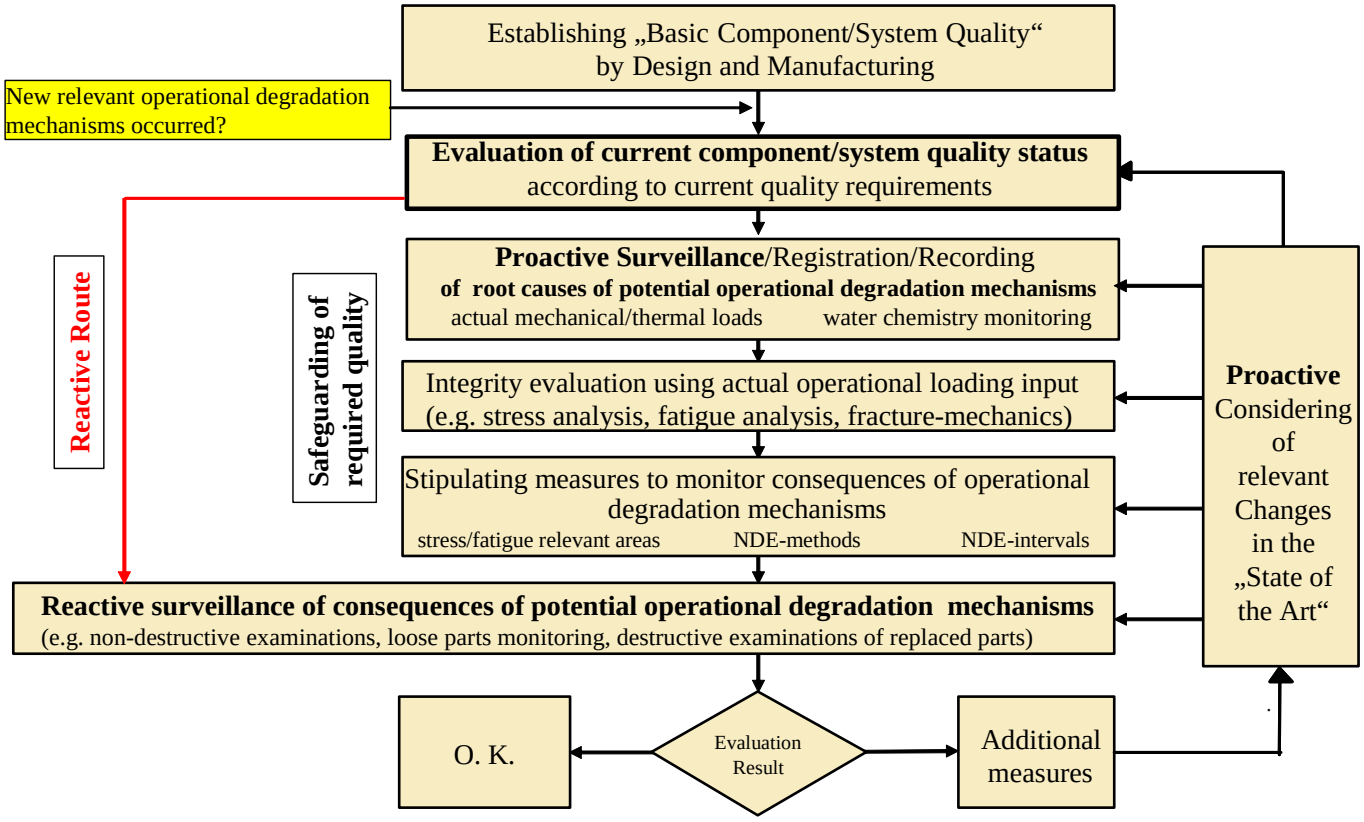

Figure 4.1: Integrity concept according to KTA 3201.4 /4.3/

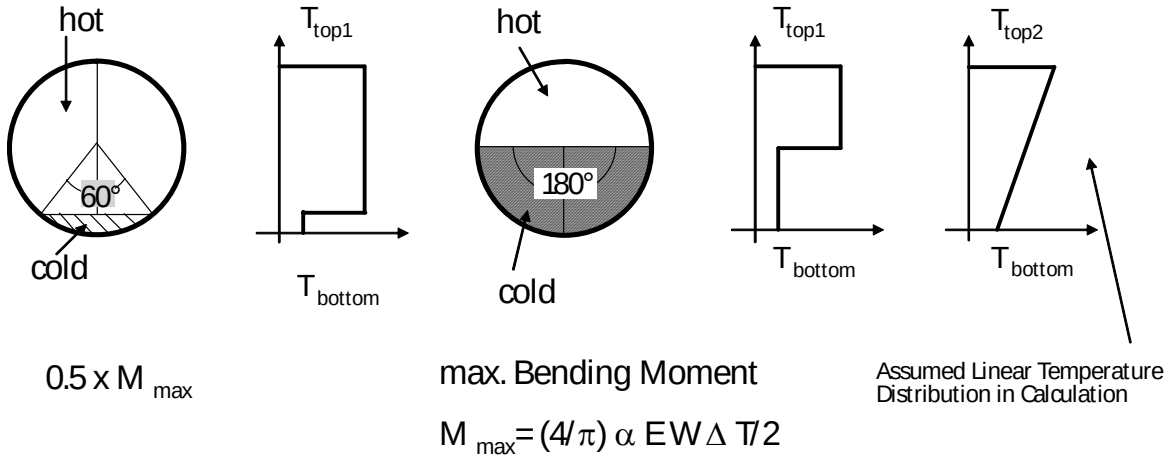

Figure 4.2: Cross sectional temperature distributions for different stratification scenarios.

In order to perform the fatigue analysis the various relevant specified load cases or measurement results have to be grouped to reference transients as suitable input for calculation. According to the approach objective – simplified or detailed – the load input is conservative or more realistic.

The fatigue evaluation may be performed as piping code analysis, e.g. for the determination of the primary + secondary stresses + peak intensity range, KTA 3201.4, Sec. 8, Eq. 8.4-3 may be applied:

$$\sigma_{III} = K_1 C_1 \frac{d_a}{2 s_c} p_o + K_2 C_2 \frac{d_a}{2I} M_{iIII} + \frac{1}{2(1-\nu)} K_3 E \alpha \left|\Delta T_1\right| + K_3 C_3 E_{rl} \left|\alpha_r \Delta T_{mr} - \alpha_l \Delta T_{ml}\right| + \frac{1}{(1-\nu)} E \alpha \left|\Delta T_2\right| \quad (4.1)$$

For determining the equivalent stresses from primary and secondary as well as stress peaks (/4.11/) the linear ΔT_1 and nonlinear ΔT_2 parts of the temperature distribution have to be considered. The symbol meanings in Equation 4.1 are:

- **first term** : with C_1=1.0 corresponds approximately to the equivalent stress of a thin walled cylindrical component (pipe);
- **second term**: with C_2=1.0 corresponds to the bending stress at the outside of a cylindrical component;
- **third term**: with K_3=1.0 corresponds to the thermal stress of a thin walled cylindrical component (pipe) caused by a linear temperature distribution ΔT_1 between the out-side surface and the inside surface and pipe ends not restrained (at the surface $\sigma_{long.max} = \sigma_{circum.max}$);
- **fourth term**: with C_3=K_3=1.0 corresponds to the thermal stress caused by range of average temperature ΔT_m on side r and l of gross structural discontinuity for a uniaxial stress state and fully restrained boundary conditions;

- **last term**: corresponds to the thermal stress at the outside ($\sigma_{long.max} = \sigma_{circum.max}$) caused by the absolute value of the range for that portion of the non-linear thermal gradient ΔT_2 through the wall thickness not included in ΔT_1.
- K_1; K_2; K_3; C_1; C_2; C_3 constants;
- E - Young modulus of component;
- E_{rl} - Young modulus corresponds to the gross structural discontinuity

Alternatively detailed FE calculations can be made. Piping code analyses require input for stress concentration and flexibility factor taken as code data or evaluated separately. At present, it is common European practice to evaluate fatigue susceptible components by FE analyses to provide more realistic data instead of conservative assumptions.

After the calculation of stresses, the K_e-factor has to be determined to take care of local plastic deformation effects at geometric discontinuities. The different codes and standards provide a variety of mechanical and thermal K_e-values (Figure 4.3). Usually, the K_e-factor for thermal loads is smaller than for mechanical loads.

The fatigue curves as in codes and standards serve as an indicator for the cyclic load bearing capability of materials (Figure 4.4). It is important to distinguish between:

- failure curves,
- crack initiation curves,
- mean curves,
- design curves or
- fatigue curves considering reduction factors (environmental effects, structural design)

These have been developed from experiments with material specimens usually under mechanical loads. In some codes separate fatigue curves are provided for ferritic and austenitic materials. Others contain just a single curve to be used for both ferritic and austenitic steels. Research work has been done primarily on ferritic materials so far. The austenitic data base is limited. Some new tests on austenitic specimen under cyclic thermal load show the same crack initiation effects as for ferritic steel but no relevant crack propagation. Safety factors are applied to the failure curve to derive the design curve. Thus, a new safety criterion may have to be defined. Partly, reduction factors have been established for structural design effects (thickness, surface, weld etc.) and for environmental effects. These factors should be handled with special care because they have largely been derived form laboratory tests and their usability under plant conditions has to be checked thoroughly.

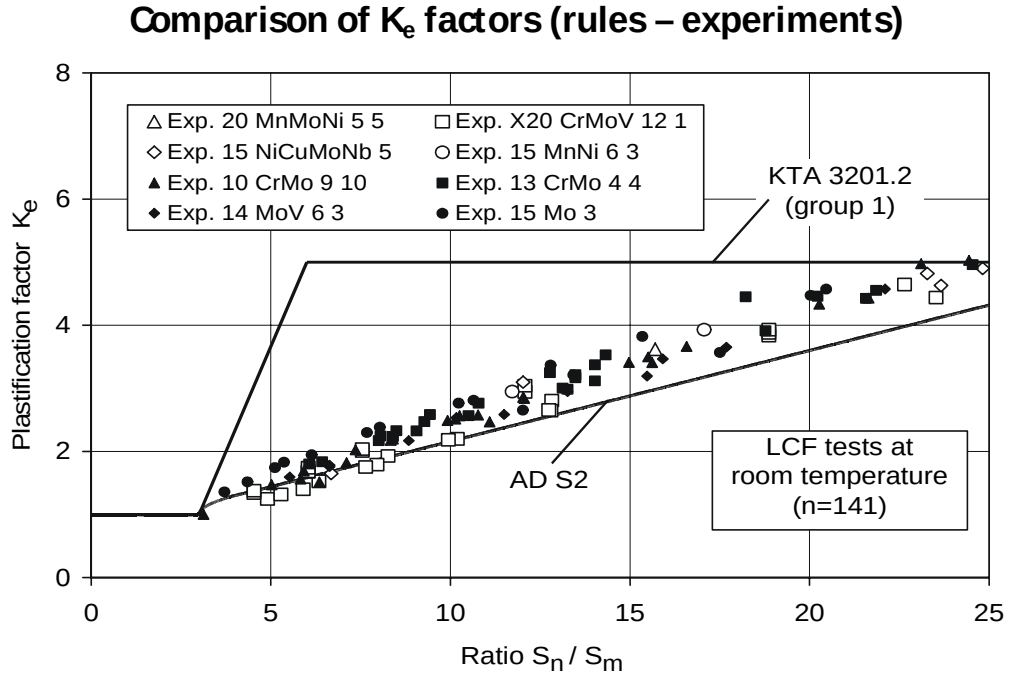

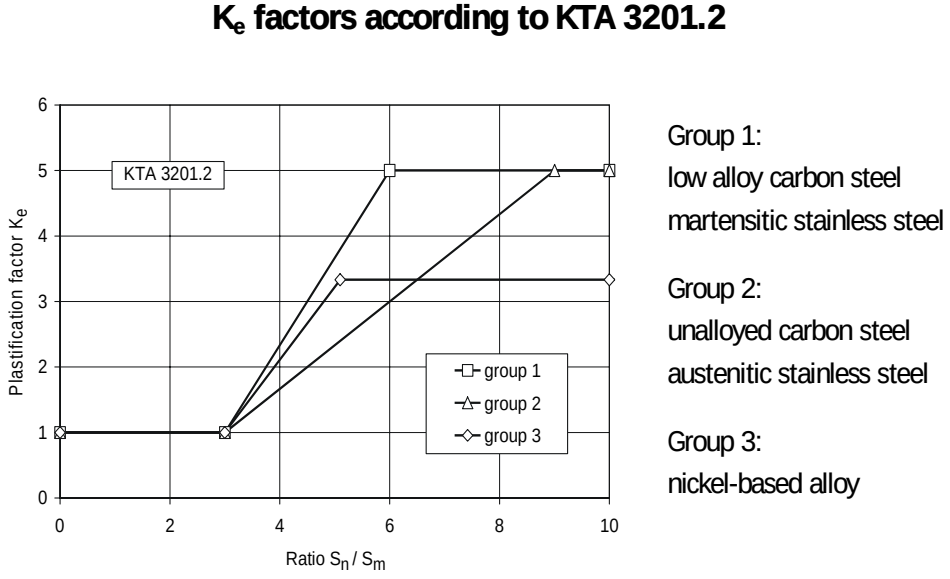

Figure 4.3: Comparison of K_e factors (rule values and experimental data) and the different KTA values /4.2/.

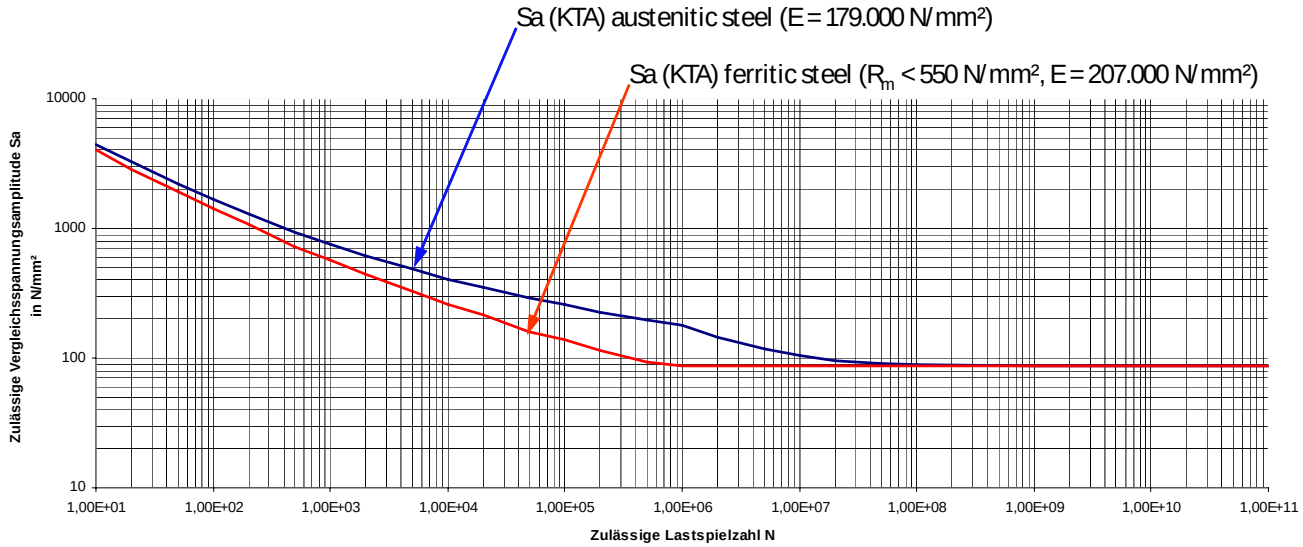

Figure 4.4: Design fatigue curve according to KTA 3201.2 /4.2/

4.1.1.2 Fatigue evaluation summary in German NPPs

The explanations above demonstrate that the determination of safety margins concerning fatigue failure or unacceptable degradation is not just a stress calculation followed by comparison with code fatigue curves. All the different integrity elements must be assessed carefully concerning their individual fatigue related significance and their interaction to the other elements. As nearly all fatigue failure incidents which occurred in NPP have several root causes (not only one), safety margins concerning fatigue cannot be provided by just one individual remedial action. The different steps on the load determination and fatigue stress calculation route as well as on the load bearing capability side using the fatigue curves as indicator have to be checked. According to the recent developments in international ageing management activities, the proactive approach to avoid/minimize premature ageing is promoted compared to the reactive approach. Concerning fatigue, load monitoring is encouraged leading to the advantage that the operational loads are known and can be compared to the design loads. Optimization of operation procedures can mitigate or even avoid fatigue significant loads. For safety relevant components, redundant NDT-measures are performed in high stressed locations to confirm the results of the integrity evaluation assisted by random sample survey in various areas to care for “unknown” effects. With the application of the integrity concept approach, potential consequences of new research results can be evaluated by assigning them to the appropriate concept element. As conclusion concerning a conceptual approach we always have to bear in mind that the most important evaluation element is the load monitoring and the determination of loads as input for the integrity evaluation. A realistically determined load spectrum may allow use of simplified stress/fatigue analyses. However the uncertainties arising from rough assumptions about the load spectrum cannot be compensated by detailed analysis, and such an approach is not acceptable for safety relevant NPP-components.

4.1.1.3 Application examples for the evaluation of temperature loads

The long term fatigue behaviour of the PWR-primary circuit may be used as integrity concept application example. The PWR primary circuit components can be classified according to their fatigue relevance, i.e. amongst others depending on the corresponding temperature loads.

The main components (reactor pressure vessel, steam generator, main coolant line, MCP, and the pressurizer) are not fatigue significant due to the limitation of thermal transient gradients to 50°K/h for operational transients. The monitoring of global operational data (temperatures, pressures, fluid mass flow etc.) is sufficient. The load cycles occurring are more or less the start up/shut down events of the plant (Figure 4.5).

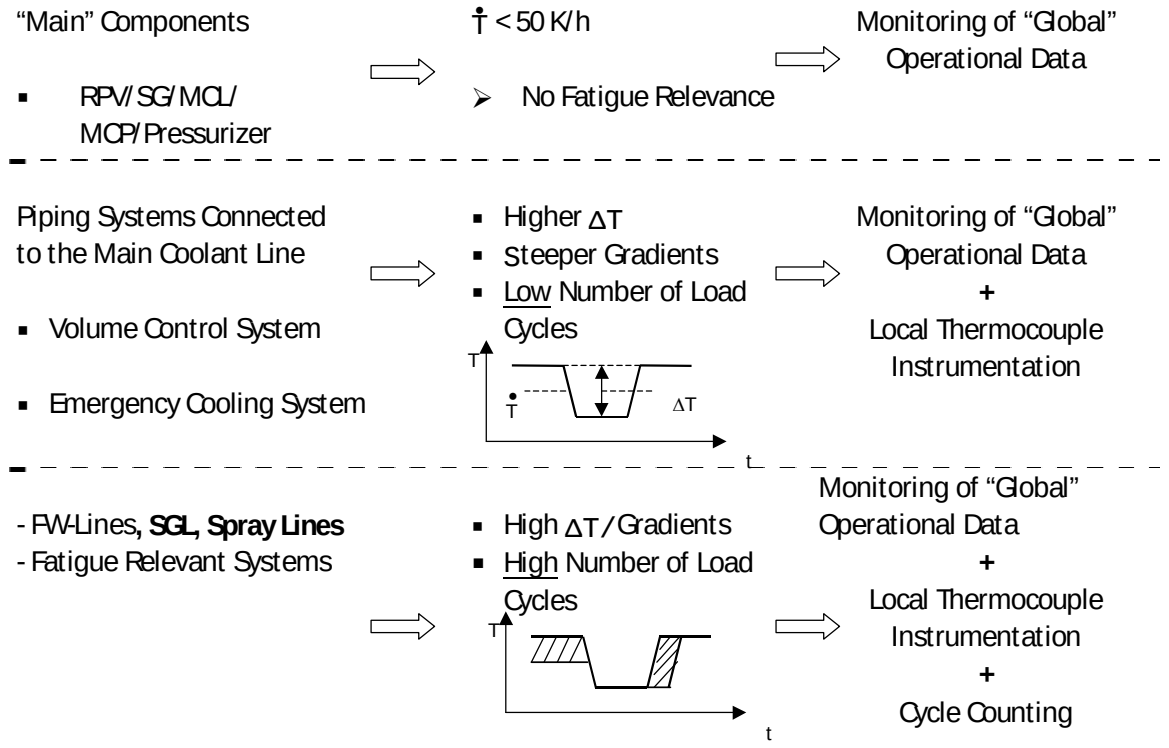

Figure 4.5: Primary circuit PWR – Temperature loadings

In piping systems connected to the main coolant line - the volume control system and the emergency cooling system - higher ΔT-differences and steeper gradients occur. But usually the number of load cycles is low. This surveillance of these systems is carried out by monitoring the global operational data and by local thermocouple instrumentations to register the transient magnitudes and the numbers of load cycles occurring (Figure 4.5).

Specific systems (feed water-lines, surge line, spray lines) with higher ΔT-differences and temperature gradients and higher number of load cycles are under specific surveillance. In addition to the monitoring of the global data and the local thermocouple instrumentations, a book-keeping of load cycles occurring (cycle counting) is performed to be able to determine the actual occurring fatigue usage factors. In particular in Germany, these long term fatigue surveillance programmes have been installed and are carried out under supervision of the responsible safety authority (Figures 4.6 – 4.8).

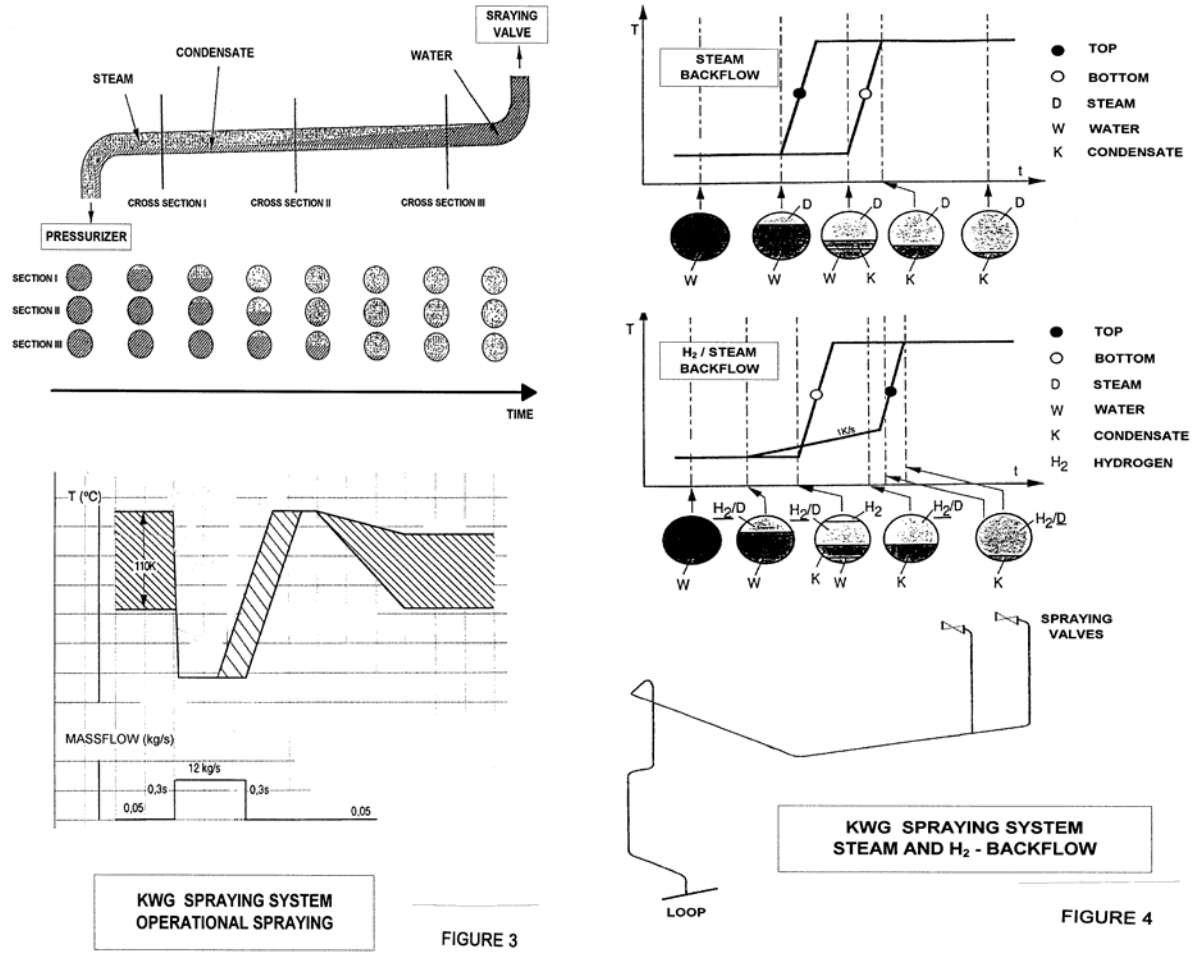

Figure 4.6: Spraying system – temperature loads

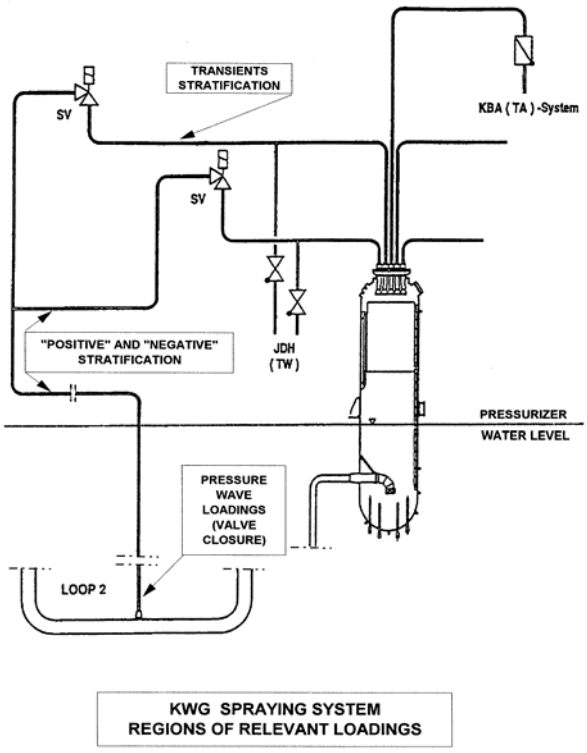

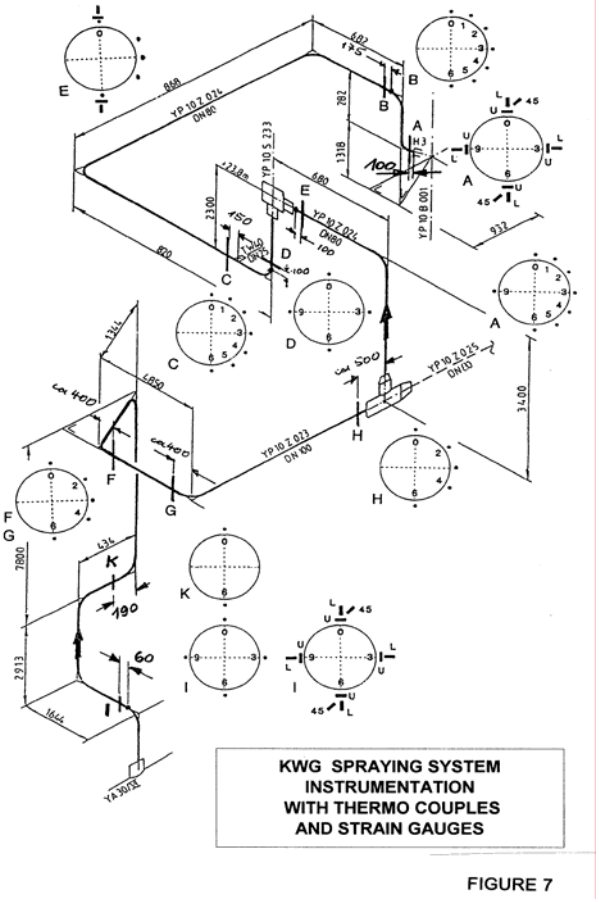

Figure 4.7: PWR spraying system – Temperature loads and thermo couple instrumentation-example

Field experience shows that high ΔT-values occur with low load cycle numbers but dominate the fatigue usage factor values. In general, with decreasing ΔT cycle numbers increase with lower usage factor contribution:

- Stratification:
  - $\Delta T \leq 180$ K (max.) limited number of cycles,
  - $\Delta T \leq 110$ K Level A,
- Transients:
  - $\Delta T \leq 300$ K $N_{specified} < 20$ (3 Sm/Fatigue),
  - $\Delta T \leq 200$ K $N_{specified} < 200$ (3 Sm/Fatigue),
  - $\Delta T \leq 100$ K $N_{specified} < 1000$ (Fatigue),
  - $\Delta T \leq 75$ K $N_{specified} < 50000$ (Fatigue),
- High cyclic loads:
  - Modify operation procedure (Reduce ΔT and occurring cycles),
  - Avoid valve leakage.

	ΔT PRESSURIZER / LOOP	REFERENCE TRANSIENT
T1	T <= 60K	A
T2	60K < T <= 90K	B
T3	90K < T <= 130K	C
T4	130K < T <= 160K	D
T5	160K < T <= 190K	E

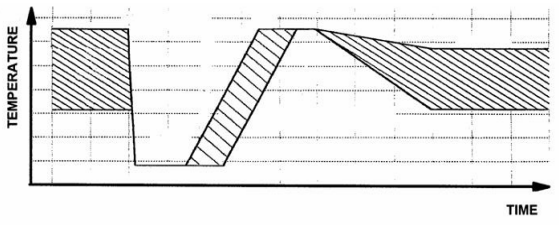

	ΔT PRESSURIZER / LOOP	VALVE	ELBOW	PRESSURIZER NOZZLE
T1	T <= 60K	$<=10^{-6}$	$<=10^{-6}$	$<=10^{-6}$
T2	60K < T <= 90K	$3,4 * 10^{-5}$	$4,5 * 10^{-6}$	$6,3 * 10^{-6}$
T3	90K < T <= 130K	$1,1 * 10^{-4}$	$1,9 * 10^{-5}$	$3,2 * 10^{-4}$
T4	130K < T <= 160K	$1,7 * 10^{-4}$	$1,8 * 10^{-4}$	$9,4 * 10^{-4}$
T5	160K < T <= 190K	$3,4 * 10^{-4}$	$6,1 * 10^{-4}$	$2,8 * 10^{-3}$

Figure 4.8: Spraying system – Temperature/fatigue usage factor.

4.1.1.4 Conclusions on the application of an integrity concept according to KTA 3201.4

In the above the sound application of an integrity concept has been demonstrated concerning the assessment of safety margins regarding the degradation mechanism “fatigue” due to temperature loads in general and for a PWR-primary circuit. For fatigue significant systems “bookkeeping of load cycles” is promoted to provide realistic and not too pessimistic evaluation results. “Load cycle counting” leads to lower fatigue usage factors than fatigue evaluation using EOL-cycle numbers (Figure 4.9). Thus, significant safety margins are available. Discussions about fatigue calculation parameters (K_e-factors, fatigue curves, F_{EN}-Factors) can be minimized because the additional introduction of “penalty factors” for the analysis results by reducing the fatigue curves and stipulating lower allowable fatigue usage limit does not necessarily lead to more targeted safety. Furthermore, this may also be misinterpreted that as a conclusion more NDT-actions are required. On the other hand, optimization of operation procedures or hardware changes may contribute to avoid/minimize fatigue relevant loads.

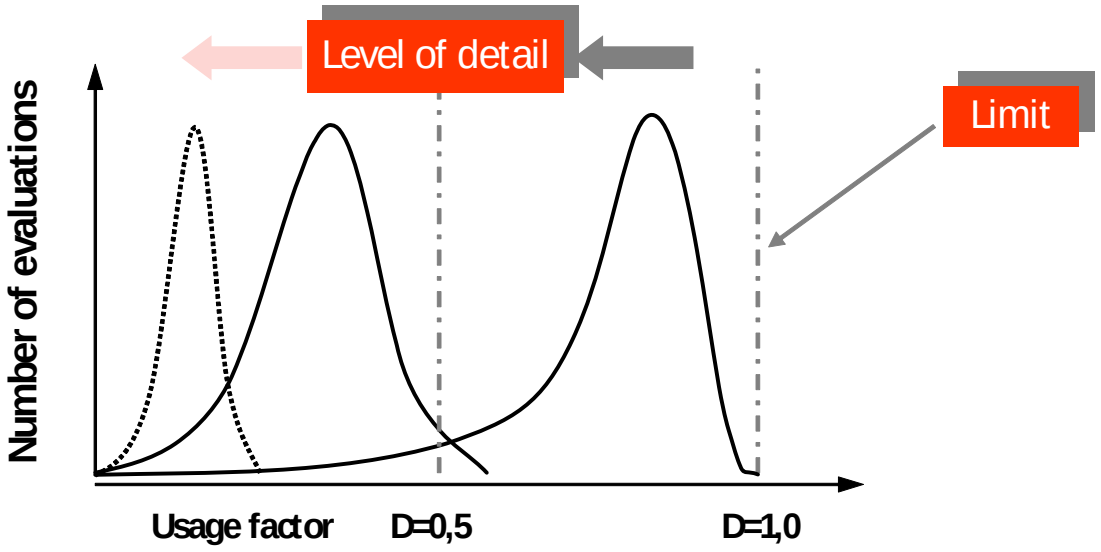

Figure 4.9: Bandwidth of possible results within allowable limits depending on level of detail of the analysis.

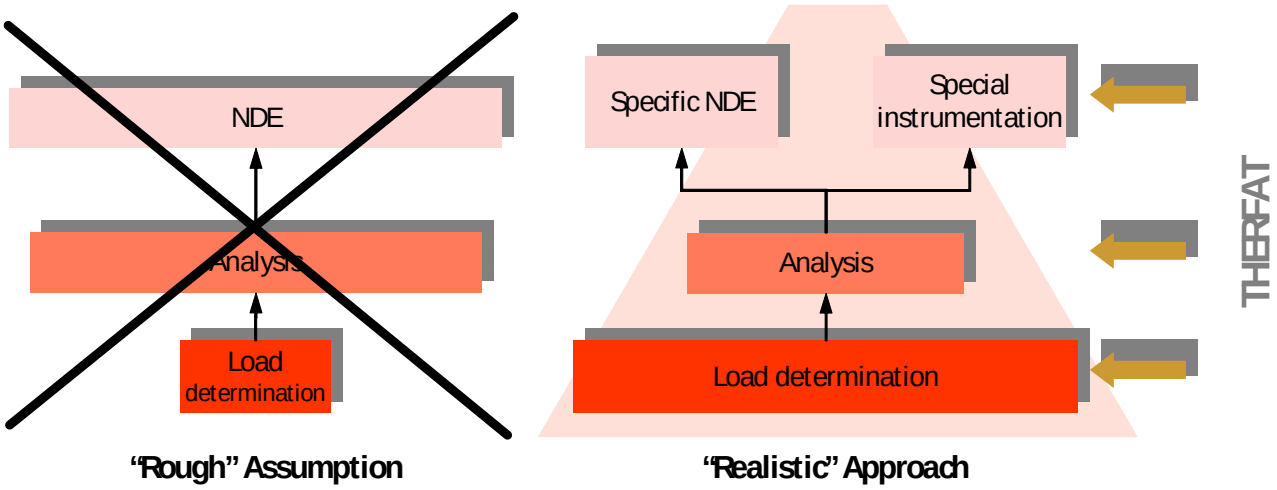

Figure 4.10: "Realistic" load/stress/fatigue determination route

A key evaluation element is the load monitoring and the determination of loads as input for the integrity evaluation. A realistically determined load spectrum e.g. stratification or transients may allow to use simplified stress/fatigue analyses. Lack of information requires conservative assumptions to care for the "unknown", with the always remaining uncertainty about the really existing safety margins. As already stated, the uncertainties arising from rough assumptions about the load spectrum cannot be compensated by detailed analysis (Figure 4.10).

Usually, it is not always required to perform a complete new integrity evaluation. But the results of the different measures performed in the different technical disciplines have to be

bundled with respect to the specific integrity related objective. People involved in the integrity evaluation process often overestimate the relevance of their own contribution, leading to an accumulation of conservatisms. To reduce unnecessary conservatism, an interactive information exchange of all the different fields contributing to the component integrity is required, promoting an improved communication and collaboration between the experts involved (Figure 4.11). Direct linkage between the different elements and the overlapping in between each other will finally lead to improved results (Figure 4.12).

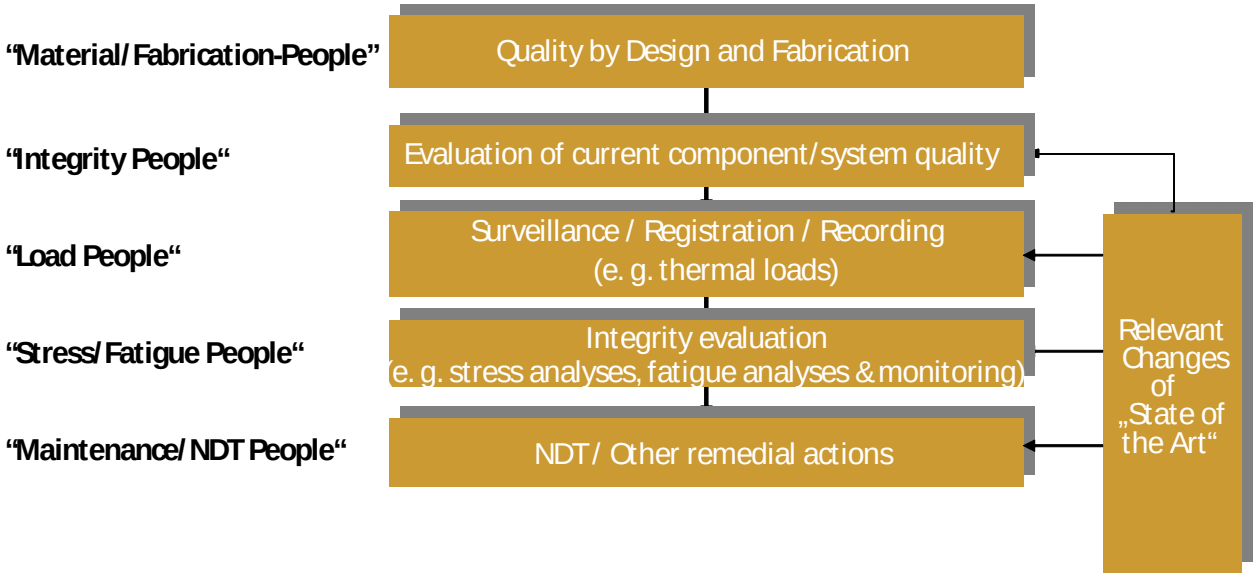

Figure 4.11: Proactive merging of different of different technical fields and expert

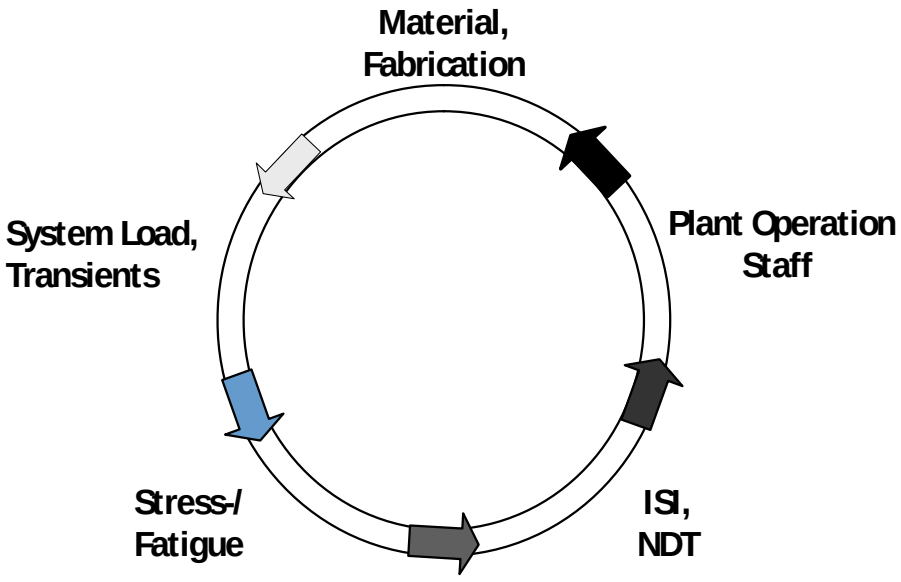

Figure 4.12: Cooperation of different technical fields in a NPP

4.1.2 French Approach (RCCM)

The French codes (RCC-M /4.12/ and RCC-MR /4.13/) have developed alternative, improved approaches to several aspects of the existing code ASME III code /4.14/:

- RCC-M requires a detailed fatigue analysis of class 2 piping
- RCC-M has proposed an alternative way to evaluate the plastic K_e (for stainless steel, K_e is greater than 1 between $2S_m$ and $3S_m$, but much less conservative above $3S_m$ with a maximum value of 1.8 instead of 3.3)
- RCC-M has proposed to include fluctuations in the fatigue exemption rules
- RCC-M has a warning to take maximum precautions during fabrication so as to minimise potential for high cycle thermal fatigue in operation
- RCC-MR has proposed an alternative way to evaluate the strain amplitude, based on the Neuber rule and included thermal load biaxiality effects on plasticity via the K_ν parameter.

4.1.3 Developments in the US & Japan

4.1.3.1 US bulletins 88-11& 88-08 and EPRI follow-up

Thermal fatigue stratification problems in the 1980's on Westinghouse 4-loop plants lead to the above two US NRC bulletins. Bulletin 88-11 /4.15/ requires a series of actions, which can be summarized as follows /4.16/.

(1) Conduct a visual inspection (ASME Section XI, VT-3) of the pressurizer surge line. Search for any gross discernable distress or structural damage in the entire surge line, including piping, pipe supports, pipe whip restraints, and anchor bolts.
(2) Demonstrate that the surge line meets the applicable design codes and other regulatory commitments, considering the effects of thermal stratification and thermal striping in the stress and fatigue evaluation. The fatigue analysis was to be performed in accordance with the latest ASME Code, including high-cycle fatigue.
(3) If the analysis showed that the surge line did not meet the licensing requirements, submit justification for continued operation, or bring the plant to cold shutdown and develop a detailed analysis of the surge line.
(4) Update the stress and fatigue analyses, based on the plant-specific or reference data and the observations in 1 above, to ensure compliance with the applicable codes. If the licensee was unable to demonstrate compliance, it was to submit a justification for continued operation and a description of the proposed corrective actions for effecting long-term resolution.

This bulletin mainly addressed the issue of stratification in surge lines, and invoked new analyses taking the stratification phenomenon into account. This pipe is intermittently subjected to stratification because of low flow rates in conjunction with temperature difference between the PWR pressurizer and a main coolant line coming from the reactor. The purpose of the new analyses was to establish the fatigue integrity of the piping systems i.e. show that the usage factors were below unity. The thermal loads were generally

determined from measurements on the piping systems and thermo-hydraulic models. Based on the instrumentation results, thermal hydraulic models the fluid and pipe wall temperature distributions for the stress and fatigue analyses were determined. The most highly stressed regions, in general elbows, were analysed with elastic-plastic FE models. Elastic shake-down in the elbows could generally not be shown, thus plasticity had to be considered.

The actions requested by Bulletin 88-08 /4.17/ are summarized as follows /4.16/:

(1) Review and identify systems where unisolatable sections of piping connected to the reactor coolant system may be subjected to thermal stratification or temperature oscillations that could be induced by leaking valves and that were not evaluated in the design analysis of the piping
(2) For susceptible locations, perform non-destructive examination of weld, heat affected zones, and high-stress locations to assure that there are no existing flaws
(3) Develop and implement a programme to provide continuing assurance that unisolatable sections of piping connected to the reactor coolant system will not be subjected to combined cycling and static stressors that could case fatigue failure. The assurance may be provided by:
    - redesigning and modifying these sections
    - instrumenting the piping to monitor for adverse temperature distributions and establishing appropriate limits on these distributions
    - providing means to ensure that pressure upstream of block valves which might leak is monitored and does not exceed reactor coolant system pressure.

The EPRI Thermal Stratification, Cycling and Striping (TASCS) Programme was funding testing and development of analytical methods to develop methodology for TF. A major starting point for this effort was Bulletin 88-08 described above. It is claimed /4.16/ that, while thermal stratification can be measured by instrumentation on the exterior of the piping, thermal striping cannot be measured in this manner. Rather it should be accounted for indirectly. TASCS developed a method to estimate fatigue damage caused by turbulent penetration thermal cycling /4.16/. As part of this a heat transfer model was developed and the results benchmarked against available data. These data indicated that the random turbulent fluctuations cause a complex loading spectrum, consisting of both high- and low-frequency content. This made the selection of a reasonable estimate of applied cycles difficult. Furthermore, /4.16/ reports problems for applying the method to cases such as elbows following a Tee. The method is reported /4.16/ to fail to predict the location of cracking in such problems as NESC ID 43 (Tihange). This discrepancy between the calculated and actual location of cracking implied that the thermodynamic phenomena that caused these failures are not well understood. Therefore, /4.16/ claims that pressure and temperature monitoring of piping susceptible to thermal cycling is the most reliable method to ensure its structural integrity.

Further work to assess stratification is also referred in /4.16/. Additional models needed to properly account for thermal stratification of pressurizer surge lines were studied, with the

conclusion that it is important to determine as accurately as possible the local temperature, pressure, and flow conditions in the pressurizer surge line.

4.1.3.2 Recent US developments

Reference /4.18/ reports on more recent development work on thermal fatigue in the US. It is reported that a final thermal fatigue management guideline is planned for release in 2005 that provides recommendations for evaluation, monitoring, inspection, and mitigation of thermal fatigue issues. This work is a continuation of the TASCS work /4.16/.

The phenomenon *swirl penetration* is discussed specifically in /4.18/. This is the type of phenomenon also referred to as *turbulent penetration*. Turbulence due to high rate flow in a main pipe partially penetrates into a dead-end branch line. Normally, the fluid in the branch is assumed to be stagnant. However, due to leakage or other reason the branch line may contain two layers of fluid temperatures, hot and cold with the cold stratified flow. The flow in the main pipe partially penetrates into the branch line and the stratification to turbulence interface is in cyclic motion, thus invoking fatigue stresses. These thermal cycling phenomena are controlled by several parameters. Screening criteria and evaluation models are proposed. These models primarily deal with the thermo-hydraulic load problem. The location, magnitude and frequency of thermal cycling are determined along with heat transfer properties. These load descriptions are intended for input to stress models. A principle sketch of the methods is shown in Figure 4.13.

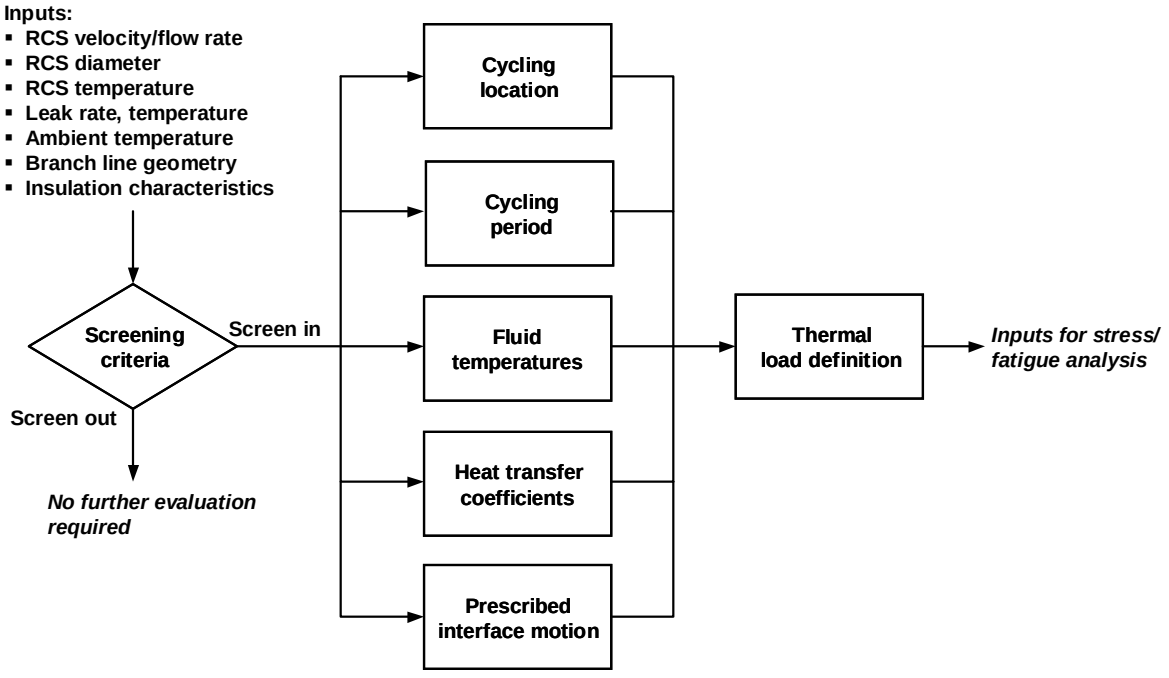

Figure 4.13: Thermal cycling evolution model as presented in /4.18/.

Three geometrical configurations are studied. These configurations with their respective notation are shown in the Figures 4.14-4.16, as given in /4.18/. Note that thermal cycling in the UH-configuration and in the H-configuration is essentially driven by the same type of mechanism and that leakage is a necessary condition. The D-configuration is different in that leakage is not necessary for thermal cycling. These more recent models are reported /4.18/ to have correlated better with such cases as the Farley and Tihange cases, which was a problem with previous models as discussed in 4.1.3.1.

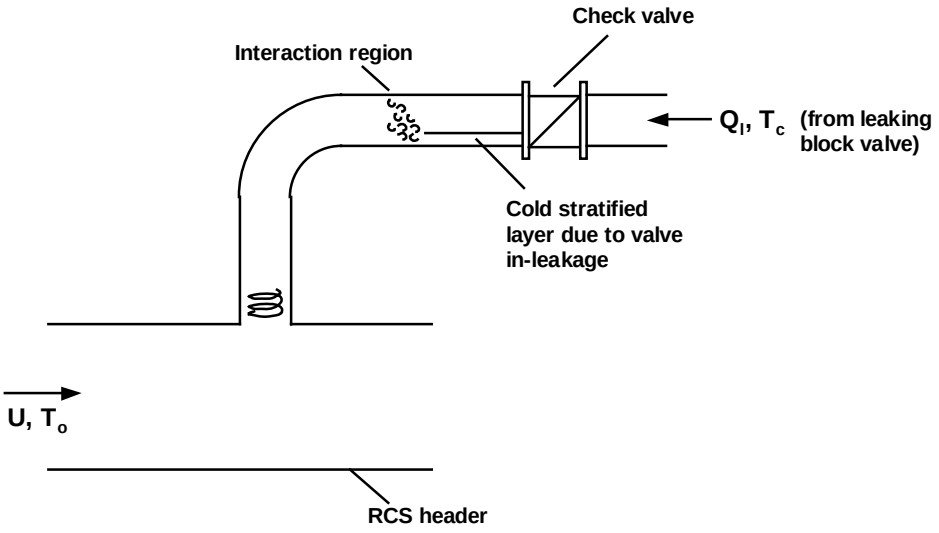

Figure 4.14: The up-horizontal (UH) configuration treated by thermal cycling evaluation models in ref. /4.18/

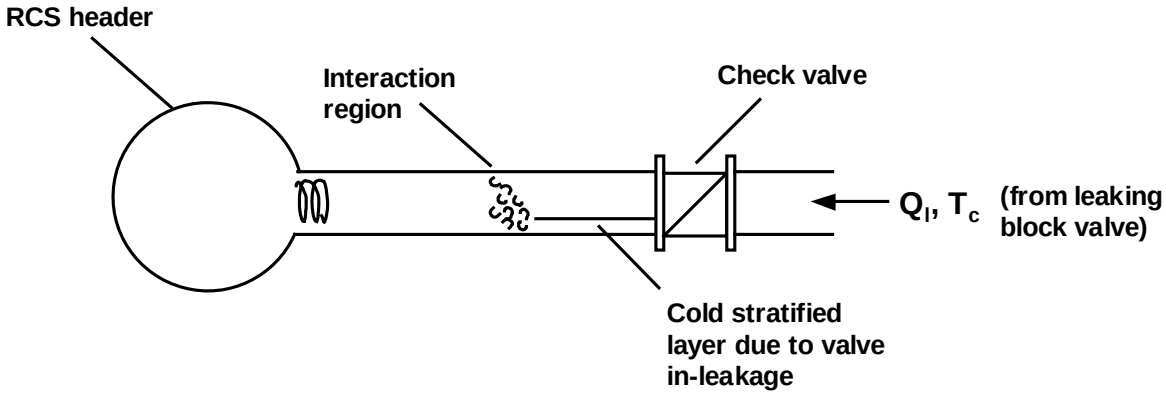

Figure 4.15: The horizontal (H) configuration treated by thermal cycling evaluation models in ref. /4.18/.

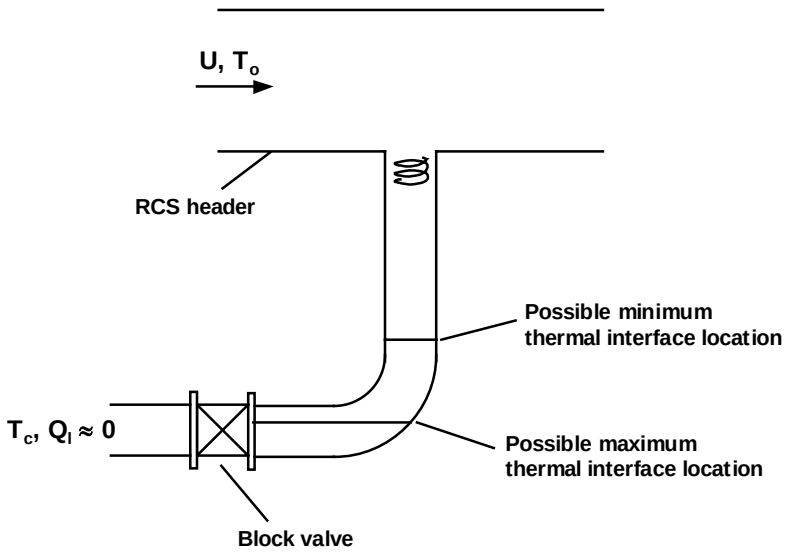

Figure 4.16: The down-horizontal (DH) configuration treated by thermal cycling evaluation models in ref. /4.18/

4.1.3.3 Thermal fatigue model development in Japan

/4.19/ provides an overview of the current status of work in Japan on thermal fatigue evaluation. The development work aims at establishing guidelines for evaluation of High-cycle thermal fatigue of a pipe and is carried out by JSME (The Japan Society of Mechanical Engineers). The "Guideline for Evaluation of High-Cycle Thermal Fatigue of a Pipe" was issued by JSME in November 2003. The proposed procedures are described briefly in /4.19/. These are separated into two sections, depending on whether the thermal load is due to striping or stratification (this is very similar to the categorisation used in NESC-TF database, see section 5). These phenomena are defined as follows /4.19/:

1) Thermal striping in a mixing tee with hot and cold water. The evaluation flow for thermal striping in a mixed tee has four steps with several charts to screen the design parameters one by one according to the severity of the thermal load predicted from the design conditions.

2) Thermal stratification in a branch pipe with a closed end generated due to cavity flow. The evaluation flow for thermal stratification has three steps with two charts to screen vertical branch pipe length according to the position of the elbow and penetration length.

The procedures are both built on the principle of different levels of analysis. The first order is a simple screening criterion based on the nominal temperature difference. If this criterion is not passed higher order analyses are proposed. For striping the following steps are described (Figure 4.17):

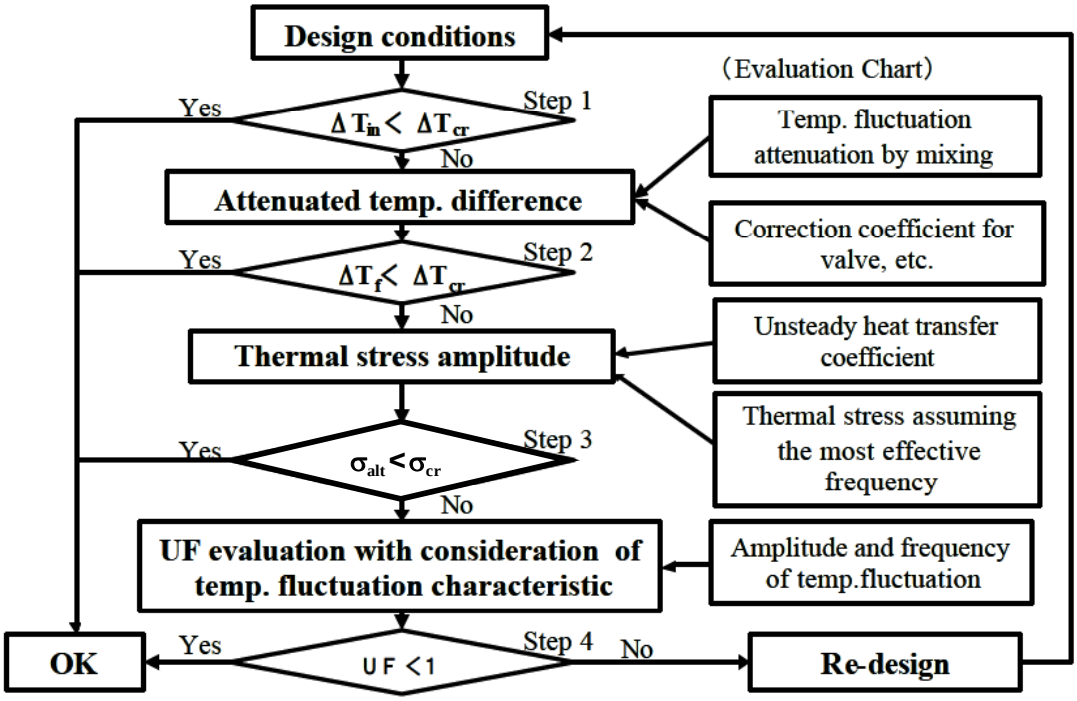

Figure 4.17: Flowchart of the proposed JSME procedure for thermal striping as described in /4.19/

Step 1: The temperature difference between the two incoming flows, ΔT_{in}, must be below the critical temperature difference, ΔT_{cr}.

Step 2: The maximum amplitude of fluid temperature fluctuation, ΔT_f, near the point being evaluated must be below the critical temperature difference. This step must consider the effects of the pipe joint configuration, the flow velocity, and the upstream and downstream pipe configurations such as valves, elbows and diffusers.

Step 3: The fluctuating thermal stress, σ_{alt}, due to thermal striping acting on the point being considered is conservatively evaluated with the assumption of the most effective frequency. The reduction effect on the fluctuating temperature due to heat transfer at the surface of the pipe wall must be taken into consideration. The fluctuating thermal stress must be below the fatigue limit, σ_{cr}.

Step 4: The cumulative usage factor, UF, is evaluated by considering the frequency characteristics of the fluctuating fluid temperature. The cumulative usage factor must be below 1.

The procedure for stratification aims at avoiding a stratified flow condition over a pipe elbow. Instead the hot-cold interface should be located a distance away from the pipe elbow. This pipe component is regarded as a significant stress raiser. The procedure steps are described in /4.19/ below and illustrated in Figure 4.18.

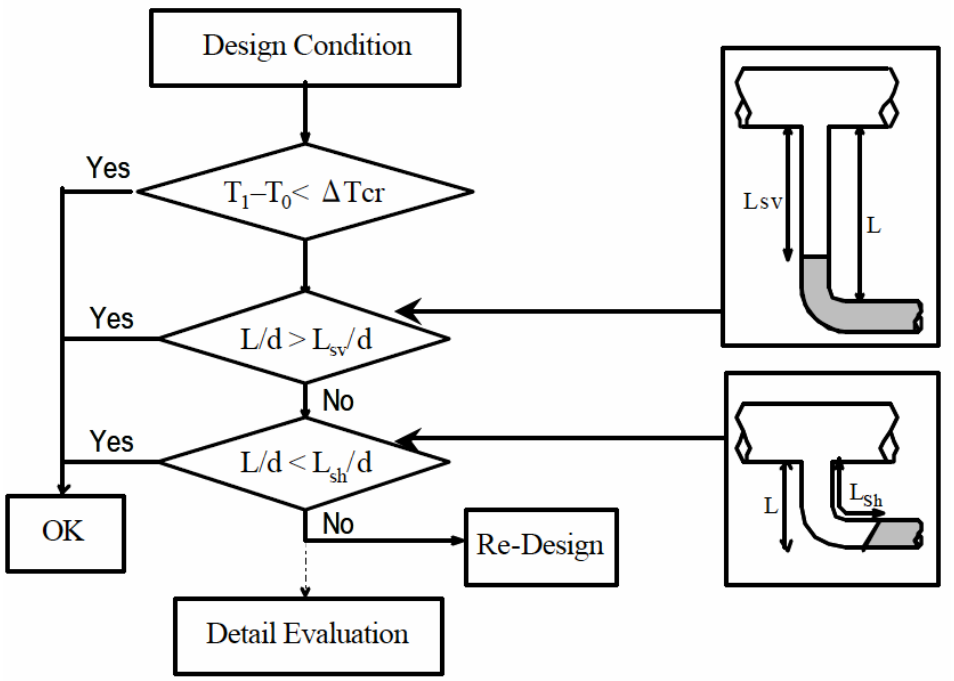

Figure 4.18: Flowchart of the proposed JSME procedure for stratification (ref /4.19/).

Step 1: The temperature difference between the main flow temperature and branch temperature, T_1-T_0, is below the critical temperature difference, ΔT_{cr}.

Step 2: The vertical pipe length, L, is longer than penetration length Lsv. In this case, cavity flow stays within the vertical pipe, and both temperature fluctuation and produced stress are small.

Step 3: The vertical pipe length, L, is shorter than penetration length Lsh. In this case, cavity flow fully intrudes into the horizontal pipe passing over the elbow, and both temperature fluctuation and produced stress are small.

4.2 European R&D Projects

4.2.1 French Programmes

EDF has launched a series of different actions /4.20/, with national and international partners. The key issues are:

- Collection of operating condition data through different monitoring devices to ensure a reasonable knowledge of the ΔT values, their corresponding durations during operation and, if possible, the related flow rates,

- Evaluation of the fluid and inner wall temperature:
  - through mock ups with transfer function from mock-up tests to plant situation
  - through CFD codes (including LES) to evaluate the steady state for crack growth analysis, to identify the surface area affected by fluctuations to ISI planning and the complete temperature spectrum in the fluid and the heat exchange coefficient for determining the inner wall temperature

  Note: For evaluation of surface temperature fluctuations, external surface measurements are not very reliable, and specific validations are needed to solve the inverse problems from outer to inner surface of a very thin wall.

- The strain range evaluation through elastic analysis and a plasticity correction factor, with, for stainless steel, a complex cyclic stress-strain curve.
- Fatigue damage evaluation for a sine-wave temperature fluctuation or the complete temperature fluctuation spectra
- The high cycle fatigue curve from 10^5 to 10^9 cycles, and the question of existence or not of an endurance limit for stainless steel
- Simulation tests on cylindrical mock-ups or bars.
- The effect of factors likely to be detrimental to fatigue resistance: un-flushed welds, counter-bore surface finish, mean strain or stress…
- Validation of a crack growth procedure for thermal cycling with a single crack or a network of small cracks
- ISI performance, mainly for thick stainless steel with welds or cast pipes
- Development, together with AREVA and CEA, of a large scale Tee test facility to perform representative tests and check all the different steps of the evaluation procedure: the FATHER program.

The main results to date include:

- Load evaluation and transfer functions: data from plexiglass and metallic mock-ups confirm the 80% transmission factor between fluid temperature difference and that on the local wall; different power spectrum density models have been developed to compare the different situations and these confirm the 1-D model for temperature distribution through the wall by modelling; a set of transfer functions from mock-ups to plant configuration have been developed (ΔT, flow rate, heat exchange coefficient etc.) and validated (Figure 4.19)
- No specific results on strain history effects on damage analysis.
- New data for stainless steel suggest a modified fatigue curve in air in the high cycle regime up to 10^9 cycles (Figure 4.20); the effect of different potentially factors (temperature, mean stress, surface finish and water environment) have been studied.

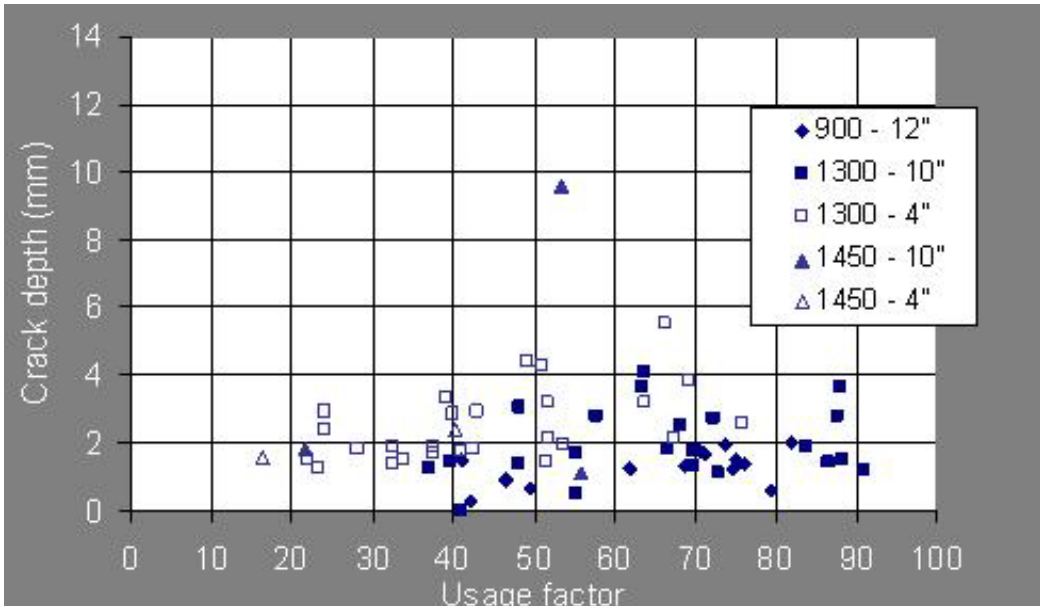

Figure 4.19: Validation of SIN-wave method by comparison with the field experience on RHR systems in French plants (ref./4.20/).

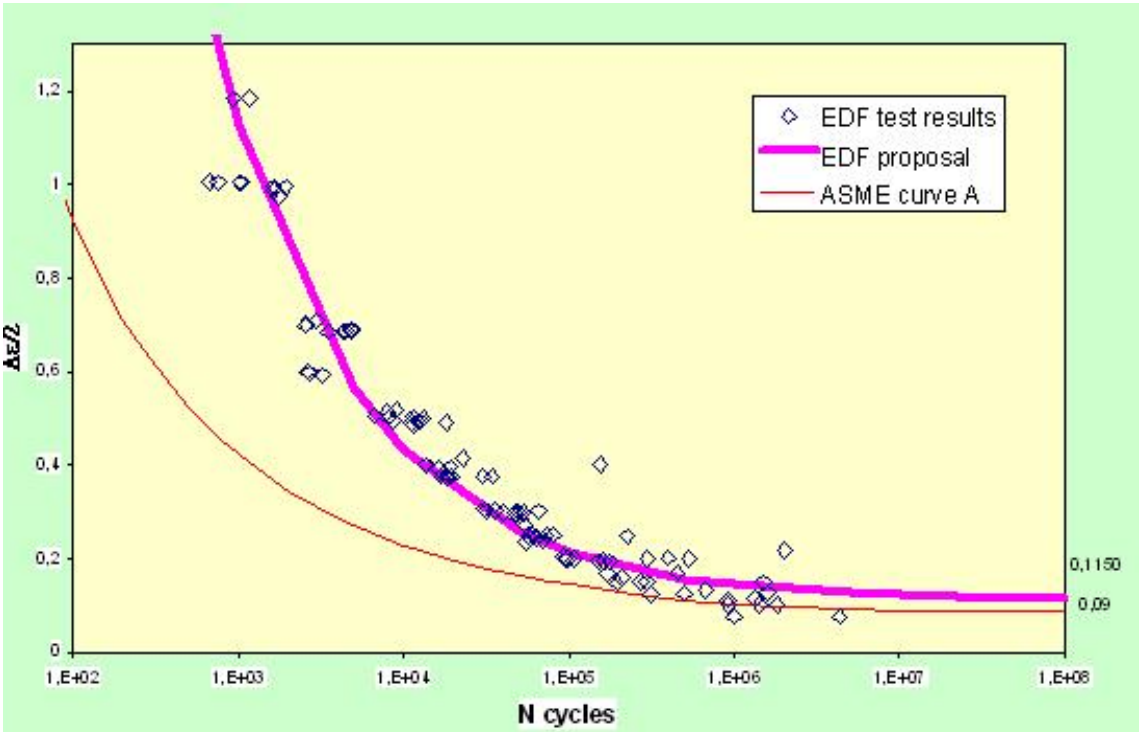

Figure 4.20: Comparison of new EDF results and the ASME fatigue curve; the mean curve "EDF proposal" is lower than existing curves when compared to ASME A design curve.

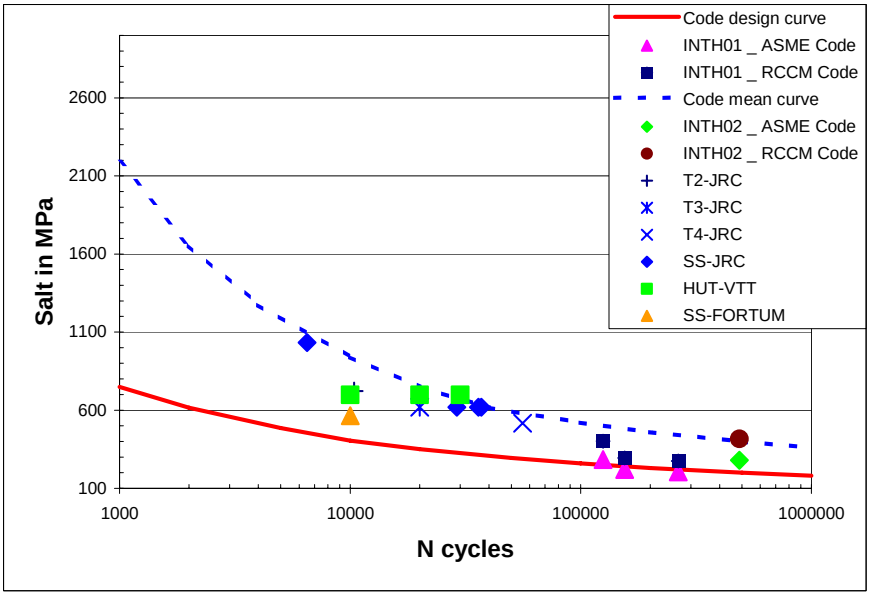

Figure 4.21: Comparison of fatigue tests results and fatigue evaluation method, from THERFAT D7 and D18.

- Detailed analysis of the existing laboratory simulation tests (Figure 4.21) confirms the approach provides good predictions in the low cycle regime using RCC-M rules (not ASME due to K_e effects).

4.2.2 THERFAT

The THERFAT project (Thermal fatigue evaluation of piping system Tee-connections, co-sponsored by the EC under FP5) was set up to advance the accuracy and reliability of thermal fatigue load determination and to outline a science-based but still practical methodology for managing thermal fatigue risks in Tee-connections susceptible to high cyclic temperature fluctuations. The project was carried out by 16 European organisations (including utilities, plants vendors/manufacturers, consultant engineers and research institutes) as a cost shared action funded by the European Commission and ran from December 2001 to November 2004 /4.21/. The project work programme (WP) comprised the following tasks:

- Load determination by experimental tests and computational fluid dynamic analyses to assess the turbulent thermal mixing effects in piping system Tee-connections and to identify the fatigue significant parameter (WP 2),
- Integrity Evaluation to quantify the existing safety margins against failure by standard methods and advanced fatigue and fracture mechanics analysis routes and to determine non fatigue relevant threshold values (WP 3),
- Experimental damage tests with cyclic thermal shock loads to verify selected aspects of fatigue assessments (WP 4),
- A "road-map" for a “European Methodology on Thermal Fatigue” (WP 5).

The THERFAT results improve the understanding of thermal fatigue issues for plant operation and safety and lead to the following conclusions /4.22/:

- In glass model tests of various Tees at ambient temperature fluid temperature differences up to 200 K were simulated by using different specific fluid densities (salt water). Equivalent fluid temperature load spectra were determined by electrical conductivity measurements.
- In steel mock-ups measurements of temperature distributions in the fluid and through the pipe wall with specific sensors ("fluxmeters") were performed with temperature differences up to 90 K. The recorded temperature load spectra at the inner surface of the pipe wall were used as input for the stress and fatigue analyses and for the important determination of realistic heat transfer coefficients.
- In addition to the experimental tests, numerical thermo-hydraulic CFD-calculations were performed for benchmark cases and for other Tee-configurations. Agreement between analytical predictions and experimental results is reasonable. However the CFD-analyses were very time consuming and still have to be fully verified for practical application. The project also examined the use virtual sensors based on neural network and fuzzy logic tools to simulate the dependency of thermal fluctuations from transient mass flow and temperature distributions of the surge lines in two pilot plants.
- Different integrity evaluation procedures were applied to assess stresses, fatigue usage, crack initiation and crack propagation for components or specimens subjected to cyclic thermal loads. In the "forward approach" the results from experimental tests and from CFD-analyses were used to determine through wall stresses, fatigue usage, crack initiation and propagation. The thermal load spectra determined in the experimental steel tests with ΔT-values of up to 90 K were extrapolated in several steps to higher temperature differences up to ΔT values of 245 K, to define the "threshold values" where fatigue degradation can be expected.
- In the stress analysis models realistic wall thickness values were used (e.g.10 mm) to calculate the thermal through wall stresses. Simplified analytic approaches as well as sophisticated FE models were used, with material laws ranging from pure elastic to complex elastic-plastic behaviour. The calculated through-wall stresses for temperature differences of $\Delta T = 245$ K show low fatigue usage factors for 32 years of full plant operation leading to the conservative assumption that potential fatigue degradation can be expected at temperature differences of approximately $\Delta T = 150$ K. These results are, of course, dependant on the geometrical Tee-configuration and the local thermal loads (temperature difference, mass flows).
- In the "reverse approach" integrity evaluations were performed to verify the results experimental damage tests on laboratory specimens and mock-up. The results confirm that the load bearing capability is higher than would be predicted by design code analysis procedures. In terms of fatigue usage, all the experimental test results showed strain ranges in agreement with or above the ASME fatigue design curve. The tests confirmed that load cycles up to crack initiation is comparable under mechanical and thermal loads. In the post-initiation phase, the current experience shows that cracks caused by mechanical loads tend to propagate, while those due to thermal loads appear to arrest.

- Turbulent thermal load spectra, the THERFAT analyses demonstrate that only significant temperature differences of ≥ 150 K in the mixing region will cause fatigue degradation effects. But as any additional global system stresses have to be added to these local through wall stresses, it was felt that a "warning threshold" for turbulent thermal load spectra would be at a ΔT-value of 100 K. It is noted that predicted crack initiation (typically evidenced by surface "crazing") does not necessarily lead to component failure if no dominant crack emerges. Nevertheless, high load cycle numbers should be avoided by proactive measures such as changing the system operation procedures or by maintenance measures, e.g. to stop potential valve leakages. If these high cyclic loads cannot be avoided in the plant or if it is uncertain whether they occur or not, engineering tools are available to predict the potential crack initiation and crack propagation, therefore allowing appropriate ISI intervals to be fixed.

Considering the application of the German integrity approach outlined in Section 4.1.1 to the Tee-connections, the THERFAT results contributed to the following areas:

- Evaluation of the "basic quality" with regard to design and fabrication of the Tee-connection under consideration;
- Monitoring of thermal load type and load cycles which occur;
- Transformation of monitored data into the load input for stress and fatigue analyses
- Performance of stress and fatigue analyses,
- Planning a long-term fatigue surveillance program (cycle counting), if appropriate,
- Fracture mechanics assessments to determine acceptable flaw sizes,
- Establishing appropriate NDT measurements to minimise eventual risks.

4.3 Experimental Case Database

Feature tests i.e. tests involving simulated thermal fatigue performed under laboratory conditions, have an important role to play for verification of assessment procedures and for establishing transferability of standard fatigue curves to component-life situations. For NESC-TF five cases have been brought together, including digital records of the induced temperature distributions, as well as calculated thermal stresses from reference finite element calculations, where available. Detailed information form each test has been collected in a dedicated report /4.23/. It is noted that further mock-up testing is on-going independently of the NESC-TF project at CEA, EDF, JRC and Serco.

4.3.1 CEA FAT3D Test

The CEA FAT3D test /4.24/ was designed produce a 3-D thermal loading field for the OECD/IAGE thermal fatigue benchmark exercise. Thus, the choice was made to design a test on a pipe submitted to a local cooling (Figure 4.22). The cyclic cooling is imposed by a local cyclic injection of cold water inside a pipe test piece fabricated in 316L(N) stainless steel, with wall thickness 6.7 mm, external diameter 166 mm and length 360 mm. The pipe is placed inside a furnace to maintain a hot temperature (600°C) at the outer surface. The

surrounding air temperature is maintained constant. First cracking was observed on the inner surface after 12000 cycles.

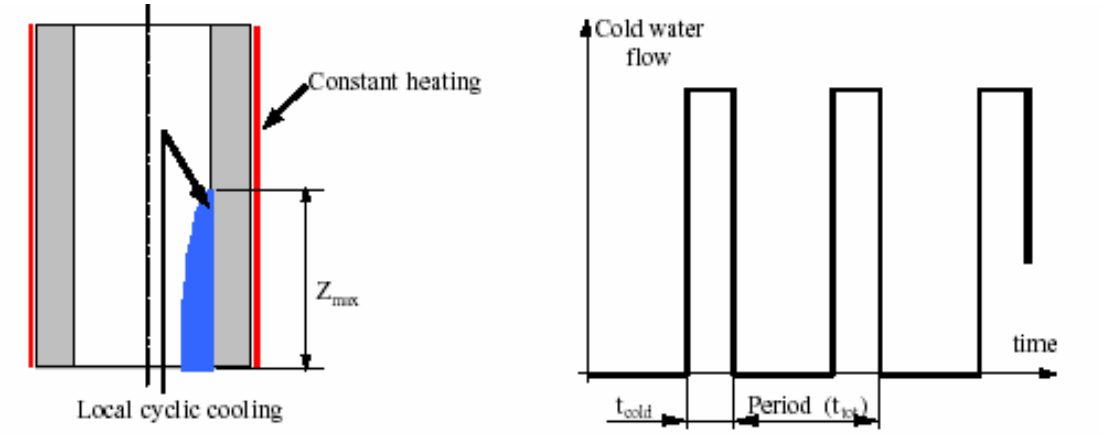

Figure 4.22: Principle of the CEA FAT3D test

The documentation available provides:

a) full geometry of the pipe and testing system
b) thermo-physical and mechanical materials information, including fatigue curves, FCG and fracture toughness data
c) details of the mechanical and thermal boundary conditions
d) benchmark results of thermal and mechanical FE simulations of the test loading cycle.

4.3.2 EDF INTERPOL Test

The INTHERPOL tests /4.25/ were design to study thermal fatigue of 304L stainless steel pipe comprising a taper and a un-flushed circumferential welded joint, subjected to cyclic thermal loadings with known amplitude and frequency. The loading frequency for this test is relatively high, to better simulate loading induced by high frequency mixing. The inclusion of welds is considered an important aspect because thermal fatigue cracking is often concentrated at a weld area. The basic geometry is pipe outer diameter: 406 mm; wall thickness: 10 mm and length : 300 mm.

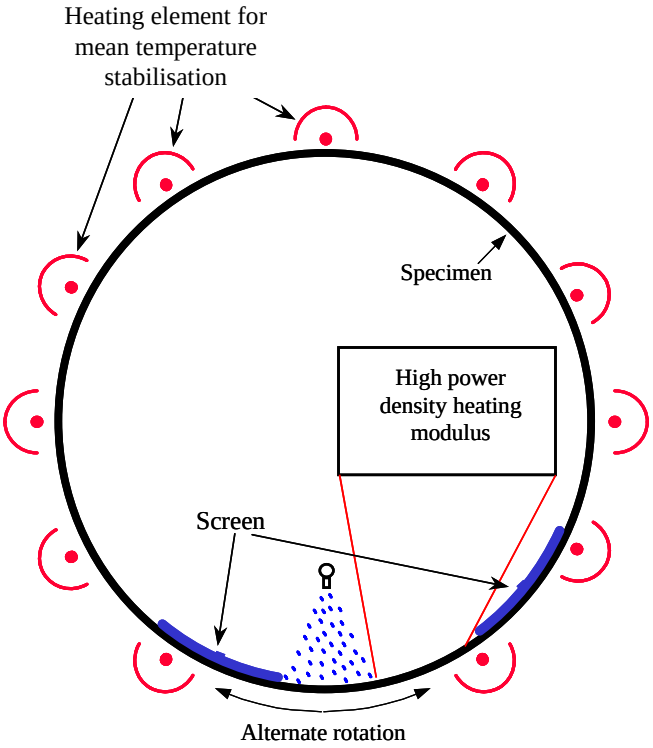

Figure 4.23: Principle of the INTHERPOL thermal loading device

The thermal loading device is illustrated in Figure 4.23. Before the test, the sector to be subjected to the fatigue loading is heated up to a homogeneous temperature of about 190°C. Thermal cycling is carried out on a 70 mm broad sector of the internal surface of the specimen. The cold shock is generated by a cold-water spray while the hot shock is obtained by subjecting the cooled surface to an intense infrared radiation. The cycling frequency for this test was 0.2 Hz for ΔT =120°C and 0.05 Hz for ΔT = 230°C.

The documentation available provides:

a) full geometry of the pipe and testing system
b) thermo-physical and mechanical materials information, including fatigue curves, FCG and fracture toughness data
c) details of the mechanical and thermal boundary conditions
d) weld residual stress profile
e) benchmark results of thermal and mechanical FE simulations of the test loading cycle

- During the test itself, the component was subjected to approximately 265000 cycles. The initiation and the evolution of the cracks were monitored by intermediate liquid penetrant inspections. The results of these are available in tabulated form.

4.3.3 JRC Cyclic Down-Shock Tests

The JRC down-shock experiments /4.26/ are a series of cyclic down-shock tests performed on 316L pipe specimens of outer diameter 48 mm and wall thickness 14 mm (Figure 4.24). The specimen is heated by an induction system from the outside and quenched internally with water at room temperature. The test procedure is as follows: the specimen is first heated until the maximum temperature is attained through the entire thickness. The specimen is then loaded cyclically by room temperature water cooling (quenched water running through bore hole) and heating (no water running thorough the pipe). The distribution and magnitude of the thermal stresses depend on the temperature difference ΔT, the duration of the quenching and heating, the material properties and the heat transfer between the pipe and the water. The ΔT in the tests conducted so far ranged from 275 to 375ºC. The duration of the quenching in the tests was typically about 6 seconds whereas the heating phase was between 40 and 50 seconds. Assessment of fatigue damage was made during periodic stops. A replica technique was used to detect initiation of surface cracks on the inner surface of the test pieces. A Time Of Flight Diffraction (TOFD) technique was used subsequently to measure the length and depth of cracks after initiation, with a resolution about 0.5 mm.

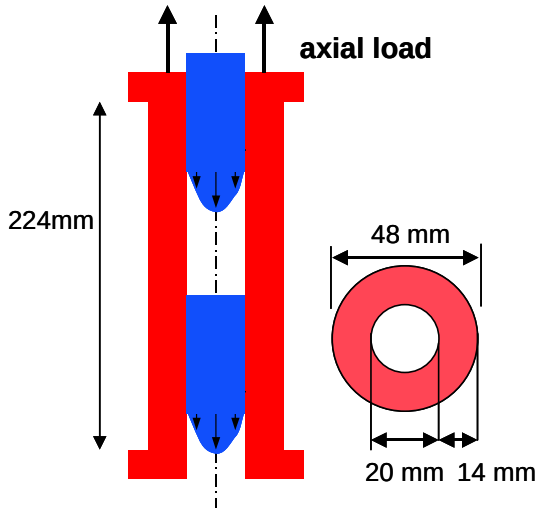

Figure 4.24: Principle of the JRC thermal cycling devic

The documentation available provides:

a) full geometry of the pipe and testing system
b) thermo-physical and mechanical materials information, including fatigue curves, FCG and fracture toughness data
c) details of the mechanical and thermal boundary conditions
d) non-destructive measurements of crack size and orientation vs. number of cycles
e) benchmark results of thermal and mechanical FE simulations of a typical loading cycle

Three thermal fatigue tests have been performed with maximum temperature values of 300, 400 and 350°C respectively. The results of the intermittent inspections, indicating crack position, orientation, length and depth are provided in tabulated form.

4.3.4 CEA SPLASH Tests

An experimental device called SPLASH was developed in CEA /4.27/ in order to reproduce simply temperature gradients on two opposite sides of a bar specimen. The specimen is continuously heated by an electrical DC current, and cyclically submitted cold shocks (corresponding to a cooling rate of about 500 to 1000°C/s) when a water-air mixture is sprayed on opposite faces (Figure 4.25). The specimens were fabricated in 304 L stainless steel, with length of 240 mm and a thickness of 20 mm between the two opposite faces where thermal shock is applied.

The documentation available provides:

a) full geometry of the flat specimen and the testing system
b) thermo-physical and mechanical materials information, including fatigue curves, FCG and fracture toughness data
c) details of the mechanical and thermal boundary conditions
d) benchmark results of thermal and mechanical FE simulations of a typical loading cycle

Results from 5 tests with initiation lives ranging from 50,000 (with $\Delta T = 200°C$) to 200,000 (with $\Delta T = 120°C$) cycles are available. These include details of the development of the networks of surface cracks.

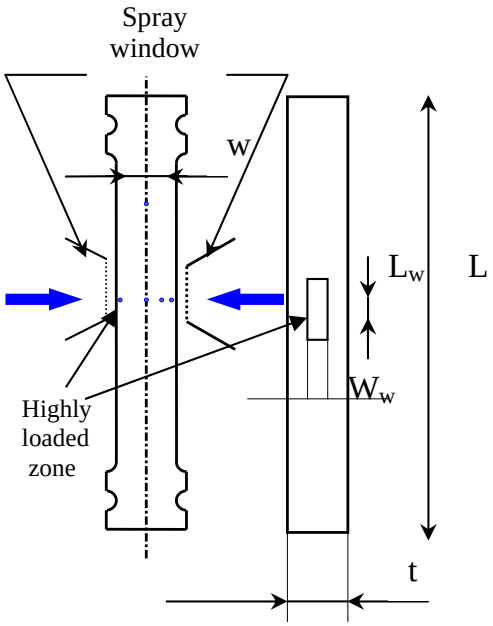

Figure 4.25: Principle of the SPLASH facility

4.3.5 CEA FATHERINO Test

The Fatherino-II series of thermo-hydraulic tests were performed by CEA /4.28/ on a ½ scale T-junction mock-up as part of the THERFAT project. The goal was to simulate the conditions on the Civaux Tee. The pipe set-up is shown in Figure. 4.26. The mock-up itself was fabricated in 304L steel (54 mm internal diameter, 1:1 branch and run, 9.5 mm wall thickness). A rotating system allowed the recording of the temperature load spectrum data at 5 different locations in the fluid and in the pipe wall of the mixing zone, from 2.2D to 5.8D.

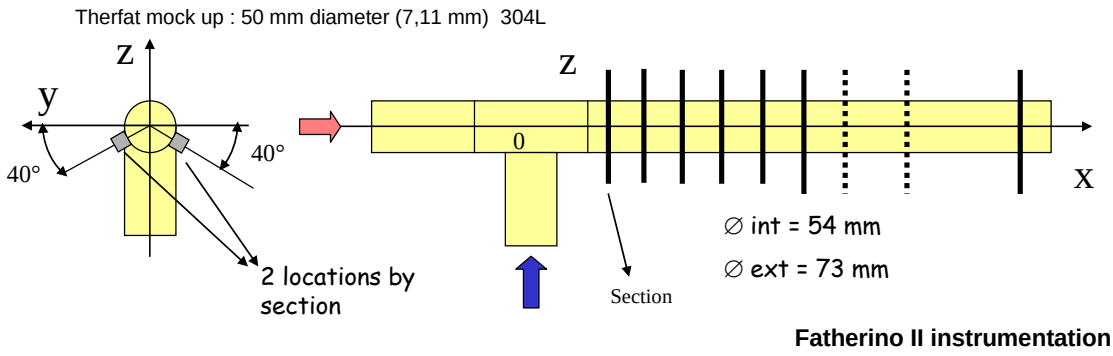

Figure 4.26: Schematic of the FATHERINO 2 test set-up.

The thermo-hydraulic conditions were identical for all the tests, with a flow velocity of 3.4 m/s and a flow ratio cold-to-total of 25%. In these conditions the Reynolds number reaches $4 \cdot 10^5$ and the mean heat flux transfer estimated by the Colburn correlation /4.29/ reaches 11000 W/m^2°K. The tests were performed with water at atmospheric pressure and a nominal ΔT of 70°C between the run and branch. The maximum fluctuation value is reached at the first measurement section located a 2.2D downstream from the tee. The attenuation of temperature fluctuation in the longitudinal pipe direction (downstream) is only 20% between 2.23 and 5.8D, showing that turbulent mixing effects occur even at this distance from the tee. In the boundary of the mixing layer large eddies of hot flow were observed in the major cold flow, but not *visa versa*. The registered thermal loading data provide a unique benchmark for CFD analyses.

The documentation available provides:

a) documentation describing the geometry and the testing system
b) digital data records of the fluid and wall temperature measurements at the five section as well as the heat flux measurements.

4.3.6 Helsinki University of Technology Tee Tests

Cyclic thermal shock tests ($\Delta T = 280°C$) were made on VVER T-connection mock-up from the Loviisa plant /4.30/. The thermal loads were generated by local induction heating and quenching in the T-junction/corner area. The temperature was measured on some surface locations. Cracks occurred after more than 10000 load cycles. The evolution of the surface cracks has been monitored with surface replicas and crack opening displacement (video technique). In the subsequent analytical investigation, the temperature fields in the T-Joint wall were determined from CFD-analysis of the fluid temperature fields and were used as data input for a FE stress analysis. Due to the required tremendous amount of computer time only a simplified T-joint could be modeled in the CFD-analysis model. The agreement to the experimental results regarding the location of high stresses is reasonable. However it was noted that the stress field generated at the crack position on the corner of the Tee is effectively uniaxial, rather than biaxial as occurs at the majority of pipe wall locations.

4.4 References

4.1 Metzner, K J "Thermal Fatigue Evaluation of Piping System Tee-Connections", THERFAT(26)/D20/2004, November 2004

4.2 KTA 3201 Part 2 "Components of the Reactor Coolant Pressure Boundary of Light Water Reactors", Design and Analysis, June 1996

4.3 KTA 3201 Part 4 "Components of the Reactor Coolant Pressure Boundary of Light Water Reactors – In-Service Inspections and Operational Monitoring", June 1999

4.4 Metzner, K J; Braillard, O; Faidy, C; Solin, J; Nilsson, K; Manoloatos, P, "Status Report – European THERFAT-project", 2nd Int. Conf. on Fatigue of Reactor Components, 2002, Snowbird, Utah, USA

4.5 Metzner, K J; Kahlisch, W; Bartonicek, J, "Integrity Concept for Safety significant Components in German NPP", Second International Conference on Fatigue of Reactor Components, July 29 – August 1, 2002, Snowbird, Utah, USA

4.6 Metzner, K J; Kohlpaintner, W; Bongartz, M; Stueber, Jo, "Application of German KTA-Code 3201.4 (6/99), ISI and Surveillance; Optimization of ISI-Intervals and NDT-Extent", 2nd Int. Conf. on Fatigue of Reactor Components, 2002, Snowbird, Utah, USA

4.7 Metzner, K J, "A European Approach to thermal Fatigue Assessment", Proc. Int. Seminar "Networking for Effective R & D" EUR 20984 EN, European Commission, 2003

4.8 Metzner, K J; Roos, E; Herter, K H; Otremba, F, "Integrity Concept for Safety significant Systems in NPP", 16th SMIRT-Conference, August 2001, Washington DC, USA

4.9 Metzner, K J, "German Utility Ageing Management Concept, Current Status", IAEA-Technical Meeting on effective Ageing Management, June, 2002, Vienna, Austria

4.10 Metzner, K J; Bartonicek, J; Boewing; W; Bongartz, M, "German Utility NPP-Ageing Management", 21st ESREDA-Seminar, November, 2001, Erlangen, Germany

4.11 E. Ross, X. Shuler, K.-H. Herter "Thermal fatigue due to Stratification and Thermal shock of piping", third international Conference on Fatigue of reactor Components, October 3-6, 2004, Seville, Spain

4.12 Design and Construction Rules for LWR Nuclear Islands, RCC-M, AFCEN, 2002

4.13 Design and Construction Rules for FBR Nuclear Islands, RCC-MR 2000 + addenda, AFCEN.

4.14 ASME – Nuclear Boiler and Pressure vessel Code – Section III – ASME 2004

4.15 USNRC, Pressurizer Surge Line Thermal Stratification, USNRC Bulletin 88-11, (1988).
4.16 IAEA, "Assessment and management of ageing of major nuclear power plant components important to safety. Primary piping in PWRs", TECDOC-1361, July 2003
4.17 USNRC, Thermal Stresses in Piping Connected to Reactor Coolant Systems, USNRC Bulletin 88-08, (1988)
4.18 Keller J. D., Bilanin A. J., Kaufman A. E., Continuum Dynamics, Inc., Carey J., "Thermal cycling screening and evaluation methodology and application to pressurized water reactor branch line piping", Int. Conf. on Fatigue of Reactor Components, Seville, Spain, 2004
4.19 Nakamura, T., The Kansai Electric Power Co., Inc., Madarame H., Research Center for Nuclear Science and Technology, The University of Tokyo, Japan, "Current Status of Development on Codes for Fatigue Evaluation in JSME", International Conference on Fatigue of Reactor Components, Seville, Spain, 4-6 October 2004
4.20 C. Faidy, High cycle thermal fatigue issues in PWRs – lessons learned from field experience and consequences, Proc. Int. Symp. Fontevraud 6, SFEN (French Nuclear Energy Society), Sept. 2006, p.1061-1068.
4.21 K.-J. Metzner & U. Wilke, European THERFAT project—thermal fatigue evaluation of piping system "Tee"-connections, Nuclear Engineering & Design, Vol.. 235, Issues 2-4 , 2005, 473-484
4.22 U. Wilke, K. Metzner, W.Kohlpaintner, P. Manolatos, Thermal Fatigue Evaluation of Piping System Tee-Connections (THERFAT), Proc. PLIM&PLEX 2006, Paris, April, 2006
4.23 NESC-TF Report "Database Of Component Mock-Up Experiments", NESCDOC (04) 08 Rev.1, June 2005
4.24 FAT3D – An OECD/NEA benchmark on thermal fatigue in mixing tee, NEA/CSNI/R(2005)2, July 2005
4.25 F. Curtit et al, INTHERPOL thermal fatigue test, NEA/CSNI/R(2004)21, Proc. 3rd Int. Conf. on Fatigue of Reactor Components, Seville, Spain, October 2004,
4.26 E. Paffumi et al, , On thermal fatigue crack initiation, propagation and arrest in 316L model pipe components, ASTM STP 1461, ASTM Int., West Conshocken, PA, USA, 2004
4.27 V. Maillot, PhD Thesis (in French), Ecole Centrale de Lille, Univ des Sc de Tech de Lille. CEA report R – 6041 (2003)
4.28 O. Braillard, Summary of thermohydraulic tests, THERFAT Report R(11)/D08/2004, December 2004
4.29 Colburn, A.P., Trans. AlChE, 29(174), 1933.
4.30 K. Calonius and J. Solin, "Case Study on thermal Fatigue Potential in a T-Joint", Third International Conference on Fatigue of Reactor Components, October, 2004, Seville, Spain

5 DAMAGE CASES SURVEY

5.1 Existing information on damage cases

Several recent studies have considered damage due to thermal fatigue in light water reactor components, with particular focus on those cases resulting in leakage. A major source of information is an IAEA TECDOC dealing with ageing of PWR piping components /5.1/. Thermal fatigue is described as a major source of concern, along with vibration fatigue. These considered the two dominating sources of fatigue loading. Much of the discussion is based on experience of reported leakage incidents. An edited list of these cases is presented in Table 5.1. These damage cases are mentioned in many other references and have provided an important basis for discussion on thermal fatigue and the development of assessment methods.

All of the 13 cases in Table 5.1 are through wall incidents leading to leakage. It is noted that 9 of the main cracks occurred in the weld and 4 in the base material. Moreover 9 of the cracks were oriented in the circumferential direction and thus 4 were oriented axially to the piping direction. It is noted that only one of the base material cracks occurred in the circumferential direction.

A statistical treatment of thermal fatigue cases (essentially those in Table 5.1) is provided in /5.2/ with the aim to capture trends of damage frequency as a function of time. Based on the various assumptions made, the leakage incident frequency is expected to double every 8 years. The difficulties to drawing generic conclusions from the damage cases are discussed and the uncertainties of the statistical models are pointed out. Much of the difficulties are attributed to the lack of quantitative understanding of the phenomenon thermal fatigue. As discussed further below, this observation is supported by the findings of the NESC group. However the trend that the frequency of thermal fatigue damages leading to leakage will increase is regarded as verified.

References /5.1/ and /5.2/ both use the following categorization of the thermal fatigue load types, (see also **Chapter 3**) and a similar breakdown is used for the NESC database:

- *Turbulent penetration and thermal cycling.* Turbulent flow in a main coolant pipe can cause penetration of hot water into a connecting pipe with water of a lower temperature. This introduces the potential for a cyclic variation of temperature in a portion of the connecting pipe, and thermal fatigue. Depending on the geometry of the piping, the penetration can also lead to thermal stratification.
- *Thermal stratification.* A horizontal pipe may have a hot water flow at the top and a cold water flow at the bottom. This introduces axial and circumferential stresses, with maximum axial stresses near the interface layer. The layout of the piping supports can further influence the stress distribution. A periodic rising and falling of the interface or mixing layer induces through wall cyclic stresses that contribute to both crack initiation and growth.

Table 5.1: Damage cases (mainly from IAEA TEC DOC 1361 /5.1/).

Plant	Location	Size
Crystal River 3	Check valve body near the valve-to-safe end weld	140-degreecircumferential crack; two crack initiation sites: one on the inside surface and one on the outside surface
Obrigheim2	Weld between a 90-degree elbow and a nozzle	Crack extended 70 degrees circumferentially at the inside surface, 12-mm long at the outside surface
Farley 2	Heat affected zone of elbow-to-pipe weld	Crack extended 120 degrees circumferentially at the inside surface, 25-mm long at the outside surface
Tihange 1	Elbow base metal	89-mm long at the inside surface, 41-mm long at the outside surface
Genkai 1	Heat-affected zone of elbow-to-pipe weld	Crack extended 97 mm circumferentially at the inside surface, 1.5-mm at the outside surface
Dampierre 2	Check valve-to-pipe weld and base metal of straight portion of pipe	Crack extended 110 mm circumferentially at the inside surface, 25 mm at the outside surface
Loviisa 2	Pressurizer auxiliary spray line control valve body	Crack extended 80 mm along the horizontal surface and 25 mm along the vertical surface of the valve body
Biblis-B	Base metal of a straight portion of the pipe	Crack extended 50 mm axially at the inside surface, 20 mm at the outside surface
Three Mile Island 1	Weld between a 90-degree elbow and a 51-mm diameter horizontal line	Crack extended 51 mm circumferentially at the inside surface, 14 mm at the outside surface
Dampierre 1	Base metal of a straight portion of the pipe	Crack extended 80 mm circumferentially at the inside surface, 22 mm at the outside surface
Loviisa 2	Weld between a T-joint piece and a reducer	65-degree circumferential crack
Oconee 2	Safe-end to pipe weld	Crack extended 360 degree circumferentially at the inside surface, about 77 degree circumferentially on the outside surface
Civaux 1	Longitudinal weld in an elbow	180-mm long through wall crack

- *Thermal striping*. This results when a pipe has thermal stratification, with a large difference in the flow velocities of the two layers. This terminology is sometimes also attributed to turbulent mixing, for example in tees.
- *Turbulent mixing*. Turbulent mixing of hot and cold coolant flows can induce local cyclic stresses on the adjacent piping wall. The stress is greatest on the inside surface, and the orientation of any resulting cracks is random.
- *Thermal shock*. Such one-time events can be crack initiators, but probably do not cause progressive crack growth.

Note: Flow-induced vibration can be a contributor to thermal fatigue, for instance when a protective thermal sleeve inside a nozzle is damaged by vibration. If the sleeve breaks loose and moves through the piping, the nozzle is left unprotected, and is subject to thermal fatigue.

Another major reference for thermal fatigue is /5.3/, which covers many aspects relevant to LWR components and discusses some of the cases in Table 5.1 in more detail.

An overview investigation of failures in nuclear piping in Sweden /5.4/ indicates that slightly more than 10% are due to thermal fatigue, which was found to be the third most important failure mechanism after IGSCC and erosion/corrosion. The occurrence of damage due to mechanical fatigue, mostly due to vibration, is at the same level. Thermal fatigue was given special consideration in the investigation. An overview of the damage incidents as a function of the recorded nominal temperature difference is presented in Figure 5.1 and as a function of the number of years is given in Figure 5.2. This latter plot indicates quite a number of incidents in the early years of operation.

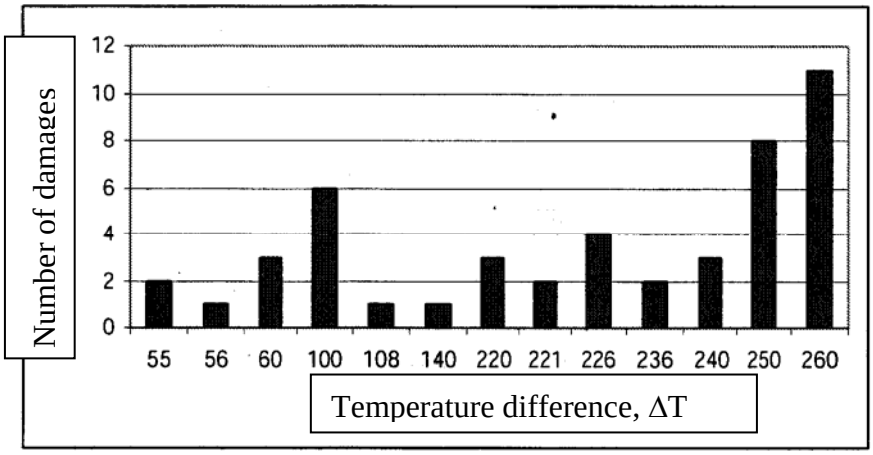

Figure 5.1: The distribution of temperatures ranges from the investigation of piping failures in Sweden (ref /5.4/).

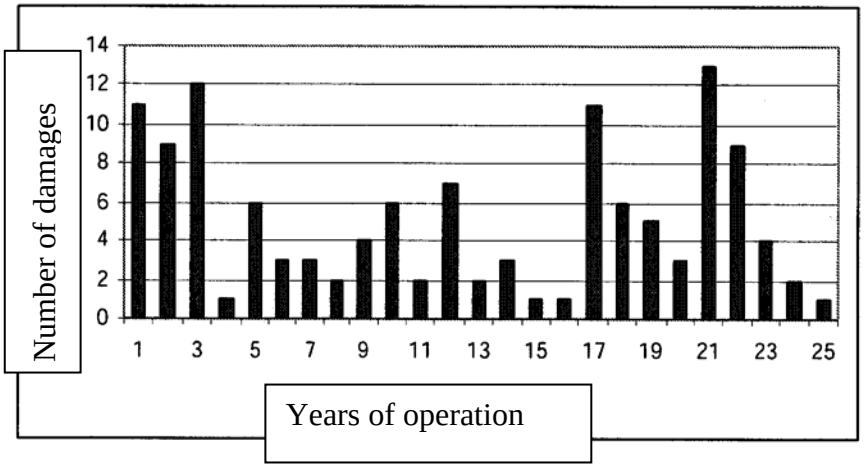

Figure 5.2: TF damage frequency versus number of years of operation from the investigation of piping failures in Sweden (ref /5.4/).

Another potential source of data is OECD OPDE project on piping failures /5.12/, the goal of which is to provide a reliable and complete source of pipe failure data in commercial NPPs world-wide (1970-present). Unfortunately the NESC group did not have access to this database for evaluation and comparison.

Reference /5.5/ provides a recent (2004) overview of damage cases. Additionally there are reports or publications dealing with individual cases. A through-wall crack in an elbow at the Tsuruga 2 plant was reported from Japan /5.6/, which is attributed to thermal fatigue. Inspection of the outer surface of the elbow found a longitudinal crack of length 44 mm on the outer surface of the pipe. After the elbow had been removed, a 99 mm crack was found in the corresponding position on the inner surface.

5.2 The NESC Database.

The purpose of the NESC-TF failure database /5.7/ was to collect cases with more detailed information, which could be to examine the parameters governing thermal fatigue in nuclear components. Primarily, thermal fatigue failure cases that were subject to root cause analysis were used as input. For this purpose a survey form was developed, see **Appendix A**. The cases were collected in a database with references to the survey forms and when available, the damage analysis report was included. The damage case descriptions and conclusions were taken in unedited form the input documentation. This documentation was generally not questioned by the authors of this report. However where different views exist, these are stated in the text.

Table 5.2:. The NESC-TF database of operational damage cases.

ID	Location	Size	Event	Load type	ΔT (°C)
1	Internal BWR part pipe connection with labyrinth type sealing	Through wall crack at the sealing at a base material part of the sealing with 5 mm thickness. Axial and circumferential cracking.	Operational	Transient	226
2	Internal BWR part pipe connection with labyrinth type sealing	See ID1.	Operational	Transient	See ID1.
3	BWR mixing tee.	Through wall crack at 16 mm thickness.	Cold water from leaking pump	Stratification	210
4	BWR mixing tee.	8.6 mm axial crack in at base material thickness 14.5 mm.	Not known	Stratification/Turbulence	280
5	BWR pipe mixing tee with inner sleeve	Axial and circumferential 2-3 mm cracking in a previous weld repair. Wall thickness	Intermittent inlet of cold water	turbulence	90 intermitently 200
6	BWR mixing tee.	Axial 11 mm cracking in the base material of wall thickness 14 mm.	Turbulent mixing under normal conditions	turbulence	64, intermittently 170
7	BWR nozzle in vessel with sleeve as thermal barrier	Through cracking in the base material of the sleeve	instable flow due to leakage, operational events, other	Instability	226
8	BWR pipe (Cone at pipe attachement)	Base material surface cracks at thickness 63 mm	operational events,	Transient	226
9	BWR pipe (Cone at pipe attachement)	Secondary cracking in supporting plate due to ID9	operational events,	Transient	--
10	BWR heat barrier sealing at a pump	Base material surface crack at thick section	Instable flow (leakage in sealing)	Instability	226
11	BWR pump	Base material surface crack at thick section	Instable flow	Instability	140
12	BWR pump thermal barrier	Surface crack at thick section.	Instable mixing cold and hot water	Turbulence	100-40
13	BWR pipe mixing tee with inner sleeve	Base material axial cracks in pressure bearing shell in contact with labyrinth sealing, maximum depth of 19	Possibly un-tight sealing	Instability	90

ID	Location	Size	Event	Load type	ΔT (°C)
		mm at wall thickness of 34 mm. Several other cracks in the vicinity			
14	PWR tee with connecting reducer	Circumferential through wall crack in weld between tee and reducer, thickness 5.5 *(mm)*	Incomplete tightness of valve	Stratification	70
15	PWR mixing tee with elbow	Through wall axial crack at elbow longitudinal weld. Thickness 9.6 mm.	Turbulent mixing, operational	Turbulence or large scale instability	160
16	PWR mixing tee	Through wall axial crack at pipe part with thickness 6 mm	Valve leakage	Stratification	230
17	PWR mixing tee	Cracking (net-work-type) in base material	Valve leakage	Turbulence or stratification	180
18-31	PWR mixing tees	Partial penetration cracks in base material and welds	Operational	Turbulence	80 and larger
32	BWR straight pipe after mixing tee	Axial through-wall crack in pipe, base material of 12.5 mm. Crack may have initiated in weld.	Valve leakage	Stratification	200
33	PWR elbow (Civaux 1 in table 5.1)	Through-wall Axial crack in axial weld in the elbow, thickness 9.6 mm	Operational	Large scale instability directly after turbulent mixing in a tee	80 and larger
34	PWR valve (Z-type geometry valve) (Loviisa 2 in Table 5.1)	Axial through wall crack at the base material, variable thickness larger than 10 mm	Leakage	Stratification	65 and intermittently higher
35	PWR elbow near tee at check valve (Tihange 2 in Table 5.1)	Longitudinal through-wall crack of about 45 mm length on the outside surface in the base metal of the last downstream elbow. Thickness 18 mm.	Leakage	Stratification	270
36	BWR pipe elbow	Through wall crack at longitudinal weld back side of elbow. Thickness 12 mm.	Leakage	Stratification	120
37	BWR pipe reducer near tee.	Through wall crack at circumferential weld of a reducer. Thickness 12 mm.	Leakage	Stratification	150

The NESC database now contains about 40 documented cases. The documentation is of varying quality, which has in some instances hampered detailed inter-comparisons. Two sources dominate, namely the cases from the Swedish Inspectorate (SKI) database and those from EDF. The rest of the cases are primarily from other NESC-TF participants. All the database cases are summarized in Table 5.2. Figure 5.3 shows the distribution of cases between contributors. A significant difference to the cases from the IAEA report in Table 5.1 is that the NESC-TF were not only selected based on a through-wall leakage criterion. It is noted that a few of the examples in Table 5.1 also appear in the NESC database and this is indicated in Table 5.2.

For analysis, the damage cases can be grouped in different ways. These are detailed in the following sections.

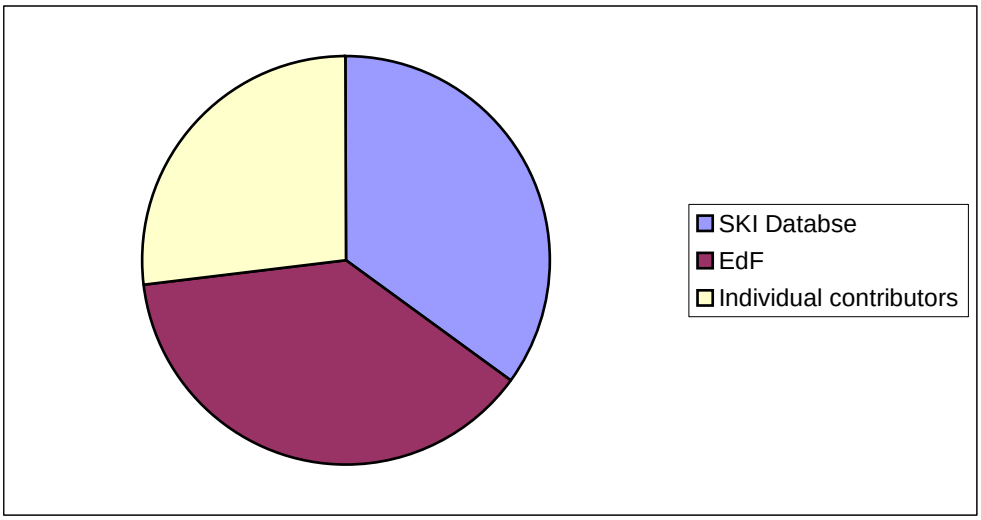

Figure 5.3: Distribution of contributors to the NESC-TF operational database.

5.2.1 Case grouping by component type

The distribution of cases according to component type is shown in Figure 5.4. It is seen that the vast majority belong to the group mixing Tees without internal mixers (sleeves). This type of component is one that is naturally subjected to temperature loadings since this is a location where fluids of different temperatures and flow rates meet. The fact that Tees with mixers (sleeves) appear as less frequent damage locations may be due to the fact that, in the population of components investigated, tees without internal mixers are more common or may simply reflect the internal mixers actually help to minimize the probability of thermal fatigue damage, as intended. More precise conclusions could only be drawn from data with larger populations. Overall it is however clear that tees are naturally sensitive to thermal fatigue.

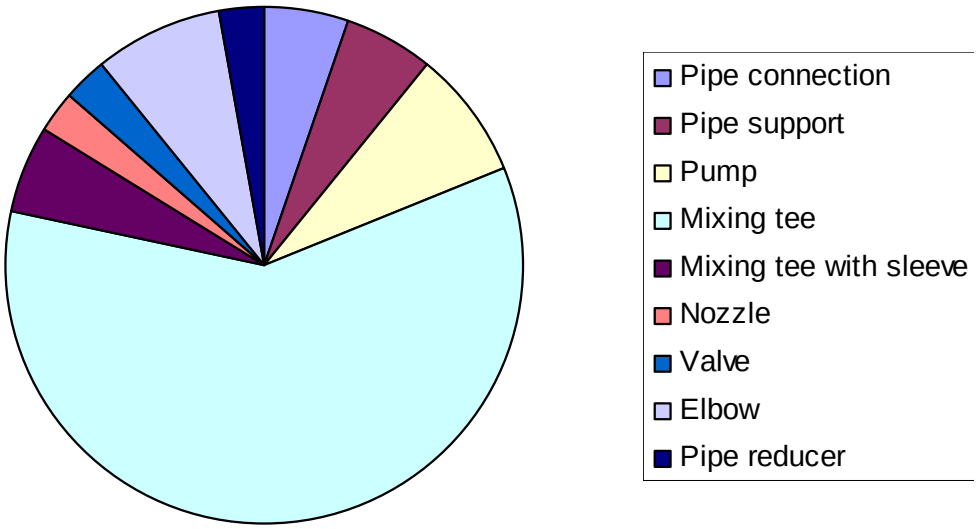

Figure 5.4: Chart showing the distribution of component type in the NESC-TF operational database

A component comparison can be made directly with the results in /5.4/. Here 64% of the thermal fatigue failures occur in the piping system. About 33% of these occur in Tees, with however valves as the dominating location for damage. Given the over-representation of Tees in the present database, different conclusions may be reached for more comprehensive component populations.

5.2.2 Case grouping by cause of failure or damage

In this case, some arbitrariness cannot be entirely avoided in making the cause of failure or damage categories, since the damage mechanism is typically influenced by several parameters. For example, residual stresses are not identified as a main parameter but may influence the fatigue process in some situations. Another such factors are environmental effects, surface condition etc. Also, the damage may have been caused by a chain of events, for example when a leakage leads to stratification, then to turbulence at the mixing interface, which finally results in damage. In such cases valve leakage is identified as the root cause, but turbulence is regarded as the nature of the load. Figure 5.5 shows the distribution of the causes of failure/damage. The results indicate that almost all of the thermal fatigue problems seem to have occurred due to an unforeseen phenomenon. This may be explained to some extent by the absence of specific provisions in the design codes for handling of such problems. It is also apparent that valve leakage is a major cause.

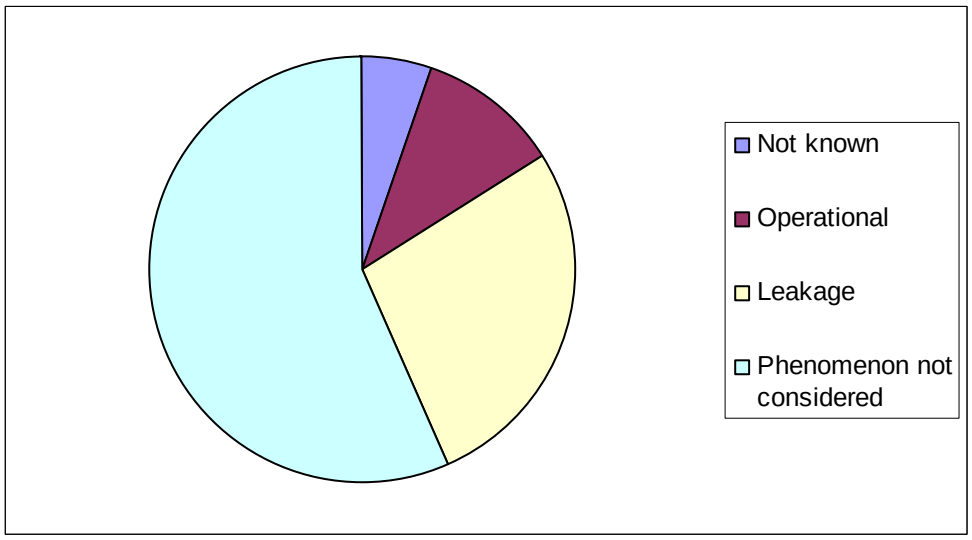

Figure 5.5: Grouping by causes of damage in the NESC-TF operational database.

5.2.3 Case grouping by load type

An attempt to categorize the components in terms of the nature of the load has been made and the results are shown in Figure 5.6. To do this several different types of unstable flow are defined: turbulence, stratification and other types. Other investigations have used similar categorization systems. For example /5.8/ divides thermal fatigue into two groups, striping and stratification, which is very similar to the grouping used here. These definitions are not entirely clear, but essentially striping has the same meaning as turbulence in the NESC database. Other types of unstable flow are, for example, flows that occur due to leakage at seals. Some of the failures have been caused by operational events other than unstable flow, and these are classed as transient type flows. The four groupings are summarised in Table 5.3.

Figure 5.6 shows a clear dominance of turbulence cases. However only limited conclusions can be drawn from this data since the contribution from EDF (which are exclusively turbulence cases) dominates the data. Direct comparison with the results reported in other references is not attempted, so the overall distribution of thermal fatigue damage for different component types remains uncertain. However, there are clear indications that stratification needs to be considered together with the turbulence in Tees problem. It should however once again be mentioned that the grey zone between the load types is large. A good example is the Civaux 1 case, which has been dealt with in detail in /5.9/. A through-wall crack appeared in an elbow near a mixing tee. Calculations showed that this cracking was due to a large scale instable flow, which arose due to local turbulent flow in the Tee.

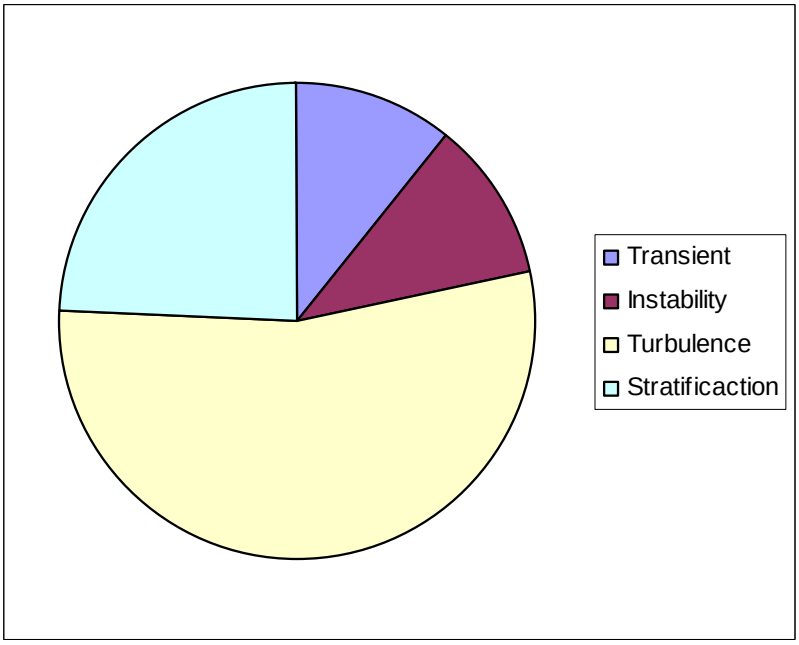

Figure 5.6: Grouping by the nature of the load in the NESC-TF operational database

5.2.4 Case grouping by crack location

Here we have looked at whether cracks are located in welds or base material. A natural feature of thermal fatigue is that the stressed area can be extensive and is not necessarily confined to notches as in the case of mechanical fatigue. The identification of a distinct crack site at a stress concentration or weld is often far from obvious. Figure 5.7 shows the distributions of damage locations in the NESC database. It transpires that the majority of cracks appear in the base material at smooth surfaces. Possibly the region of thermal fluctuations is confined to a rather small area, which does not generally coincide with the weakest location in the component. This remains an open question and further systematic studies are needed. In terms of fatigue evaluation this question is linked to the issue of weld fatigue life reduction factors. Considering the contribution from EDF, i.e. only Tees, welds would seem to have an influence: out of a total of 28 crack sites, about 58% are confined to welds. Network cracking occurs over large areas of base material. The location of the cracking is shown, for the three types of tees, in Figures 5.8-5.10. However, if the depth of the cracks is considered, the weld locations dominate, as is shown in Figure 5.11. In fact the nine deepest cracks occur in the welds. The cracks that appear in the base material remain relatively shallow in comparison to those that appear in the circumferential welds.

Table 5.3: Categorisation of thermal loads

Category	Example	Comment
Turbulence	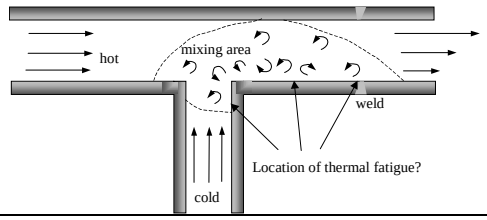	Turbulent mixing in a tee without inner sleeve
Stratification	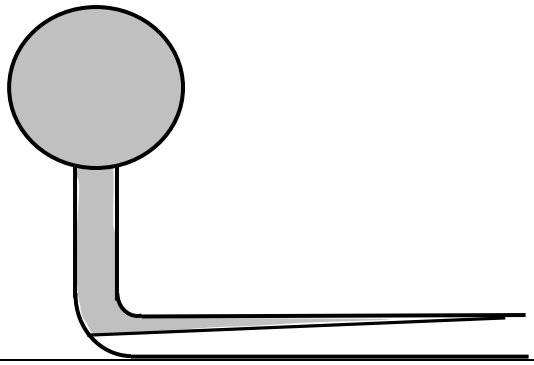	Stratification near a tee. Stresses occur as a consequence of insufficient mixing over the section of the pipe
Other instability	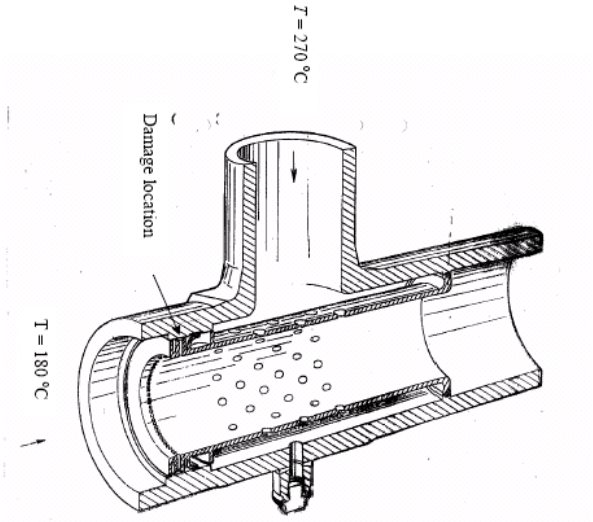	Varying flow near a sealing
Operating transient	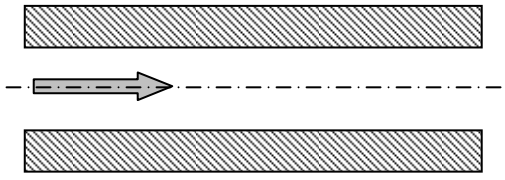	Pipe with axi-symmetrical flow

The question about crack location is linked to the issue of crack orientation. In the case of a thermal shock load in pipes the stress state is typically bi-axial and accounts for the network-type crack patterns. Taken as a whole, the NESC database results indicate that axial cracks are more frequently the dominating crack at a given damage location. This is however not supported by the subset of EDF data, in which circumferential cracks at welds are the most frequent, as shown in Figure 5.11.

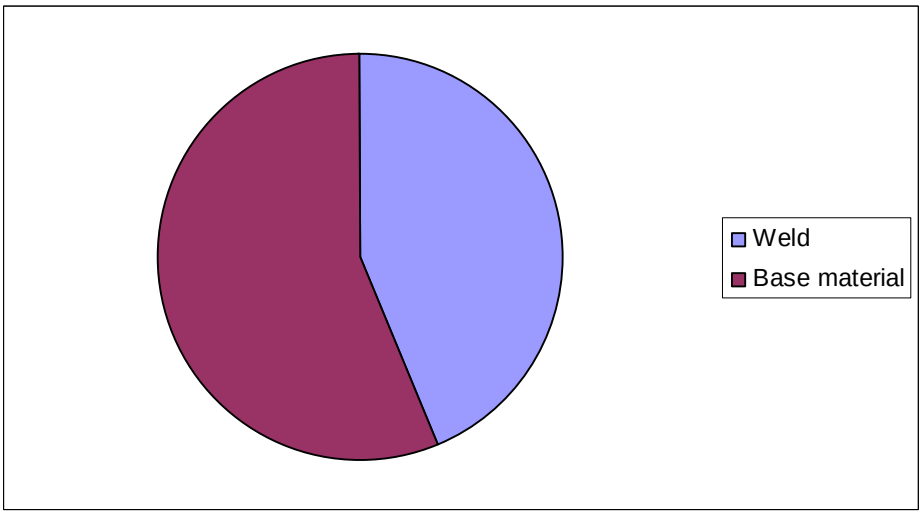

Figure 5.7: Location of cracks (base material or weld) in the NESC-TF operational database.

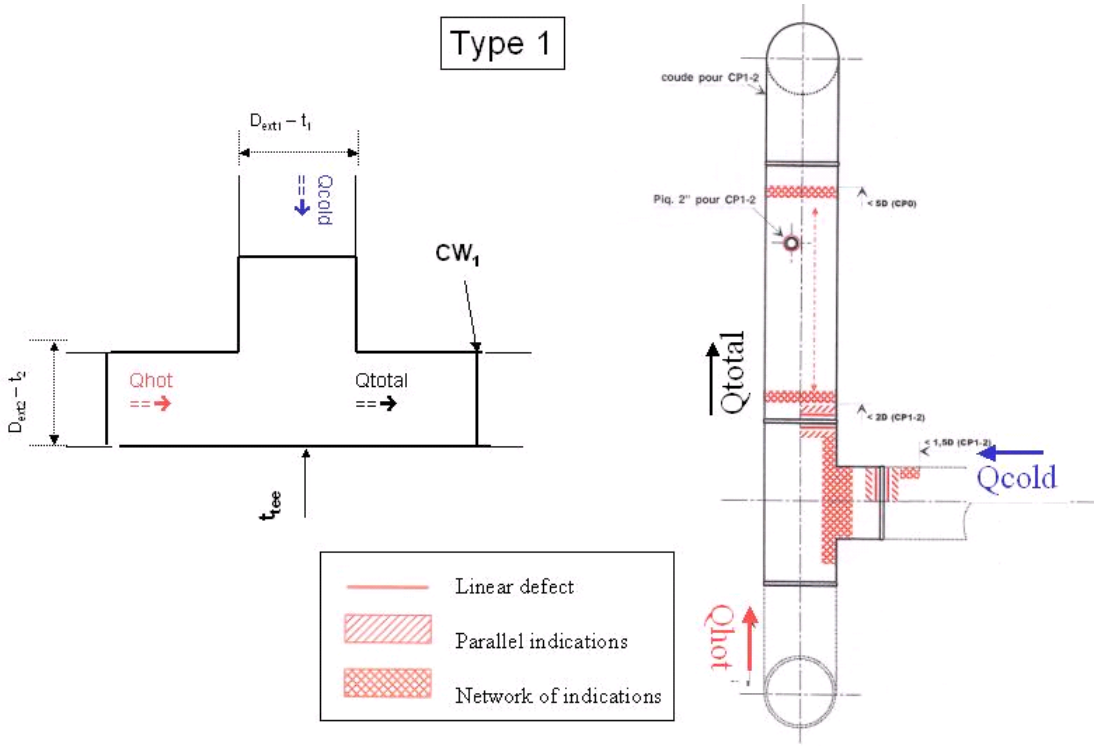

Figure 5.8: Location of cracks in a Type 1 Tee, from the EDF generic dataset

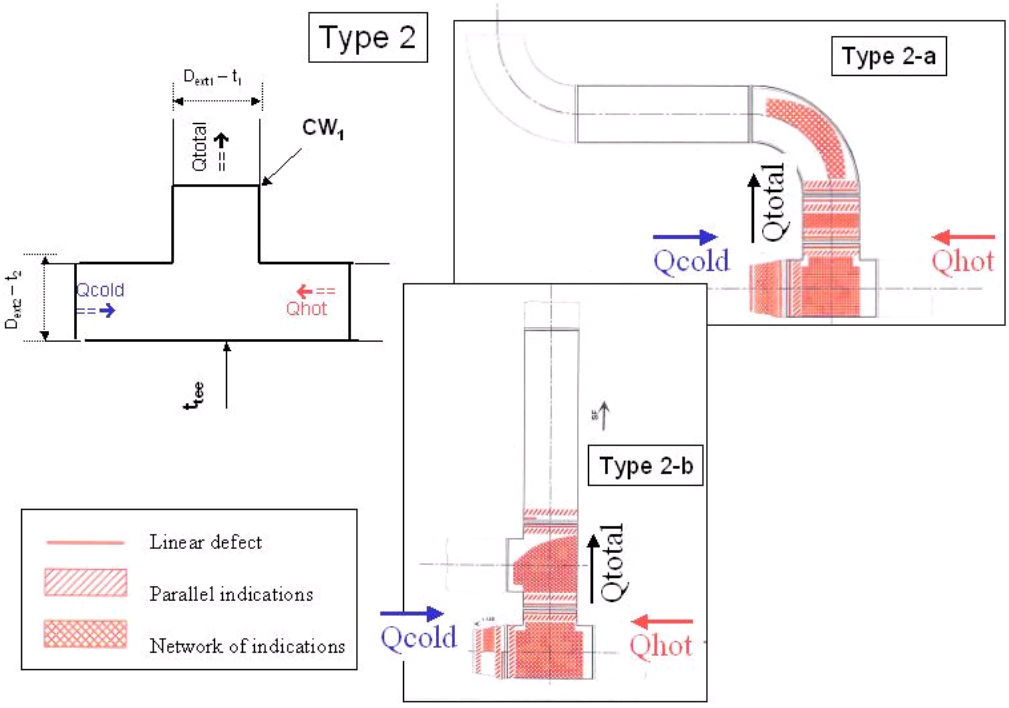

Figure 5.9: Location of cracks in a Type 2 Tee, from the EDF generic dataset.

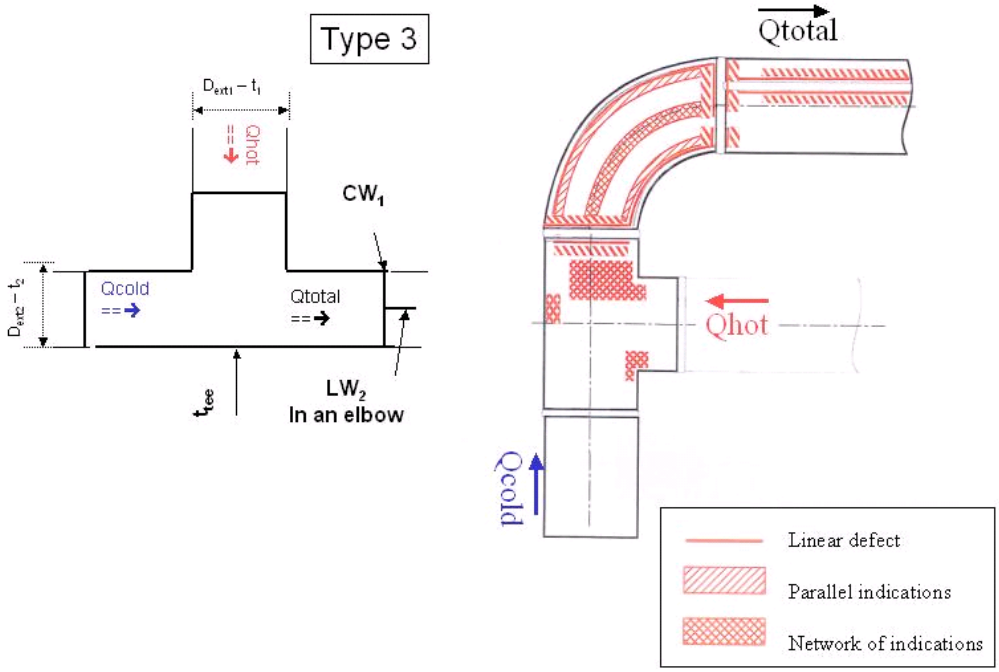

Figure 5.10: Location of cracks in a Type 3 Tee, from the EDF generic dataset.

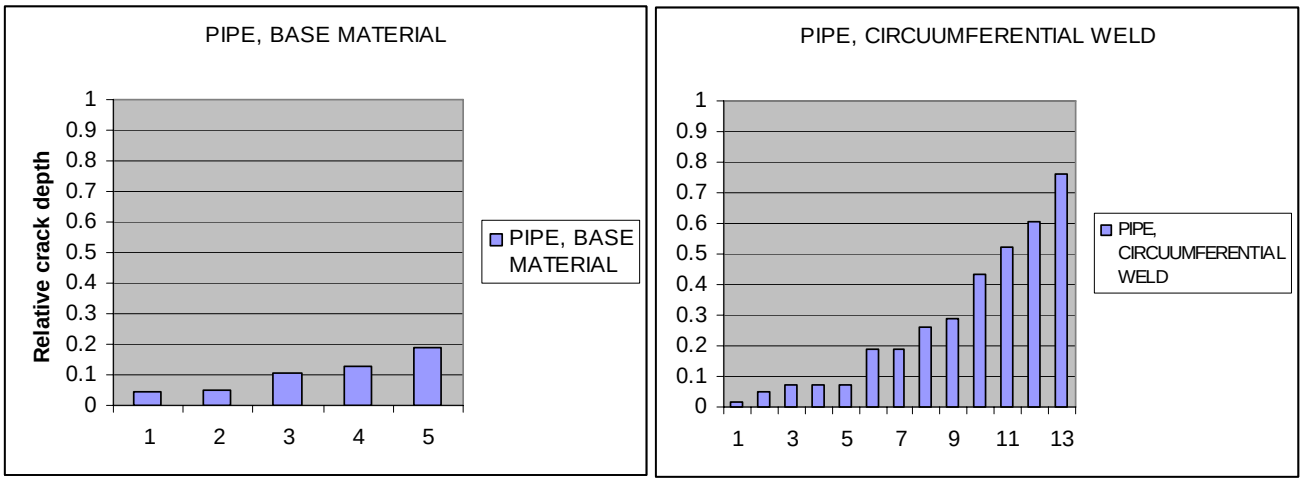

Figure 5.11: Relative crack depths (a/t) , from the EDF generic dataset

5.2.5 The EDF cases of turbulent mixing in tees

The largest data set on damages in Tees comes from EDF. Operational data for three different geometries have been studied. The Tee geometries and the observed crack patterns are shown in Figures 5.8-5.10. Crack depth data are shown in Figure 5.11. The Tee itself is similar in each of the geometries; however the adjacent components may be different[1]. It is noted that the cases also cover three different loading conditions in terms of flow directions. The results are summarized in Table 5.4.

It is of interest that the cracks in the cases in Table 5.4 appear within short operational times. All cracks appear within six months and all the components were run with quite large variations in operational conditions. This situation is also reported in /5.4/ where cracking within short operational times is reported. Many of these damage cases occurred in Tees without mixers. The Civaux through wall case (No.14 in Table 5.4) occurred within two months of operation. Furthermore the nominal ΔT clearly exceeded $80^{o}C$ for long periods.

[1] The Civaux 1 case in Tables 5.1 and **5.2** (ID33) is represented by geometry Type 3 (Figure 5.10).

Table 5.4: EDF generic Tee thermal loading cases.

ΔT in °C between T_{hot} and T_{cold}	**1**	**2**	**3**	**4**	**5**	**6**	**7**	**8**	**9**	**10**	**11**	**12**	**13**	**14**
	Duration (hours)													
80-120	117	322	323	454	582	189	596	424	348	348	410	278	298	62
120-150	310	258	173	507	915	807	285	373	293	242	463	550	338	1431
150-180	107	639	754	1712	1309	2125	630	1001	705	906	1576	1311	1460	11
total time	535	1219	1251	2673	2806	3120	1511	1799	1347	1496	2448	2138	2096	1504
Type of Tee	3	1	2-a	2-a	1	3	1	1	2-a	2-b	2-a	3	3	3
D_{ext} branch, mm	273	324	273	273	324	273	324	324	273	273	273	273	273	273
Pipe thickness in mm	9.6	12.7	9.6	9.6	12.7	9.6	12.7	12.7	9.6	9.6	9.6	9.6	9.6	9.6
Thickness of the tee, mm	25	25	25	25	25	25	25	25	25	25	25	25	25	25
$Q_{hot} + Q_{cold} = Q_{total}$, m^3/hour	1000	1800	1150	1150	1800	1000	1800	1800	1150	1150	1150	1000	1000	1000
Crack depth in tee (base metal), mm	1.1		2.2	2.4				1.47		1.37		0.89		0.71
Crack depth in pipe (base metal), mm			1.23	1.8	0.6			0.59						1.03
Crack depth in weld[4] $\mathbf{LW_2}^2$	0					3.22							3.22	9.6
Crack depth in weld $\mathbf{CW_1}^2$	1.82	0.9	2.52	1.8		5.82	0.24	0.61	0.7	0.71	2.8	4.15	5	7.3

5.2.6 Cases other than turbulence in Tees.

The Civaux case, No.14 in Table 5.4, is analysed in more detail /5.9/ and is identical to ID33 in the NESC database. It is seen from Figure 5.12 that the through wall crack occured in the pipe elbow a short distance downstream of the Tee. The large elbow crack grew from the outside of the elbow. CFD analyses were performed /5.9/ in order to seek an explanation for this. These revealed a large scale instability which would induce high membrane stresses in the pipe at the crack location. Thus it could be stated that this case is not exactly a case of turbulent mixing, but may be an example of instable flow conditions as a consequence of turbulence in the Tee junction.

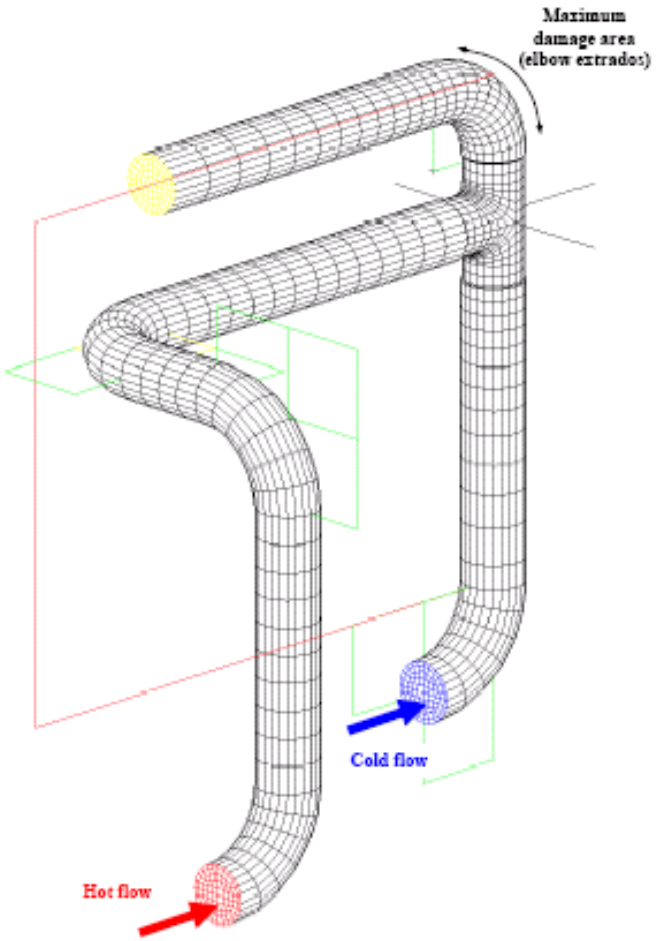

Figure 5.12:. Location of the through-wall crack in ID33 (Civaux 1 case).

Another example of damage in an elbow is shown in the Figure 5.13. This is case ID35 in the NESC database, which is the Tihange 2 case in Table 5.1. This crack was caused by a small flow from a leaking valve. The nature of the load can hardly be categorised as turbulence, and stratification is considered more likely. It is noted that the through wall crack (crack no. 1 in the Figure 5.13) was located in the base material. This damage is believed to have been caused by the same type of phenomenon as the Farley 2 case in Table 5.1, the mechanism for which is shown schematically in Figure 5.14. The cyclic stratification in the branch is caused by the turbulence in the main pipe, with turbulent penetration into the branch. Variations in operational conditions lead to different lengths of the turbulent penetration (see **Chapter 3**).

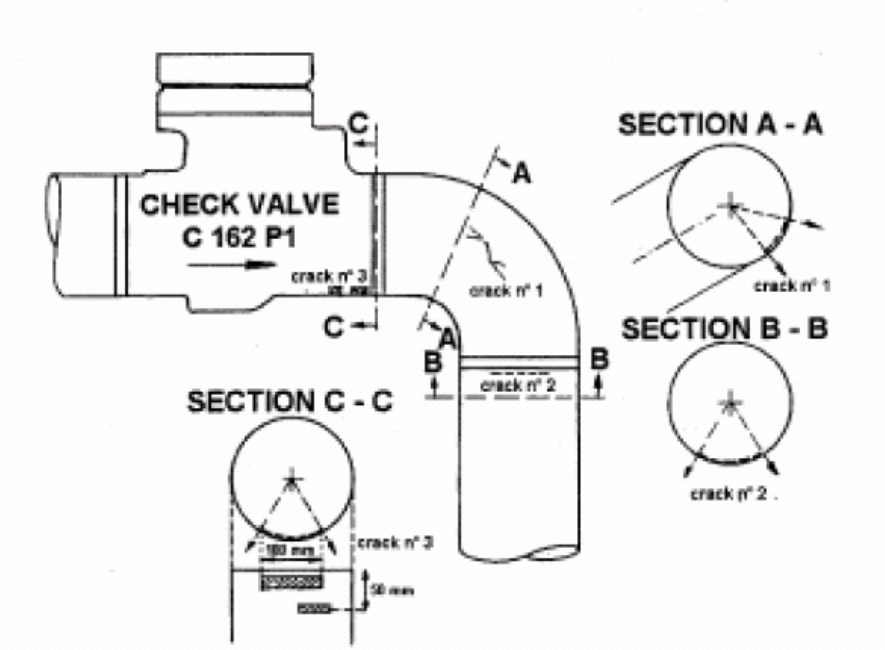

Figure 5.13: An example of through wall cracking (Case ID35)

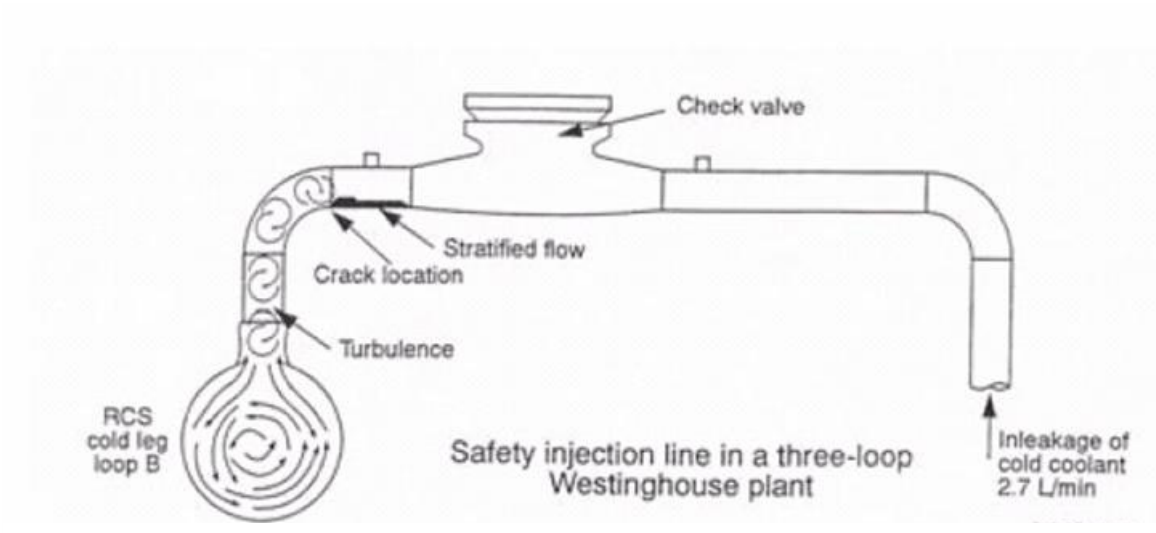

Figure 5.14: Sketch from ref /5.1/ of the loading condition for Farley 2, which is believed to be of the same type of for case ID35 (Tihange).

A further example of stratification is shown in Figures 5.15-5.17. This is case ID36. As in many other cases of stratification, the temperature load is caused by a leakage, here in the valve indicated in the figure. Typically the flow rates in the branch are low. The crack occurs in the axial weld in the pipe. The measured cycling period of the stratification layer is comparatively long, about 20 to 50 secs. The temperature difference at the steep gradient between the hot and the cold layer is estimated to be about 120^{o}C. However the nominal temperature difference is larger, up to 200^{o}C. Furthermore the temperature difference was measured by means of a heat camera. The results are shown in Figure 5.17. The existence of sections of hot and cold water is confirmed. Note also the heated zone where the through-wall crack is positioned. A somewhat similar loading situation occurred in the Genkai case in Table 5.1**,** which described in more detail in /5.3/. Here stratification cycling with a period of 20 minutes was identified on a similar piping geometry. The inlet of cold water also came from a leaking valve, with a variable leak rate. A schematic of loading is shown in Figure 5.18, as taken from /5.1/. The penetration length can vary according to either to different operation conditions or to variations in the leak rate from the branch valve.

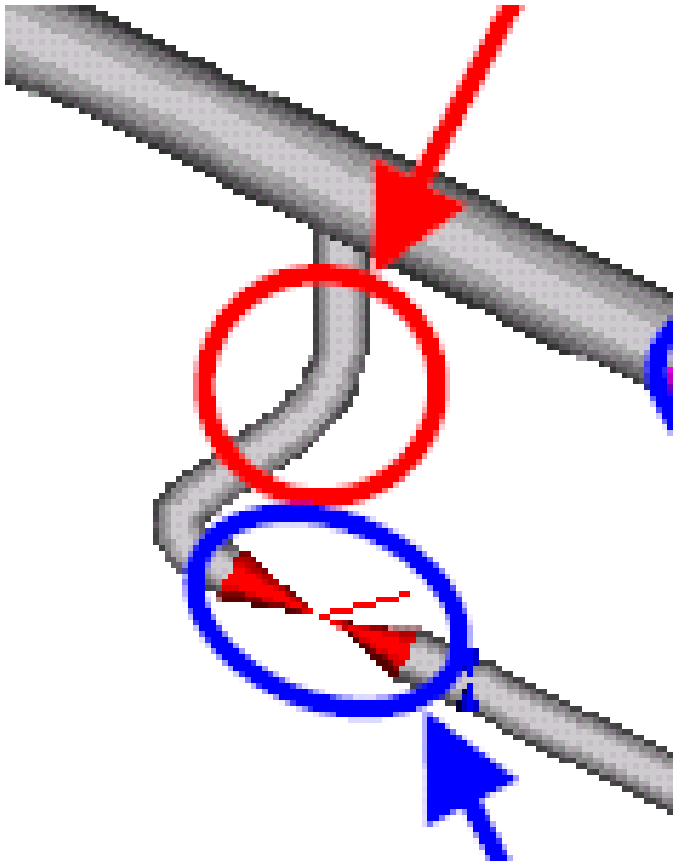

Figure 5.15: Case ID36, showing the location of pipe elbow where the leak occurred (red circle) and that of the leaking valve (blue circle)

Figure 5.16: Case ID36, showing a photo the leaking crack in the pipe bend.

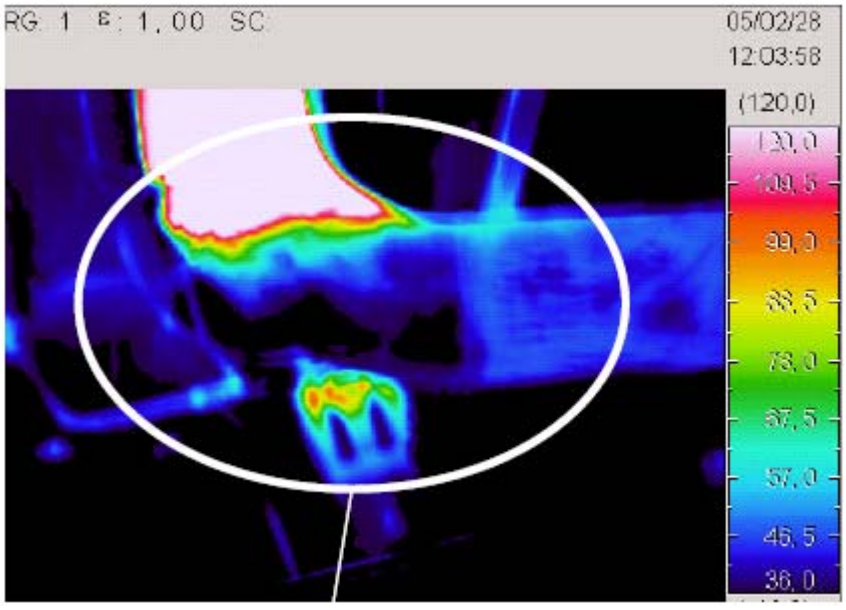

Figure 5.17: Case ID36, showing the measured heat distribution in the pipe elbow and providing evidence of the stratification and striping which occurred

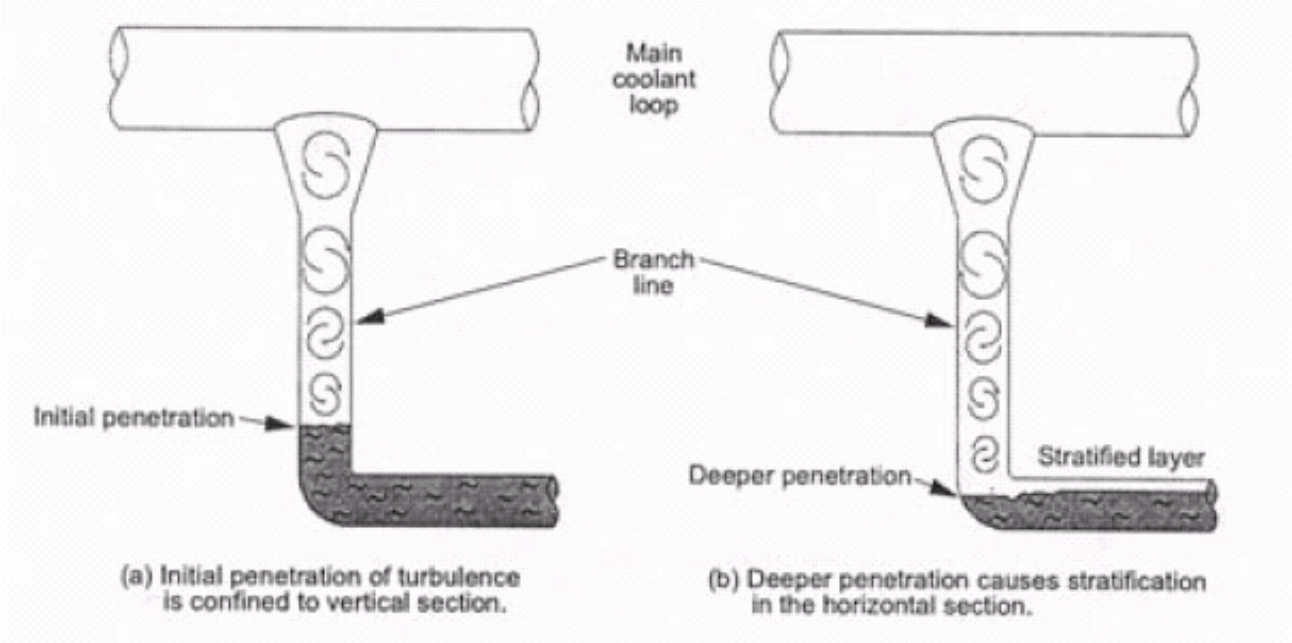

Figure 5.18: Idealisation of Case ID36, showing a stratification layer with cyclic motion in a elbow (ref /5.1/).

A further example (ID37) of a through-wall crack in piping is shown in Figure 5.19. Here a reducer was damaged due to thermal cycling. Once again, flow rates are low, as is the period time, which was estimated to be about 100 s with a temperature variation of 100°C. The cause for the unintended temperature variation is a small leakage through a pump, which was on standby. The nature of the load is assumed to be stratification; however this was not fully investigated. Figure 5.20 shows a similar type case (ID32) that seems to have been created due to a comparatively high temperature difference, with a nominal ΔT of 200°C. The crack in this case is axial and was not confined to the weld in the vicinity of the crack. The mixing occurred unintentionally due to a leaking valve. There appears to have been significant plastic deformation along the mouth of the crack (Figure 5.21), which would indicate a low-cycle fatigue process and high cyclic stresses.

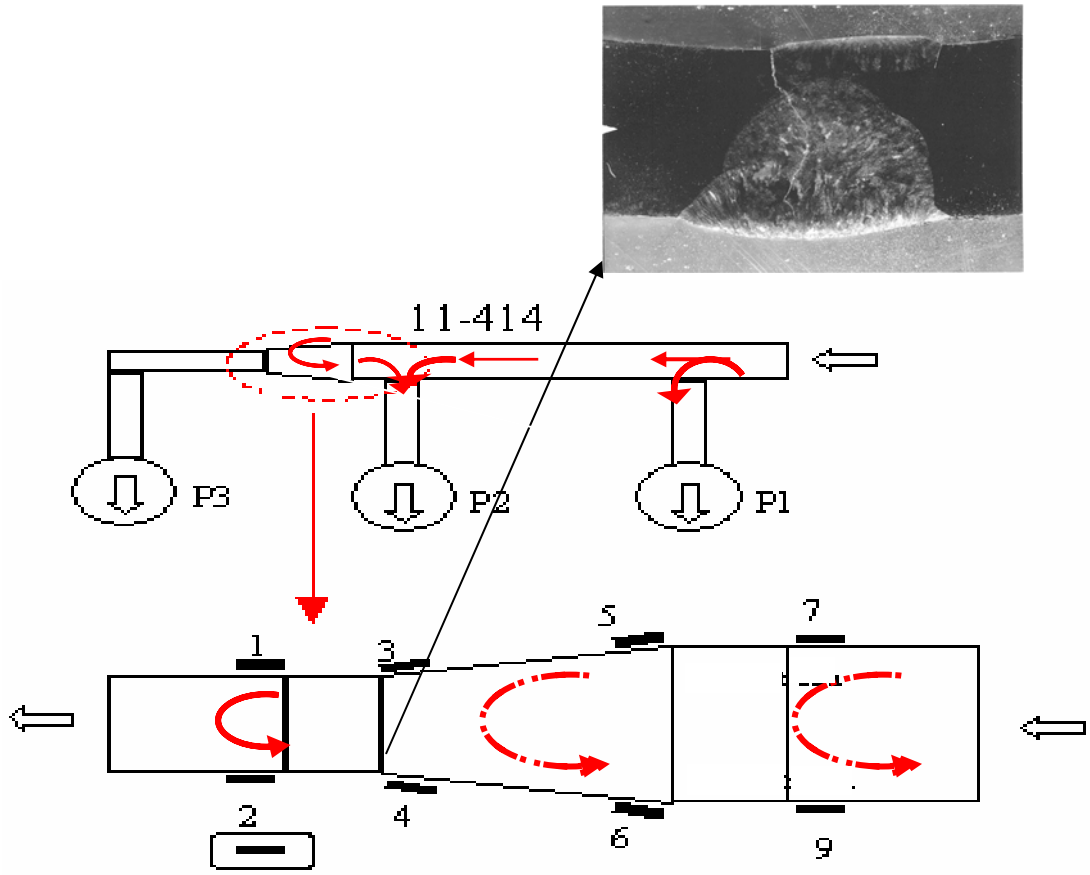

Figure 5.19: Damage location in a reducer (Case ID37); the red lines show the assumed flow directions.

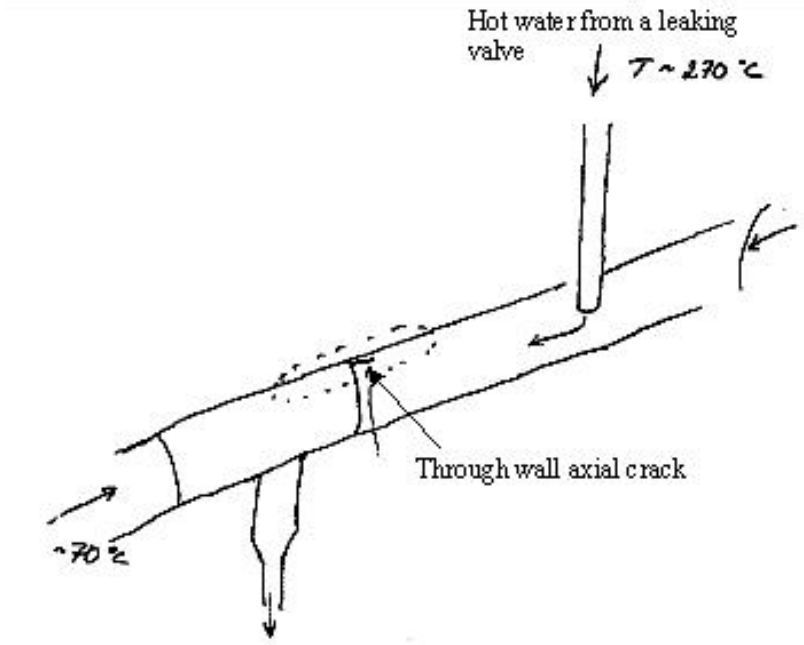

Figure 5.20: Sketch of the situation in case ID32, with a through-wall crack near a Tee.

Figure 5.21: Case ID32: photo of the axial crack indicated in Figure 5.20

Further examples of stratification are shown in the Figures 5.22-5.23, all of which led to through wall cracking. In all these cases the mixing of hot and cold happened unintentionally and was due to an internal leakage in the system. Figure 5.22 shows a valve (Loviisa 2, ID34), in which steam at 325^{o}C and hot water at 250^{o}C unintentionally met. It should be mentioned that /5.7/ reports that occasionally the temperature difference was higher, and values in excess of 200^{o}C are believed to have occurred during the initial operation of the valve. The orientation of the crack indicates high circumferential stresses. However, this could not be shown with 2D analyses according to the failure report in /5.7/, with the conclusion that 3D modelling may be needed to fully capture the local stress state.

A leakage near a T-joint is described in Figure 5.23, case ID18. The failure investigation found clear signs of stratification. Leakage in combination with insufficient isolation is assumed to have influenced the damage. Observations of sulphur on the crack faces may indicate environmental assistance to the process.

The case shown in Figure 5.24 highlights the problem of using simplified load definitions. Here, local fluctuating flow and unintended leakage through the sealing was believed to be the crack driving load. Temperatures were measured in the vicinity of the sealing and a slow temperature variation (10-20 seconds) in the circumferential direction was measured. The cracks were relatively deep, 17 mm in a thickness of 34 mm. The internal mixer with holes is placed in the tee in order to avoid turbulent mixing, however the temperature variation in the sealing was not foreseen. It is also noteworthy that the cracking appears upstream in the run and not downstream as in Tees without mixers. It is assumed that some instability other than stratification or turbulence is present. However, the rather deep crack indicates that the stress variation is not only at the surface. Hence a 3D stress state (as in stratification) with a non-negligible net force/moment through the wall thickness is likely.

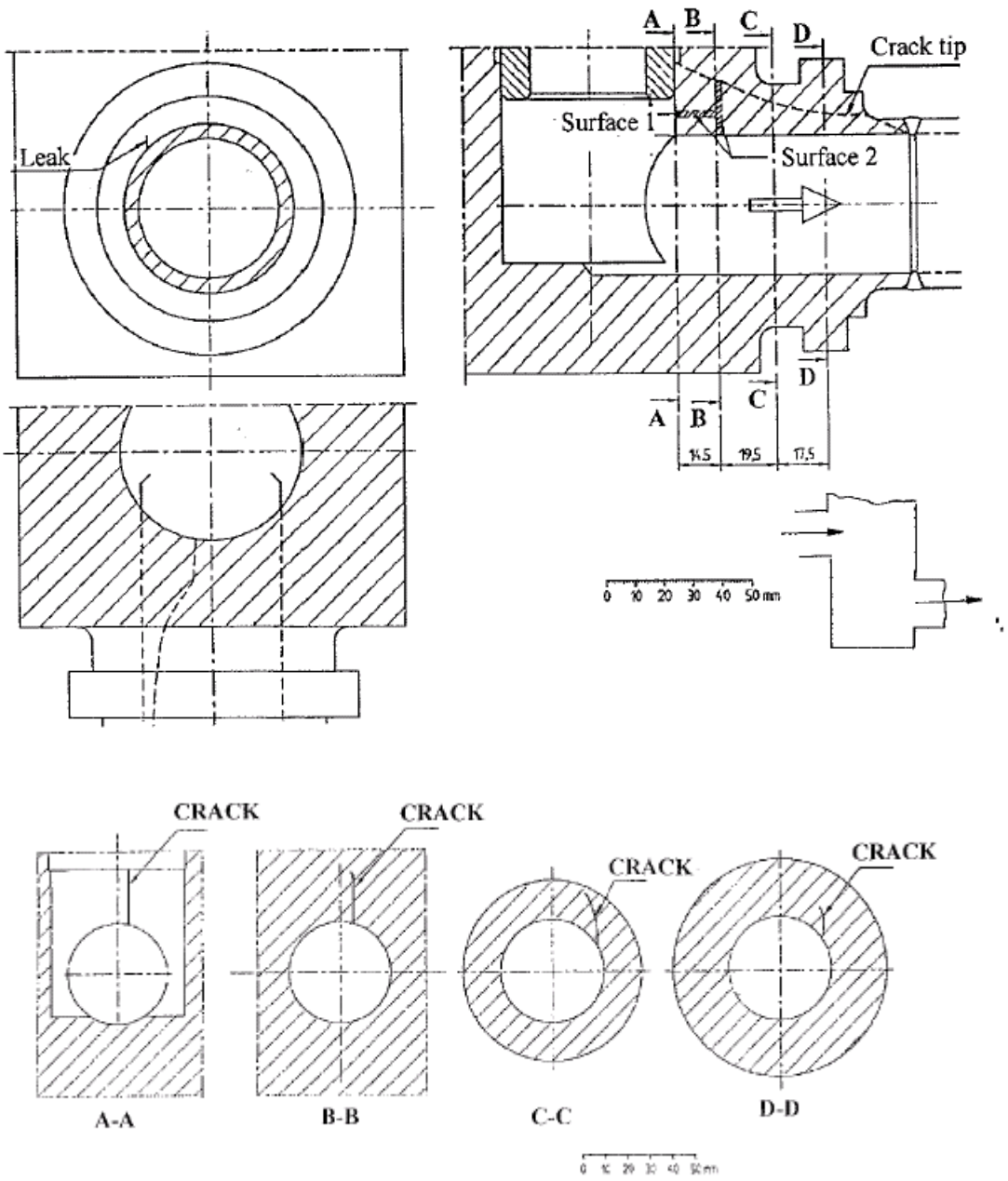

Figure 5.22: Case ID34 (Lovisa 2): stratification damage in a valve; the nominal temperature difference was about 60-65^{o}C, but occasional values of more than 200^{o}C were reported.

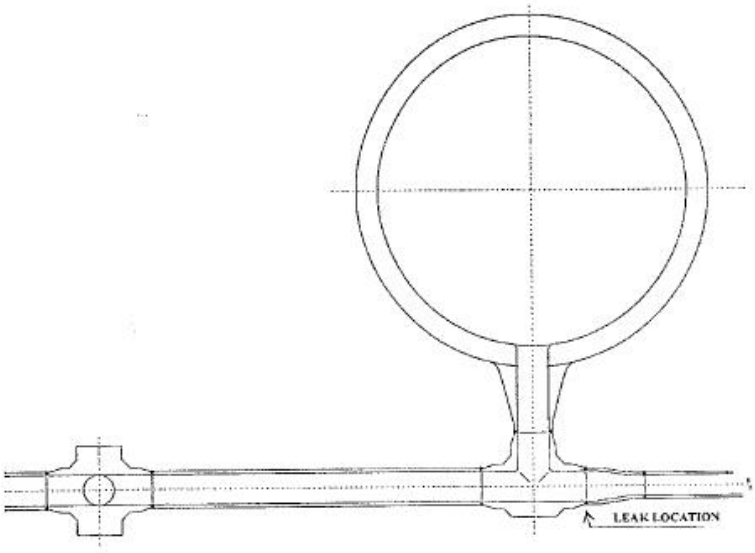

Figure 5.23: Case ID18: sketch of the location of the through wall circumferential crack in a T-joint

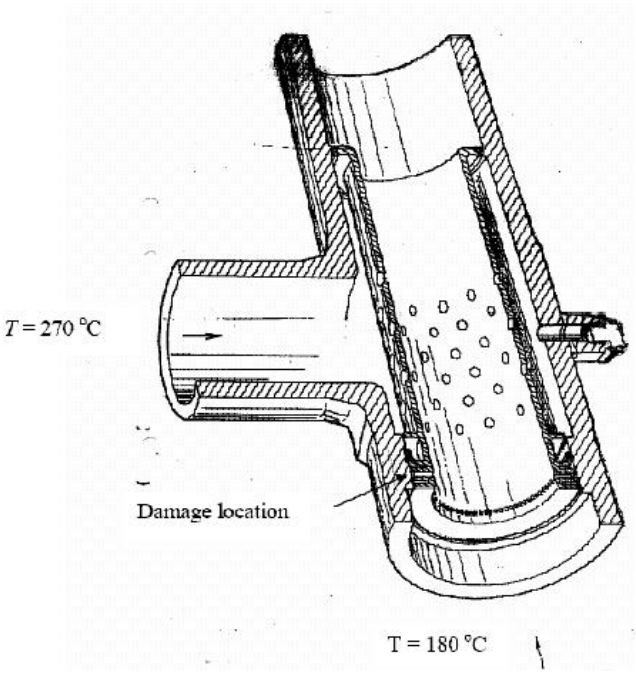

Figure 5.24: Cracking in a Tee with an internal mixer /5.10/.

Tees with internal mixers have been subjected to design changes in order to avoid thermal fatigue problems such as those depicted in Figure 5.24. An example of a modified design is shown in Figure 5.25. The sealing, that was the source of the previous problems, is located at the internal mixing device and thus is not in direct contact with the pressure-bearing pipe surface. Thermal fatigue problems have also been reported for this design, however apparently in the internal mixer (in the vicinity of the labyrinth sealing) and not in the pressure bearing part of the Tee.

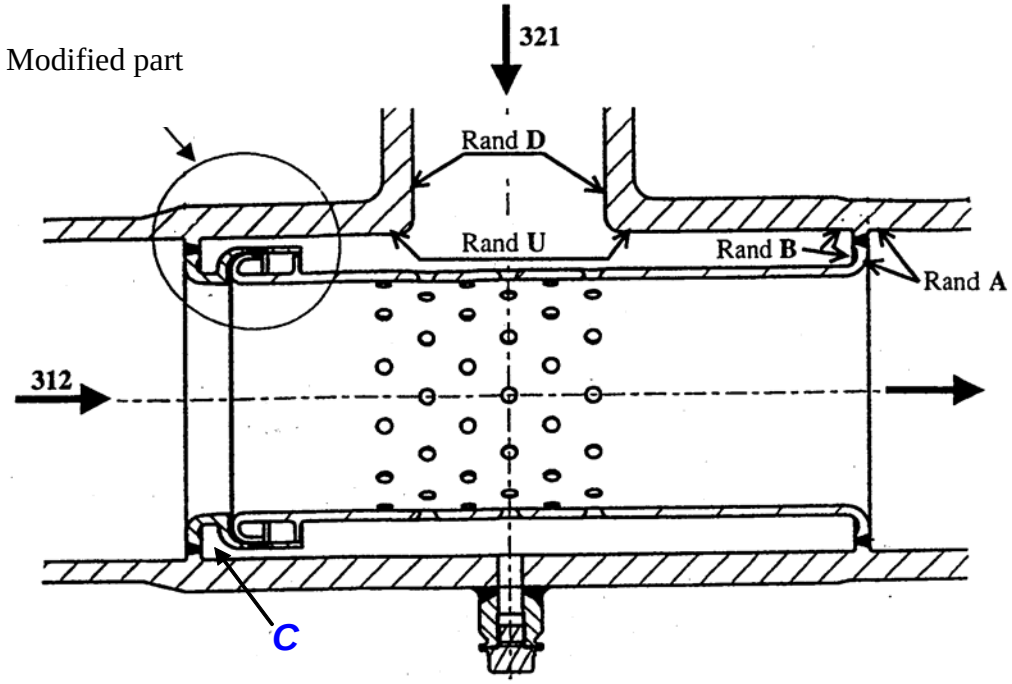

Figure 5.25: Modified Tee with an internal mixer (compare to Figure 5.24).

5.3 Discussion

The failure cases examined essentially fall into two groups, as observed in other thermal fatigue studies:

- In the first group the loading is characterised by turbulent mixing (or striping), with or without stratification. Typical components affected by this process are Tees without internal mixers. It is noted that none of the through wall cracking cases can be attributed to turbulence alone. However, the observed damage is not just superficial, and cracks penetrating to more than 50% of the wall thickness were observed in a few cases.
- In the second group the thermal loading is predominantly stratification. Damage caused by stratification appears much more likely to cause leakage, and almost all the cases of through-wall cracking referred to in the present report are associated with this phenomenon. The damage occurs at much lower flow rates than in the turbulent case. The combination of a low flow rate in at least one of the fluids and a high temperature difference controls the damage evolution. It is clear that different forms of stratification exist, the most harmful being the case with a moving interface between a stratified and a non-stratified state.

No cases of component rupture were found and any crack growth seems to have been stable up to the point it was detected.

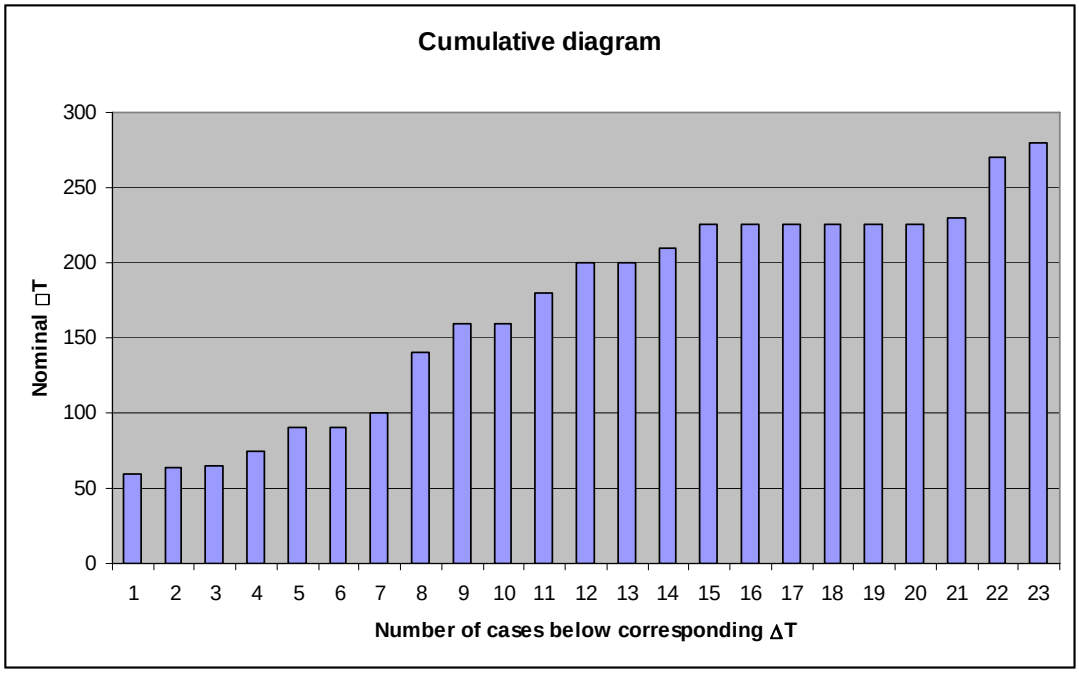

Figure 5.26: Number of NESC-TF operational database cases below a given ΔT (excluding the generic EDF cases)

An important issue in this study concerns the evidence to support the use of screening criteria at mixing Tees, based on the nominal temperature difference between flows, i.e. to establish if there is a threshold below which no significant fatigue damage occurs. In this regard EDF have proposed a threshold value of ΔT=80°C at mixing Tees fabricated in stainless steels /5.11/ and this concept has been taken up in the proposed European procedure (see Chapter 8 below). The Swedish study /5.4/, which collected a substantial dataset of temperature difference values for damaged components (Figure 5.1), shows a small number of cases (2 with ΔT=55°C, 1 with ΔT=56°C and 3 with ΔT=60°C) below the 80°C level. However, when an attempt was made to examine these in more detail, only limited information was found; at least one case had a nominal temperature difference above 60°C and the component was occasionally operated with a considerably higher temperature difference. The project's own database was also evaluated to verify this approach. The EDF cases for mixing Tees, which all show some damage, were operated with nominal temperature differences higher than 80°C for most of the time. For all the other cases in the NESC database, the number of damages cases for increasing nominal ΔT values is summarised in Figure 5.26. The distribution is similar to that for the Swedish cases in Figure 5.1. Of the 4 cases with a nominal ΔT less than 80°C, 3 were occasionally operated with higher temperature differences. This points clearly to the detrimental influence of even short periods of higher temperature difference values, and confirms the conclusions of the Swedish study /5.4/ and the fact that in all of the EDF cases damage occurred within a time significantly shorter than one year. In conclusion, there is strong evidence supporting the proposed screening criterion level of ΔT=80°C for stainless steel components subject to turbulent mixing conditions. Of the relatively small number of damage cases with slightly lower nominal ΔT values, several apparently experienced periods

of operation at higher ΔT values. Rather than invalidating the proposed screening level, this highlights the need to verify that the "nominal" ΔT value used for the screening properly reflects the full range of past (or planned) operating conditions.

Concerning the requirements for more detailed fatigue damage evaluation procedures, the database results underline the need to carefully consider the type of loading and individual component geometry. The variety of damage types observed (in terms of location, orientation and depth) reveals that the local stress state strongly influences the fatigue damage evolution. The multiaxiality of the stress is significant in some cases, but in others it may be predominantly a one-dimensional. In particular the stratification cases are quite diverse, and susceptibility such damage is also strongly influenced the piping lay out itself.

There are several instances in which thermal fatigue damage has developed within short times, even less than a year. These cases are generally associated with the turbulent mixing in tees and underline the importance of reliably representing the actual operating conditions in the damage assessment process. Hence the common classification of thermal fatigue as an ageing process (implying that its probability increases progressively with time) is potentially misleading.

From an inspection viewpoint it is interesting that cracking seem to be less confined to the presence of welds than in mechanical fatigue. The data shows that cracks occur even in straight piping sections and frequently in base material, and shows the strong influence of the coolant thermohydraulics in determining the potential thermal fatigue sites.

The database confirms that leakages (such as those at valves or pumps) are a significant risk parameter for fatigue damage. A significant proportion of the through-wall cracking cases were associated with leakages in the system. It is now well recognised that tighter checks on valve leak-tightness can significantly reduce the problems with thermal fatigue, and the damage case statistics in the coming years will hopefully bear this out.

Lastly, no general conclusions on environmental effects can be drawn, since only one case reported visible traces of environmental effects.

5.4 References

5.1 IAEA, "Assessment and management of ageing of major nuclear power plant components important to safety. Primary piping in PWRs", TECDOC-1361, July 2003
5.2 Atwood C. L., Shah V. K., Galyean W. J., Analysis of Pressurized Water Reactor Primary Coolant Leak Events Caused by Thermal, ESREL '99 – European Safety and Reliability Conference, September 99
5.3 NEA/CSNI Specialists' Meeting on Experience with Thermal Fatigue in LWR Piping Caused by Mixing and Stratification, OECD Nuclear Energy Agency, 7-12 June 1998, Paris.
5.4 Gott, K., "Skador I svenska kärnkraftanläggningars mekaniska anordningar 1972-2000" SKI Rapport 02:50 (Sweden)
5.5 Deardorff, A. et. Al., "A Survey of Current US Nuclear Plant Fatigue Issues", International Conference on Fatigue of Reactor Components, Seville, Spain, 4-6 October 2004
5.6 Details emerge on Tsuruga 2 leak, Nuclear Engineering International, Wilmington Publishing Ltd. Sep 1999
5.7 Dahlberg M., et. Al., "NESC Thermal Fatigue Failure Case Database", 2005

5.8 Nakamura, T., The Kansai Electric Power Co., Inc., “Current Status of Development on Codes for Fatigue Evaluation in JSME”, International Conference on Fatigue of Reactor Components, Seville, Spain, 4-6 October 2004

5.9 Chapuliot S. et al., “Hydrothermalmechanical Analysis of Thermal fatigue in a mixing tee”, International Conference on Fatigue of Reactor Components, Seville, Spain, 4-6 October 2004

5.10 Efsing, P., RTTB, ”Blandare (Mixers)”, Presentation vid Kärnteknik 2004, Swedish Nuclear Symposium, 2004

5.11 C. Faidy, ‘Thermal Fatigue in Mixing Areas: Status and Justification of French Assessment Method’, Proc. 3rd Int. Conf. on Fatigue of Reactor Components, EPRI 1011958, 2005.

5.12 OECD pipe failure data exchange project (OPDE) – 2003 status report, Proc. ICONE-12, April 2005, Arlington, Virginia, USA

6 THERMAL LOAD DETERMINATION

Load determination is a fundamental aspect in the fatigue evaluation of components. In general, thermal loads depend on the component geometry, flow velocity and temperature ranges of hot and cold fluid. These factors determine the flow distribution and turbulence, resulting in a certain amount of mixing in the component. For the case of a mixing tee, the thermal load that is associated with these flows is determined by (local) temperature fluctuations (amplitude and frequency) close to the wall, and the (local) heat transfer coefficient.

6.1 Specified Loads

Loads taken from the design specification include all potential system load cases – enveloping stipulated – up to "End-of-Life" (EOL). Even plant level C loads (emergency condition) which are not likely to occur, are sometimes classified as operational load cases on the system level. Therefore, they are included in the EOL-fatigue evaluation with specified loads, although they may never appear. Trying to specify additional complex temperature phenomena may result in too conservative simplification or is done in such a detailed manner which is not suitable as data input for the common piping system fatigue analyses (Figure 6.1).

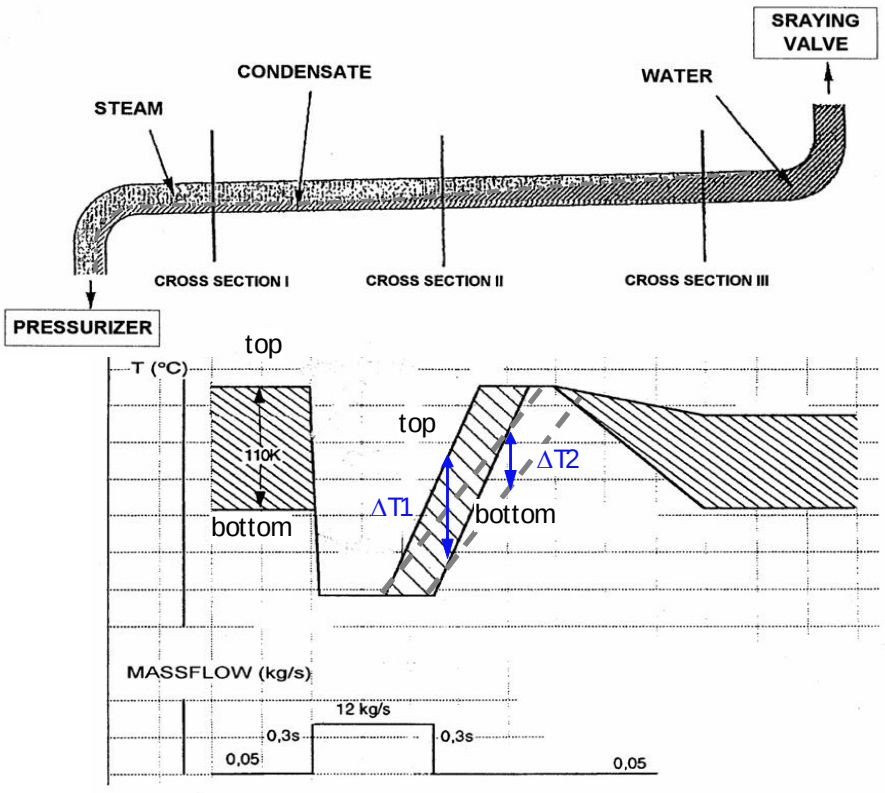

Figure 6.1: Parameters involved in the thermal fatigue analysis of a spray line

6.2 Load Determination by Thermocouple Instrumentation

For fatigue relevant temperature transients and stratifications, thermocouple measurements provide suitable data input concerning the cross section temperature distribution at important locations and the temperature variation along the length of piping system segments (Figures 6.2 – 6.3).

Heat transfer coefficients derived from measurements are more realistic than nominal values specified in codes or procedures. Mostly, operational load cycle numbers are smaller than the design specification data. The “book-keeping” of occurred load cycles provides the advantage that a realistic “today fatigue usage factor” can be determined and a prediction for future time periods is available.

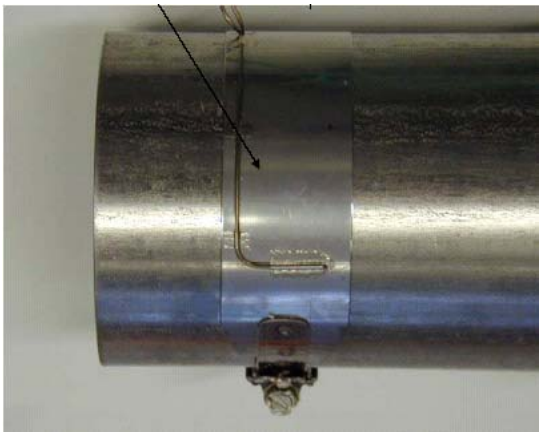

FANP “New”-Example

Installation	Sketch
TUEV Cologne I	
FANP new	
FANP old	
TUEV Cologne II	
AMTEC	

Figure 6.2: Different thermocouples installation methods

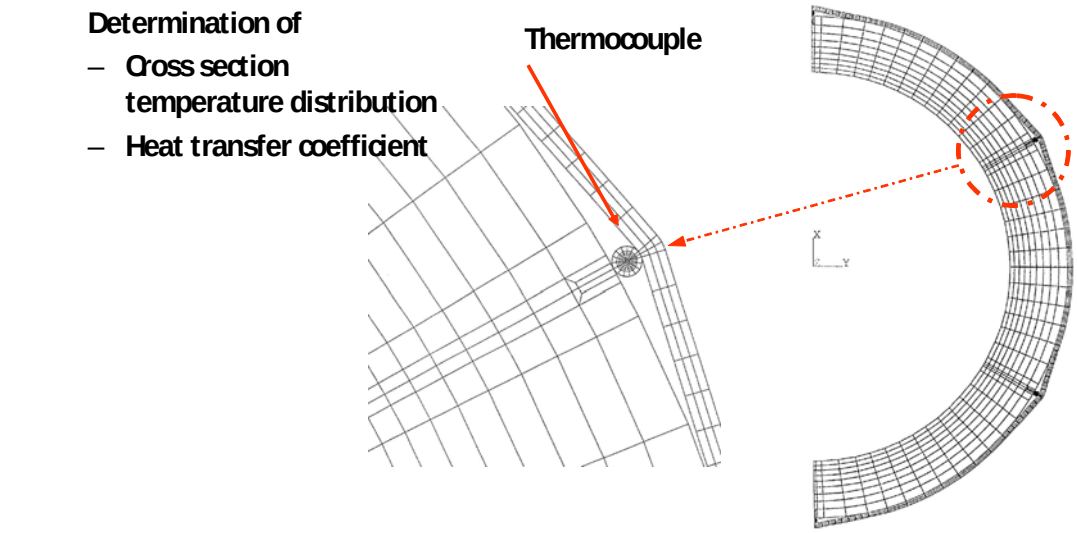

Figure 6.3: Conversion of measured thermocouple data into thermal boundary conditions

6.3 Load Determination by Experiments

- THERFAT Work Package 2 was devoted to load determination by experimental tests and supporting computational fluid dynamic analyses to assess the turbulent thermal mixing effects in piping system Tee-connections (Figure 6.4) and to identify the fatigue significant parameter.
  - In glass model tests of various Tee configurations at ambient temperature fluid temperature differences up to 200°C were simulated by using different specific fluid densities (salt water). Fluid temperature load spectra were determined by electrical conductivity measurements (electrical conductivity fields are analogous to temperature fields).
  - In steel mock-ups measurements of temperature distributions in the fluid and through the pipe wall with specific sensors (e.g. the so-called “fluxmeters”) were performed with temperature differences up to 90°C. The recorded temperature load spectra at the inner surface of the pipe wall were used as input for the stress and fatigue analyses and for the important determination of realistic, but not too conservative, heat transfer coefficients.
  - In addition to the experimental tests, numerical thermo-hydraulic CFD-calculations have been performed for benchmark cases and for other Tee-configurations. Agreement between analytical predictions and experimental results is reasonable. Additional highly sophisticated aspect in the load determination field covers the development of virtual sensors based on neural network and fuzzy logic tools to simulate the dependency of thermal fluctuations from transient mass flow and temperature distributions of the surge lines in two pilot plants.

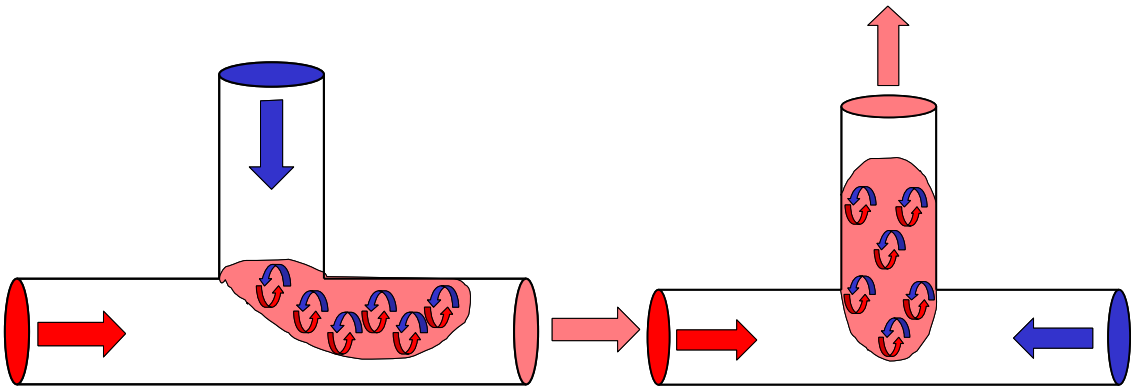

Figure 6.4: Two mixing Tee flow scenarios and the resulting turbulence zones

6.4 Load Determination by CFD Analysis

Computational fluid dynamics can in principle be used to compute the flow in a component and thus predict the thermal load. However, if one wishes to fully model turbulence at all length scales (using the so-called direct numerical simulation), computational times are excessive even with current processing performance. Therefore, several alternative modelling strategies have been developed, with the Reynolds Averaged Navier-Stokes (RANS) approach being the most widely used. Its advantage lies in a simple model and numerical formulation. On the downside, RANS does not resolve the turbulent spectrum and provides only limited information on unsteady mixing processes.

In recent years, an intermediate approach called Large Eddy Simulation (LES) is being increasingly applied. LES aims at resolving all large scales in the flow domain. Only small (dissipative) structures are modelled by the sub-grid scale eddy viscosity. The advantage of LES is that only a small portion of the flow is modelled, whereas most of the turbulence is a result of the numerical solution of the unsteady-state, three-dimensional Navier-Stokes equations. A disadvantage is that LES is computationally more expensive than the RANS approach.

In order to determine thermal load in a mixing tee, the use of LES is imperative. The RANS approach simply does not provide enough detailed information. On the other hand, thermal stratification problems e.g. in elbows, can still be evaluated accurately with RANS.

6.4.1 Linking CFD with the SIN-Method

In the sinusoidal method (SIN-method) substantial simplifications are made to arrive at a conservative estimate of loads due to turbulent mixing (see further descriptions in Sections 8 and 9, as well as /6.1/). These include:

- Neglecting the local nature of the load, and assume it to be axisymmetric;
- Reducing the full load spectrum to a sinusoidal one with a single (critical) frequency and amplitude.

With these simplifications, there remain three main parameters to be specified in relation to the thermal load for application of the SIN-method:

- Heat transfer coefficient (set to the constant value of 15.000 W/m^2/K);
- Amplitude of the sine wave (set to 80% of the nominal temperature difference $\Delta T=T_{hot}-T_{cold}$);
- Frequency of the sine wave (most severe frequency in terms of fatigue is chosen).

The LES simulation that has been performed provides a local solution of the heat transfer coefficient. From Figure 6.5 it can be seen that the heat transfer coefficient varies between 5000 and 33.000 W/m^2/K. So, the heat transfer coefficient chosen in the SIN-method is not the most conservative one. However, one has to notice that the thermal load is determined by the combination of transfer coefficient and temperature difference.

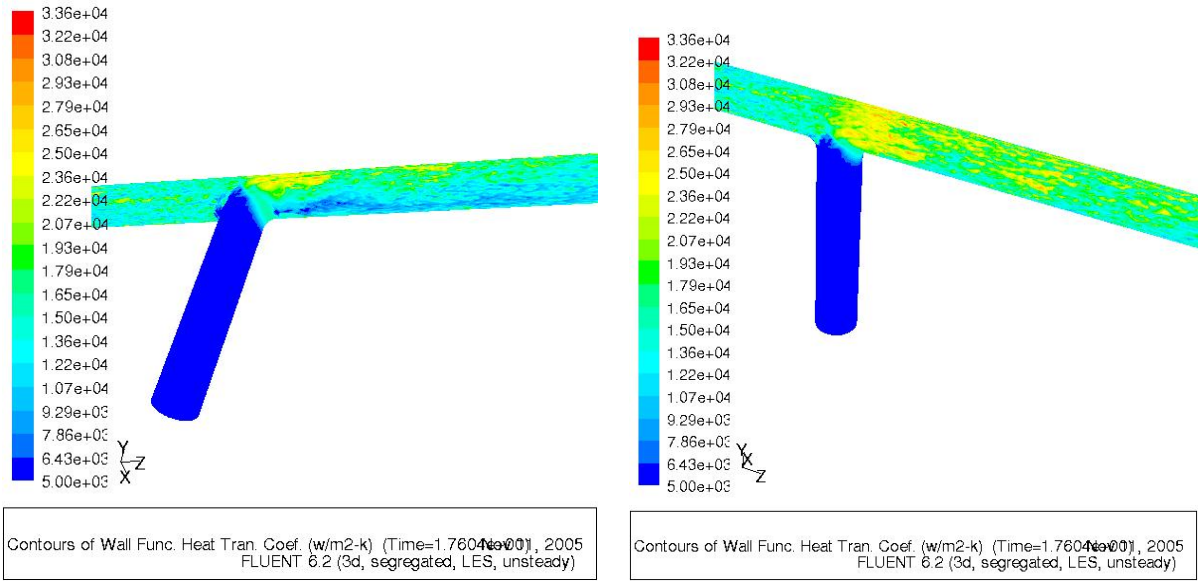

Figure 6.5: Heat transfer coefficient at the boundary of the fluid domain

In Figure 6.6 the average and RMS temperature at the boundary of the fluid domain is shown. For comparison, the nominal temperature difference in this simulation is $\Delta T=T_{hot}-T_{cold}$ = 72°C. Thus, with a maximum of RMS temperature of 18 °C the choice in the SIN-method 80% ΔT = 58°C is conservative for this particular mixing tee configuration and flow speed.

Unfortunately the LES study performed so far, turned out to be computationally too demanding to be able to draw clear conclusion regarding the frequency of the temperature fluctuations. Also, since no solid was modelled in this initial investigation, the "low-pass-filtering" effect of the solid could not yet be quantified.

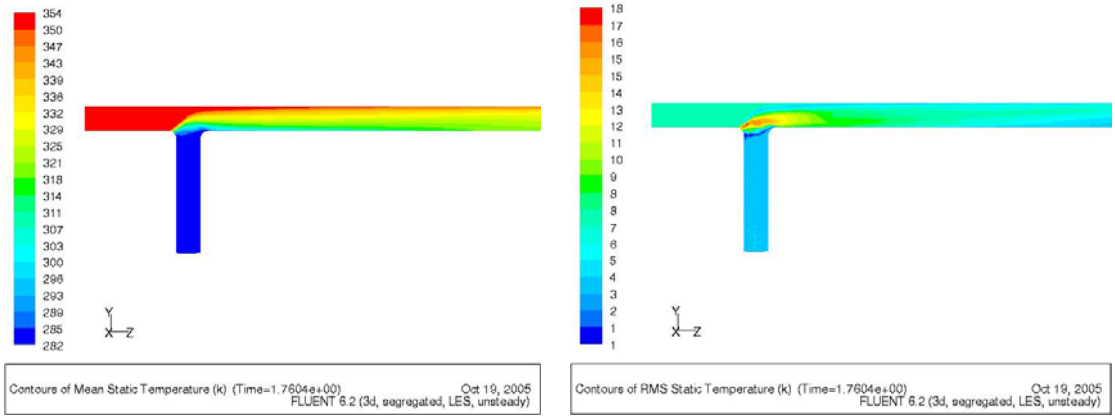

Figure 6.6: Average and root mean square temperature at the boundary of the fluid domain

6.4.2 Outlook for further improvements

As stated, the LES model for the tee junction has to be improved by taking into account the heat transfer with the component itself. The temperature variations will then be solved in the solid and the fluid simultaneously. Furthermore, the highest frequency fluctuations predicted by the current model are in practice not relevant for thermal fatigue applications. Therefore they could be omitted, thus potentially reducing the computational effort.

With such an improved LES model, it will become clear whether it is more practical to try to transfer the heat transfer coefficient and the RMS temperature to the SIN-method, or to try and transfer the actual temperature in the solid, which has the benefit of being a more local approach.

6.5 References

6.1 H.-Y. Lee et al, Tee-Junction of LMFR Secondary circuit Involving Thermal, Thermomechanical and Fracture Mechanics Assessment on a Striping Phenomenon, IAEA TECDOC 1318-5, 1999

7 FATIGUE ASSESSMENT

7.1 Fatigue Curves

This section is intended to provide guidance on the selection of an appropriate fatigue curve for use with the procedure when calculating the fatigue usage factor. The choice of fatigue curve will depend on whether the analyst is assessing a working component or is confirming (or making) the initial design calculations for the component. The data used are similar in that they are derived form fatigue endurance tests on approximately 10mm diameter laboratory specimens, which are presented in terms of applied total strain range versus numbers of cycles to failure. For use in design, the laboratory data are modified by an appropriate factor to allow for unknowns or uncertainty and are sometimes presented in terms of applied stress (range or amplitude) versus fatigue endurance. Fatigue endurance can also be defined in a number of different ways, such as cycles to complete sample separation or cycles to a particular decrease in tensile load from its peak or steady state value etc. The best advice would therefore be to consult an expert, although the use of the ASME /7.1/ design curve should provide conservatism in the majority of cases.

The most widely used of the design procedures is that presented in the ASME Section III Division 1 code. In ASME, the design fatigue curves have been obtained from laboratory tests by reducing the fatigue life at each point on the curve by a factor of 2 on strain (or stress) or 20 on cycles, whichever is the more conservative. Cooper /7.2/ noted that the intent of introducing these factors was to account for such factors as data scatter (including material variability), differences in surface condition and size differences between the test specimens and the actual components. Cooper further noted that the factors of 2 and 20 were not safety margins but rather uncertainty factors that should be applied to the small–specimen data to obtain reasonable estimates of the lives of actual reactor components. He believed that the factor 20 was made up from the product of the following three uncertainties:

- Scatter on data between the minimum and mean, 2.0
- Size effects (difference in scale between laboratory samples and plant), 2.5
- Surface finish, atmosphere (moderate environmental effects), metallurgy, etc. 4.0

Cooper based these observations on comments by Harvey /7.3/, although there has been further discussion as to the make-up of these factors by Porowski et al /7.4/ and Manjoine & Tome /7.5/, who assign equal weighting to either four or five variables in the list above. However, whatever the historical origin of the safety factors in the ASME design codes, the fatigue design curves have been adopted in both the French RCC-M /7.6/ and German KTA /7.7/ codes and so are widely used around Europe.

For Type 304 stainless steel at temperatures up to 427ºC, ASME /7.1/ recommends a single design curve. This can be represented using the following Coffin-Manson type equation:

$$\varepsilon_a = 0.73677 * (N)^{-0.14913} + 7.07136 * (N)^{-0.55268} \qquad (7.1)$$

where ε_a is the strain amplitude (%) and N is the number of cycles to failure; the equation is valid between strain amplitudes of 0.1 and 2.5%. The equation is only valid for $N < 10^6$.

There have been discussions within the ASME committees about extending the curves to higher numbers of cycles. To accomplish this, the curve would have to modified into a stress based formula (using an appropriate modulus) and the effects of mean stress would have to be taken into account using a method such as the Goodman diagram.

If a base line fatigue curve is required which excludes the design factors then for Type 304 stainless steel at temperatures up to 400ºC the following mean curve proposed by Jaske and O'Donnell /7.8/ could be adopted:

$$\sigma_{aJaske}(N) := 62610\,N^{-0.5} + 218 \qquad (7.2a)$$

where σ_a is the stress amplitude (MPa) and N is the number of cycles to failure. The equation is valid for cycles to failure, N, up to 10^8. Equation 7.2a expressed with strain amplitude, assuming E = 195 GPa, is:

$$\varepsilon_a = 0.321 \cdot (N)^{-0.5} + 1.118 \cdot 10^{-3} \qquad (7.2b)$$

More recently Chopra and Shack /7.9/ have proposed an alternative fatigue curve:

$$\ln(N) = 6.703 - 2.030 * \ln(\varepsilon_a - 0.126) \qquad (7.3)$$

where ε_a is the strain amplitude (%) and N is the number of cycles to a 25% drop in tensile stress. Caution should be exercised when using these latter two fits, as they contain no inherent margins of safety within the data.

The ASME design curve and the best-fit curve proposed by Jaske and O'Donnell are plotted together on Figure 7.1. New low cycle fatigue data presented by PSI /7.10/ are also included. The majority of the new data lie to either side of the Jaske curve, with the exception of one data point from Type 321H stainless steel.

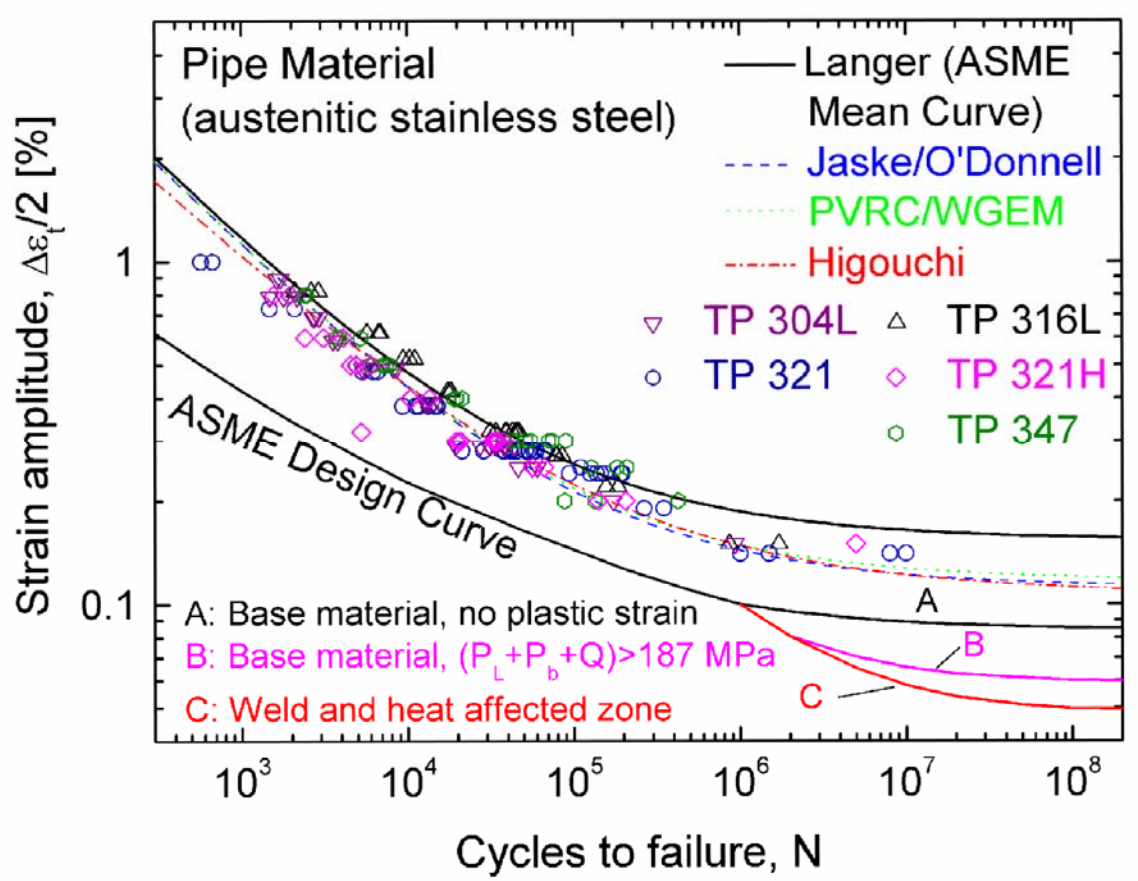

Figure 7.1: Comparison of data presented by PSI (/7.10/) with the ASME design curve for stainless steel.

7.2 Fatigue Reduction Factors

Advice exists within various codes and procedures to account for variables not accounted for by the safety factor applied to the endurance data. Use of the factors from the international procedures needs to be treated with caution because in some procedures the additional factor is applied to the endurance data, whereas in others it is applied as an enhancement to the elastically calculated stress range as part of the structural analysis. The advice of an appropriate expert should be sought where uncertainty or ambiguity exists.

7.2.1 Welds

The fatigue endurance of welded joints are designed or assessed based on the fatigue endurance of the parent material with a strength reduction factor applied to account for their observed inferior performance. These fatigue strength reduction (or weld usage) factors are applied to account for variables that may contribute to the early failure of weldments when compared to the parent material. Such variables include:

- metallurgical discontinuities across a weld (weld metal, fusion line, heat affected zone and base metal) whose differing stress-strain properties result in the deformation being concentrated in one or other of the constituent regions;
- surface finish effects;

- geometric discontinuities including misalignment;
- welding residual stresses;
- inclusions and voids.

The severity of the fatigue strength reduction factor applied will depend on the combination of the above factors. For instance if a weld has received a post weld heat treatment and has received a full NDT inspection then the latter two variables need not be considered. In addition if the geometrical discontinuity has been fully modelled in the stress analysis then an additional factor need not be applied. If the surface has been returned to its original condition following welding, then this need not be considered in the analysis. However, the metallurgical discontinuity is always present in a welded joint and it is unlikely that all the material regions (eg HAZ, strain affected zone) can be fully modelled in an assessment. The proposal is to adopt similar recommendations to RCC-MR in the code of practice, however the intention would be to include the factor 1.1 on strain to account for the material discontinuity, which is not present within RCC-MR (see Tables 7.1 and 7.2). Note though these factors were intended for use with globally applied loads and may be overly conservative for thermal striping loading which is a local phenomenon.

Table 7.1: RCC-MR weld strength reduction factors, *f*, on strain

Type of welded joint inspection and surface finish	**AUTHORISED**		**TOLERATED**
	I.1, I.2, I.3, III.1	**II.1, III.2**	**II.2, III.3, IV, V, VI, VII**
Volumetric examination or surface examination during welding (between passes). Dressed flush welds with good surface finish.	1.1	1.1	
Volumetric examination or surface examination during welding (between passes). As-welded joints where the profile is modelled.	1.25	1.25	
Surface examination after welding (both sides) with poor surface finish.	1.5		
Other examinations	2	2	4

Table 7.2: Proposed weld strength reduction factors (on strain) for common weld types.

Weld Geometry Schematic	RCC-MR Type	Definition/ geometry	f
	I.1	Dressed Butt Weld two sides accessible	1.1*
	I.1	Butt Weld two sides accessible	1.25
	I.2	Dressed Butt Weld two sides accessible	1.25
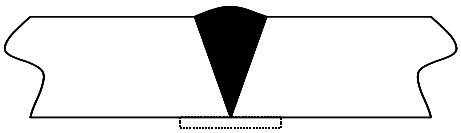	I.3	Butt Weld with temporary backing strip	1.5
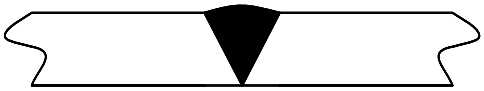	II.1	Butt Weld back side inaccessible	1.5
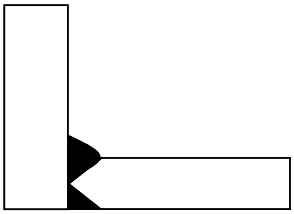	III.1	Dressed Full penetration Tee Fillet Weld Undressed	1.5 2
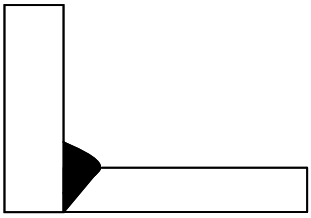	III.2	Full penetration Tee Fillet back side inaccessible Undressed	2 3

*Factor proposed for use with RCC-MR but not adopted

These factors are generally applicable to cases were the principal stress is at right angles to the welded feature. There is evidence to suggest that where the direction of the maximum principal stress is parallel to the weld then only a single factor of 1.25 is required to account for all the variables. A further Table 7.2 is included which gives examples of the weld geometries together with proposed strength reduction factors on strain.

7.2.2 Environmental Effects

The need for the inclusion of additional environment factors is debatable, as the data used in the construction of the original design curves were often not conducted in fully environmentally controlled laboratories. Thus it is possible that part of the scatter in the data was due to the presence of high levels of moisture or salt in the atmosphere. Some of the data were also produced at above ambient temperature and may include an oxidation effect. However Article B–2131 in Appendix B to Section III of ASME states that the owner's design specifications should provide information about any reduction to fatigue design curves that is necessitated by environmental conditions.

The applicability of ASME III fatigue design curves in LWR environments is still an issue of debate. The code itself does not give specific curves or quantitative factors for adopting the influence of coolant to fatigue calculation. Moderate environmental effects were accounted for through the design curve definition, but the responsibility of considering eventual environmental effects was left to the designer. This is clearly stated in the Criteria Document for the ASME III Design by analysis procedure as follows: "protection against environmental conditions such as corrosion and radiation effects are the responsibility of the designer".

Sensitivity studies on different water chemistry parameters have yielded a list of important parameters, which can influence the fatigue life of materials used in primary circuits. Some are listed below:

- Type, composition and heat treatment of material
- Oxygen content of coolant
- Service temperature
- Material impurities
- Strain rate.
- Coolant dosing agents such as lithium and boron.

In addition, flow rate seems to be an important parameter for carbon and low alloy steels, but possibly less important for stainless steels. Note that many factors need to be considered for assessing the possible environmental effects present in an LWR. In extreme cases, at particularly low strain rates, environmental effects may be significant, but certain thresholds need to be exceeded to observe notable environmental effects. It has been shown that moderate environmental effects are applicable to most plant transients. For example, if the strain rate is greater than 0.4%/s or the dissolved oxygen content of the water is >0.5ppm or the temperature is <180ºC then the factors in the ASME curve should adequately cover the effect of environment for stainless steels /7.9/. However for carbon steel the oxygen content of the water should be <0.5ppm. This illustrates that in some cases environmental factors may have opposite effects for different materials and operating outside these limits may introduce environmental effects. A further consideration is that environment effects are not

generally considered relevant in the high or very high cycle fatigue ranges associated with turbulent mixing.

So in general if the component being assessed is suspected of being subjected to a notable environmental effect then a relevant expert must be consulted or a conservative factor applied.

Finally, it should be noted that a discussion on plasticity correction factors is given in **Appendix D**.

7.3 References

7.1 ASME – Nuclear Boiler and Pressure vessel Code – Section III – ASME 2004

7.2 Cooper, W. E., "The Initial Scope and Intent of the Section III Fatigue Design procedure," in Welding Research Council, Inc., Technical Information from a Workshop on Cyclic Life and Environmental Effects in Nuclear Applications, Clearwater, Florida, January 20–21, 1992.

7.3 Harvey, J.E., Pressure Component Construction, Van Nostrand Reinhold Company, New York, 1980.

7.4 Porowski, J.S., et al., Fatigue Criteria for Remaining Life Assessment of Shell Structures Programme Plan, Submitted to the Subcommittee on Shells and Ligaments of the Pressure Vessel Research Committee, May (1988).

7.5 Manjoine, M.J. and Tome, R.E., Proposed Design Criteria for High Cycle Fatigue of Austenitic Stainless Steel, ASME Pressure Vessel and Piping Conference, Portland (1988) or ASME H00255, 51–57.

7.6 Design and Construction Rules for LWR Nuclear Islands, RCC-M, AFCEN, 2002

7.7 KTA 3201 Part 2 "Components of the Reactor Coolant Pressure Boundary of Light Water Reactors", Design and Analysis, June 1996.

7.8 Jaske C.E and O'Donnell W.J., Fatigue Design Criteria for Pressure Vessel Alloys, ASME 77-PVP-12, November 1977.

7.9 Chopra O.K. and Shack W.J., Environmental Effects on Fatigue Crack Initiation in Piping and Pressure Vessel Steels, NUREG/CR–6717, ANL–00/27, May 2001.

7.10 Leber H., PSI fatigue data supplied by private communication at CEA Headquarters Paris meeting, November 2005.

8 PROPOSED HIGH CYCLE FATIGUE ASSESSMENT PROCEDURE UNDER TURBULENT THERMAL LOADS

This section describes the proposed procedure for assessing the fatigue life of mixing tees subjected to turbulent mixing of the incoming fluids, Figure 8.1. The procedure is mainly intended for mixing tees of class 1, 2 and 3 piping systems without internal devices. The procedure may be applicable to other components, but that has not been investigated in this project. The piping system should be designed with a nuclear piping code, such as ASME III, RCC-M or similar.

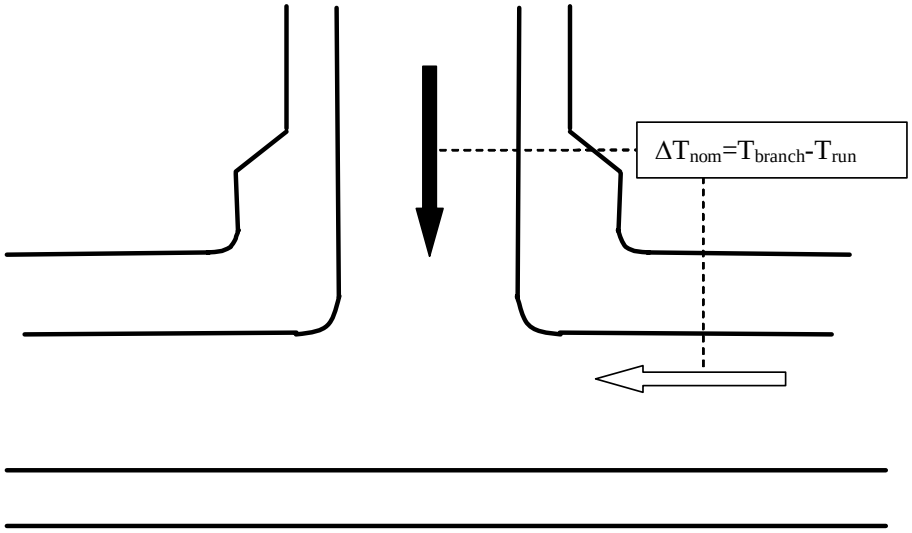

Figure 8.1: Definition of nominal ΔT for a given flow scenario at a mixing Tee

The proposed multi-level approach (Figure 1.1) has four levels:

- Level 1 uses a simple screening criteria expressed in terms of the (nominal) ΔT between the two mixing fluids.
- Level 2 requires no other information about the loads than the amplitude of the temperature variation. The stresses and strains are computed from a heat transfer analysis and elastic stress analysis assuming sinusoidal variation of the temperature. The usage factor is determined from the appropriate fatigue curve and the stress or strain variations at the surface using the frequency that gives the shortest duration.
- Level 3: the fatigue usage factor is determined by analysis of the complete local load spectra together with fatigue curves.
- Level 4 is based on fracture mechanics and deals with the calculation of the growth of detected or postulated crack-like flaws.

Generally the required amount and the quality of data increases with higher analysis level. The complexity of the analysis also increases but the user is rewarded by better accuracy. Conservatism should be built into each level but it decreases with the higher levels. In the following the first two assessment levels are described. Work on the 3rd and 4th levels is ongoing and will be completed as part of follow-up work to the current project.

8.1 Level 1: Screening Criteria

The screening criteria are intended as a simple way of assessing whether a particular Tee requires further fatigue assessment. The value is based on knowledge of the nominal temperature difference (Figure 8.1) between the two flows and weld reduction factor. The values for a particular material can be determined from experimental data or analysis.

For stainless steel (304, 304L, 316 and 316L), no specific fatigue analysis or fabrication improvements are necessary if

$$\Delta T_{nom} \leq 80^{o}C \text{ .} \qquad (8.1)$$

If ΔT_{nom} varies during operation, the criterion refers to its maximum value. K_r is the fatigue strength reduction factor.

For ferritic steels the corresponding value is**,**

$$\Delta T_{nom} \leq 50^{o}C \text{ .} \qquad (8.2)$$

This value for ferritic steel has less experimental support and should be further verified if used.
The values recommended above are based on the work reported by EDF in ref. /8.1/. The validity of these values in relation to the NESC operational case database is discussed in **Chapter 5** and to the analytical SIN-method in **Chapter 9**. For the application of the screening criteria only the nominal temperature variation, the steel type and fabrication data are required. An extension of the concept to include component specific details such the weld type (for austenitic steels the above value of 80°C was derived assuming a fatigue strength reduction factor K_r= 1.7 for un-flushed welds applied to the ASME design curve fatigue limit at 10^6 cycles) and the material fatigue limit, as well as potential environmental effects has been proposed in ref. /8.2/, but has not been validated.

8.2 Level 2: Sinusoidal method (SIN-method)

For the sinusoidal method the following data are required.

- *Load*; only the temperature variation in the fluids ΔT is needed as direct input. However for computation of heat transfer coefficient flow rates is also needed for the non-dimensional Reynolds and Prandtl parameters.
- *Heat transfer coefficient.* From direct measurements or computed.

- *Basic geometry:* only the wall thickness is directly used in the analysis. However, understanding the overall geometry may be important to take constraints into account. These may be accounted for as boundary conditions.
- *Material type and material properties*: basic mechanical and thermal properties such as thermal conductivity, cyclic stress strain curves, fatigue curves; all with temperature effects in the appropriate range.
- *Fabrication*: location and type of welds, surface finishing parameters, residual stresses

8.2.1 Basic steps

The basic assumption is that the temperature variation is described as sinusoidal. The total analysis includes the following four basic steps.

1) Thermal analysis with heat transfer between fluid and component by convection and conduction through the pipe wall. The temperature in the fluid is sinusoidal $T = \Delta T / 2 \cdot \sin(2\pi f \cdot t)$. ΔT the local temperature range, f is the frequency to be determined and t is time. This analysis is repeated for different temperature variations and frequencies.
2) The time dependent temperature distribution is used directly as input to an elastic stress analysis. The resulting stress or strain variation as function of the frequency is determined.
3) Appropriate reduction factors are then applied on the stress/strain variation.
4) The number of cycles for a specific ΔT is determined from the computed stress/strain variation and appropriate fatigue curves. The frequency, f, which gives the shortest life (in duration) is selected. This procedure is repeated for different temperature variations resulting in a curve which gives the fatigue life (in duration) versus temperature variation. The fatigue usage factor can be directly determined from the ratio between duration of the thermal load and the computed fatigue life at this temperature.

8.2.2 Uncoupled thermal stress analysis (Step 1 and 2)

The idealization that temperature variations are sinusoidal is more important for the fatigue life than details of the modelled geometry. Moreover the SIN method is a robust but rough method for fatigue life assessment. The heat transfer and stress analysis problems are therefore analysed with very simple geometries.

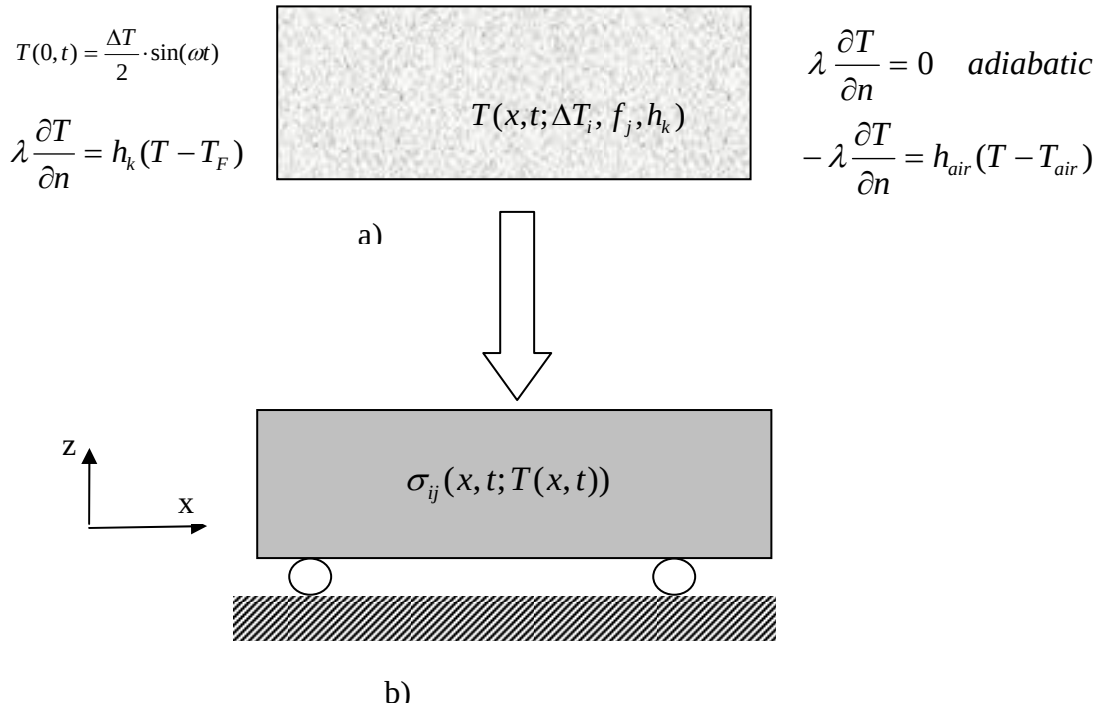

Figure 8.2: Schematic illustration of the uncouples thermal-stress analysis

The heat transfer analysis is generally one-dimensional. The fluid has a sinusoidal temperature variation and the heat is transferred from the fluid to the pipe by convection as illustrated schematically in Figure 8.2a). The value of the heat transfer coefficient has a large impact on the temperature distribution and consequently also for the resulting stresses and the computed fatigue life as illustrated below. The heat transfer coefficient is not a simple material property. It depends on the properties of the fluid as well as the pipe material, but it is also a function of the flow velocity. It is up to the user to use the best available estimate. The value used could be measured, computed from CFD calculations or derived from simple semi-empirical formulas such as the Colburn formula:

$$h = \lambda \cdot 0.024 \cdot \mathrm{Re}^{0.8} \cdot \mathrm{Pr}^{0.4} / D_h \ . \qquad (8.3)$$

Here λ is the water thermal conductivity in $(W/m/°C)$, Re and Pr the Reynolds and Prandtl non-dimensional numbers respectively and D_h the hydraulic diameter[2]. Formulas such as Eq (8.3) refer to an average heat transfer, which may differ from a local value. A typical value for h from measurements is $15000\, W/m^2/°C$. It should be noted that the adopted heat transfer is an approximate value and uncertainty by a factor 2-3 is not unusual.

The boundary condition at the other side of the pipe can be adiabatic or convection with air. The heat transfer coefficient for air is generally much lower than for water so the results are not very sensitive to the value used or if adiabatic conditions are assumed.

[2] $D_h = 4S/L$, where S is the internal cross section area of the pipe and L the internal length of the section.

The time dependent temperature distribution in the pipe,

$$T(t, x; \Delta T_i, f_j, h_k), \tag{8.4}$$

is computed by the standard one-dimensional Fourier heat conduction analysis and the boundary conditions. The temperature field is subsequently used directly in the elastic stress analysis as schematically illustrated in Figure 8.2b). The computed stresses and strains depend on the assumed geometry. As discussed above simple geometries such as plate or axisymmetric thick pipes are recommended. In addition boundary conditions can also be used to model various levels of constraint as discussed in the next chapter. The thermal analysis and the stress analysis can be performed using semi-analytical methods or more general method such as finite elements. One implementation is described in Appendix B. Figure 8.3a) shows computed stress range at the inner surface of the pipe versus the frequency for an axisymmetric geometry for different Biot numbers ($Bi = h \cdot H / \lambda$) where *h*, *H* and λ denote heat transfer coefficient, wall thickness and thermal conductivity respectively. The stress range, $\Delta\sigma^* = \Delta\sigma(1-\nu^2)/(E\alpha)/\Delta T$, as well as the frequency, $f^* = f\rho c_p H^2/\lambda$, are presented as dimensionless quantities. Here *E*, ν, α, ρ, λ and c_p denote the Young's modulus, Poisson's number, thermal expansion coefficient, density, heat conductuctivity and specific heat respectively. The results can therefore be adjusted to changes in geometry or material properties. The Biot number gives a relation between the heat transfer between fluid and heat conduction. Figure 8.3b) shows the corresponding stress range distribution through the thickness. The peak stress amplitude and the frequency for which the peak stress is attained increases with the Biot number. It is obvious that the stress amplitude will have a maximum at a certain frequency. The stress amplitude may formally be written as

$$\Delta\sigma(f; \Delta T_i, h_k). \tag{8.5}$$

The Biot numbers are typically in the range 5–50 whereas the frequency factor $\rho c_p H^2/\lambda$ could be between 5 and 100 for a typical austenitic steel and pipe geometry[3].

[3] Typical values for 316L are $\rho = 8 \cdot 10^3 kg/m^3$, $c_p = 480$ J/kg/K, $\lambda = 15$W/m/K , $\alpha = 17 \cdot 10^{-6}$ /K, E = 185 GPa. *Typical wall thickness is 5 – 30 mm.*

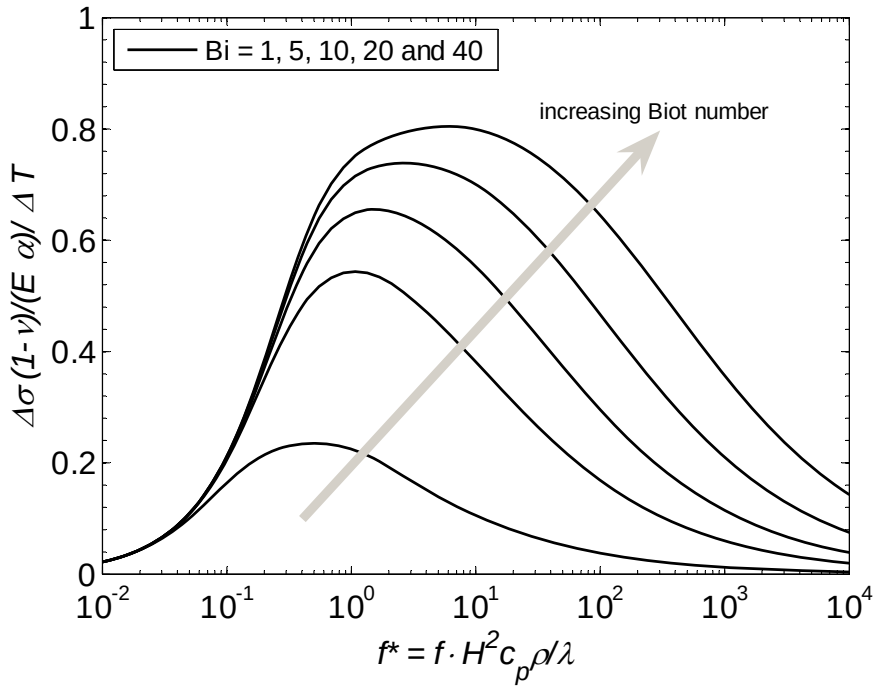

a)

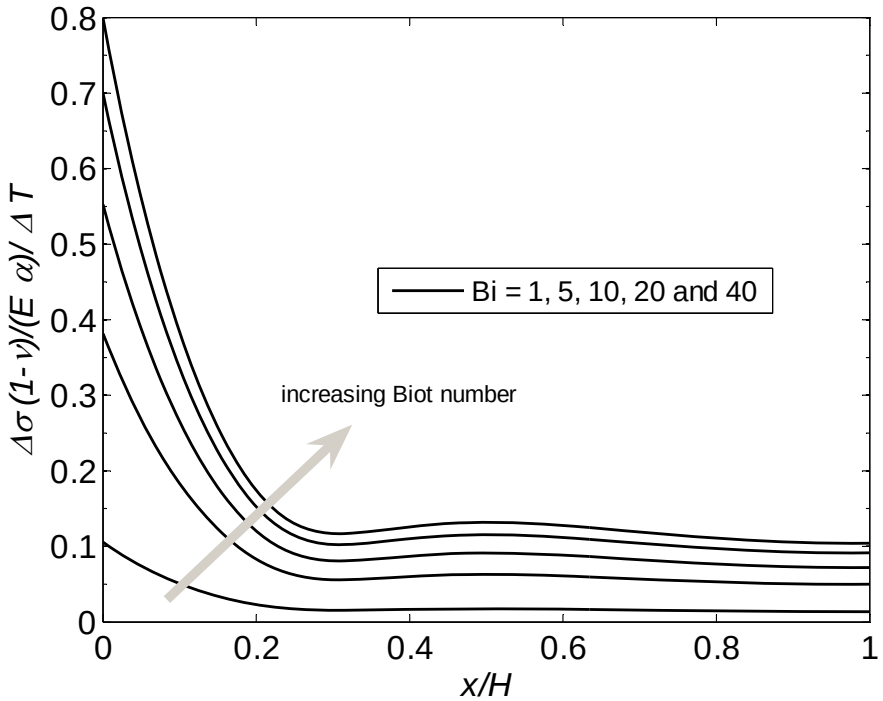

b)

Figure 8.3: a) Normalized stress range for different Biot number) a) surface stress versus frequency b) Through thickness distributions at the frequency $f^* = 10$.

8.2.3 Correction factors for load amplitude (Step 3)

When applied in a fatigue analysis the stress amplitude needs to be adjusted for the appropriate reduction factors

$$\left.\begin{aligned}\Delta\sigma_{app} &= \Delta\sigma \cdot \frac{E_C}{E} \cdot K_r \cdot K_\nu \\ \Delta\varepsilon_{app} &= \frac{\Delta\sigma}{E} \cdot K_r \cdot K_\nu\end{aligned}\right\}. \tag{8.6}$$

Here K_r is the fatigue strength reduction factor and K_ν the plastic strain amplification due to bi-axial thermal stresses (Figure 8.4) as discussed in Appendix B. E is the material Young's modulus whereas E_c is the Young's modulus inferred from the fatigue curve. The latter is needed since fatigue curves are generally derived from controlled strain tests. Strain amplitudes can be used instead of stress amplitudes and $E_C = E$. It should be emphasized that austenitic steels have a very low yield stress and the plasticity correction factor has a significant effect even when the loading is not in the long-cycle fatigue range.

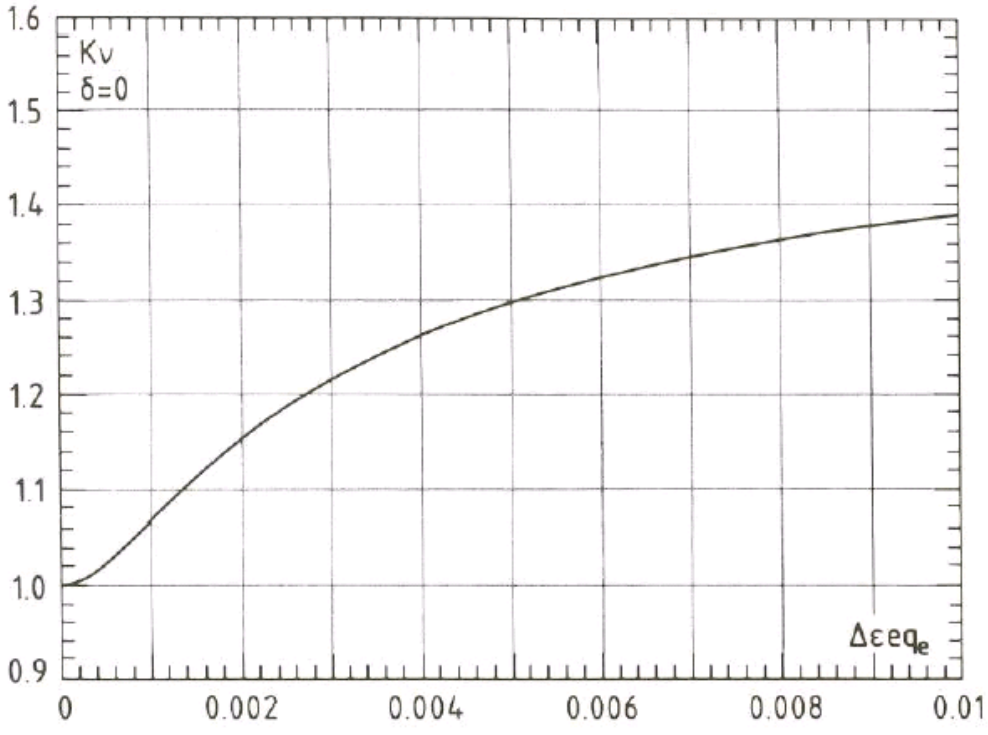

Figure 8.4: Plastic correction factor for the biaxial case.

8.2.4 Fatigue Life Assessment (Step 4)

For a given temperature variation ΔT , heat transfer coefficient, *h*, material properties and pipe thickness, the number of cycles for failure can be inferred directly from the material's fatigue curve,

$$N(\Delta\sigma_{app}(f;\Delta T_i)). \tag{8.7}$$

It is recommended that the equivalent stress amplitude based on Tresca or von Mises is used rather than a stress component. The corresponding duration is given by the number of cycles divided by the frequency. There is a frequency for which the duration is minimized. We refer to this as the admissible life. To find its value requires that we solve the optimization problem:

$$D_{Adm,i}(\Delta T_i) = \min\left\{\frac{N(\Delta\sigma_{app}(f;\Delta T_i))}{f}\right\}. \tag{8.8}$$

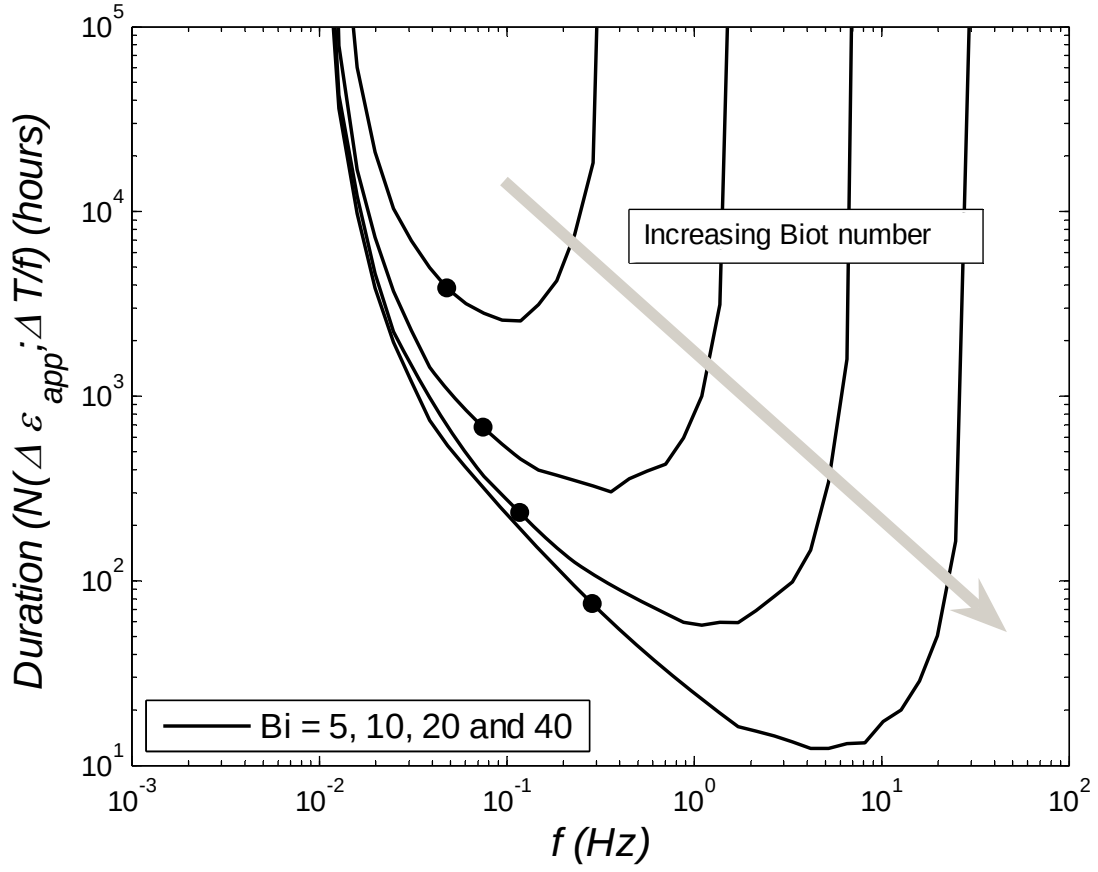

Figure 8.5: The life function N/f versus the frequency, $\Delta T = 160°C$, H = 9.6 mm. The circles indicate the frequency at which the stress amplitude has its peak value.

The stress transition curves as well as the fatigue curves are generally smooth functions and the optimization scheme to determine the admissible life can be solved by simple Newton-Rapson scheme. Figure 8.5 shows the curve N/f when the stress amplitude has been taken directly from Figure 8.3a) for the Biot numbers 5, 10, 20 and 40, with $\Delta T = 160°C$ and thickness H = 9.6 mm, material properties as in the footnote and the Jaske mean curve. The filled circles denote the frequency at which the peak stress range is attained. The frequency that gives the admissible life is generally slightly higher than the frequency with the highest stress amplitude. This effect increases with the Biot number.

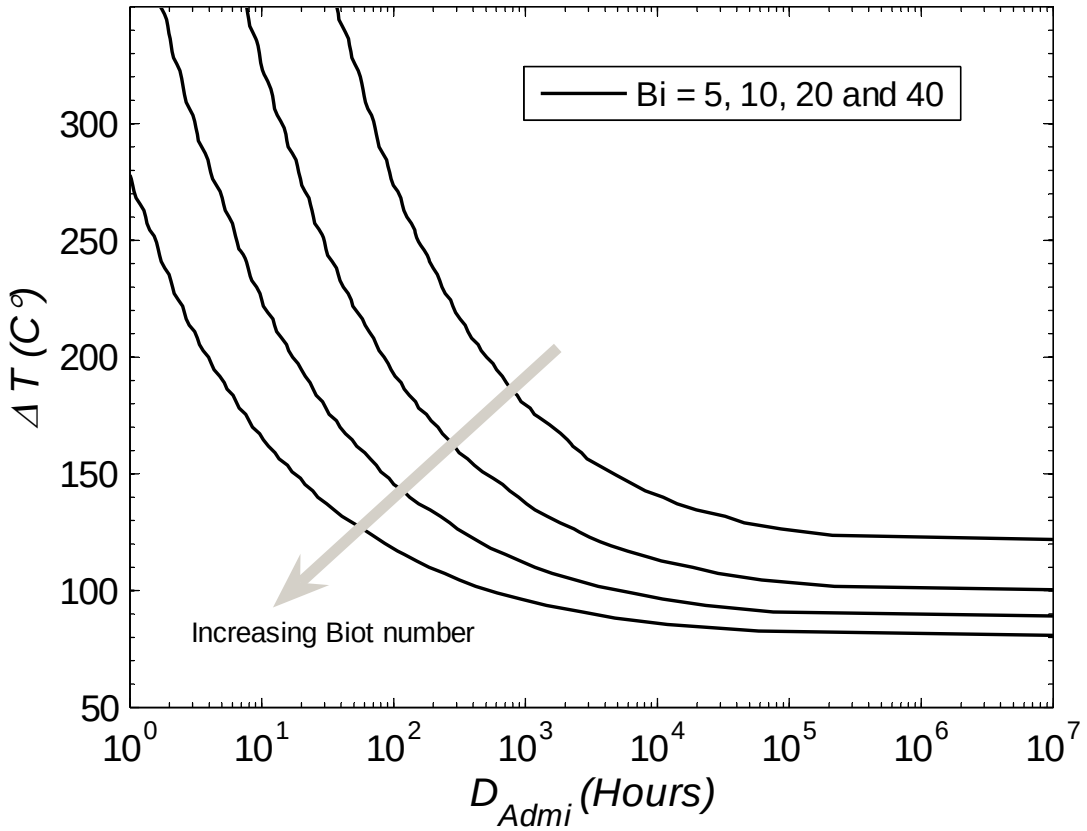

Figure 8.6: Computed fatigue life reference curve using the SIN-method for the temperature variation, $K_r = 1.25$, K_v as described in Appendix B and Jaske mean curve.

A thermal fatigue life curve describing the admissible life versus the temperature variation can then be derived by repeating this procedure for different values of ΔT. Typical computed fatigue life curves are shown in Figure 8.6 using the Jaske mean curve for austenitic steel,

$$N = \left(\frac{0.321}{\Delta \varepsilon_{app} - 1.185 \cdot 10^{-3}} \right)^2 \quad . \tag{8.9}$$

material data in the footnote, wall thickness H = 9.6 mm and weld correction factor 1.26. A heat transfer value of 15 000 and 30 000 $W/m/°C$ correspond in this case to Bi = 10 and 20 respectively. Clearly the value of the heat transfer coefficient has a very large impact on the computed life.

The usage factor, F_u, is directly given by the ratio between the duration the component has been subjected to the temperature load, D_i, and the computed admissible life

$$F_{u,i} = D_i / D_{Adm,i} \,. \tag{8.10}$$

If the durations for different temperature variations of a component are known ($D_i, \Delta T_i$) then the total usage factor is computed from a Miner-Palmgren damage accumulation,

$$F_u = \sum_{i=1}^{N} D_i / D_{Adm,i} \,. \tag{8.11}$$

8.2.5 Application of SIN method

The SIN-method should normally give conservative fatigue life estimates. There are two major modelling aspects that contribute to this conservatism.

- Firstly, of all frequencies, the admissible life, $D_{Adm,i}$, is based the frequency that minimizes the life. The local frequency in the pipe can be quite different.
- Secondly the stresses and strains have their maximum value at the inner surface. The peak stress/strain at the surface is used in the fatigue life assessment but the fatigue curves are derived from specimens with constant stress/strain distribution. For instance if the wall thickness is increased then the Biot number increases, and as seen from Figure 8.3, the peak stresses increase and the fatigue life is decreased. In reality the fatigue initiation would be faster due to the higher peak stresses but the total life would increase since the crack propagation phase would be longer. A more detailed discussion can be found in Appendix B on the stress distribution with respect to initiation and crack propagation.

The assumption that the temperature varies sinusoidally may results in non-conservative stress amplitudes, in particular for lower frequencies. This aspect is further discussed in the Appendix B where results based on sinusoidal and square shaped temperature variations are compared. The SIN method is based on simple geometries. There may be three-dimensional effects from pipe geometry and local variations in the temperature field that increase the local peak loads.

As seen in Figure 8.6, the value of the heat transfer coefficient influences strongly the computed fatigue life. As discussed above, there is no precise value for the heat transfer coefficient. A too low value would reduce the conservatism in the analysis. The user should use his best judgement for the selection of *h*. It should be noted though that a higher heat transfer coefficient increases the computed peak stress gradient at the surface wall (which is accounted for in the analysis) but the positive effect that the stress gradient increases at the wall and the stresses decay is not accounted for. The overall effect is therefore exaggerated by the SIN method.

The temperature variation used in the analysis should correspond to the local temperature variation, which is normally lower than the nominal temperature difference between fluids in the two branches. Measurements from operational experience and mock-ups indicate that the

local temperature difference is 80% or less of the nominal value. To avoid undue conservatism this 80% rule can be used for the SIN-method,

$$\Delta T = 0.8 \cdot \Delta T_{Nom} . \qquad (8.12)$$

The choice of the fatigue curves has a very significant effect on the computed fatigue life. The fatigue curve to be used depends on the purpose of the analysis and it is up to the user to select a proper curve and to provide the rationale for his choice. The design fatigue curve is the natural candidate for design of components whereas a mean curve is the natural choice to assess the life of components in the operational phase. The fatigue evaluation may be based on a rather traditional approach as suggested for example by ASME or RCCM-R. Note also the fatigue curves proposed by Jaske et al (see **Chapter 7,** ref. /7.8/) are suitable for use with the SIN-method. This reference contains mean failure probability curves as well as design curves. The curves are also extended to have a fatigue limit at $N=10^8$ cycles which is in contrast to curves with the fatigue limit at $N=10^6$ cycles.

The analysis can be based on strain as well as stress variations. The stress approach is more commonly used by engineers but the strain approach is more logical, in particular for low cycle fatigue, since fatigue curves are generally based in strain controlled tests.

Note that the thermal fatigue curve as illustrated by Figure 8.6 gives an endurance limit for the temperature variation. This value can be used as the screening value in Level 1. The temperature variation should then be based on the nominal temperature amplitude. This will be further discussed in the next chapter.

8.3 References

8.1 C. Faidy, 'Thermal Fatigue in Mixing Areas: Status and Justification of French Assessment Method', Proc. 3rd Int. Conf. on Fatigue of Reactor Components, EPRI 1011958, 2005.

8.2 C. Faidy, European Thermal Fatigue Procedure, version A3, distributed to NESC-TF project participants in January 2005

9 APPLICATION EXAMPLES

9.1 Modelling and assumptions

In this section implementations of the sinusoidal method by NRG and Inspecta are presented. The analyses are uncoupled thermal stress analyses where the temperature fields are input to the stress analysis as illustrated in Figure 8.2. The thermal problem is one-dimensional in both cases. On one edge a sinusoidal temperature variation is applied in the assumed fluid which is transferred to the inner surface of the component by convection whereas the other edge has adiabatic conditions. The computed temperature field is used as input to the elastic stress analysis. For the stress analysis Inspecta assumes axial symmetry and globally unconstrained ends whereas NRG adopted a plate model with different boundary conditions at the edge of the plate.

The results of the computational predictions are evaluated and compared with the EDF cases (1-14) described in section 5.2.5. These cases are relatively well documented and enable relevant evaluation of the method. Furthermore the sensitivity to the different model implementations and assumptions are also investigated.

9.1.1 Cylindrical model

An axi-symmetric finite element formulation was used to determine the time dependent temperature distribution $T(t,x;\Delta T_i, f_j, h_k)$. There is no heat transfer through the outer surface (adiabatic condition). Depending on the type of time variation the system equation may be solved either in the frequency domain or by direct time integration. Since the edges are traction free all stress components and strains are given by the expression from the computed temperature field:

$$\begin{cases} \sigma_x(r) = \dfrac{E\alpha}{(1-\nu)}\left(\dfrac{2I_1}{r_o^2-r_i^2} - T(r)\right) \\ \sigma_\theta(r) = \dfrac{E\alpha}{(1-\nu)r^2}\left(\dfrac{(r^2+r_i^2)I_1}{r_o^2-r_i^2} + I_r(r) - r^2T(r)\right) \\ \sigma_r(r) = \dfrac{E\alpha}{(1-\nu)r^2}\left(\dfrac{(r^2-r_i^2)I_1}{r_o^2-r_i^2} - I_r(r)\right) \\ \tau_{x\theta} = \tau_{r\theta} = \tau_{xr} = 0 \end{cases} \quad ; \quad \begin{cases} I_1 = \int_{r_i}^{r_o} T(r)\cdot r\cdot dr \\ I_r(r) = \int_{r_i}^{r} T(r)\cdot r\cdot dr \end{cases} \tag{9.1}$$

Further details of the implementation of the cylindrical model can be found in Appendix B.

9.1.2 Plate model

The model adopted by Inspecta is based upon a cylinder heated at the internal surface. Internal constraint in the circumference is inherently imposed as a function of geometry defined in terms of cylinder radius and wall thickness. This model is representative if the

temperature variation occurs over a large area. Self-equilibrating stresses are induced in the axial direction by the component's internal constraint. However, if temperature fluctuations are more localized as "hot spots", constraint is also exerted by the surrounding and underlying material. This imposed constraint may have a significant influence on the resulting fatigue behaviour. To consider this aspect in more detail, NRG developed a simplified plate model with resulting moments and forces are imposed at the plate edge to model the constraint (Figure 9.1).

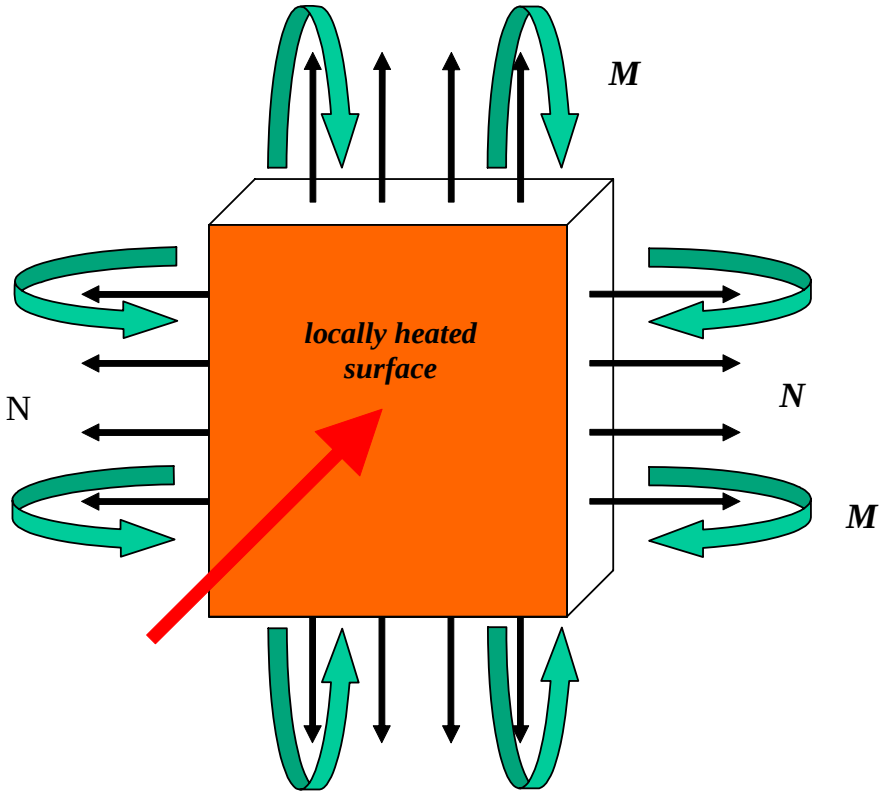

Figure 9.1: Local Plate Model, allowing membrane and bending constraint (NRG)

The response to a sinusoidally varying bulk fluid temperature is described using a conventional 1-dimensional heat transfer analysis as outlined above. The biaxial stress field can be described by:

$$\sigma_{xx}(x) = \sigma_{yy}(x) = -\frac{\alpha E}{1-\nu} T(x,t) + Cx + D, \qquad (9.2)$$

where C and D are constants that depend on the constraint conditions. In the case of globally free edges the expression becomes:

$$\sigma_{zz}(x,t) = \sigma_{yy}(x,t) = \frac{\alpha E}{1-\upsilon}\left(-T(x,t) + \frac{1}{H}\int_0^H T(x,t)dx + \frac{12\left(y - h/2\right)}{H^3}\int_0^H T(x,t)(y - H/2)dx \right) \qquad (9.3)$$

In /9.5/ details are provided of thermal stress profiles for which constraint levels are varied independently in orthogonal directions on the wall surface. In the present work this full flexibility has not been invoked. Instead, since 'hotspots' occur locally, it is assumed that locally constraint at the surface is uniform in the plane of the surface and essentially provided by the surrounding material.

A finite difference formulation was adopted for the stress analysis, thus allowing cyclic conditions to be implemented efficiently. The routine generates surface stress levels for the symmetric constraint conditions indicated in Figure 9.1:

- no constraint,
- full constraint (clamped),
- bending constraint; and
- membrane constraint.

For an unconstrained case the through-thickness temperature variation will bend and expand/contract the plate. In the clamped case both these global deformations are suppressed. In the constrained bending case moments act along the plate edge with a magnitude that exactly cancels the thermal bending. In the membrane constraint case the resulting force cancels the expansion/contraction of the plate centre line.

9.2 Analysis cases

The EDF generic failure cases for operational with tees in operation were chosen for the evaluation of the SIN-method. Details are given in Table 5.4. Note that 14 different combinations of damage location are reported. Essentially there are four different geometries, including two pipe geometries as well as the tee itself, where the wall thickness locally is higher. The geometries are shown in the Figures 5.8-10. The dimensional and material data used in the calculations are given in Tables 9.1 and 9.2. Different fatigue reference curves were also considered as part of the exercise.

Table 9.1: Geometrical data.

Geometry type	***D***	***t***	**Corresponding pipe type**
A	273	9.6	Pipe
B	324	12.7	Pipe
C	273	25	Tee section
D	324	25	Tee section

Table 9.2: Material properties data.

$C_p\left[\frac{J}{kg\cdot C}\right]$	$\lambda\left[\frac{W}{m\cdot C}\right]$	$\rho\left[\frac{kg}{m^3}\right]$	$\alpha\left[\frac{1}{C}\right]$	$E\left[\frac{N}{m^2}\right]$	v
533	17.2	7800	$18.02\cdot10^{-6}$	184 GPa	0.3

9.3 Computational results

9.3.1 Cylinder Model

Two types of fatigue curves are used in the evaluation, a *mean curve* and a d*esign curve*. The former is based upon the mean endurance response for austenitic steels provided by Jaske and O'Donnell /9.1/. The latter is derived with the conventional factors of 2 and 20 applied to stress amplitude and mean cycles to failure respectively, consistent with the ASME approach. The two curves are shown in Figure 9.2. A list of the parameters used for each of the so-called analysis cases is shown in Table 9.3.

Table 9.3: Analysis cases considered.

Case	Model	Fatigue curve**	80%-rule	Plasticity correction factor	Fatigue correction factor	Heat transfer coefficient $W/m^2/K$
I	Cylindrical	Mean	Yes	K_υ	$K_r = 1.25$	$h = 15000$
II	Cylindrical	Mean	Yes	K_υ	$K_r = 1.25$	$h = 30000$
III	Cylindrical	Design	No	No	No	$h = 15000$
IV	Plate*	Design	Yes	No	No	$h = 15000$

* Consideration of mechanical constraint
** No environmental correction considered

The choice of fatigue life reduction factor for cases I and II is based on the description in chapter 7.2; $K_r = 1.25$ is applied for both the un-flushed welds and the base material. This should possibly imply some very slight over-conservatism for the base material but is considered a reasonable approximation.

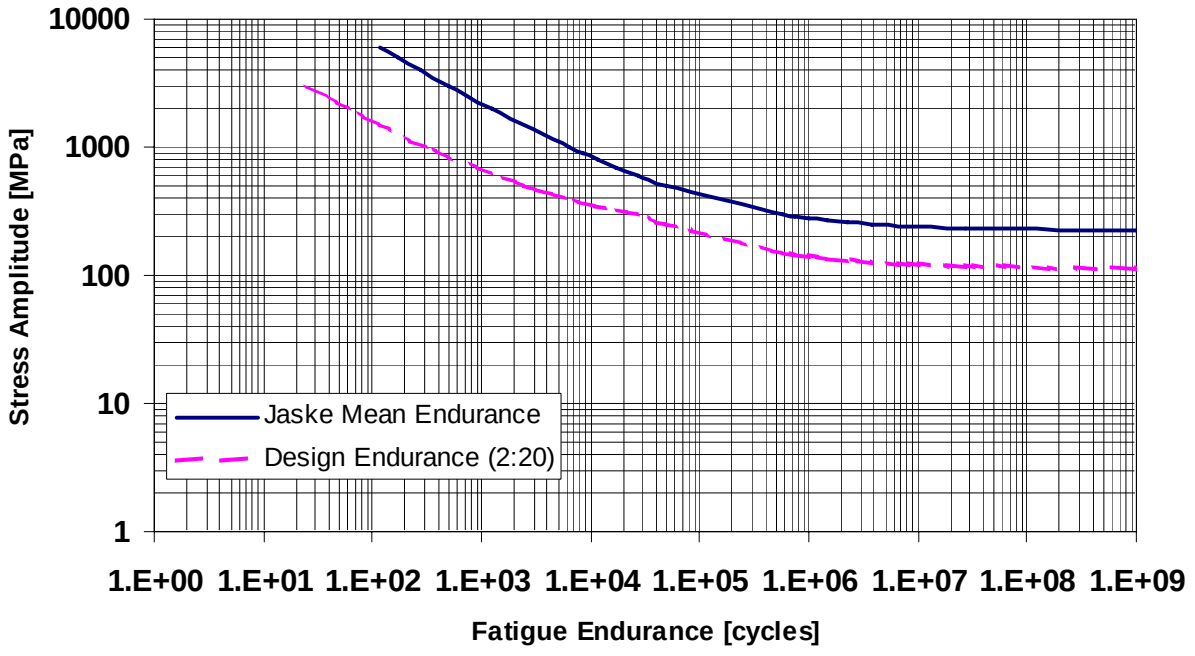

Figure 9.2: Mean and design fatigue curves (from Jaske and O'Donnell /9.1/).

The plasticity correction factor is applied assuming a cyclic plasticity response comparable to that for standard type austenitic steel material. The cyclic stress-strain curve used is shown in Figure 9.3 and is defined by:

$$\Delta\varepsilon(\%) = 100 \cdot \frac{\Delta\sigma}{E} + \left(\frac{\Delta\sigma}{K}\right)^{\frac{1}{m}} \qquad (9.4)$$

where $\Delta\sigma$ is the stress range in MPa, $\Delta\varepsilon$ is the strain range in %, K and m are material constants (K = 712 and m = 0,351) and E is Young's modulus

The objective in analysis cases I and II is to compare best-estimate predictions with the reported operational data, so that theoretically the usage factor should be close to unity i.e. U=1. However, the loading and other important parameters differ between the standard uniaxial specimen fatigue tests used to define the fatigue curve and the actual components, so that deviations from unity are to be expected.

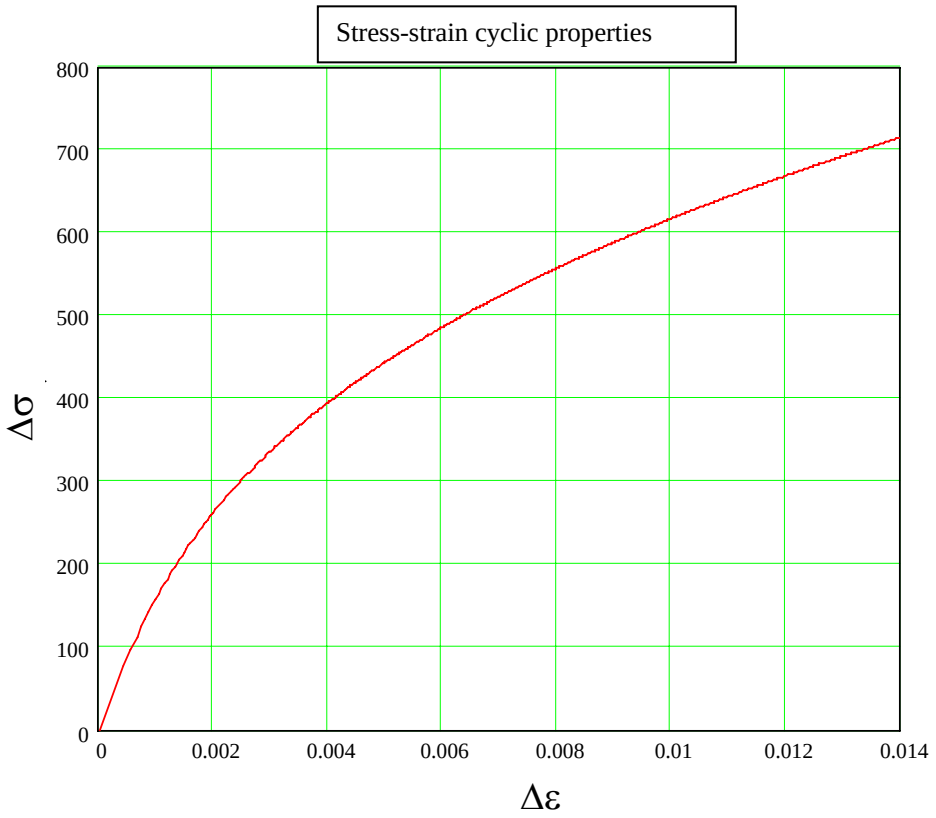

Figure 9.3: Cyclic stress-strain properties applied for the austenitic material

The computed thermal fatigue damage reference curves are shown in Figures 9.4-9.5 for each of the analysis cases, where the symbols indicate the computed duration, $D_{Adm,i}$, for the reported temperature ranges ΔT_i in the EDF cases. The corresponding results and usage factors are reported in Tables 9.4-9.5. The usage factors are calculated from the Miner-Palmgren damage accumulation relation, Eq, (8.10). It is interesting to note that the mean curve results for case I give a usage factor consistently below 1 whereas the results for case II

are closer to unity. This suggests that the heat transfer coefficient might be set higher than the value $h = 15000\ \mathrm{W/m^2/K}$ proposed in the present version of the procedure. A higher heat transfer coefficient is in line with through wall measurements of cyclic down-shocks by JRC /4.26/. However all cases with the design curve, analysis case III (Figure 9.6), give usage factors well above unity, so this potential non-conservatism becomes a negligible factor. It should also be noted that no correction factors are applied in this case, which would further increase the usage factors. For comparison with the plate model, the case where the 80% rule is applied to the design curve was also performed. The usage factor was reduced by a factor 2 compared to the case with the nominal temperature difference. Calculations were also done when the plasticity correction factor for cases I and II was set to 1. The usage factor then decreases significantly. This is also expected because of the early onset of plastic deformation in the cyclic stress-strain curve.

Table 9.4: Fatigue life results for the analysis cases.

Nominal Temperature load	**Geometry Class**			
	Analysis Case I			
ΔT, °C	**A**	**B**	**C**	**D**
100	Infinite	Infinite	Infinite	Infinite
135	3.61E+05 h	45226 h	10670 h	10744 h
165	3406 h	2455 h	1404 h	1406 h
	Analysis Case II			
ΔT, °C	**A**	**B**	**C**	**D**
100	Infinite	Infinite	Infinite	Infinite
135	4042 h	2697 h	1557 h	1571 h
165	408 h	351 h	283 h	283 h
	Analysis Case II			
ΔT, °C	**A**	**B**	**C**	**D**
80	4666 h	3684 h	2542 h	2548 h
120	348 h	301 h	235 h	235 h
150	101 h	91 h	77 h	77 h

Table 9.5: Usage factors for the analysis cases.

EDF Case	**1**	**2**	**3**	**4**	**5**	**6**	**7**	**8**	**9**	**10**	**11**	**12**	**13**	**14**
Analysis Case I														
Pipe	0.03	0.27	0.22	0.50	0.55	0.63	0.26	0.42	0.21	0.27	0.46	0.39	0.43	0.01
Tee	0.11	0.48	0.55	1.27	1.02	1.59	0.47	0.75	0.53	0.67	1.17	0.99	1.07	0.14
Analysis Case II														
Pipe	0.34	1.92	1.89	4.32	4.07	5.41	1.90	2.99	1.80	2.28	3.98	3.35	3.66	0.38
Tee	0.58	2.42	2.78	6.37	5.21	8.03	2.41	3.78	2.68	3.36	5.87	4.98	5.38	0.96
Analysis Case III														
Pipe	2.0	8.0	8.0	18.5	17.6	23.4	8.0	12.4	7.9	9.7	17.0	14.6	15.5	4.2
Tee	2.8	9.5	10.7	24.6	21.1	31.1	9.6	14.8	10.5	12.9	22.6	19.5	20.5	6.3

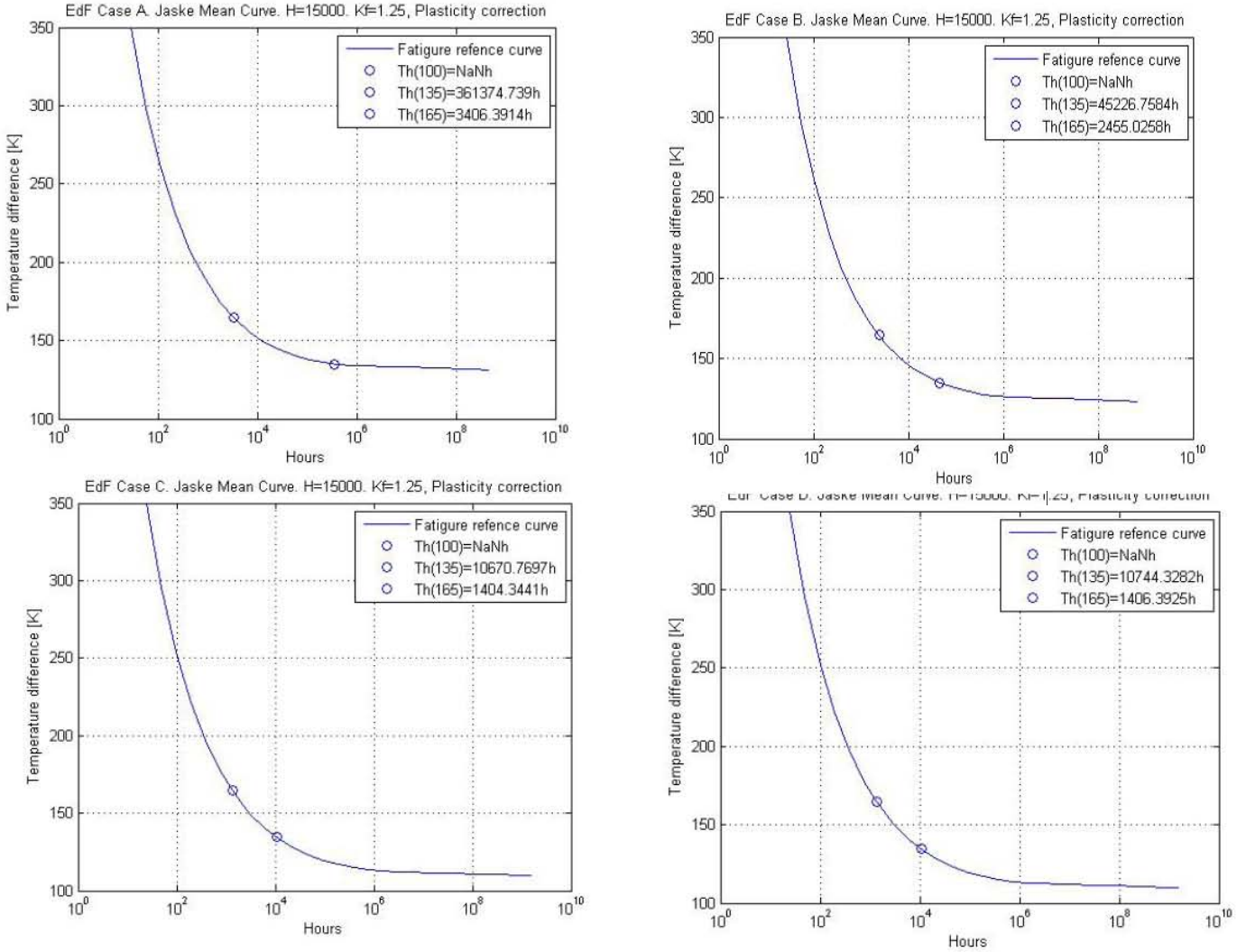

Figure 9.4: Fatigue reference curves for analysis case I.

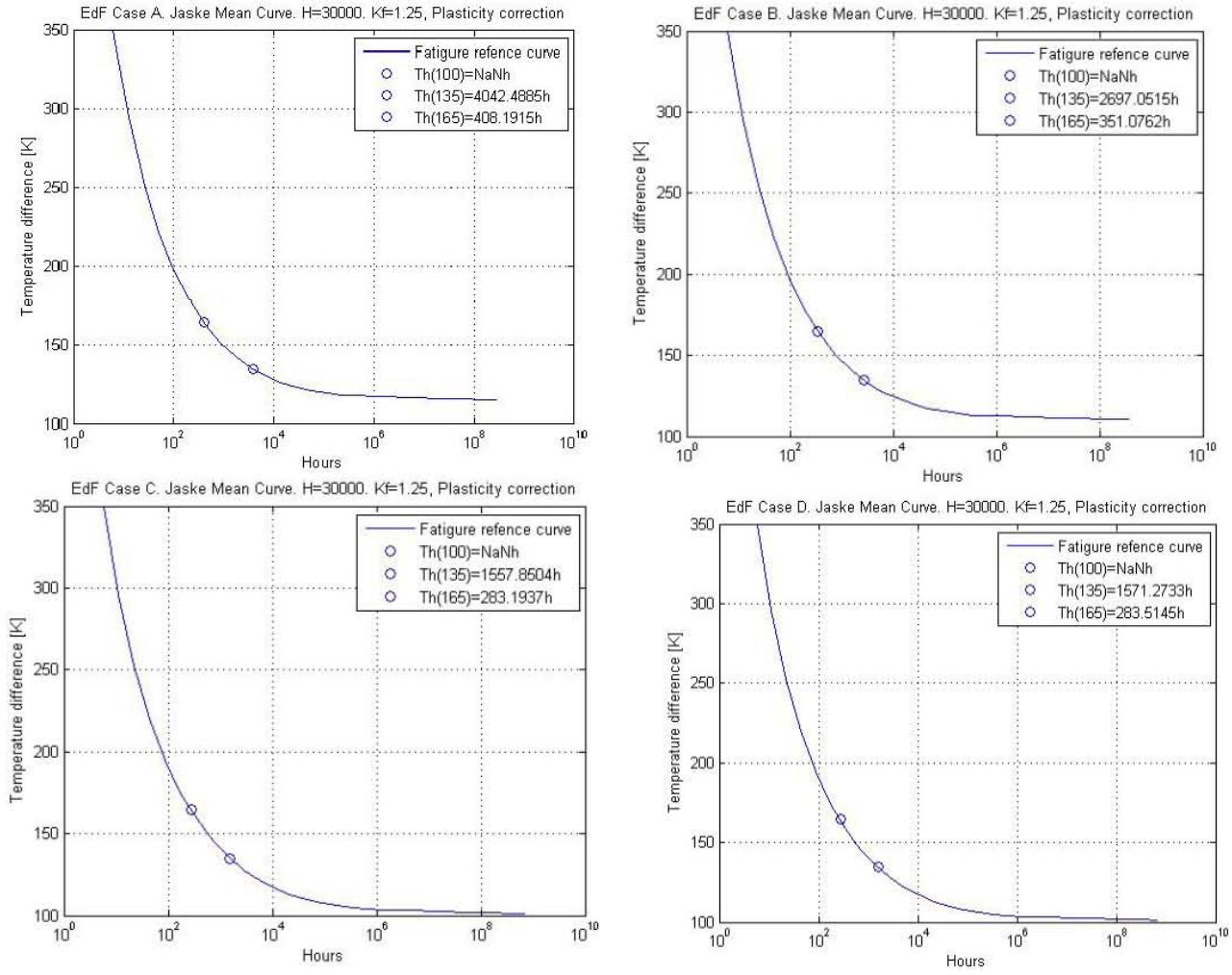

Figure 9.5: Fatigue reference curves for analysis case II.

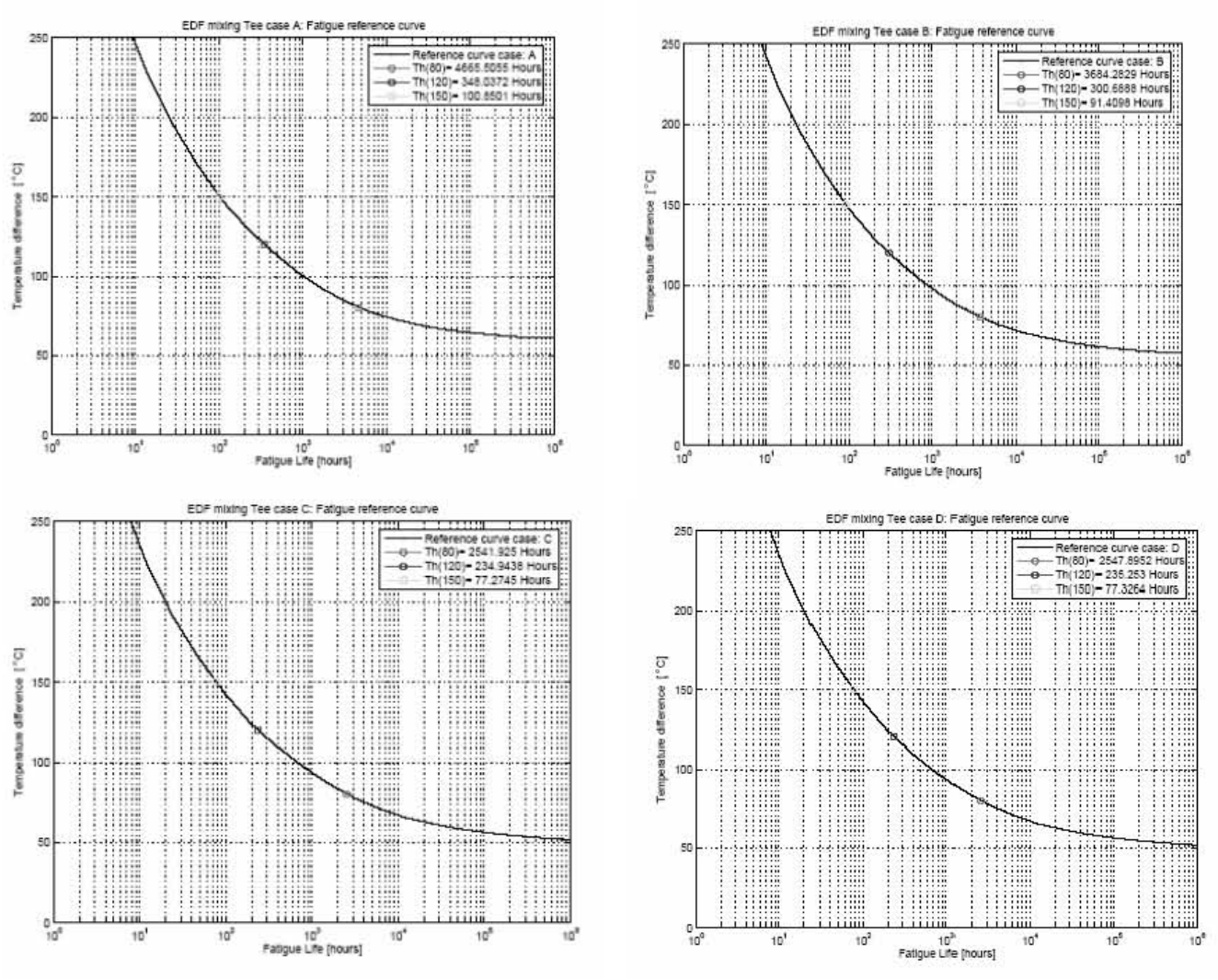

Figure 9.6: Fatigue reference curves for analysis case III

9.3.2 Plate Model

For the plate model, the full constraint option is the most conservative. Table 9.6 and Figure 9.7 present the initial assessment results with the predicted lifetime in hours for a range of temperature differences between the main fluid flows, using ASME design curves. In the first instance, thermal response is based on 80% of the bulk fluid temperature difference. Specifically indicated on the figure are the lifetimes associated with temperature differences of 80, 120, 150 and 180 °C, in line with the temperature ranges defined in the EDF cases. In the case of the fully constrained model the predicted response is independent of wall thickness. Also included in Figure 9.7 is a prediction based upon 100% of the bulk temperature difference between the hot and cold flows. As expected, the predicted lifetimes are consistently shorter.

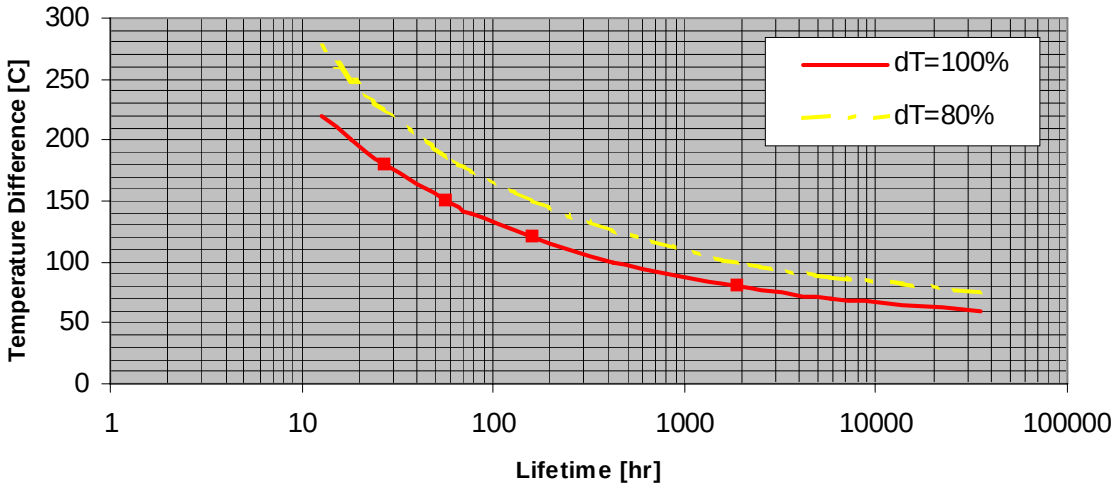

Figure 9.7: Fatigue temperature reference curve, fully constrained model, 100% and 80% bulk temperature difference

Table 9.6: Summary of NRG results, full constraint, 80% temperature difference, h=15000 $W/m^2/K$

Fluid ΔT, °C	87.5	100	125	150	175	187.5	225	250
Wall ΔT, °C	70	80	100	120	140	150	180	200
Frequency, Hz	0.052	0.095	0.200	0.316	0.457	0.525	0.743	0.906
Δσ/2, MPa	135.3	143.9	161.1	177.4	191.3	198.6	219.4	231.4
Lifetime, hrs	5756.3	1895.0	428.1	160.6	77.7	57.4	27.0	18.2
Lifetime, years	0.66	0.22	0.05	0.02	0.01	0.01	0.00	0.00
Lifetime, cycles	1.088E+06	6.515E+05	3.075E+05	1.828E+05	1.279E+05	1.085E+05	7.234E+04	5.921E+04

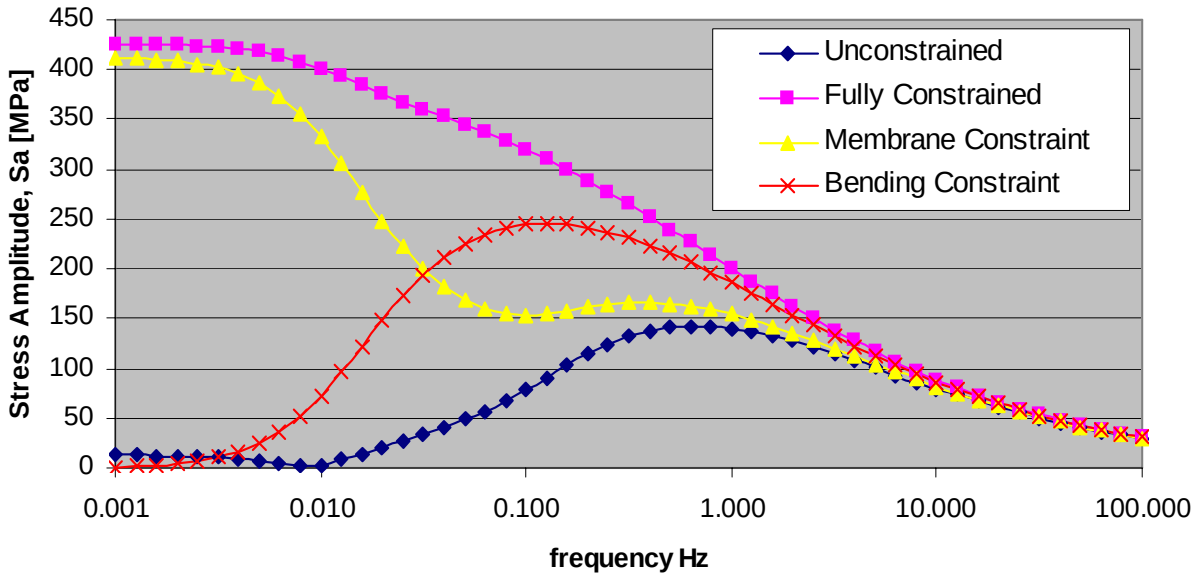

Figure 9.8: Thermal stress amplitude versus frequency. Constraint options: unconstrained; fully constrained, membrane constraint, bending constraint

In Figure 9.8 surface stress amplitudes are presented as function of frequency, based upon the four constraint options: no constraint; full constraint; membrane constraint; bending constraint. The example uses a 9.6mm wall thickness scenario. At high frequencies the stress amplitude tends towards zero, independent of the constraint option chosen. This is consistent with the expectation that when temperature fluctuations are sufficiently rapid the wall has no time to respond thermally. At intermediate and lower frequencies surface response is quite sensitive to the chosen constraint model. At low frequencies, quasi-static conditions are achieved with essentially a stationary linear temperature distribution[4]. Under full constraint, a combination of bending and membrane stress conditions results. The exact stresses depend on the initial stress free condition and the heat transfer assumption at the outer wall. When the plate edges are unconstrained the static stresses will be zero. At intermediate frequencies, variations in stress amplitude reflect the constraint options, through-wall force and compatibility requirements, and the conduction and local heat capacity characteristics of the wall. The full constraint option gives consistently the highest stress range. In the range 0.1-1 Hz, bending restraint provides peak surface stress ratios, essentially reflecting temperature changes local to the heated surface. Membrane stresses only dominate at lower frequencies when through wall temperature gradients close to the heated surface become less severe.

[4] The temperature distribution is linear if the thermal boundary is convection at the outer surface. If adiabatic conditions are prescribed then the steady-state temperature is constant.

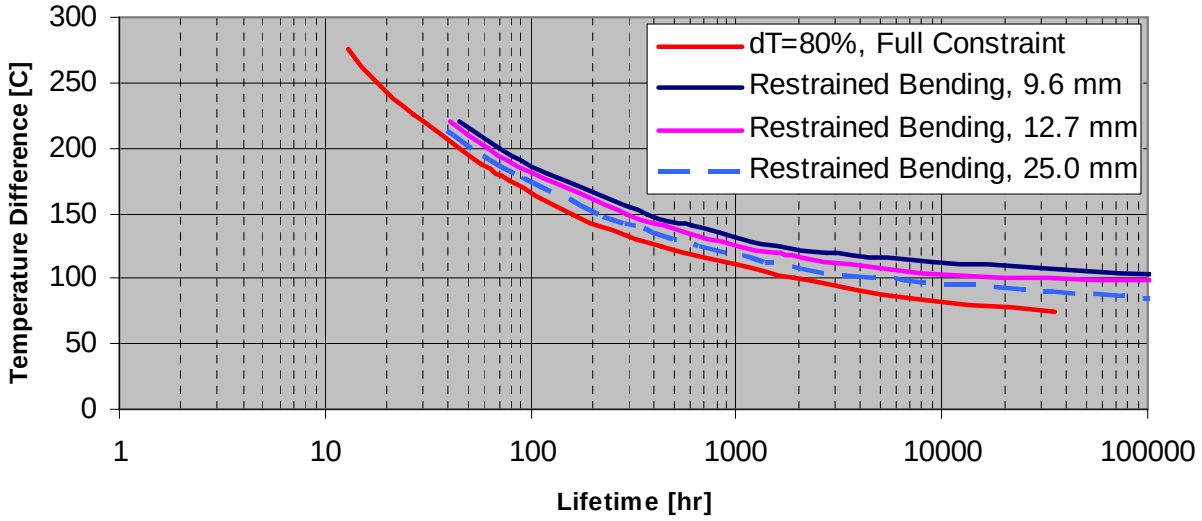

a)

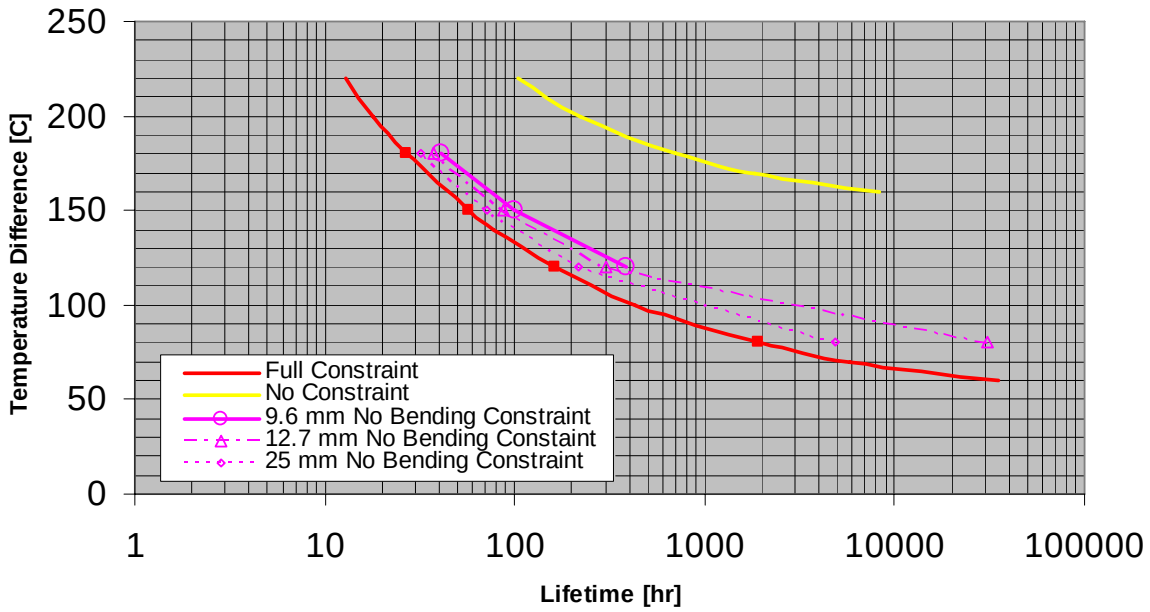

b)

Figure 9.9: Influence of model constraint on temperature reference curves: a) 80% ΔT rule with full constraint and bending constraint + wall thickness effect. b) 100% rule with full constraint, no constraint and bending constraint + wall thickness effect

Figure 9.9a compares reference temperature curves with the sinusoidal approach for situations of full constraint with wall thickness 9.6mm and restrained bending for wall thickness 12.7 and 25 mm respectively, all with the 80% rule. Under restrained bending conditions response is sensitive to section thickness. This is expected since the Biot number doubles as discussed in Chapter 8. For a given temperature difference (ΔT), increased thickness leads to additional constraint (and thereby higher surface stresses) and shifts the reference curve back towards the fully constrained solution. The difference in computed lifetime for the two constraint conditions is less than one would first expect from difference in stresses shown in Figure 9.8.

The reason is that the shortest life from the SIN-method is attained for the frequency range 0.1 – 1 Hz for which the stress ranges in Figure 9.8 do not differ dramatically. The underlying data for the reference curves for restrained bending conditions are included in Table 9.7. Figure 9.9b) shows the reference curves for full constraint and no constraint for H= 9.6mm along with the bending constraint case with the three thicknesses. The un-constrained case gives significantly lower stress amplitudes (Figure 9.8) and the reference curve is significantly shifted towards longer lifetimes. The unconstrained case is not a realistic model of a pipe since it dose not account for the internal constraint.

Fatigue life usage factors have been calculated for the 14 case studies on the basis of the plate model (Table 9.8). Predicted fatigue endurance is based on the constrained bending model, assuming 80% of the bulk temperature difference, a heat transfer coefficient of 15000W/m^{2}K and taking wall thickness into account. No strength reduction factors or plasticity correction factors were applied. Further, fatigue life consumption is based upon the design endurance limit.

Mixing conditions for the mixing-Tees of the case studies have been described in terms of temperature ranges. For each temperature range (80-120°, 120-150° and 150-180°C) bounding usage factors can be determined on the basis of the upper and lower temperature limits. On the basis of these bounding usage factors a nominal average value for the usage factor has also been defined.

The case study data include data on observed crack depths. In Figures 9.10-9.12 the calculated usage factors (upper, lower and average respectively) are plotted against the associated observed crack depths from the case studies. In the figures a distinction is made between the pipe data (9.6 and 12.7 mm) and the mixing-Tee data (25 mm), but no distinction is made between weld and base metal characteristics (i.e. $K_r = 1$).

All three figures are clearly variations on a theme and are therefore similar. However for the lower bound correlation, cracking is observed at usage factors below unity. Whilst distinctly possible /9.3/, this is undesirable for a potential damage indicator. Further, for the T-intersection, the data appear to follow a nominal trend with a usage factor of 1 nominally relating to a crack depth of 1 mm. This is consistent with the observations of /9.6/. For the pipework and weld data, the correlation is less well established. In particular two out-lying points from case #14 distort the general trend of the data. It is also noteworthy that the crack depth data versus the computed usage factor is very flat. This indicates that crack initiation and short crack propagation (to 1-2 mm) occurred early in life but that subsequent crack propagation was rather slow. This is not unexpected since the stress amplitude through-wall distribution has a peak value at the surface and then falls off, as was illustrated in Figure 8.3b.

Table 9.7: NRG SIN-method predictions for fatigue life vs. temperature range reference curves (bending restraint, 80% temperature difference, h=15000 W/m^2/K)

	Thickness = 25 mm							
Fluid *T*, °C	80	100	120	140	150	180	200	220
Wall *T*, °C	53.0	59.7	65.9	70.6	73.9	82.2	85.5	91.4
Frequency, Hz	0.042	0.108	0.186	0.297	0.334	0.476	0.625	0.703
Δσ/2, MPa	125.5	141.3	156.1	167.2	175.0	194.6	202.6	216.4
Lifetime, hrs	1249302.8	4593.8	891.8	321.2	215.6	85.0	52.7	35.1
Lifetime, years	142.61	0.52	0.10	0.04	0.02	0.01	0.01	0.00
Lifetime, cycles	1.9E+08	1.8E+06	6.0E+05	3.4E+05	2.6E+05	1.5E+05	1.2E+05	8.9 E+04
	Thickness =12.7 mm							
Fluid *T*, °C		100	120	140	150	180	200	220
Wall *T*, °C		58.6	64.5	70.5	73.2	79.8	85.4	89.3
Frequency, Hz		0.121	0.209	0.297	0.348	0.535	0.625	0.760
Δσ/2, MPa		138.8	152.9	167.1	173.4	189.0	202.2	211.5
Lifetime, hrs		19703.0	1570.7	455.6	289.8	104.3	62.5	40.8
Lifetime, years		2.25	0.18	0.05	0.03	0.01	0.01	0.00
Lifetime, cycles		8.6E+06	1.2E+06	4.9E+05	3.6E+05	2.0E+05	1.4E+05	1.1E+05
	Thickness =9.6 mm							
Fluid *T*, °C		100	120	140	150	180	200	220
Wall *T*, °C		57.5	63.9	69.5	72.1	79.6	83.9	86.1
Frequency, Hz		0.137	0.220	0.319	0.374	0.543	0.671	0.874
Δσ/2, MPa		136.3	151.3	164.6	170.7	188.4	198.7	203.9
Lifetime, hrs		434251.8	2704.4	608.9	367.2	121.6	70.9	45.4
Lifetime, years		49.57	0.31	0.07	0.04	0.01	0.01	0.01
Lifetime, cycles		2.1E+08	2.1E+06	7.0E+05	5.0E+05	2.4E+05	1.7E+05	1.4E+05

Table 9.8: NRG SIN-method predictions for usage factors (linear damage summation, full constraint model, 80% nominal temperature difference, h=15000 W/m^2/K)

Case No.	***#1***	***#2***	***#3***	***#4***	***#5***	***#6***	***#7***	***#8***	***#9***	***#10***	***#11***	***#12***	***#13***	***#14***
Operational Hours, Fluid δT = 80-120°C	117	322	323	454	582	189	596	424	348	348	410	278	298	62
Operational Hours, Fluid δT = 120-150°C	310	258	173	507	915	807	285	373	293	242	463	550	338	1431
Operational Hours, Fluid δT =150-180°C	107	639	754	1712	1309	2125	630	1001	705	906	1576	1311	1460	11
Pipe:														
Lower Bound	0.41	2.37	2.12	4.85	5.10	6.08	2.36	3.69	2.03	2.56	4.46	3.77	4.10	0.56
Upper Bound	1.77	7.22	6.80	15.63	16.08	19.74	7.41	11.16	6.73	8.24	14.37	12.38	13.04	4.01
Average Usage Factor	1.09	4.80	4.46	10.24	10.59	12.91	4.88	7.43	4.38	5.40	9.42	8.08	8.57	2.29
Mixing-Tee:														
Lower Bound	0.84	3.25	3.69	8.51	7.10	10.76	3.24	5.06	3.60	4.47	7.83	6.70	7.15	1.66
Upper Bound	2.83	9.07	10.04	22.99	20.29	28.94	9.40	13.98	10.05	12.16	21.14	18.28	19.07	6.84
Average Usage Factor	1.84	6.16	6.86	15.75	13.69	19.85	6.32	9.52	6.82	8.32	14.48	12.49	13.11	4.25

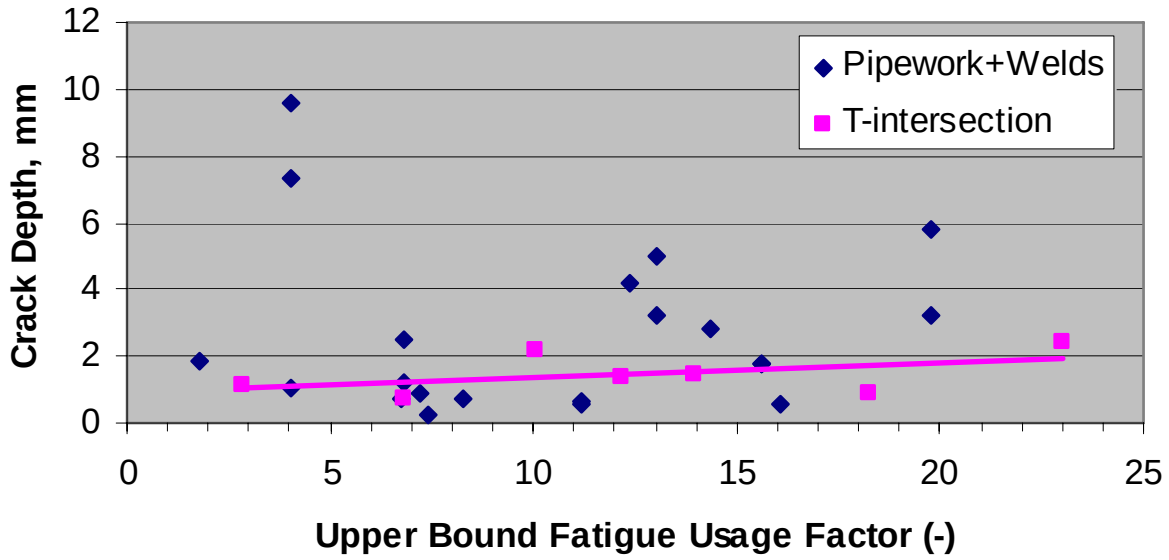

Figure 9.9: Correlation of upper bound fatigue usage factor with observed crack depth.

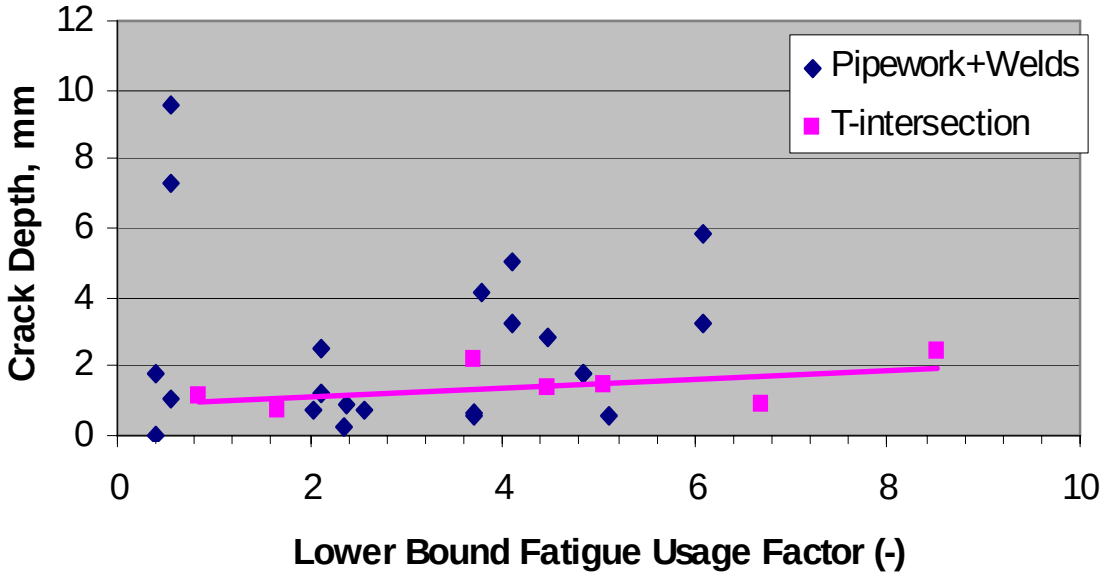

Figure 9.11: Correlation of lower bound fatigue usage factor with observed crack depth.

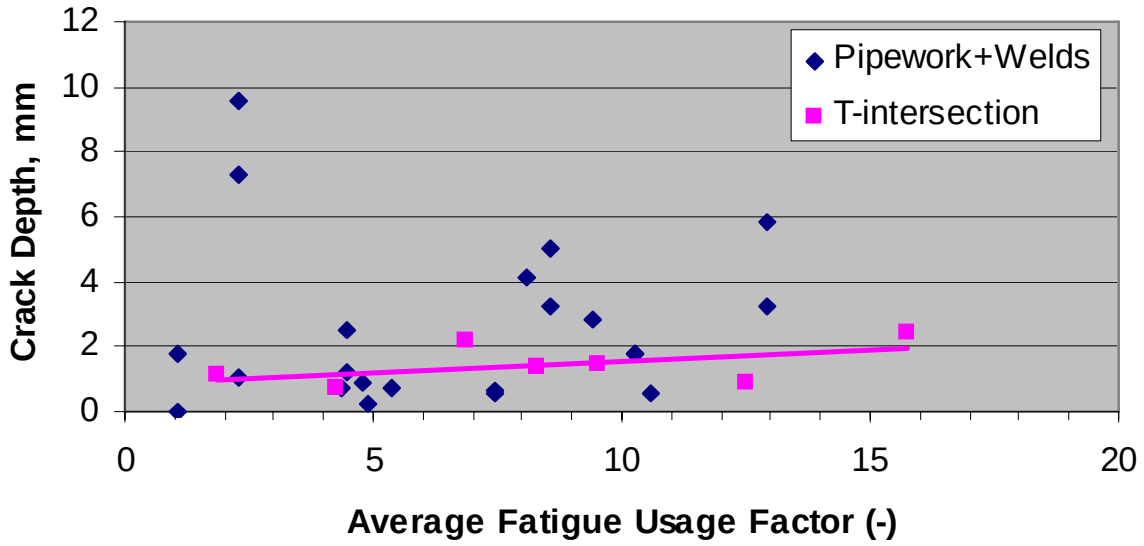

Figure 9.12: Correlation of average fatigue usage factor with observed crack depth.

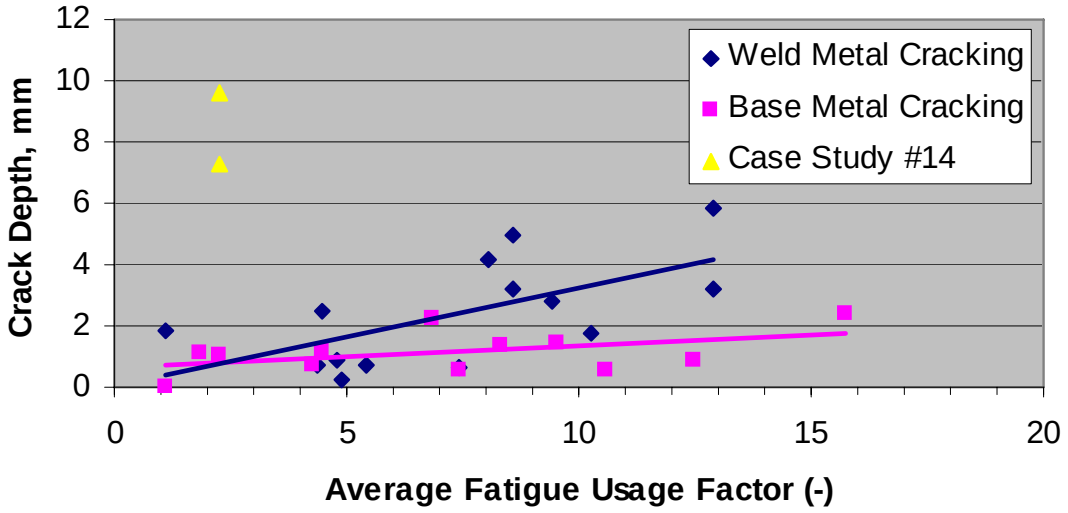

Figure 9.13: Correlation of average bound fatigue usage factor with observed crack depth for weld and base metal

In Figure 9.13 the data are re-arranged on the basis of material type (weld or base material) instead of section thickness. Further the two out lying points of case #14 have been separated from the weld dataset. For the base material the flat slope is even lower than in Figure 9.12, indicating that it is dominated by initiation and short crack growth. The trend of the weld metal data is also clearer by the revised presentation with an approximate usage factor of 3 associated with 1 mm cracking on the basis of the nominal interpretation. This tendency is also consistent with the observation of /9.6/, where a usage factor of 4 is related to 1 mm weld metal cracking. The gradient of the fitted trend curve is steeper than for the base metal indicating that crack propagation is more important and propensity for through-wall cracking is larger. The analysis does not include a strength reduction factors. If strength reduction factors were applied for the weld case then the computed usage factors would increase accordingly and difference between weld and base material would be reduced but there would still be a higher slope for the weld than for the base material.

The correlation provides no explanation for the divergent behaviour observed in case #14. Whilst further details pertaining to this particular study are not available at this time, it is evident that the crack depths observed are significant when compared to many other of the available data. The present method makes no distinction between crack initiation and crack growth. It is often the case with crack formation and growth that the initiation phase consumes something in the region of 70-90% of the total available lifetime, with subsequent crack extension occurring relatively quickly. Given the size of the defects in case #14 it might reasonably be argued that crack initiation has been superseded by a local growth mechanism with greater crack extension per cycle, or that an alternative mechanism is responsible for the crack formation. As a further alternative, the stress analysis results of Figure 9.8 demonstrate that at low frequencies constrained situations are dominated by membrane stresses rather than local bending stresses. If the true loading frequency were low the applied cyclic (membrane) stress would be higher than adopted in the present analysis, thereby promoting earlier crack initiation. Through wall cracking would also be more likely.

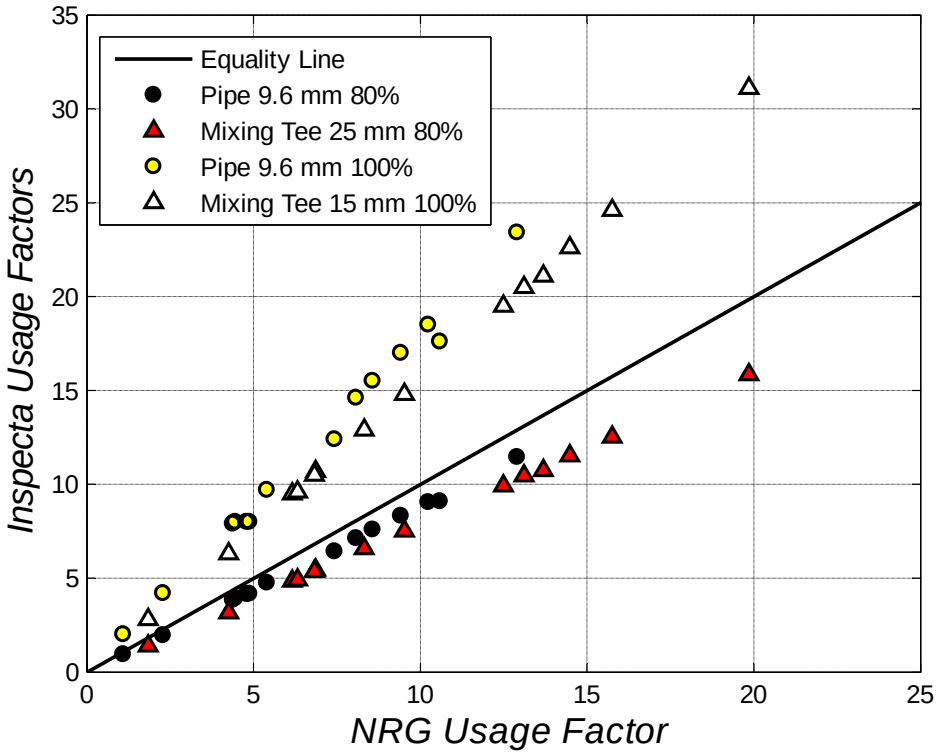

Figure 9.14: Comparison of usage factors from the NRG plate model (restrained bending, 80% ΔT rule) and the Inspecta cylindrical model (analysis case III, 80% and 100% ΔT rule; all cases use a design curve with no plasticity or weld corrections

9.4 Comparison of Results Cylinder and Plate Models

In Figure 9.14 predicted usage factors for the 14 case study examples are compared for the averaged plate model results with the 80% rule and those from case III of the cylinder based analysis with 80% rule and 100% rule. The same modeling assumptions have been applied in each case with respect to physical and material property data, fatigue curve and corrections factors. The only essential difference for the two 80% cases is the geometric model. The usage factors are consistently slightly higher for the plate with bending constraint compared to the cylinder case: 10% for the mixing tee with H = 25 mm and 15% for the pipe with H = 9.6 mm. Whether or not the 80% rule is invoked affects the computed usage factor much more than the geometry model. Hence the geometry assumed is a secondary factor compared to other modeling assumptions.

9.5 Discussion

Given the simplifying assumptions of the method its purpose should be to provide conservative yet practical screening criteria. The SIN-method together with design fatigue curves seems to give conservative predictions. It is questionable whether it is too conservative. To reduce the conservatism mean curves with appropriate reduction factors can

be used. Looking at other factors, it is clear that the heat transfer coefficient, *h*, is the most important and also is subject to some uncertainty as discussed in Chapter 8. The Inspecta Case II with the higher heat transfer coefficient (30000 $W/m^2/K$) gives overall usage factors closer to unity than when applying the lower standard value (15000 $W/m^2/K$). However, too much significance should not be drawn from the non-conservatism of the lower heat transfer coefficient. If, for instance, the 80% rule hadn't been applied, then usage factors would have been higher.

The plasticity and fatigue correction factors are also important. Because austenitic steels begin to yield at a relatively low stress, the plasticity factor should be applied when mean curves are used. At the fatigue limit K_v is typically 1.1. The two geometry model (axisymmetric pipe and plate with bending constraint) give very similar usage factors. This does not mean that any geometry model can be used. It must simulate the inherent constraints of a pipe. The unconstrained plate (Figure 9.9b) would clearly be non-conservative if used together with mean fatigue curves.

It should also be kept in mind that the SIN-method is intended for mixing tees with only turbulence loading. The lower usage factors for EDF cases #1 and #14 could be explained by global stresses from superimposed stratification, for instance. Morerover the SIN method is essentially intended for crack initiation and possibly short crack growth. Nevertheless the comparison of crack depth versus usage factor suggests that a correlation can be made between predicted fatigue usage factors and observed crack depth. Further, a distinction is possible between the performance of base and weld metal. In the case of base metal, based upon the available data, a fatigue usage factor of approximately 1 corresponds to a 1 mm crack depth. For welds the usage factor (for 1 mm cracking) is in the region of 2-3 if no correction factor is applied. These criteria are consistent with the criteria specified in /9.2, 9.6/, despite slight differences in model assumptions. Equally encouraging, the data trends of usage factor against crack depth are relatively shallow suggesting that inspection, planned on the basis of the assessment results, should identify crack initiation before extensive through wall cracking can occur.

A possible concern is case #14 that is an outlier from the general trend. Insufficient data have been made available to determine the reason for this. However, it would be prudent to understand this if the method is to be made generally applicable. As discussed in section 5.2.6, it is likely that this case involved loads other than those due solely to turbulent loads and surface stresses. Some type of larger instability leading to high membrane stresses in the pipe bend seems likely and would explain the rapid crack growth. It is also noted that the values for operational hours associated with cracking reported in the case studies are based upon inspection intervals rather than being the actual time to crack initiation; this is also a source of scatter for the correlations presented above.

9.6 Note on screening criteria for turbulent mixing in tees

In France a systematic evaluation of the SIN-method and the screening criterion has been carried out /9.2/. The implementation is somewhat different from those described above. The ASME III fatigue curve up to 10^6 cycles is used, with an (amplitude) endurance limit of 180 MPa for stainless steel. The fatigue reduction factor for un-flushed welds is set to 1.7 which is in accordance to ASME NB 3600. The local fluid fluctuation level is 80% of the nominal

temperature difference ΔT_{nom} and the heat transfer coefficient is set to $h=15000W/m^2K$. This approach leads to a screening criterion of $\Delta T_{nom} = 80^oC$. The validity of this value has been demonstrated by field experience, as also discussed earlier in this report. All the mean curve analyses in the present report (Figures 9.4-9.5) indicate a value somewhere above $\Delta T_{nom} = 100^oC$, demonstrating some margin. However, if the design curve (based on factors of 2 for σ/ε and 20 for N) data are evaluated with the SIN method (see Figures 9.6, 9.7 and 9.9) the threshold is reduced by factor 2. For the austenitic steel this implies a criterion of about 50^oC, which is significantly lower than the proposed value.

9.7 References

9.1 Jaske C.E., O'Donnell W.J., 'Fatigue Design Criteria for Pressure Vessel Alloys', Trans ASME Energy Technology Conf. and Exhibition, Houston Texas 18-22 Sept. 1977, Paper No. 77-PVP-12.

9.2 Faidy C., 'Thermal Fatigue in Mixing Areas: Status and Justification of French Assessment Method', Proc. 3rd Int. Conf. on Fatigue of reactor components, Seville, Spain 3-6 October 2004.

9.3 Dittmar S., Huttner C., 'Fatigue Analyses as Aid for the In-Service Monitoring, Possibilities and Limitations', Proc. 3rd Int. Conf. on Fatigue of reactor components, Seville, Spain 3-6 October 2004

9.4 Incropera F.P., De Wit D.P., 'Fundamentals of Heat and Mass Transfer', 3rd edition, John Wiley and Sons, 1990.

9.5 Jones I.S., 'The Effect of Various Constraint Conditions in the Frequency Response Model of Thermal Striping', Fatigue and Fracture of Engineering Materials and Structures, vol. 18, 1995.

9.6 Faidy C., 'Thermal Fatigue in Nuclear Power Plants: French Experience and On-going Program', Proc. 3rd Int. Conf. on Fatigue of reactor components, Seville, Spain 3-6 October 2004.

10 CONCLUSIONS

The NESC Thermal Fatigue project has focused on two aspects:

c) creating a database of service and mock-up data for better understanding thermal fatigue damage mechanisms and for validating the procedure.

d) developing a multi-level thermal fatigue damage procedure that reflects the multi-disciplinarity of the phenomenon (thermo hydraulic, material, strain evaluation through FEA, damage analysis, fracture mechanic, ISI performance).

The conclusions from the work are grouped below under three headings: the database of thermal fatigue damage cases, the proposed best-practice procedure and recommendations for further work.

Database thermal fatigue damage cases

- The project created a database of thermal fatigue damage cases, 45 of which relate to operational components and 5 to laboratory simulation tests. From the analysis of the operation data the following points emerge:
  - The cases examined confirm that the thermal loads are the main unknown factor for detailed assessment of thermal fatigue damage.
  - In several instances thermal fatigue damage has developed within short times, even less than a year. Hence the common classification of thermal fatigue as an ageing process (implying that its probability increases progressively with time) is potentially misleading.
  - A small number of damage cases with low nominal ΔT values (60 to 80^{o}C), were identified, but most of these apparently experienced periods of operation at higher ΔT values.
  - Cracks can appear both on un-flushed welds (not used in class 1 piping) and in the base material and can be oriented axially or circumferentially. Cracks in welds tend to be deeper than those in base material (although it is noted that some deep cracks initiated in the weld counter bore radius).
  - None of the through-wall cracks have lead to a pipe rupture during normal operation (although in some cases the dimensions would be assessed as critical for accident loads). All the cracks were detected by leakage in the system.
  - Turbulent mixing alone rarely causes through-wall cracking of pipes, but leads to the development of local surface crazing. Crack depths depend on the mean stress values that are connected to the steady state stresses. Additional system or thermal loads can provide a level of stress sufficient to create through wall cracking.
  - Stratification may occur in conjunction with turbulent mixing in dead legs. It is worth mentioning that stratification loads are easier to handle than turbulence and can frequently be controlled by temperature monitoring and application of suitable transfer functions (an exception is for steep gradients

through the height of a pipe, for instance due to low velocity cold water flows in feedwater systems).

– A main risk factor for stratification is valve leakage. Thus valve leakage control is an effective measure against thermal fatigue in dead legs.

- Examination of the 5 laboratory simulations confirmed that these can successfully reproduce thermal fatigue damage. It is noted, however, that to achieve this under controlled test conditions these experiments used relatively high ΔT and low frequency values, so that the cycles to crack initiation ranging from several hundred up to several hundreds of thousands of cycles.

European Procedure for Assessment of Fatigue Damage under Turbulent Mixing

- A multi-level approach is proposed, which recognizes that despite recent R&D work on measurement and simulation of mixing conditions at Tee junctions, the description and quantification of the associated thermal loads remains a difficult task. The 4 levels are:
  - Level 1 uses a simple screening criteria expressed in terms of the (nominal) ΔT between the two mixing fluids
  - Level 2: the fatigue usage factor is determined by the so-called sinusoidal method, whereby the thermal loading is treated as an idealised sinusoidal wave at most damaging frequency.
  - Level 3: the fatigue usage factor is determined by analysis of the complete local load spectra
  - Level 4 deals with the calculation of the growth of a detected or postulated crack-like flaw and is based on fracture mechanics principles.

  The first two levels have been considered in detail in this study.

- In Level 1 a screening criterion of $\Delta T = 80^{o}\mathrm{C}$ is proposed for turbulent mixing in Tees of austenitic materials. This can also be extended to other types of thermal loadings i.e. stratification and transients, for all types of components fabricated in austenitic materials. For Tees in carbon steel, a lower value of 50°C is set, reflecting the lower endurance limit of such steels and the greater uncertainty concerning the environment effect on fatigue strength. The project database of component damage cases broadly supports the validity of the screening criterion approach. Of the relatively small number of damage cases with slightly lower nominal ΔT values, several apparently experienced periods of operation at higher ΔT values. Rather than invalidating the proposed screening level, this highlights the need to verify that the "nominal" ΔT value used for the screening properly reflects the full range of past (or planned) operating conditions.
- Level 2 provides for the calculation of a fatigue usage factor based on the assumption of a sinusoidal thermal loading at the most damaging frequency for a given ΔT. Advice is given on selection of heat transfer coefficient, fatigue curves, fatigue strength reduction factors and plasticity correction factors. The inherent conservatism of the method has been demonstrated with the database of operational failure cases.
- In applying the above methods, other sources of thermal loading and/or system loads should be taken into consideration.

- Fatigue environmental effects have not to be taken in high cycle fatigue, but should be considered on a case-by-case basis for lower frequency stratification loads.

Further Work

- Level 3 and 4 of damage assessment methodology (detailed consideration of the thermal loading spectra and fatigue crack growth of detected or postulated crack-life flaws) should be detailed and validated.
- The database of thermal fatigue damage cases should be maintained and, where possible, further extended. Analysis of the data is relation to positive operating experience should be considered i.e. to account for cases where no damage has occurred (notwithstanding ΔT levels above the screening criterion level) in the assessment. For instance, the most recent EDF INTHERPOL test confirmed that a Class 1 piping weld with good surface finish can resist more than 500,000 cycles with $\Delta T = 120°C$ without any damage.
- The procedure should be expanded to provide a more comprehensive basis for assessing the different aspects of thermal fatigue damage assessment and mitigation measures, for instance:
  - temperature monitoring to monitor low frequency phenomena, stratification and support better understanding of how fluid temperatures and flow rates versus time
  - load sequence effects, in particular the effect of intermittent occurrence of large ΔT values on fatigue behaviour.
  - effective in-service inspection technology and procedures.

APPENDIX A

FAILURE CASE SUMMARY FORM FOR THERMAL FATIGUE DAMAGE IN NUCLEAR POWER PLANT COMPONENTS

Question	Response
Reactor type: *BWR, PWR, VVER*	
Method of detection *ultrasonic testing, radiographic testing, dye penetrant testing, magnetic particle testing, eddy current testing, visual testing, leakage, other*	
Type of component: *pipe, pipe elbow, valve, pipe mixing tee, pipe mixing tee with inner sleeve, reactor vessel, reactor vessel head, nozzle in vessel, internal part, core barrel, pump, turbine, heat exchanger etc.*	
Material group and type of material: *carbon steel, low-alloy steel, stainless steel, Ni-base alloys, welds./ AISI 304L, 316L, 316NG, X6CrNiNb18-9, X6CrNiTi18-9, Inconel 600, 690, 882, X-750, SS2333*	
Outer diameter or other relevant measure at the location of the damage:	*(mm)*
Thickness at the location of the damage:	*(mm)*
Location of the damage: *base material, heat affected zone (HAZ), weld, back side or belly side of pipe elbow, branch, run, upstream, downstream, other* [7)]	
Type of damage*:* *single crack/multiple cracks*	
Crack orientation: *axial, circumferential*	
Maximum surface length of damage:	*(mm)*
Depth of damage:	*(mm)*
Medium at the location of damage: *fluid*/gas	
Medium at opposing side: *fluid/gas*	
Nature of temperature variation at the location of damage: *turbulence, stratification, other type of instable flow, operational events, other*	
Max temp θmax of medium at the location of the damage:	*(^oC)*[6)]
Nominal temp variation $\Delta\theta_{nominal}$ of medium [1)]:	(^oC)[6]
Local $\Delta\theta$ of medium [2)]:	(^oC)[6]
Estimated frequency of local $\Delta\theta$ [3)]:	*(Hz)*[6)]
Max temperature difference of media between opposing sides:	(^oC)[6)]
Max temperature difference through thickness of material:	*(^oC)*[6)]
Max temperature difference in material at location of damage:	*(^oC)*[6]
Mass (or volume) flows v[4)]:	(*kg/s*)
***P*max**:	*(MPa)*

Question	Response
Δ*P*:	*(MPa)*
Other mechanical loads:	
Stress variation at the location of the damage[5)]:	*(MPa)*
Was the temperature spectrum at the location of the damage known at design stage?	*yes/no*
Could the damage be predicted with the current temperature design spectrum?	*yes/no*
Has the component been subjected to variable operational conditions? [8)]	*yes/no*
Possible interacting parameters: *stress corrosion, oxidation, manufacturing defects, weld residual stresses, corrosion fatigue, other*	
Estimated number of fatigue cycles: (*number of cycles or high/low cycle fatigue*)	
Years in operation:	
Other information:	

Notes:

1) In case of a T-joint supply temperatures for run and branch, θ_{run}, θ_{branch} or $\Delta\theta_{nominal} = \theta_{run}$-$\theta_{branch}$
2) Local temperature variation of the fluid/gas at the location of the damage. Supply estimated characteristic value or supply power spectral density and/or corresponding parameters
3) Supply estimated characteristic frequency or supply power spectral density and/or corresponding parameters
4) In case of a T-joint supply flows for run and branch, v_{run}, v_{branch} or $\Delta v = v_{run}$,-v_{branch}
5) If available supply a stress variation estimate, and also indicate the method of stress assessment, for example FE calculations and the corresponding local temperature variation.
6) Indicate if calculated or measured
7) If possible supply sketch of component with damages indicated
8) If yes, please indicate the change in temperature and flow parameters over time

APPENDIX B

CHARACTERISTICS OF THE SIN-METHOD

B1 INTRODUCTION

This appendix presents an investigation of some of the properties of the SIN-method, and discusses one possible numerical implementation scheme. In order to evaluate the proposed criteria and procedures, system equations for the time varying temperature and stress/strain field in a hollow cylinder are derived and implemented in a a computer code. For the temperature field a FE formulation, suitable for the axis-symmetrical case, is used. For the stress/strain field an analytical solution is used for the axis-symmetrical case, based on the FE solution of the temperature field.

B2 STRESS CALCULATION PROCEDURE

For the axis-symmetrical case thermal loading caused by sinusoidal time variation of flow convection is studied. In addition a loading characterised by a square wave time variation is considered. A FE mesh for computing the temperature field is defined by nodal points along a radius in the pipe material. The geometry is defined in Figure B.1. Two-node linear elements are used.

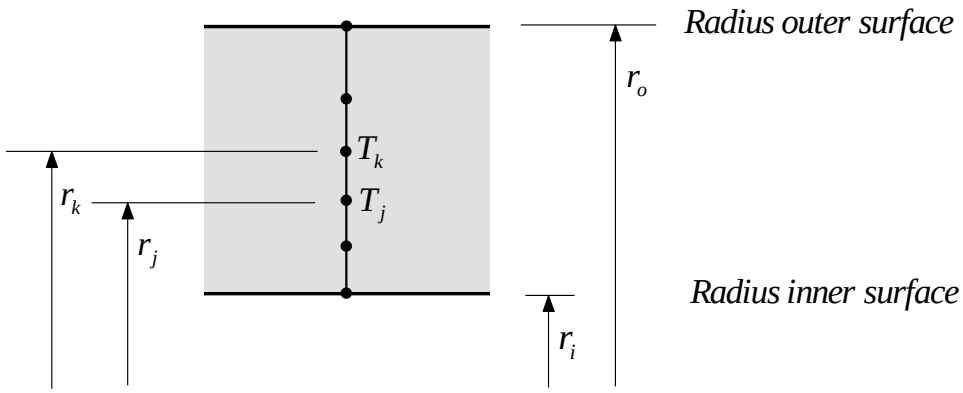

Figure B1. Geometry of axis-symmetric heat transfer model

By assuming no heat transfer through the outer surface (adiabatic conditions), defined by the radius r_o, element matrices and the heat convection load vector are integrated. By assembling the element matrices, a system equation for heat transfer problem is formed. Depending on type of time variation, the system equation may be solved either in the frequency domain or by direct time integration.

For an axis-symmetrical temperature field in a cylinder, stress values can be derived from analytical expressions, see refs./B4/ to /B6/. For a long cylinder the so-called generalized plane strain condition gives the stress field, except for the local effects in the end sections. Based on the computed temperature field $T(r)$ given by the FE solution, all stress

components and strains are given in closed form by the expressions (B.1) and (B.2) (ref/B4,B6/),

$$\begin{cases} \sigma_x(r) = \dfrac{E\alpha}{(1-\nu)}\left(\dfrac{2I_1}{r_o^2 - r_i^2} - T(r)\right) \\ \sigma_\theta(r) = \dfrac{E\alpha}{(1-\nu)r^2}\left(\dfrac{\left(r^2 + r_i^2\right)I_1}{r_o^2 - r_i^2} + I_r(r) - r^2 T(r)\right) \\ \sigma_r(r) = \dfrac{E\alpha}{(1-\nu)r^2}\left(\dfrac{\left(r^2 - r_i^2\right)I_1}{r_o^2 - r_i^2} - I_r(r)\right) \\ \tau_{x\theta} = \tau_{r\theta} = \tau_{xr} = 0 \end{cases} \quad ; \quad \begin{cases} I_1 = \int_{r_i}^{r_o} T(r)\cdot r \cdot dr \\ I_r(r) = \int_{r_i}^{r} T(r)\cdot r \cdot dr \end{cases} \tag{B.1}$$

The stresses above are those obtained under general plane strain, i.e. the pipe has no end restraints, which is appropriate for this application. The corresponding strains[5] are:

$$\begin{cases} \varepsilon_x = 1/E\left(\sigma_x - \nu\left(\sigma_r + \sigma_\theta\right)\right) \\ \varepsilon_\theta = 1/E\left(\sigma_\theta - \nu\left(\sigma_r + \sigma_x\right)\right) \\ \varepsilon_r = 1/E\left(\sigma_r - \nu\left(\sigma_\theta + \sigma_x\right)\right) \end{cases} \tag{B.2}$$

By transforming the system equations into the frequency domain, a frequency response function (*FRF*) $Z_{\bar{T}}(\omega)$ may by established, which gives the relation between a fluctuating bulk flow temperature T_f and the temperature in any point in the pipe material. $Z_{\bar{T}}(\omega)$ is fully defined at any point and at any frequency by the three non-dimensional parameters given in (B.3).

$B^* = (h \cdot t)/\lambda$ Biot number (B.3a)

$f^* = f \cdot \left(\rho c t^2\right)/\lambda$ Non-dimensional frequency (B.3b)

$t^* = t/r_m$ Ratio thickness to mean radius of pipe (B.3c)

The parameters are as follows

λ	Conductivity of material in component and in fluid, [W/m/K]
h	Convection heat transfer coefficient, [W/m^2/K]
ρ	Mass density of material in component and fluid, [kg/m^3]
c	Specific heat of material in component and fluid, [J/kg/K]
r_m	Radius, radius of mean surface, radius of outer and inner surface of component, [m]
t	Thickness of material in component, $t = r_o - r_i$, [m]
t^*	Non-dimensional thickness of material in component, $t^* = t/r_m$, [-]
E	Youngs modulus of material in component, [Pa]
ν	Poisson ratio of material in component, [-]
α	Expansion coefficient of material in component, [K^{-1}]

[5] These are the mechanical and not the total strains, since only the mechanical strains cause fatigue damage.

B^* Biot number, $B^* = (h \cdot t)/\lambda$, [-]

d Thermal diffusivity in component, $d = \lambda/(\rho \cdot c)$, [m^2/s]

f Frequency, [Hz]

f^* Non-dimensional frequency, $f^* = f \cdot (\rho c t^2)/\lambda$ [-]

For a thin walled cylinder, the pipe material temperature is only dependent of the Biot number B^* and the frequency, f^*. The thin walled cylindrical temperature solution approaches that of a pure one dimensional problem. Values of the Biot number for heat transfer between flowing water and pipe steel are typically in the range 1-20. By combining these, a relation between the fluctuating flow temperature and the pipe material stress is obtained.

Figure B.2 shows the frequency dependence of the normalised surface stress for different Biot number values. In the main report the ASME III code acceptance criterion for fatigue stresses due to operational loading in a pipe component is discussed. For a pipe section, leaving aside dimensional changes, the stress intensity range S_p is based on two parameters, ΔT_1 and ΔT_2. ΔT_1 is the range between two conditions of the linearised temperature through the thickness of the pipe wall. By subtracting from the actual surface temperature the mean temperature and the linearised part of the distribution, the range of the remaining temperature difference gives the parameter ΔT_2. In Figure B.3 the frequency dependence of the parameters ΔT_1 and ΔT_2 is presented in the same manner as done for surface stress in Figure B.2.

Figure B.4 compares the amplitude of the normal surface stress $\Delta\sigma_x/2$ and alternating stress intensity S_{alt} based on the temperature parameters ΔT_1 and ΔT_2. It is clear that for low frequency cycling the surface stress is dominated by the linear variation of the temperature through the thickness. At high frequency cycling the local surface temperature given by ΔT_2 completely dominates surface stress. In addition, the combined effect of ΔT_1 and ΔT_2 is compared to that of the actual surface stress σ_x. It is clear that stress intensity parameter S_{alt} based on ΔT_1 and ΔT_2 leads to a conservative estimate of the alternating stress. This may be due the method used to estimate the ranges of ΔT_1 and ΔT_2; a time lag between the maximum/minimum of the time signals representing the linearized temperature and remaining part is most likely cause. In other words, the time signal of the linearized temperature is not in phase with the time signal of the remaining part.
In Figure B.5 the peak amplitude at “resonance” frequency of the surface stress FRF and the stress intensity due to the parameters ΔT_1 and ΔT_2 (independently) are given versus the Biot number. The values of “resonance” frequency related to these peak amplitudes are given in Figure B.6.

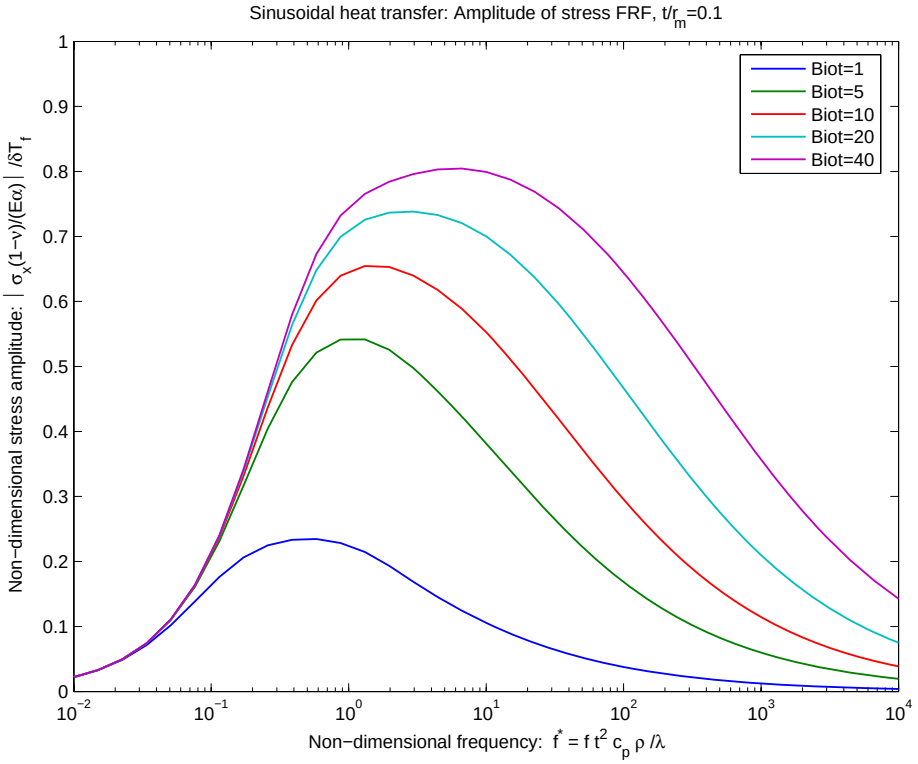

Figure B.2: Frequency response function of alternating surface stress

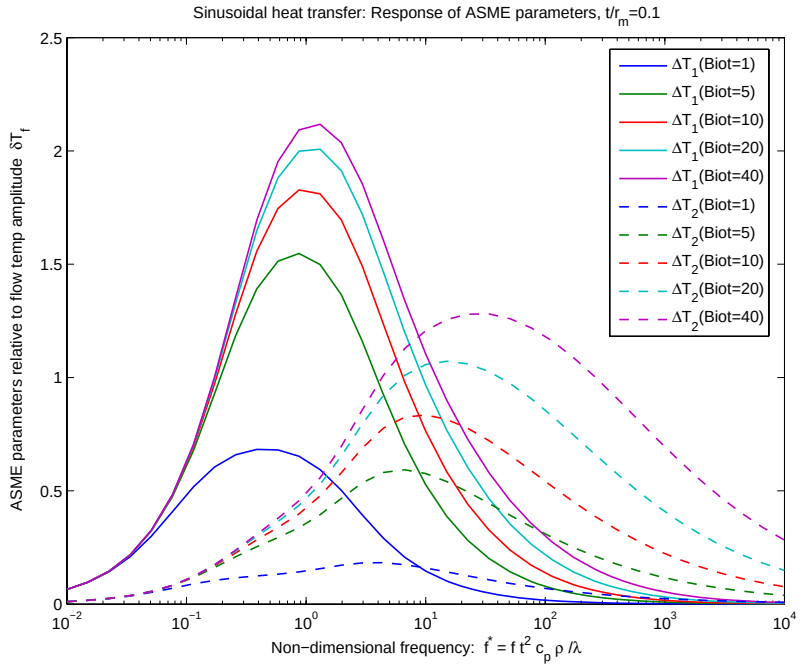

Figure B.3: Frequency response of ASME-code related temperature parameters

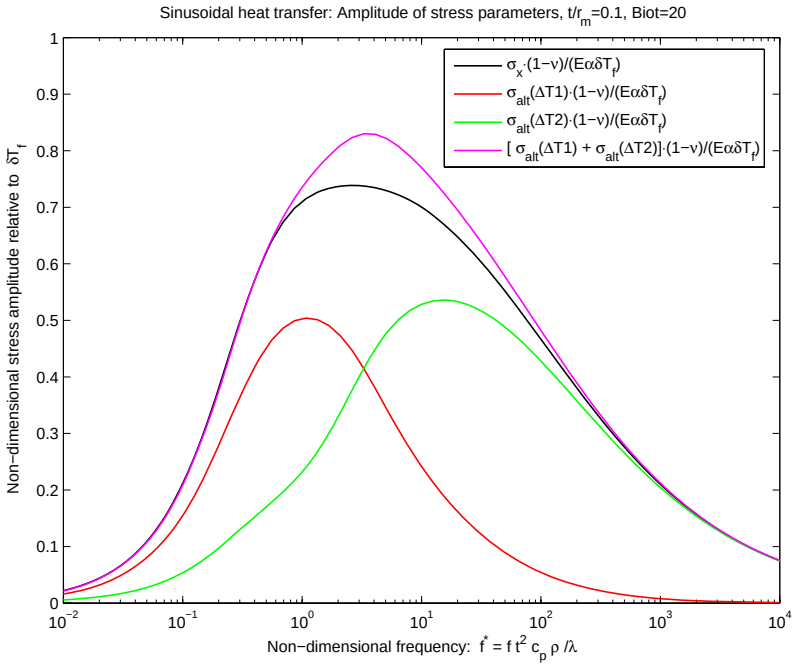

Figure B.4: Alternating surface stress compared to ASME-code related stress parameters.

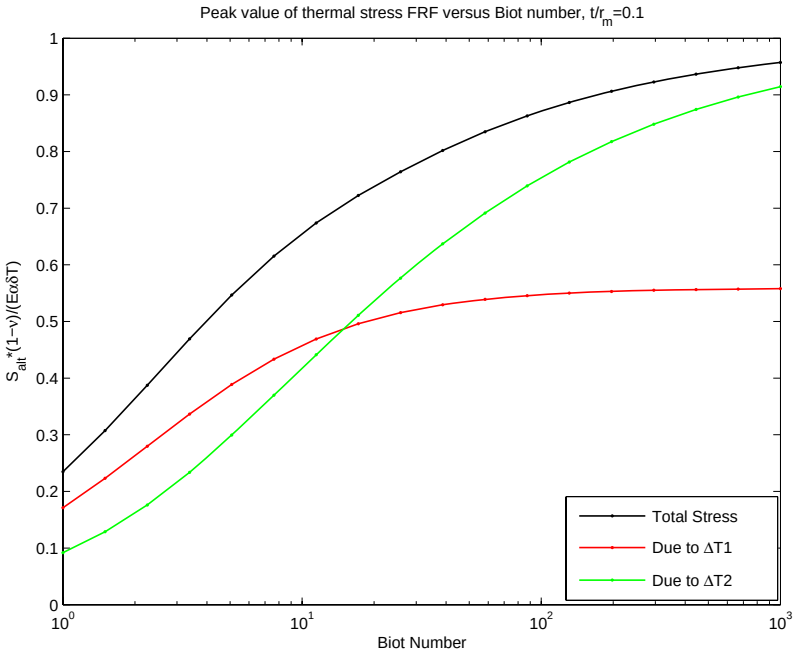

Figure B.5: Peak amplitude of stress FRF versus Biot number

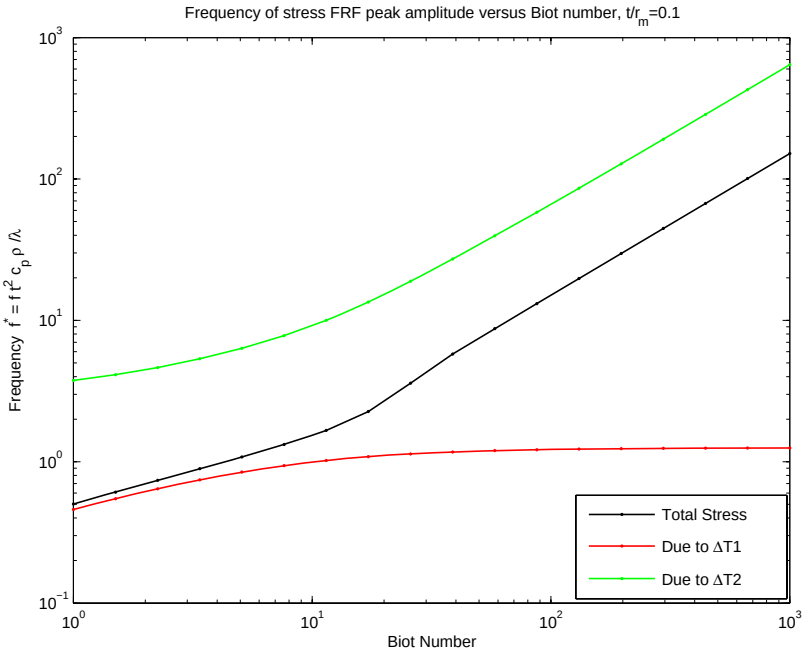

Figure B.6: Frequency at peak amplitude of stress FRF versus Biot number

B.3 INFLUENCE OF THE ASSUMED WAVE FORM

For the sake of comparison, the use of a square-type wave form instead of a sin one was analysed. Stationary square wave excitation was used to define the heat convection. The convection is described by a temperature variation $T_f(t)$ for given a Biot number, similar what was done for the sinusoidal loading case. However, this particular problem is solved in the time domain by integration. The total integration time is set so that a stationary response cycle is obtained in the last computed cycle. The range parameters are evaluated based on that last cycle.

Figure B.7 shows the periodic excitation wave, with the amplitude given by δT_f and the period by τ. For comparison with the sinusoidal case, the frequency parameter f is defined as the inverse of period time. This means that the fundamental tone of the Fourier spectrum of the square wave is equal to the frequency, f. Figure B.8 shows the variation of the normalised surface stress amplitude with normalised frequency for different Biot numbers. For comparison the values resulting from sinusoidal excitation, representing the fundamental tone only, are included.

In Figures B.9-B.10 the ASME-code temperature range parameters ΔT_1 and ΔT_2 are plotted. In addition the range of the mean temperature of pipe material ΔT_m is plotted in Figure B.11. In Figure B.12, the normalised surface stress is compared to alternative stress parameters based on the temperature range parameters ΔT_1 and ΔT_2. The Biot number is set to 20. A distinct cut-off frequency may be identified in the response curves at very low frequencies, below which there is no influence of the period of excitation. That means that the response is dominated by the higher order harmonics. For such long periods of excitation the loading may

simply be characterized as a series of repeated and independent transient step loads. In such transients each individual load step will be equal to $\pm 2 \cdot \delta T_f$. This phenomenon is clearly explained by the mean temperature response range curves, ΔT_m, in Figure B.11. As can be seen the range ΔT_m is equal to the flow temperature range $2 \cdot \delta T_f$. This means that the temperature in the pipe material will reach the fluid flow temperature during each cycle at fundamental tone frequencies below the cut-off value.

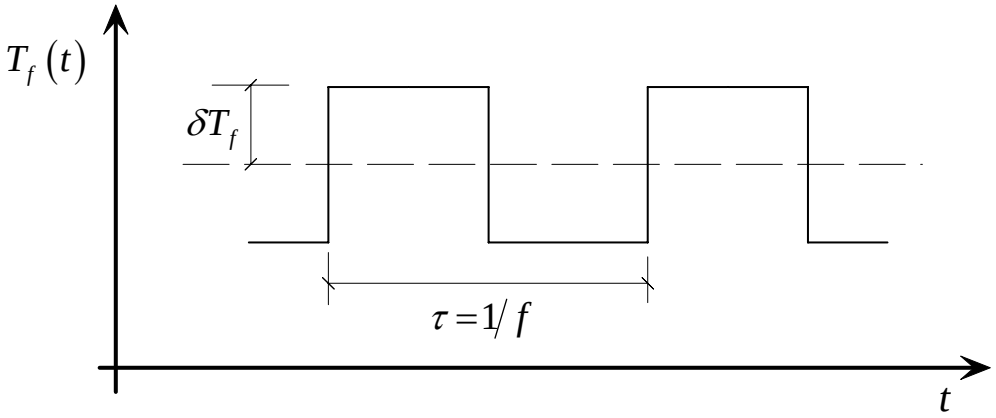

Figure B.7: Definition of square cycle excitation

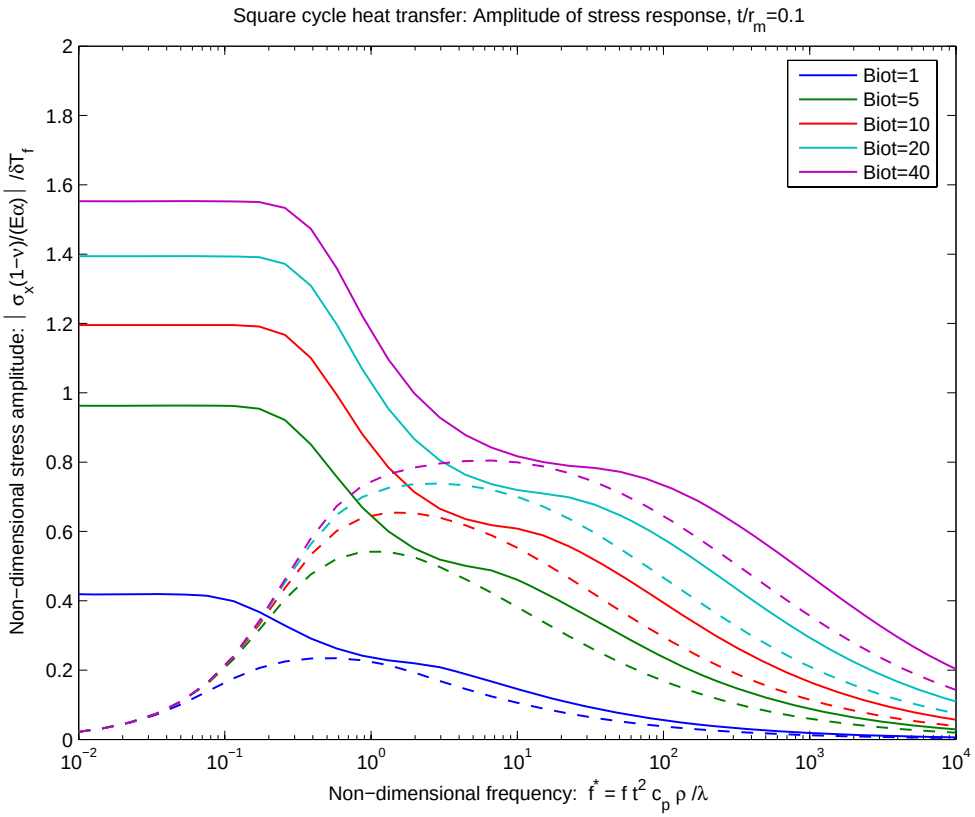

Figure B.8: Stress amplitude when square cycle excitation

(full lines = square wave; dashed lines = sinusoidal wave).

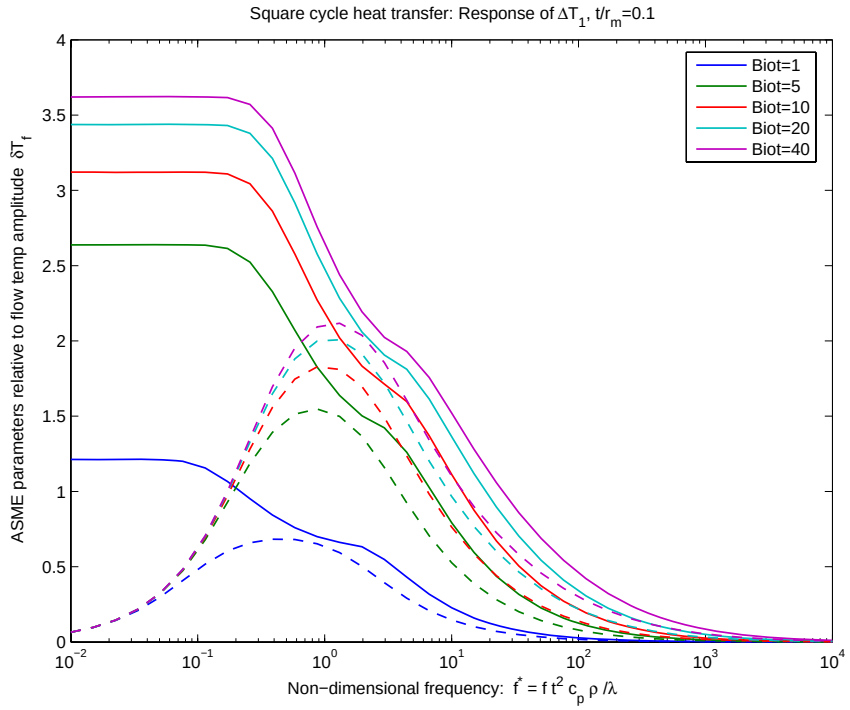

Figure B.9: Response of parameter ΔT_1, square cycle excitation (full lines = square wave; dashed lines = sinusoidal wave).

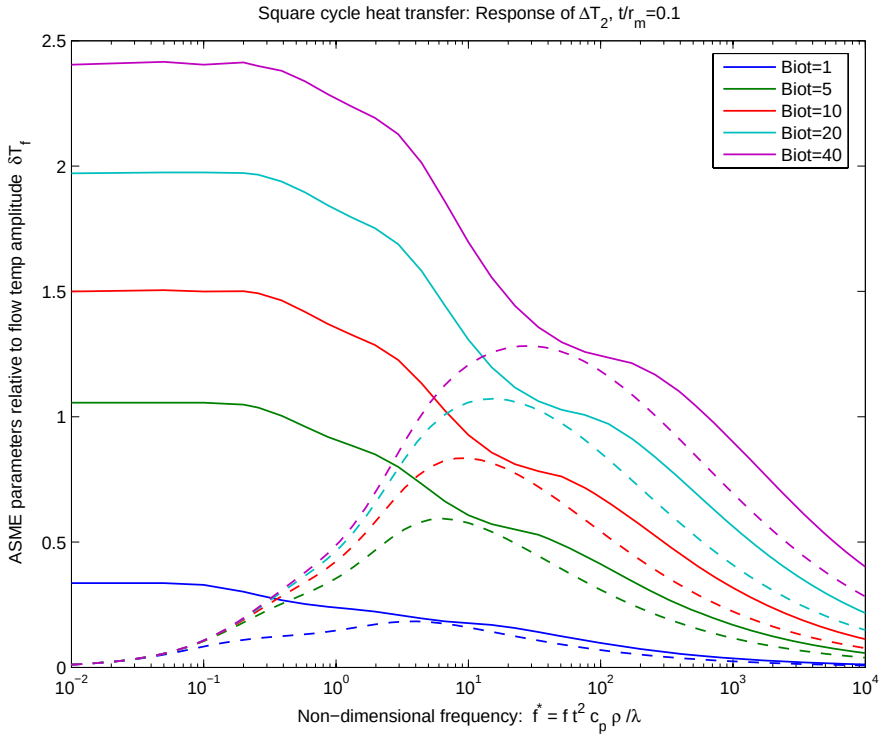

Figure B.10: Response of parameter ΔT_2, square cycle excitation (full lines = square wave; dashed lines = sinusoidal wave).

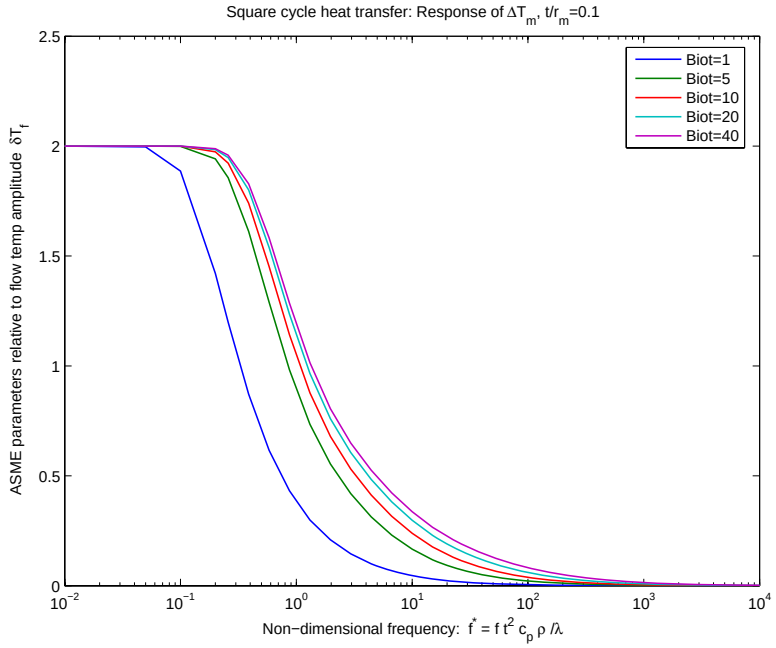

Figure B.11: Response of parameter ΔT_m, square cycle excitation.

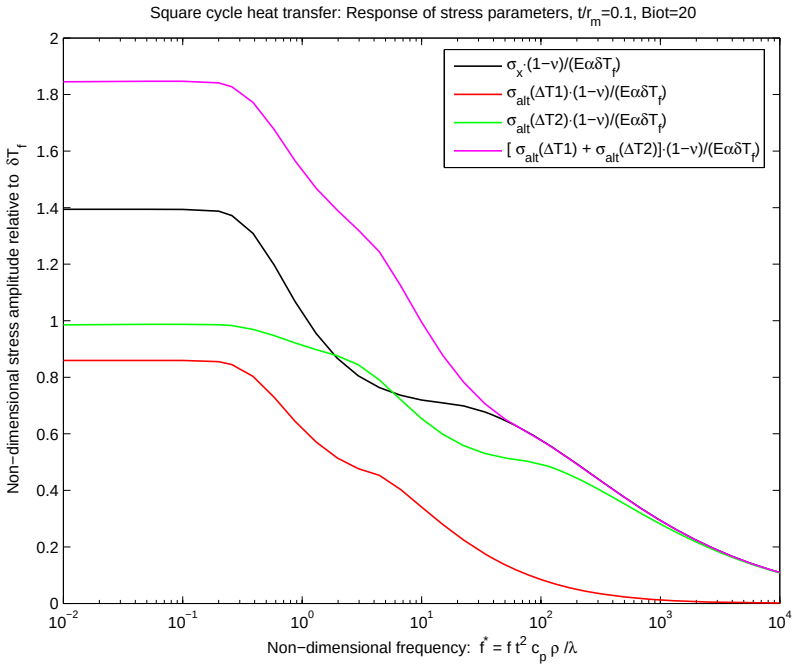

Figure B.12: Surface stress compared to ASME-code stress parameter (square wave excitation)

B4 REFERENCES

B1 Claude Faidy, European Procedure for Thermal Fatigue Analysis, rev A2 EDF-SEPTEN, March 5, 2004

B2 ASME III Division 1 – Subsection NB, Rules for construction of nuclear facility components The American Society of Mechanical Engineers.

B3 Cook R. D. et al, Concepts and Applications of Finite Element Analysis, John Wiley & Sons, 1989

B4 Timoshenko S. & Goodier j. N., Theory of Elasticity, 2nd edition, 1951

B5 Brown M. W., Multiaxial Fatigue Testing and Analysis, Fatigue at High Temperature. Ed. R. P Skelton, Applied Science Publishers Ltd, 1983.

B6 Goodier J. N., Thermal stress in long cylindrical shells due to temperature variation round the circumference, and through the wall, Canadian Journal of Research, vol 15, 1937, 49-58

B7 Goodier J. N., Thermal stress and deformation, Journal of Applied Mechanics, vol 24, Trans. ASME, Vol 79 (1957), 467-474

B8 Miller A. G., Crack propagation due to random thermal fluctuations: Effect of temporal incoherence, Int. J. Pres. Ves. & Piping, vol 8 (1980), 15-24

B9 Miller A. G., Equivalent strain range due to random thermal fluctuations: Effect of spatial incoherence, Int. J. Pres. Ves. & Piping, vol 8 (1980), 105-130

APPENDIX C

CODE BASIS FOR THERMAL FATIGUE

C1 GENERAL RULES

C1.1 Design-by-analysis

Nuclear Class 1 components are studied using a design-by-analysis approach, as implemented in the Code ASME III NB-3200 and other similar Codes (RCC-M, KTA, etc.). In the design-by-analysis approach, a detailed evaluation of stresses at critical areas of the component is performed, generally by means of a FE calculation. Membrane and bending stresses are determined. A further categorization of stresses into primary, secondary or peak is done for comparison with Code allowable values.

C1.2 Fatigue analysis

Fatigue evaluation is based on the assumption that the equipment is running in steady state with this steady state perturbed by some service (level A/B) transients (thermal or mechanical, such as seismic). Each transient starts from and returns to a steady state situation. The order of succession of the transients is generally unknown and the analysis must take all possibilities into account. Each transient is characterized by:

- two extreme situations for which total stress intensity is minimum or maximum; these extreme situations are called “load sets”
- the number of times the transient will occur in the life of the equipment (number of occurrences)

Figure C1 illustrates the load set definition for a 1-D stress state.

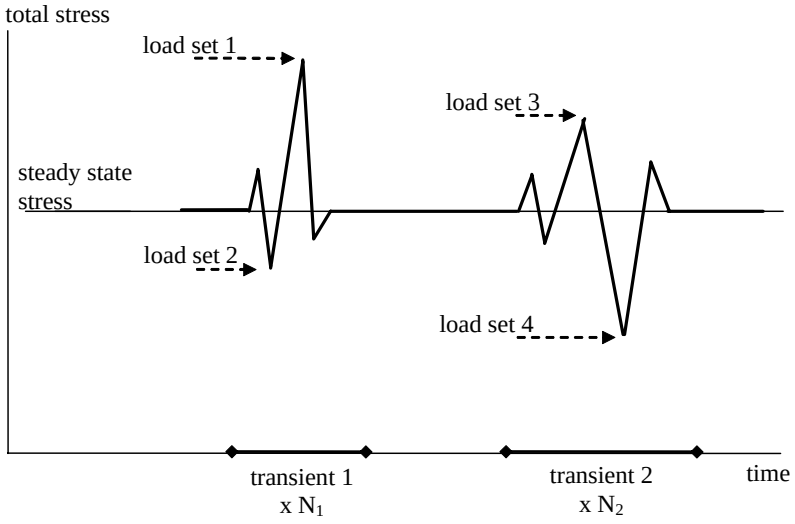

Figure C1: Load set definition

The peak stress intensity ranges $S_{p,ij}$ between any load set pair (i,j), with $i \neq j$, are computed. The alternating stress intensity is defined as:

$$S_{a,ij} = \frac{S_{p,ij}}{2}$$

The allowable number of cycles for the load set pair N_{ij} is obtained from the applicable design fatigue curve.A partial usage factor is then calculated:

$$UF_{ij} = \frac{n_{ij}}{N_{ij}}$$

where n_{ij} is the number of occurrences for the load set (i,j).

When dealing with more than two load sets, load sets are arranged in such a manner that the total usage factor is maximized:

1. A table of stress intensity ranges between all possible pairs of extreme situations is set up:
   $k \quad l \quad \Delta S_{kl}$
   M M M
2. The pairs are ordered in decreasing order of stress intensity range
3. A pair with the largest stress intensity range is taken with its maximum possible number of occurrences i.e. :
   $n_{kl} = \max(n_k, n_l)$
4. The number of occurrences is updated by subtracting the number of occurrences of the treated pair:
   $n'_k = n_k - \min(n_k, n_l)$
   $n'_l = n_l - \min(n_k, n_l)$
   (the number of occurrences of one of the pairs becomes 0)

The process is continued for the largest pair having a non-zero residual number of occurrences. It is stopped when all residual number of occurrences is 0. The usage factor is calculated for all pairs with non zero number of occurrences and summed:

$$CUF = \sum \frac{n_{kl}}{N_{kl}}$$

Stress intensity ranges $S_{p,ij}$ are usually computed by means of a linear elastic analysis, i.e. it is assumed that the material remains globally elastic. This is ensured by verifying the elastic shakedown criteria:

$$S_{n,ij} \leq 3 S_m \text{ for all load set pairs}$$

where S_n is the range of primary plus secondary stress intensity and S_m is the allowable design stress. When the shakedown criterion is exceeded, it is necessary to perform a plastic analysis. A simplified elasto-plastic analysis, using the elastically computed stress intensity ranges, is however possible under certain conditions. In this case a penalty factor K_e is applied to the stress intensity range to take into account strain concentration effects under plastic cycling:

$$S_a^* = K_e S_a$$

In the ASME Code, K_e is given by the equation:

$$K_e = 1 + \left[\frac{1-n}{n(m-1)}\right]\left[\frac{S_n}{3S_m} - 1\right] \quad \text{(NB-3228.5 (b))}$$

where $1.0 \leq K_e \leq 1/n$, and for carbon steel: m = 3.0, n = 0.2, while for austenitic stainless steel: m = 1.7, n = 0.3. Figure C2 illustrates the variation of K_e with load.

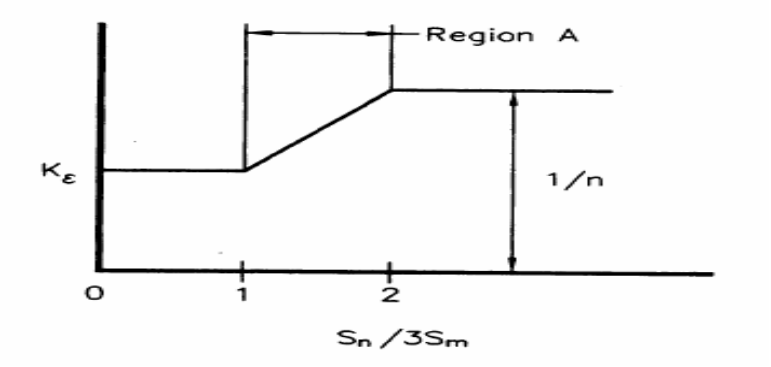

Figure C2: K_e factor

The RCC-M Code has a somewhat different approach and makes a distinction between the mechanical and thermal part of the stresses.

$$S_a^* = \frac{1}{2} . [\, K_{e,mech} \times S_{p,mech} + K_{e,ther} \times S_{p,ther} \,] = \frac{1}{2} \, . K_{e,alt} \times S_p$$

Where:

S_p range of the total stresses

$K_{e,alt}$ elastoplastic stress concentration factor

$S_{p,mech}$ range of the mechanical part of the stresses

$K_{e,mech}$ elastoplastic stress concentration factor for the mechanical part

$K_{e,mech} = 1.0$ for $S_n \leq 3\ S_m$

$$K_{e,mech} = 1.0 + \frac{1-n}{n(m-1)} . \left(\frac{S_n}{3S_m} - 1\right) \text{ for } 3\ S_m < S_n < 3m\ S_m$$

$$K_{e,mech} = \frac{1}{n} \text{ for } S_n \geq 3m\ S_m$$

the values m and n are material parameters (RCC-M B 3234.6 [C1]) (m = 1.7 and n = 0.3 for austenitic stainless steel material).

$S_{p,ther}$ range of the thermal part of the stresses.

$K_{e,ther}$ elastoplastic stress concentration factor for the thermal part.

$$K_{e,ther} = \max\left\{1.86\left(1 - \frac{1}{1.66 + \frac{S_n}{S_m}}\right); 1.0\right\}$$

C2 RULES FOR PIPING

A detailed analysis using the above rules is generally not required for every type of piping. Simplified methods for performing a design-by-analysis have been developed in the Codes (e.g. ASME III NB-3600) based on a stress index approach.

A flexibility analysis is performed to determine the moments in the piping as a result of the loading. In the stress index method, the primary, secondary or peak stresses in a fitting are determined by multiplying the nominal bending stress by the appropriate stress index. The maximum stress intensities from different loads are added together regardless of location in the fitting, what is a conservative simplification. The temperature distribution in the pipe thickness is supposed to be axisymmetric. It is described by two parameters: ΔT_1 and ΔT_2.

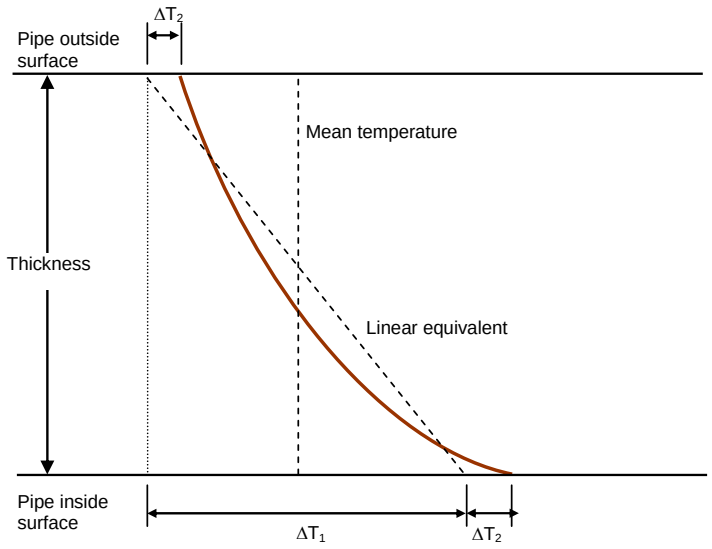

Figure C3 Temperature distribution through thickness

ASME III NB-3653.2 Eq. 11 gives the peak stress intensity range between two load sets:

$$S_p = K_1 C_1 \frac{PD_o}{2t} + K_2 C_2 \frac{M_i}{Z} + K_3 C_3 E_{ab} \left| \alpha_a T_a - \alpha_b T_b \right| + \frac{1}{2(1-\nu)} K_3 E \alpha \left| \Delta T_1 \right| + \frac{1}{2(1-\nu)} E \alpha \left| \Delta T_2 \right|$$

Where:

P	range of service pressure
Mi	resultant range of moment
$E_{ab}\lvert\alpha_a T_a - \alpha_b T_b\rvert$	range of gross structural discontinuity stress, where E_{ab} (average E at either sides of the discontinuity), α_a and α_b are taken at RT temperature
S_m	average value of allowable stress intensity at highest and lowest material temperature during transient
$E\alpha$	material characteristics at room temperature
ν	Poisson ratio (= 0.3)
ΔT_1	absolute value of range of equivalent linear temperature difference
ΔT_2	absolute value of range of non-linear temperature difference

K_1, K_2, K_3, C_1, C_2, C_3 secondary and local stress indexes, as per Table C1

The three last terms of the equation are of particular interest:

$K_3 C_3 E_{ab} \left| \alpha_a T_a - \alpha_b T_b \right|$ is the stress intensity range due to interaction of adjacent components *a,b*

$\frac{1}{2(1-\nu)} K_3 E \alpha \left| \Delta T_1 \right|$ is the stress intensity range due to linearized temperature range ΔT_1

$\frac{1}{2(1-\nu)} E \alpha \left| \Delta T_2 \right|$ is the local stress intensity range due to nonlinear temperature range ΔT_2

C3 DESIGN CODES AND THERMAL FATIGUE

First of all it is underlined that in addressing component design, the codes embody a due degree of conservatism. For monitoring or fatigue assessment of parts subject to a well-described loading history, the conservatism may be excessive. Moreover, the codes focus mainly on service transients such as plant start-up and shutdown, etc. A major difference between these transients and the phenomena related to thermal fatigue is the temperature distribution: typically axisymmetric for the transients covered by the codes, and non-axisymmetric for thermal fatigue. This means that the simplified stress index approach of the ASME NB-3600 or RCC-M is normally not applicable. The more general NB-3200 rules should be used instead. Two cases of thermal fatigue can be distinguished.

C3.1 Local, high frequency thermal fatigue

Small parts of the piping are subject to rapid temperature variations (typical in the range: 0.1 to 1 Hz). Examples include mixing tee and vortex penetration. The stress intensities are generally low in comparison with those of the design thermal transients. A reasonable approximation for the total usage factor can be therefore expressed as the sum of:

- the usage factor taking into account the design transients only, calculated with the NB-3600 piping rules
- the usage factor due to local temperature variation only, calculated according to NB-3200 by means of a local FE analysis or by other analytical methods, such as the sinusoidal method discussed elsewhere in this report.

C3.2 Global, slow frequency thermal fatigue (stratification)

Stratification phenomena are relatively slow and involve large portions of the piping. They are characterized by a top-to-bottom temperature gradient in the pipe.

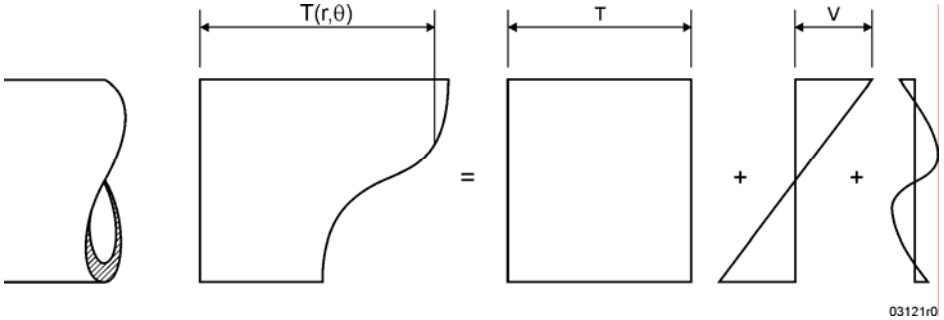

Figure C4: Temperature distribution through the pipe

C3.2.1 Global effects

The global effects of stratification are considered by determining the bending moments due to differential thermal expansion. Bending moments can be obtained by means of a flexibility analysis, taking as input the mean pipe temperature T and linear temperature gradient V:

$$V = \frac{6}{\pi(r_o^3 - r_i^3)} \int_{-\pi/2}^{\pi/2} \int_{\pi r_i}^{\pi r_o} r^2 T(r,\theta) \sin\theta \, dr \, d\theta$$

The resultant bending moments are treated the same as those due to thermal expansion. In particular, the moment range Mi in ASME III NB-3653.2 Eq. 11 includes the global stratification effects.

C3.2.2 Additional stresses

The non-linear top-to-bottom temperature distribution in a pipe produces a non-uniform stress distribution around the pipe circumference (primarily axial stresses). These stresses have the same characteristics as a non-linear through-wall stress distribution in that they will not result in gross thermal displacement of the piping system and contribute only to fatigue. The nonlinear distribution can be described by the parameter ΔT_3:

$$\Delta T_3 = \max\left|\left(T(r,\theta) - T - Vr\sin\theta / r_o\right)\right|$$

Two different approaches can be used at this point:

A) Stick to the NB-3600 rules … and simply add another term to ASME III NB-3653.2 Eq. 11: + $K_4 \, E \, \alpha \, |\Delta T_3|$. Values of K_4 still need to be developed. As a first approximation, K_4 can be taken equal to K_3; however several questions need to be considered:

i. Are stress indices that were determined for axisymmetric loading valid for non-axisymmetric loading?
ii. Since local stratification stresses are not surface-only stresses, should they be included in the check for thermal stress ratcheting?
iii. Is the local stratification stress uniaxial (axial only) or biaxial?
iv. Does the fact that the ΔT_1, ΔT_2, and T_a-T_b stresses are not uniform around the pipe affect the Code acceptance criteria?

B) Conduct a detailed analysis using the rules of NB-3200, in which the combination of stress terms at multiple locations around the circumference of the piping can be considered.

	Internal pressure			Moment loading			Thermal loading			
	B1	**C1**	**K1**	**B2**	**C2**	**K2**	**C3**	**C3'**	**K3**	
Straight pipe, remote from welds or other discontinuities	0.5	1.0	1.0	1.0	1.0	1.0	1.0	…	1.0	see NB-3683.3
Longitudinal butt welds in straight pipe										see NB-3683.4(a)
(a) flush	0.5	1.0	1.0	1.0	1.0	1.1	1.0	…	1.1	
(b) as welded, t> 4.76 mm (3/16 in)	0.5	1.1	1.2	1.0	1.2	1.3	1.0	…	1.2	
(c) as welded, t≤ 4.76 mm (3/16 in)	0.5	1.4	1.5	1.0	1.2	1.3	1.0	…	1.2	
Girth butt welds between nominally identical wall thickness items										see NB-3683.4(b)
(a) flush	0.5	1.0	1.2	1.0	1.0	1.1	0.6	0.5	1.1	
(b) as welded	0.5	1.0	1.2	1.0	1.0	1.8	0.6	0.5	1.7	
Girth fillet weld to fittings, socket weld, SW valves, SW flanges										see NB-3683.4(c)
All	0.8	1.8	3.0	1.5	2.1	2.0	2.0	1.0	3.0	
Transitions NB-4250										see NB-3683.5(a)
(a) flush	0.5	…	1.1	1.0	…	1.1	…	1.0	1.1	
(b) as welded	0.5	…	1.2	1.0	…	1.8	…	1.0	1.7	
Transitions within a 1:3 slope envelope										see NB-3683.5(b)
(a) flush	0.5	…	1.2	1.0	…	1.1	…	0.6	1.1	
(b) as welded	0.5	…	1.2	1.0	…	1.8	…	0.6	1.7	

Table C1: Stress indexes according to ASME Table NB-3681(a)-1

APPENDIX D

PLASTICITY CORRECTIONS IN THERMAL FATIGUE

D1 MEASURES OF EQUIVALENT STRESS AND STRAIN

In cases of thermal loadings it is necessary to decompose the total strain into the thermal and the mechanical portions:

$$\varepsilon_{total} = \varepsilon_{mechanical} + \varepsilon_{thermal} \quad \text{D1}$$

The thermal strains are generally computed as:

$$\varepsilon_{thermal,ij} = \alpha(\theta - \theta_{ref})\delta_{ij} \quad \text{D2}$$

Where θ is temperature and δ_{ij} indicates that these strains act only in principal directions.

The mechanical strains, $\varepsilon_{mechanical}$, are associated with the evolution of fatigue damage and these strains, or the stresses associated with these strains, should be input to the fatigue design curves.

In thermal fatigue multiaxial effects almost always need to be considered. The typical approach is to use scalar stress- or strain-based parameters, which are derived from the various stress/strain components. The ASME Code Case N-201-4, ref /D1/ proposes the parameter:

$$\Delta\varepsilon_{equiv1} = \frac{1}{(1+\nu^*)\sqrt{2}}\sqrt{(\Delta\varepsilon_x - \Delta\varepsilon_y)^2 + (\Delta\varepsilon_x - \Delta\varepsilon_z)^2 + (\Delta\varepsilon_y - \Delta\varepsilon_z)^2 + \frac{3}{2}\left(\Delta\gamma_{xy}{}^2 + \Delta\gamma_{xz}{}^2 + \Delta\gamma_{yz}{}^2\right)} \quad \text{D3}$$

In terms of the principal strains the same equivalent measure is:

$$\Delta\varepsilon_{equiv1} = \frac{1}{(1+\nu^*)\sqrt{2}}\sqrt{(\Delta\varepsilon_1 - \Delta\varepsilon_2)^2 + (\Delta\varepsilon_1 - \Delta\varepsilon_3)^2 + (\Delta\varepsilon_2 - \Delta\varepsilon_3)^2}$$

Here, ν* is the effective Poisson ratio. Two analysis options are given: elastic and inelastic for which ν* is given the value 0.3 or 0.5 respectively. Specific design curves are given in the Code Case. In the elastic analysis option, it is suggested that the maximum equivalent strain $\Delta\varepsilon_{\max}$ be computed, neglecting the influence of local geometric stress concentrations. It is furthermore proposed (with a few options) that stress concentration or notch effects should be considered via a Neuber-type correction:

$$\Delta\varepsilon_{\mathrm{mod}} = K^2 \frac{S}{\bar{S}}\Delta\varepsilon_{\max} \quad \text{D4}$$

where *K* is the stress concentration factor. Furthermore, *S* and $\Delta\varepsilon_{\max}$ are elastically computed entities and $\Delta\varepsilon_{\mathrm{mod}}$ and $\bar{S}$ are obtained from a non-linear stress-strain curve, also given in the Code Case. Finally, the strain range value $\varepsilon_t = \Delta\varepsilon_{\mathrm{mod}}$ is input to the design curve, applying a

factor K_ν to incorporate effects of the higher Poisson ratio in the plastic regime. This influence of the Poisson ratio, expressed via K_ν, is treated in detail in ref /D2/. In this document the definition the equivalent strain used is:

$$\Delta\varepsilon_{equiv2} = \frac{\sqrt{2}}{3}\sqrt{(\Delta\varepsilon_x - \Delta\varepsilon_y)^2 + (\Delta\varepsilon_x - \Delta\varepsilon_z)^2 + (\Delta\varepsilon_y - \Delta\varepsilon_z)^2 + \frac{3}{2}\left(\Delta\gamma_{xy}{}^2 + \Delta\gamma_{xz}{}^2 + \Delta\gamma_{yz}{}^2\right)} \qquad \text{D5}$$

And once again, in principal strains:

$$\Delta\varepsilon_{equiv2} = \frac{\sqrt{2}}{3}\sqrt{(\Delta\varepsilon_1 - \Delta\varepsilon_2)^2 + (\Delta\varepsilon_1 - \Delta\varepsilon_3)^2 + (\Delta\varepsilon_2 - \Delta\varepsilon_3)^2} \qquad \text{D6}$$

It is noted that this measure is identical to the equivalent strain in the Code Case, letting ν*=0.5. Furthermore in /D2/ the secant modulus E_s and the effective Poisson ratio $\bar{\nu}$ are defined. The secant modulus can be simply obtained from the uniaxial cyclic elastic-plastic relation, with $E_s = \Delta\sigma/\Delta\varepsilon$, so the effective Poisson ratio is obtained by:

$$\bar{\nu} = \nu\frac{E_S}{E} + 0.5\left(1 - \frac{E_S}{E}\right) \qquad \text{D7}$$

Then K_ν is computed as the correction of expression D5, assuming that the surface strains are computed:

$$K_\nu = \frac{\Delta\varepsilon_{equiv2}(\nu = \bar{\nu})}{\Delta\varepsilon_{equiv2}(\nu = \nu_{elastic})}. \qquad \text{D8}$$

Hence K_ν will depend on the cyclic elastic-plastic stress-strain relationship as well as the degree of multiaxiality of the load state. It should be noted that the K_ν defined in /D2/ is not exactly the same as the one defined in the Code Case /D1/. A feature of it is that a correction is needed to correlate $\Delta\varepsilon_{equiv2}$ to the strain Δε in the load direction in the uniaxial case. This correction reads: $\Delta\varepsilon = \left(3/2\left(1+\bar{\nu}\right)\right)\Delta\varepsilon_{equiv2}$.

Finally, in /D3/ the use of an effective measure is discussed further. The measure proposed is

$$\Delta\varepsilon_{equiv3} = \frac{1}{\sqrt{2}\left(1+\bar{\nu}\right)}\sqrt{(\Delta\varepsilon_x - \Delta\varepsilon_y)^2 + (\Delta\varepsilon_x - \Delta\varepsilon_z)^2 + (\Delta\varepsilon_y - \Delta\varepsilon_z)^2 + \frac{3}{2}\left(\Delta\gamma_{xy}{}^2 + \Delta\gamma_{xz}{}^2 + \Delta\gamma_{yz}{}^2\right)} \qquad \text{D9}$$

Or, expressed in terms of principal strains

$$\Delta\varepsilon_{equiv3} = \frac{1}{\sqrt{2}\left(1+\bar{\nu}\right)}\sqrt{(\Delta\varepsilon_1 - \Delta\varepsilon_2)^2 + (\Delta\varepsilon_1 - \Delta\varepsilon_3)^2 + (\Delta\varepsilon_2 - \Delta\varepsilon_3)^2} \qquad \text{D10}$$

It is furthermore noticed that the relation between the von Mises effective stress and the equivalent strain is:

$$\sigma_{VM} = E_S \cdot \varepsilon_{equiv3}. \qquad \text{D11}$$

It is noted that $\Delta\varepsilon_{equiv3}$ will be exactly the strain Δε is the uniaxial case and no correction is needed. It is also noted that $\Delta\varepsilon_{equiv3} \geq \Delta\varepsilon_{equiv2}$ and equal only in the case of entirely plastic deformation. Moreover, it is possible to define a $K_\nu^{'}$ similar to that of eq. D8, reading:

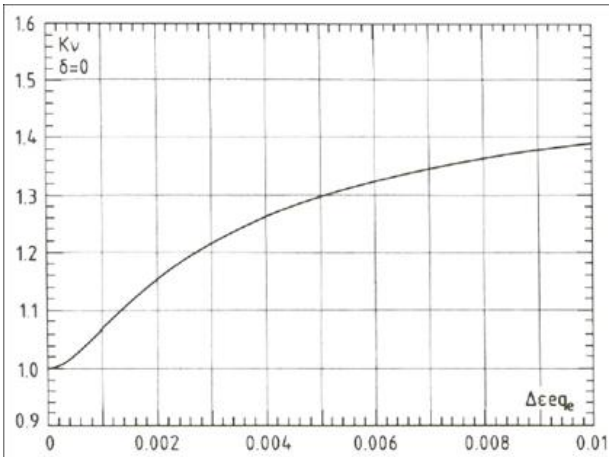

Figure D1: Plastic correction factor K_v for the biaxial loading (/D2/).

D2 FE MODELLING OF CYCLIC PLASTICITY

In ref /D3/ the computation of the surface strain under thermal cyclic loading is discussed. Calculations were performed using inelastic models and were compared to those of elastic calculations. It was shown that the surface strains $\Delta\varepsilon_1$ and $\Delta\varepsilon_2$ could be quite accurately computed even in cases where the level of plastic deformation is rather high. This would indicate that elastic calculations can often be used to capture the level of mechanical surface strains in cases of thermal loading, even when comparatively high levels of plastic deformation are present. This is possibly due to the fact that the surface strains are controlled by the elastic response beneath the surface. An example is that of thermal shock (ref /D2/) where the total surface strains are zero and hence $\Delta\varepsilon_1 = \Delta\varepsilon_2 = -\alpha\Delta\theta$.

The Chaboche model /D4/ is a non-linear kinematic hardening material model. It is an able to model cyclic plastic behaviour, such as ratchetting, mean stress relaxation and cyclic hardening or softening. It can easily be combined with an isotropic hardening to model combined behaviour. In order to use the model, a set of 3 material parameters is necessary. Using fixed material parameters limits the strain range for which the model is applicable. The feature which allows it to model shakedown and ratchetting is the “memory term” representing the accumulated plastic strain.

In Figure D2 the size of the inner surface corresponds to von Mises yield stress and is represented by the constant *k*. This yields for the hardening rule:

$$da_{ij} = \frac{2}{3} C d\varepsilon_{ij}^{p} - \gamma a_{ij} \mid d\varepsilon_{a}^{p} \mid \qquad \text{D15}$$

Where: da_{ij} is the increment in kinematic hardening.
$|d\varepsilon^{p}{}_{a}|$ is the increment of the accumulated plastic strain.
C and γ are characteristic coefficients of the material.
$d\varepsilon^{p}{}_{ij}$ is the increment in plastic strain.
a_{ij} is a tensor representing the centre of the yield surface.

The yield criterion is given by:

$$f = J_2(\sigma_{ij} - a_{ij}) - k \qquad \text{D16}$$

Where: f is the yield surface.

J_2 is the second invariant of the stress deviator.

σ_{ij} is the stress tensor.

k is the material parameter corresponding to the von Mises yield stress.

In Figure D3 plots hysteresis loops for 0.2, 0.5 and 2% strain ranges for both the Chaboche model (with a fixed set of parameters) and the empirical RCC-MR relation. The solid curves connect the hysteresis peaks for each relation. Even though the hysteresis loops do not match perfectly, their endpoints do match very well, leading to accurate predicted strain-amplitudes. The difference grows bigger for large strain amplitudes, showing the limited applicability of the model with a single set of parameters.

In order to check how well the two peak curves match, the relative difference is plotted in Figure D4. Using the Chaboche model for evaluation of a pipe-geometry exposed to cyclic thermal loading, one can show that, even though the material enters the plastic region, the in-plane strains can be sufficiently accurately calculated with a purely elastic model. The rougue component is the out-of-plane strain component. This is markedly different from that determined in an elastic evaluation and is therefore suspected to strongly depend on material behaviour beneath the surface. This component can easily be derived from elastic calculations of the in-plane-strains using an assumption of total plasticity by:

$$\varepsilon_r = \frac{-\nu'(\varepsilon_\theta + \varepsilon_y)}{1-\nu'} \qquad \text{D17}$$

Where $\varepsilon_r, \varepsilon_\theta, \varepsilon_y$ are the principal strains and ν' is the effective Poisson ratio, fixed at 0.5 under fully plastic conditions.

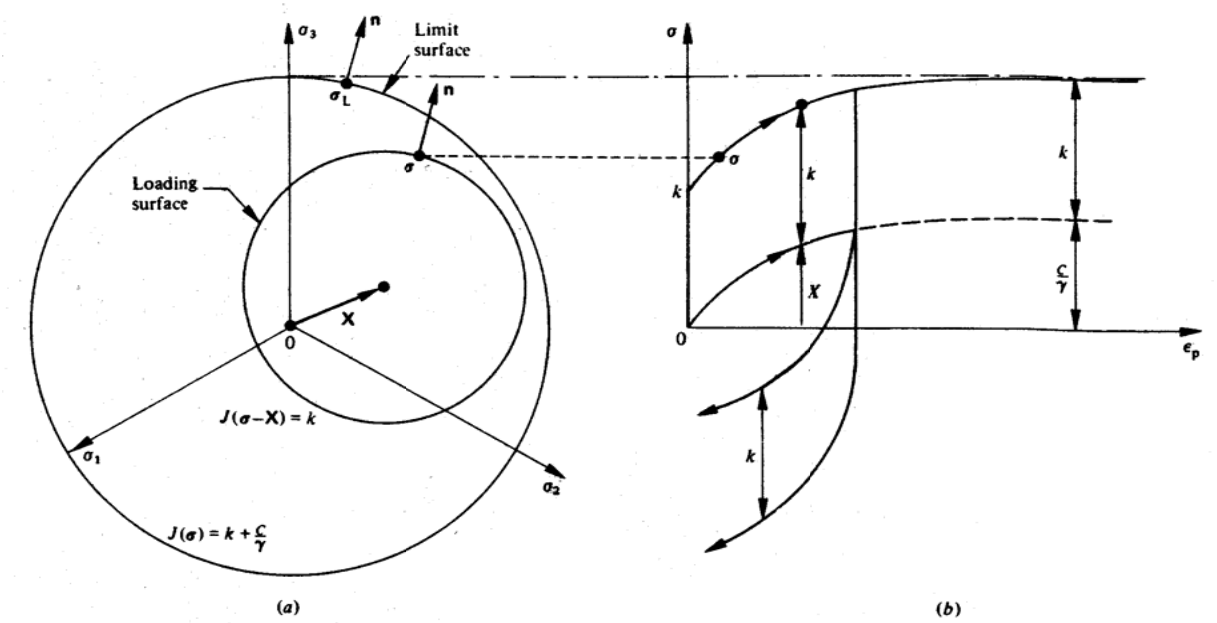

Figure D2: The limit surface and the yield surface showing and the significance of the material parameters; the outer surface is fixed and represents total plasticity.

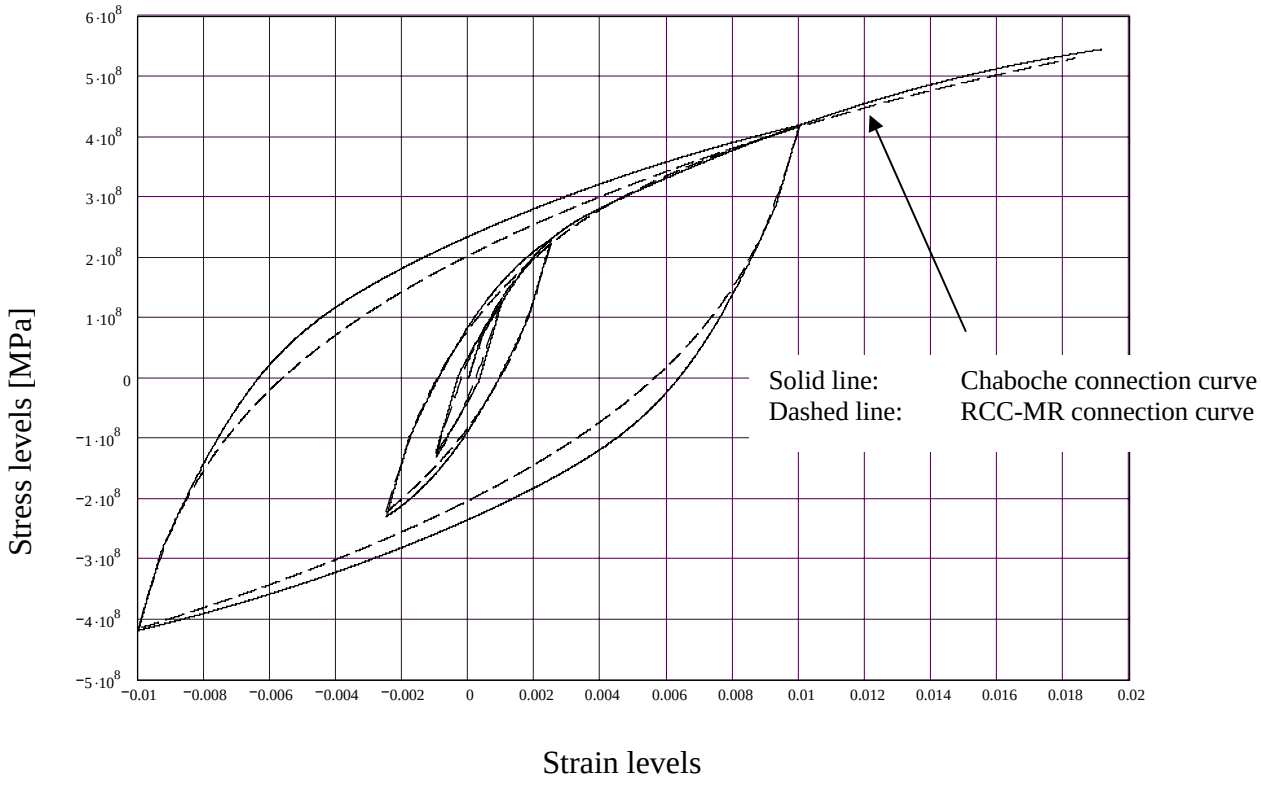

Figure D3: Cyclic stress-strain curves and peak connection curves; the connection curves are functions of strain amplitudes.

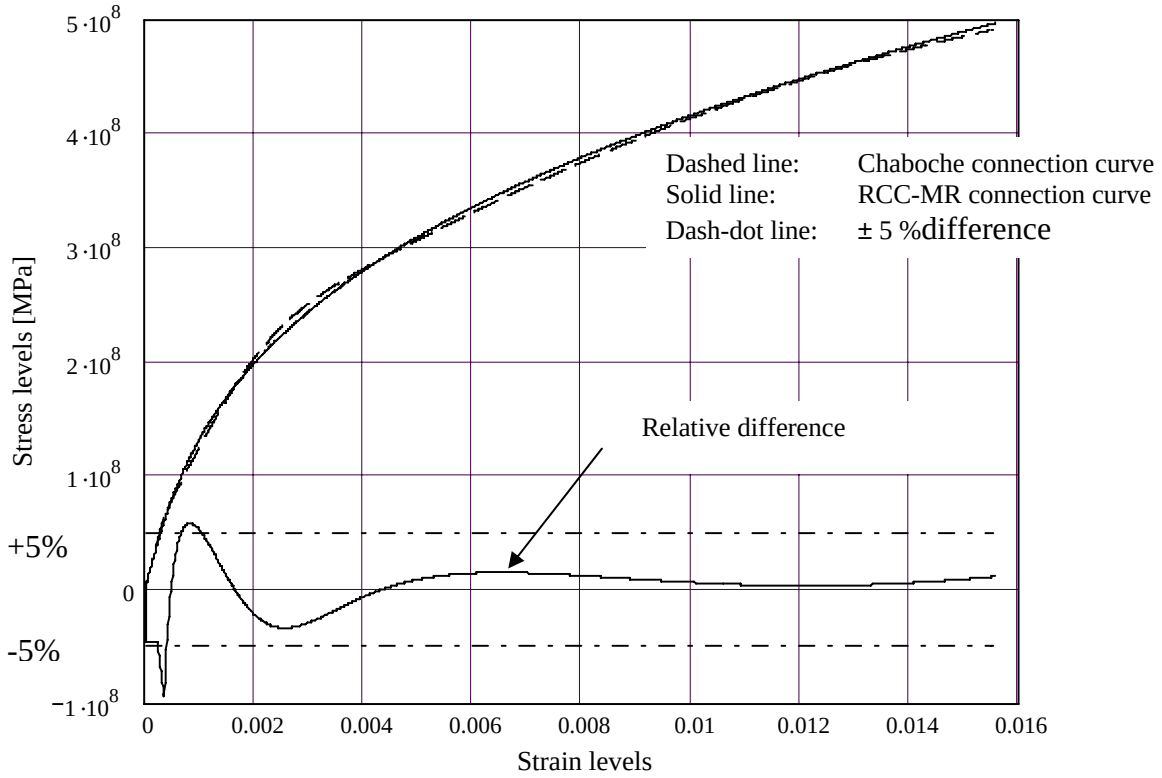

Figure D4: Relative difference between peak-curves for Chaboche and the RCC-MR relation; the dash-dot line represents 5% difference between the two curves.

D3 REFERENCES

D1 ASME, Code case N-201-4, Appendix Y

D2 Moulin, D., Roche R. L., ”Correction of the Poisson Effect in the Elastic Analysis of Low-Cycle Fatigue” Int. J. Pres. Ves. & Piping 19 (1985)

D3 Södergren, F., “Thermal Fatigue”, DNV Research Report, RSE R&D Report no.2004/03

D4 Lemaitre, J., and J.-L. Chaboche, “Mechanics of Solid Materials”, Cambridge University Press, 1990.

APPENDIX E

FRACTURE MECHANICS TREATMENT OF CRACK PROPAGATION IN THERMAL FATIGUE

E1 INTRODUCTION

Although foreseen as Level 4 in the proposed procedure, a detailed methodology for assessing thermal fatigue crack propagation was not derived in the NESC-TF project. The following guidelines have however been formulated. These are restricted to cases where fracture mechanics concepts can be applied, thus short cracks and compression/compression loading cases are excluded. The crack depth at which a crack becomes "long crack" depends on the material and the load level. From engineering point-of-view, a crack depth of 1 mm should be sufficient.

Some basic concepts for fracture mechanics-based fatigue crack growth (FCG) models are discussed below. Formulas and experimental data are often derived for stress-controlled conditions and for more or less constant loadings. In thermal fatigue, however, the loading is essentially strain-controlled and with large through thickness gradients.

E2 GENERAL CRACK PROPAGATION LAW

Consider a growing crack with a plastic zone at the crack tip. The crack propagation per cycle, *da/dN*, can be expressed by the functional relationship:

$$\frac{da}{dN} = F(\Delta L, R, \kappa), \qquad \text{(E1)}$$

where ΔL is the crack tip loading variation, R is the ratio between the minimum and maximum value of the crack tip loading ($L_{\min} / L_{\max}$) and κ indicates the history dependence from previous plastic deformation. The number of cycles needed to propagate a crack from an initial length a_0 to a final length a_f, is given by integration of Eq. (E1):

$$N = \int_{a_0}^{a_f} \frac{da}{F(\Delta L, R, \kappa)} \quad . \qquad \text{(E2)}$$

E2.1 Small-scale yielding crack propagation model under constant amplitude loading

If the plastic zone ahead of the crack tip is small compared to other lengths (crack length and dimension of component) then the propagation is described by the stress intensity factor and

$$\Delta L = \Delta K = \begin{Bmatrix} K_{\max} - K_{\min} & if\ K_{\min} > 0 \\ K_{\max} & if\ K_{\min} < 0 \end{Bmatrix} \qquad \text{(E3)}$$

$$R = K_{\min} / K_{\max} \qquad \text{(E4)}$$

Figure E1 shows a schematic log-log plot of da/dN versus ΔK, which illustrates typical fatigue growth behaviour in metals. At intermediate values of ΔK the relationship is linear and can be described by the so-called Paris law:

$$\left.\begin{array}{ll} da/dN = C\Delta K^{m} & \Delta K > \Delta K_{th} \\ da/dN = 0 & \Delta K \le 0 \end{array}\right\} \qquad \text{(E5)}$$

where C and m are material constants and ΔK_{th} is the threshold value, which is typically defined by the ΔK value when da/dN < 10^{-7} m/cycle.

The fatigue threshold and the lower end of the Paris' law are affected by the R-ratio. The reason is that crack faces come in contact at a certain load, K_{op}, which is above K_{min} (see Figure E2). There are different reasons for this so-called crack closure effect. The most important one is plasticity induced crack closure (PICC), which is caused by the plastic wake behind the crack tip. Only the portion of ΔK when the crack remains open, ΔK_{eff}, contributes to the crack propagation. The Paris law is then:

$$\frac{da}{dN} = C\left(\Delta K_{eff}\right)^{m} = C\left(U\Delta K\right)^{m} \qquad \text{(E6)}$$

where the effective stress intensity factor is,

$$\Delta K_{eff} = K_{\max} - K_{op} \qquad \text{(E7)}$$

and the reduction factor, U, is

$$U = \frac{\Delta K_{eff}}{\Delta K} = \frac{1}{1-R} - \frac{K_{op}}{\Delta K} \qquad \text{(E8)}$$

To apply this, the simplest approach is to assume K_{op} to be a material constant. The threshold can be directly inferred by setting U = 0 (i.e. $K_{max} = K_{th}$)

$$\Delta K_{th} = K_{op}(1-R), \qquad \text{(E9)}$$

and

$$\Delta K_{eff} = \frac{\Delta K - \Delta K_{th}}{1-R} \qquad \text{(E10)}$$

In reality the K_{op} is not a material constant and it depends among other thing on the load history. For instance, it has been shown from fatigue tests with a constant R but decreasing ΔK that Eq. (E9) overestimates ΔK_{th}, whereas increasing ΔK has the opposite effect. A number of more or empirical expressions for K_{op} can be found in the literature /E2/, /E3/.

There are more general expressions than the Paris law, capable of describing the da/dN vs. ΔK relation for the entire sigmoidal shape in Figure E1. The most popular one is the so-called Forman-Mettu equation, which is used in the NASGRO and ESACRACK procedures:

$$\frac{da}{dN} = C\left[U \cdot \Delta K\right]^m \frac{\left(1-\frac{\Delta K_{th}}{\Delta K}\right)^p}{\left(1-\frac{K_{\max}}{K_c}\right)^q} \quad . \qquad \text{(E11)}$$

Note that this model requires four material calibration parameters. (*p, q, m* and *C*) and that *m* and *C* may deviate slightly from the values determined from for the Paris law.

E2.2 Calculation of ΔK

It is not feasible to re-calculate ΔK for each cycle from a cracked body FE-analysis in a cycle-by-cycle propagation. The best procedure is then to use available K-solutions for semi-elliptical cracks at the outer or inner pipe surface subject to an arbitrary stress distribution, Figure E3. These were first presented by Raju and Newman /E4, E5/; recently CEA have published more refined solutions covering a wider range of geometries and material properties /E6/. The expression for K is:

$$K(a/t, a/c, a/R_i, \sigma) = \sqrt{\frac{\pi a}{Q}}\left[b_0 i_0 + b_1 i_1 \frac{x}{t} + b_2 i_2 \left(\frac{x}{t}\right)^2 + b_3 i_3 \left(\frac{x}{t}\right)^3\right] \sec\sqrt{\frac{c}{2R_i}\sqrt{\frac{a}{t}}} \qquad \text{(E12)}$$

where the coefficients b_i are fitted to the stress distribution for a un-cracked body:

$$\sigma(x/t) = b_0 + b_1 \frac{x}{t} + b_2 \left(\frac{x}{t}\right)^2 + b_3 \left(\frac{x}{t}\right)^3 \quad \text{for } 0 \le x \le a\,; \quad b_0, b_1, b_2, b_3 \text{ are fit coefficients} \qquad \text{(E13)}$$

The coefficients i_0, i_1, i_2 and i_3 depend on the relative crack depth, *a/t*, on the shape of the crack, *a/c*, on the curvature t/R_i and on the location along the crack front. $Q = 1 + 1.464(a/t)^{1.65}$ is a shape factor while *x* is the variable of distance across the wall thickness. For a given crack geometry and loading *K* can then be calculated as function of time over a cycle and K_{max}, K_{min} and thus ΔK can be calculated at different points along the crack. The crack propagation rate is then obtained from a Paris or Foreman-Mettu law. If this procedure is repeated cycle-by-cycle the evolution of the crack shape can be modelled.

E2.3 Large-scale yielding crack propagation model under constant amplitude loading

When the plastic zone is not small compared to the defect size, as would be expected for low-cycle fatigue or when a crack is short, the stress intensity factor concept is no longer valid. However, it has been shown that crack propagation can be described by Paris law models using the contour "J-integral", *ΔJ*, /E7/ or crack tip opening as crack tip loading parameters, *ΔCTOD* /E8/:

$$\left.\begin{aligned} \frac{da}{dN} &= C_J \Delta J^{m_J} \\ \frac{da}{dN} &= C_{CTOD} \Delta CTOD^{m_{CTOD}} \end{aligned}\right\} \qquad \text{(E14)}$$

In small-scale yielding situations J and CTOD are proportional to K^2, but $\Delta J, \Delta CTOD$ are proportional to $\sqrt{K_{\max}^2 + K_{\min}^2 - K_{\min}K_{\max}} \neq (K_{\max} - K_{\min})$. The Paris law parameters (c_{CTOD}, m_{CTOD}) or (c_J, m_J) can therefore not be directly inferred from *c* and *m* established using ΔK data. Thus the crack growth law parameters need to be evaluated for the associated crack loading parameter.

E2.4 Variable amplitude loading and history effects

The loading in thermal fatigue is generally of variable amplitude and described by a spectrum. Analysis of crack propagation in these circumstances is very complex. The most common approach is to use a rainflow technique to compute the cycles in combination with a cumulative Miner-Palmgren damage law. This should normally give conservative estimates since history effects are not accounted for, in particular crack retardation due to compressive residual stresses following overloads.

E3 APPLICATION OF FCG MODELS TO THERMAL FATIGUE

For a safety assessment it is typically required to demonstrate that a crack cannot propagate to a depth that may jeopardise the structural integrity during operation. If a simple and conservative model predicts crack arrest or very slow crack propagation, then compliance with this safety concept is shown. If not, a more advanced model could be applied. An alternative requirement is to determine the potential crack growth rate as part of planning in-service inspection intervals. To address these needs, a hierarchy of models with increasing complexity is foreseen.

E3.1 Constant amplitude loading.

Model 1a: Elastic model with constant amplitudeΔK

a) The distribution of the stress component normal to the crack versus time is computed from an elastic analysis, $\sigma_{el}(x,t)$. This can be done with different levels of geometrical complexity. However, it is important that the through-wall distribution is captured, bearing in mind that this can be 1-D, axi-symmetric or 3-D.
b) The cyclic stress intensity factor, $\Delta K\left(a,t,c,R_i,\sigma(x,t)\right)$, is computed from Eq. (E12) for the given geometry and stress distribution.
c) The crack propagation is computed using Paris law (Eq. (E5)) and the crack length versus time is calculated using Eq. (E2).
d) The evolution of crack depth and shape is computed by integration of Paris law.

The procedure can be applied for axial as well as radial cracks. It should give a conservative estimate since:

a. An elastic analysis overpredicts ΔK for strain-controlled loadings,
b. It uses a stress-based rather than a strain-based formula for K, which should overestimate the actual driving force value with increasing crack depth due to the increased compliance.
c. Crack closure effects are not accounted for.

It can be noted that the K-solutions assume axi-symmetric stresses. In a 3D case, the maximum stresses should be used for the K-calculation.

Model 1b: Elastic FCG model with constant amplitudeΔK_{eff}

This is the same as Model 1° except that ΔK is replaced by ΔK_{eff} using the simple formula (E10). This model should also give conservative estimates since conditions a) and b) above are still relevant. In addition, due to the large strain gradients $\frac{dK}{da}$ will become negative at a certain crack depth so ΔK_{th} is expected to increase. More advanced approaches could be adopted by applying more specific formulas for the crack closure than (E10).

Model 1c: Elastic-plastic FCG model for small-scale yielding conditions and constant amplitudeΔK

As Model 1a or 1b but the stress distribution is computed from stabilized cycles using a cyclic plasticity model. This model should give a conservative estimate since condition a) above still holds. Note that the stress intensity formulas (E12) and (E13) rely on superposition and sufficient conservatism when applying these to plastic deformation may need to be demonstrated. Nevertheless, this model has proved to be conservative when applied to laboratory tests /E9/.

Model 1d: Elastic-plastic FCG model for large scale-yielding conditions and constant amplitude loading

To apply this model crack propagation data in terms of $\Delta CTOD$ are needed. More importantly, simple formulas for $\Delta CTOD$ similar to Eq. (E12) and (E13) are only available for simple crack geometries such as axisymmetric cracks and for most practical cases require detailed cracked body FE analyses.

E3.2 Variable amplitude loading

Models 1a-1d can be extended to variable amplitude loading. If there is no knowledge of the load spectrum, then the sinusoidal approach (Level 2) can be used. Thus stresses are calculated for ΔT with the 80% rule and the crack propagation versus time is calculated as function of the frequency using Model 1a. This gives the number of cycles needed propagate the crack to the depth, a_f, which is defined as end of life. We write this formally as $N(a_f,f)$. The life in time is given by: $T(a_f, f) = N(a_f, f)/f$. The life is then $T_{Life} = \lfloor N(a_f, f)/f \rfloor_{\min}$. This approach is expected to provide very conservative estimates since in addition to the features mentioned above, the worst-case frequency value is used.

If the spectrum is known, then the rainflow technique should be used for cycle counting and Miner-Palmgren accumulation law for crack propagation. This should provide conservative estimates since crack retardation after overloads is not accounted for.

E3.4 Other Effects

The stresses and strains in thermal fatigue are typically biaxial and there are usually a large number of cracks (although the number of cracks of a given depth decreases with increasing depth). Multiple cracking increases the local material compliance, and would be expected to

reduce magnitude of the crack driving force for a strain controlled loading. Biaxiality has no effect on the computed ΔK. Fatigue propagation data show a biaxiality effect when plotted against ΔK but not when plotted against $\Delta CTOD$ for crack propagation rates close to the threshold value.

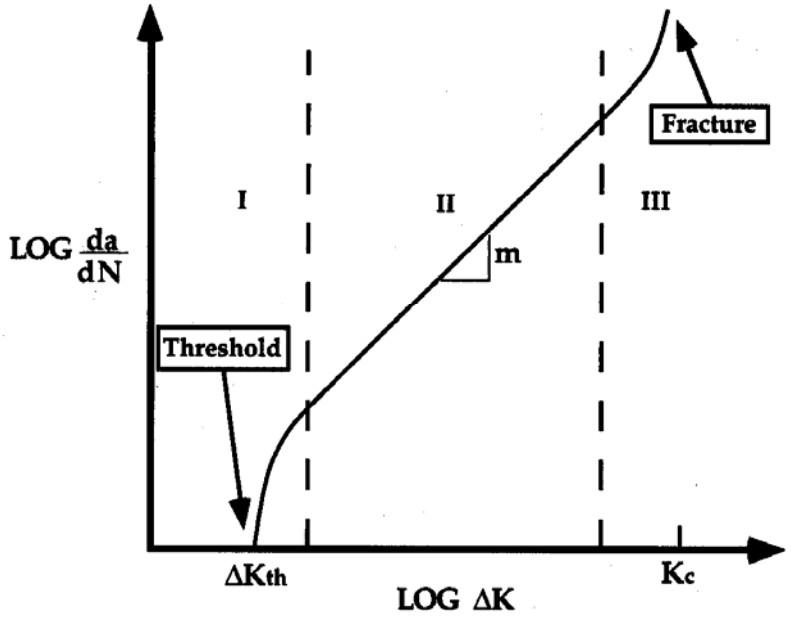

Figure E1: Schematic illustration of da/dN versus ΔK.

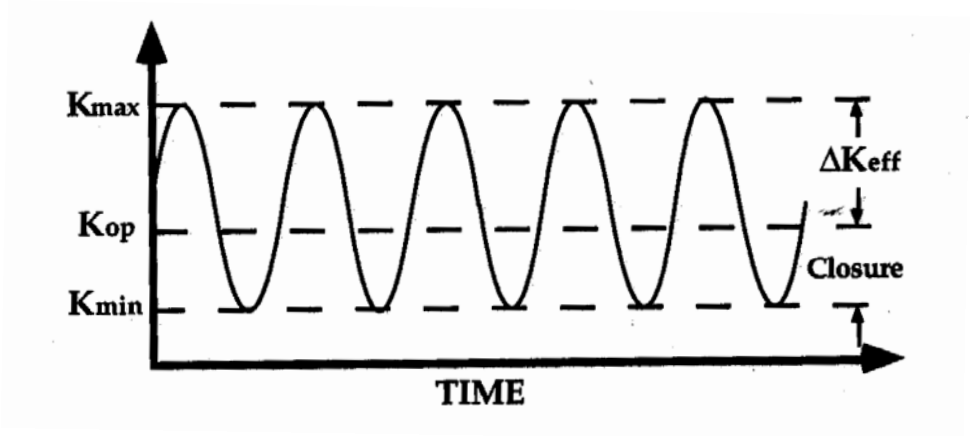

Figure E2: Constant amplitude crack tip loading where $\Delta K_{eff} < \Delta K$.

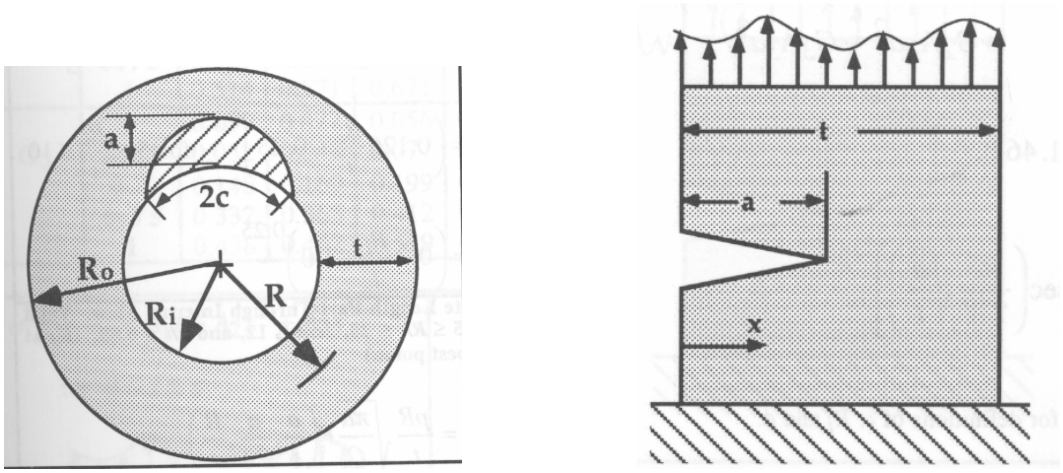

a) b)

Figure E3: Tube with semi-elliptical defect at arbitrary loading. a) Definition of crack and tube geometry b) illustration of through-wall stress distribution.

E4 REFERENCES

E1 Hetzberg R.W, Newton, C.H, and Jaccard, R., 1988, Crack closure: Correlation and confusion, ASTM STP 982, ASTM Philadelphia pp. 139-148.

E2 S. Suresh Fatigue of Materials 2nd Edition, 1998, Cambridge University Press, UK

E3 T.L Anderson, Fundamentals and Applications, Second Edition, 1995, CRC Press, USA.

E4 Newman J. C., and Raju I.S., Stress Intensity Factors for Internal Surface Cracks in Cylindrical Pressure vessels, *ASME Journal of Pressure Vessel Technology*, Vol. 102, Nov. 1980, pp.342-346

E5 I.S. Raju, J. C. Newman Jr., *Stress-Intensity factors for internal and external surface cracks in cylindrical vessels*, Journal of Pressure Vessel Technology, Vol. 104, pp. 293-298, 1982

E6 Chapuliot S., Formulaire de K_I Pour les Tubes Comportant un Defaut de Surface Semi-elliptique Longitudinal ou Circonferentiel, interne ou externe, Direction de l'information scientifique et technique, CEA/SACLAY-R-5900, France, ISSN 0429 3460, 2000

E7 Dowling N.E and Begley J.A., 1976, Fatigue crack growth during gross plasticity and the J-integral. In Mechanics of Crack growth, ASTM STP 590, pp. 82-103.

E8 Tanaka K, Hoshide T., Yamada A. and Taira S., 1979, Fatigue crack propagation in biaxial stress fields, Fatigue Eng. Mater. Struct, 2. 181-194.

E9 Paffumi E., Nilsson K-F, Taylor N., Hurst R. and Bache M.R., Measurement of shallow crack growth during thermal fatigue of 316L tubular test piece, Proc., Third International Conference Fatigue of Reactor Components, OECD/EPRI Seville, 3-6 October,2004

European Commission

EUR 22763 EN – DG JRC – Institute for Energy
Development of a European Procedure for Assessment of High Cycle Thermal Fatigue in Light Water Reactors: Final Report of the NESC-Thermal Fatigue Project
Authors:
M. Dahlberg, Inspecta
K.F. Nilsson, EC DG JRC
N. Taylor, EC DG JRC
C. Faidy, EDF
U. Wilke, EON
S. Chapuliot, CEA
D. Kalkhof, PSI (now HSK)
I. Bretherton, Serco (now HSE)
M. Church, NRG
J. Solin, VTT
J. Catalano Tractebel

Luxembourg: Office for Official Publications of the European Communities
2007 –158pp. – 21 x 29.7 cm
EUR - Scientific and Technical Research Series; ISSN 1018-5593

Abstract
In nuclear plant piping systems thermal fatigue damage can arise at locations where there is turbulent mixing of different temperature flows. The severity of this phenomenon can be difficult to assess via plant instrumentation due to the high frequencies involved. In Europe the existing approaches to high cycle thermal fatigue have been successful in providing margins against pipe ruptures. Nonetheless there have been instances of thermal fatigue damage and over the last 10 years several recent R&D programmes have been devoted to developing better understanding of the induced thermal loads and associated damage mechanisms. To exploit this work, in 2003 the Network for Evaluation of Structural Components (NESC) set up a project involving both utilities and R&D organizations. Its aim was to produce a consensus methodology for assessing high cycle thermal fatigue in piping components, with special attention to turbulent mixing phenomena at mixing tees in light water reactor systems. It has involved the collaboration of over 10 organisations from 5 European countries. All have participated on an 100% in-kind basis. Wherever possible, advantage has been taken of recent R&D work at national, European and international levels. The work programme focused on two main aspects:

a) creating a database of service and mock-up data for better understanding thermal fatigue damage mechanisms and for validating the procedure.

b) developing a European multi-level thermal fatigue damage procedure, which should reflect the multi-disciplinarity of the phenomenon (thermo hydraulic, material, strain evaluation through FEA, damage analysis, fracture mechanic, ISI performance).

The mission of the Joint Research Centre is to provide customer-driven scientific and technical support for the conception, development, implementation and monitoring of EU policies. As a service of the European Commission, the JRC functions as a reference centre of science and technology for the Union. Close to the policy-making process, it serves the common interest of the Member States, while being independent of special interests, whether private or national.

EUROPEAN COMMISSION
DIRECTORATE-GENERAL
Joint Research Centre

Publications Office
Publications.eu.int